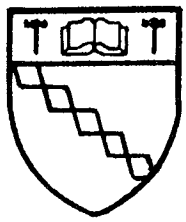

TEMPERATURES AND FRICTION AT LUBRICATED ROLLING / SLIDING CONTACTS

by

STANLEY MICHAEL MANTON

A Thesis submitted for the Degree of

DOCTOR OF PHILOSOPHY

DEPARTMENT OF MECHANICAL ENGINEERING
THE UNIVERSITY OF ASTON IN BIRMINGHAM

MAY 1969

SUMMARY

The parameters affecting the temperatures and friction at lubricated rolling/sliding contacts of the Hertzian type are investigated and examined in relation to the failure of contacts by scuffing and their performance under traction conditions.

Based on the critical temperature criterion for scuffing, an experimental technique for the direct measurement of a lubricant's critical temperature is proposed and evaluated.

Blank temperature studies are carried out and further information concerning the heat transfer coefficients of machine components made available.

On the question of heat generation at the contact, a thermal analysis of the lubricant film is developed, providing complete distributions of temperature, shear rate, viscosity, and shear stress throughout the contact region. A marked dependence of these characteristics upon the physical properties of the lubricant is observed and the results assist not only in the prediction of scuffing but also in understanding the frictional behaviour of rolling/sliding contacts.

By comparison with friction measurements made on a traction machine, the theory gives a reasonable estimate of the friction-sliding characteristic provided the non-Newtonian behaviour of the lubricant is represented by a suitable model in the calculations. The Maxwell fluid model is that adopted for the present investigation.

The results for shear stress are considered to be of further use in the study of failure by pitting.

CONTENTS

ACKNOWLEDGEMENTS

The author acknowledges with thanks the opportunity given to him by the Senate of the University of Aston in Birmingham and the Directors of Joseph Lucas Ltd. to work for this degree.

Thanks are due to Mr. J.A.C. Thorne of the Mechanical Engineering Department for his help and guidance throughout the supervision of the work and also to Dr. J.P. O'Donoghue of Lanchester College of Technology, Coventry who originally suggested the subject for research and offered so much advice and encouragement during his position as external supervisor.

The author wishes to express his gratitude to Dr. S.S. Chang of the Lucas Group Research Centre for his continued support of the research programme particularly as external supervisor during the later stages of the work.

The advice and useful suggestions on the research programme offered by Dr. A. Cameron of Imperial College, London, Mr. T.C. Askwith of the Institute of Tribology, Leeds and Dr. H.E. Merritt are gratefully acknowledged.

The lubricant samples were supplied by Dr. H. Naylor of Shell Research Ltd, Chester and the author would like to thank M.S. Ali and M.P. Thomas of David Brown Industries Ltd. for providing samples of their test lubricants.

Finally to all those at the Lucas Group Research Centre who have assisted in the design and construction of the equipment reported in this thesis, the author's sincere thanks are recorded.

NOMENCLATURE

a	Half Hertzian contact width = $b/2$
b	Hertzian contact width
B	Box size (length of side)
C	Specific heat /unit mass
Cp	Specific heat at constant pressure
D	Diameter
E	Young's Modulus
E_1	Young's Modulus of body 1
E_2	Young's Modulus of body 2
$\frac{1}{E^1}$	$\frac{1}{2}\left[\frac{1-\gamma_1^2}{E_1} + \frac{1-\gamma_2^2}{E_2}\right]$
Ee	Internal energy per unit mass
E_t	Total energy per unit mass
$\frac{\partial e_1}{\partial z}$	Viscous shear strain
$\frac{\partial e_2}{\partial z}$	Elastic shear strain
f	Coefficient of friction
G	Shear modulus of elasticity
G_∞	Limiting high frequency shear modulus
Gr	Grashof number = $\frac{\epsilon\, g \Delta T\, D^3 \rho^2}{\eta^2}$
h	Oil film thickness
hm	Oil film thickness at $dp/dx = 0$
h_o	Oil film thickness on line of centres
h_c	Convective heat transfer coefficient
I	Non-dimensional temperature = $\frac{2\pi T k}{q}$
Ie	Enthalpy
i, j, k	3-D coordinates (as x, y, z)
k	Thermal conductivity
K	Thermal constant in flash temperature equation $(k \rho c)^{\frac{1}{2}}$

L	Distance between heat sources
N	Speed of revolution
n	Number of revolutions
Nu	Nusselt number = $\frac{h_c D}{k}$
P, p	Pressure
Pe	Potential energy
Po	Reduced pressure $1/\delta$
P_H	Hertzian contact pressure
Pr	Prandtl Number = $Cp\ \mu/k$
Q	Heat injected into metal surface
Q^1	Heat source strength = $q_\rho c$
q	Heat flow = Q/t
q^1	$q/2$
R_N	Reduced radius = $\frac{R_1 R_2}{R_1+R_2}$
R_1	Radius of contact of surface 1
R_2	Radius of contact of surface 2
Re	Reynolds Number $\rho UD/\eta$
Re_c	Reynolds Number of cross flow on cylinder $\frac{\rho U_c D}{\eta}$
S	Slip $\frac{U_1 - U_2}{U_1}$
T	Temperature
Tb	Blank temperature
Tc	Critical temperature
Tf	Flash temperature
Tt	Total contact temperature
t	Time
U	Velocity
U_1	Velocity of surface 1

U_2 Velocity of surface 2

U_c Crossflow velocity in forced convection

U_e Entraining velocity $= \frac{U_1 + U_2}{2}$

w Contact load/unit width

y Distance across face of contact

z Distance across contact oil film

α Heat transfer quantity $2\kappa_{hc}/Uk$

α'' Heat partition ratio $= q_2/q_1$

α^1 Heat sharing factor $q_1 = \alpha^1 q$

β $U/2K$

Υ Temperature-viscosity coefficient $(1/T)$

δ Pressure-viscosity coefficient $(1/p)$

ϵ Coefficient of thermal expansion $(1/T)$

κ Thermal diffusivity $= k/\rho c$

λ Second coefficient of viscosity

μ Surface finish in micro inches RMS

μ'' Surface finish in micro inches CLA

η Viscosity

η_o η_s Inlet viscosity to contact at ambient

Pressure

η_x Viscosity at metal surfaces at distance x

$\bar{\eta}_m$ Effective viscosity at contact from traction results

ϕ Dissipation function

ρ Density

θ Temperature in Crook's theory

θ_c Temperature on median plane of film

θ_s Inlet surface temperature

τ Shear stress

τ_c Critical shear stress in plastic shear hypothesis

τ_{ij} Shear stress in direction i in plane i j (If i = j then τ ij represents direct stress in direction i)

γ Poission's ratio

1.0 INTRODUCTION

Many machine components involve contact between surfaces possessing relative motion and carrying high loads. In the operation of gears for instance, torque is transmitted by contact between the flanks of meshing gear teeth. The application of a lubricant considerably increases the life of the gears but a limiting load capacity is experienced at which failure of the mating surfaces occurs. The conditions of load and speed and the nature of the lubricant determine the type of failure.

Various empirical relationships for the failure of lubricated rolling/sliding contacts have been derived from extensive testing under controlled laboratory conditions from which certain failure criteria have been proposed, particularly in the case of failure by scuffing

Recently, considerable progress has been made in the study of the lubrication mechanism at highly loaded contacts. The existence of a substantial oil film between the contacting surfaces has been confirmed and both analytical and numerical solutions to the problem provide important information relating to the pressures and the behaviour of the lubricant at the contact.

The results are not only relevant to the study of material failure or lubricant breakdown but also extend to the operation of machines known as friction drives, where the traction afforded by the lubricated contact is the important factor in determining the performance of the unit.

Further to this the surface shear distributions within the contact are vital to the calculation of contact stresses and to the understanding of pitting failures occurring in roller bearings, cams, and in the dedendum of gears.

The objects of the work presented in this thesis were to

examine the parameters affecting the failure of lubricated contacts in the light of the proposed scuffing criteria and to investigate the extention of existing theoretical solutions to predict failure by scuffing.

At the same time, the calculation of frictional traction would be possible and by comparison with previous and further experimental work, the accuracy of the solutions could be assessed.

The following chapters describe the experimental techniques and apparatus employed in obtaining data relating to the temperature and friction at lubricated contacts. Also, a thermal solution of the contact is proposed that results in the prediction of interesting characteristics of the lubricant's behaviour that are found to have a marked influence on the magnitude of the calculated temperatures and friction.

2.0 FAILURES AT LUBRICATED ROLLING/SLIDING CONTACTS

2.1 Types of failure

At the contact between gear teeth in mesh, considerable wear and power loss would occur if it were not for the low friction provided by the applied lubricant. With the correct design of gear form and right choice of lubricant, a substantial fluid film is built-up between the sliding surfaces. The load transmitted by the gears is carried by a finite area of contact between the teeth and high compressive stresses are produced at the metal surfaces. The application of these stresses is repeated every cycle of engagement and if at some point in the contacting bodies, the fatigue strength of the gear material is exceeded, then subsurface cracks or cracks at the surface are initiated. The first of these failures produces "flaking", characterised by the removal of large areas of material in the form of surface layers. Pitting is the phenomenon occurring as a result of the second type of failure and is characterised by the formation of small pits or craters produced by the propogation of the surface cracks under the action of the hydrodynamic pressures of the lubricant. Pitting usually occurs in the dedendum of gears just below the pitch line where the sliding speed is a minimum and the friction force a maximum.

Roller bearings and cam followers also exhibit the above failures, the contact conditions being very similar to those at the pitch line of gears. Various designs of friction drive also involve the same type of contact but with a small amount of sliding introduced between the surfaces. This resembles the contact between gear teeth at points a little removed from the pitch line but whereas the sliding in the gear tooth contact

is fixed by the geometry of the involute action, the sliding in friction drives is determined by the shear rate adopted by the fluid in transmitting the applied torque. Material failures are often encountered in friction drives, but the major design problem results from the limiting frictional force attainable by the contact. Should the device be overloaded, "skidding" of the drive takes place accompanied by surface damage of the driving members. The damage resembles that occurring at the tips of gear teeth where the same conditions of high surface sliding speed exist; this type of failure is known as scuffing.

Scuffing occurs initially at the tip and root of a gear tooth but may progress towards the pitch line. This type of failure is associated with the breakdown of the lubricant film, whereupon the metal surfaces make contact and under the high local stresses form welds and tear material from the surfaces. On the next cycle of engagement the surfaces make further contact with more severe welding and progressive deterioration of the surface condition is observed. A form of wear known as abrasion occurs as a result of metallic particles carried by the lubricant through the contact. With a low film thickness however, abrasion may also occur as a result of surface asperities penetrating the film and contacting the mating surface. More adequate filtering of the lubricant supply will help remove the particles whilst a more viscous lubricant increases the film thickness and prevents the contact of asperities.

2.2 Survey of investigations into scuffing failures

Many attempts have been made to relate material and lubricant properties to failure by scuffing. The earliest was that of Almen (1) who proposed the simple PVT factor which took

into account the tooth surface pressure, tooth velocity, and length of tooth contact path. A design limit of PVT = 1.5×10^6 was proposed (2) and has been widely used by gear designers, particularly in the U.S.A.

However, Shipley (3) showed that the scuffing results published by Borsoff (4) and those by Manhajm and Mansion (5) on the I.A.E. $3\frac{1}{4}$" gear testing rig did not conform to the design limit and many gears operated satisfactorily above the critical PVT factor. Shipley further showed that the results could be correlated by the "Temperature Flash" method proposed by Kelley (6). This work was in fact based upon the original theoretical work of Blok (7) who developed expressions for calculating the momentary rise in temperature experienced by rubbing contacts and who later suggested (8) that lubrication failed and surfaces scuffed when the maximum temperature at the contact exceeded a value characteristic of the lubricant and material of the rubbing surfaces.

The Blok flash temperature equation is:-

$$Tf = \frac{1.11\ f\ w\ (U_1^{\frac{1}{2}} - U_2^{\frac{1}{2}})}{K(b)^{\frac{1}{2}}}$$

Kelley obtained an empirical equation based on his scuffing results for case-carburised spur gears:-

$$Tt = \left[T_b + .00317\ w\ \frac{(U_1^{\frac{1}{2}} - U_2^{\frac{1}{2}})}{(b/2)^{\frac{1}{2}}} \right] \frac{55}{55 - \mu}$$

where μ is the surface finish after initial run in micro-inches R.M.S.

With this equation Shipley was able to reduce his scuffing results and those of Borsoff to a series of narrow bands or straight lines representing a constant scuffing temperature for any given lubricant.

Since the introduction of the Blok equation several research workers have been able to correlate their scuffing results. Although no criterion or explanation for scuffing failure of gear teeth has been found, scuffing temperatures remain the only method by which results can be correlated. In gear tests however, the coefficient of friction appearing in the flash temperature equation, cannot be measured and some estimate of its value is required. In this respect, disc machines have proved themselves extremely useful. Any gear tooth-tip contact can be represented by two discs rolling together and geared to have a predetermined sliding speed between them. Measurement of frictional force is a relatively simple matter and owing to the simplicity of the specimens, data can be rapidly accumulated. Two such investigations have been carried out by O'Donoghue and Cameron (9) and Benedict and Kelley (10) and provide the research worker with values of coefficient of friction for the gear contact conditions experienced in his tests. The empirical equations are easy to handle:-

The O'Donoghue and Cameron expression is:-

$$f = \frac{\mu' + 22}{35} \quad \frac{0.6}{\eta_S^{\frac{1}{8}} (U_1 - U_2)^{1/3} (U_1 + U_2)^{2/3} R_N^{\frac{1}{2}}}$$

where η_S is Centipoise at Tb

μ' = total initial surface roughness micro-inches CLA.

The Benedict and Kelley expression is:-

$$f = 0.0127 \log_{10} \left[\frac{3.17 \times 10^8 \, w}{\eta_S (U_1 - U_2) (U_1 + U_2)^2} \right]$$

η_S is centipoise at Tb.

In the absence of these expressions, Lane and Hughes (11) carrying out scuffing tests on the IAE $3\frac{1}{4}$-in gear rig derived

an empirical equation for scuffing load:-

Scuffing load in lbf = $N^{-2/3}$ $(1400\eta - 40\ T_b)$

where η = viscosity C.S. @ 140°F.

The relationship was derived from the Blok flash temperature equation and applied to the IAE gear specimen only. Blok (12) later converted these results to scuffing temperatures by assuming upper and lower values to the unknown quantities f and K in the flash temperature equation and produced a curve relating scuffing temperature to viscosity, with upper and lower limits.

De Gruchy and Harrison (13) reported the development of a disc machine for the study of scuffing. Although the disc machine had been widely used for examining material failures such as pitting and surface fatigue, little had previously been published concerning its use in scuffing tests. The load capacity obtained by De Gruchy and Harrison gave good correlation with the load capacity of the $3\frac{1}{4}$ inch centres gears of the IAE rig by matching the sliding speeds. O'Donoghue (14) however considered this to be quite fortunate as the results had been compared on a load capacity basis, with no reference to the blank temperature and apart from the sliding speed the discs did not represent the tooth-tip conditions of the IAE gears. O'Donoghue showed that the heat transfer coefficients of discs and gears where totally different. Discs tended to run at higher temperatures and therefore underestimated the load

capacity. For a true comparison between disc and gear machines it is necessary to calculate the scuffing temperature by summing the bulk operating temperature and the flash temperature in accordance with Blok's hypothesis. O'Donoghue converted the disc results of De Gruchy and Harrison and illustrated the near constancy of the scuffing temperature for a range of operating conditions.

Other investigators reported scuffing results for disc machines that supported the constant scuffing temperature concept. Meng (15) gave an account of tests in which each disc was of a different steel so that the contact acted as a thermocouple (the same method used by Blok in 1937) and found that over a whole range of speed, the contact temperature at which scuffing occurred was constant.

Genkin, Kuzmin, and Misharin (16) found that by measuring bulk temperature and friction and calculating the flash temperature rise, the scuffing temperature tended to rise with increasing rolling speed for one combination of steels and with another pair to fall.

Leach and Kelley (17) and Ali and Thomas (18) reported experimental results for scuffing of discs under varying conditions of sliding speed and operating temperature, recording the latter by thermocouples trailing on the disc surfaces. The scuffing temperature again was constant for a given oil for all conditions.

With so much evidence to suggest the constancy of scuffing temperature it is interesting to see how ratings of lubricants obtained from one machine and testing procedure compare with another. If the scuffing temperature concept is to be at all useful to the gear designer in predicting safe working loads, then there must be correlation of scuffing temperatures

obtained under the controlled conditions of the laboratory before the theory of scuffing can be extended to gears in service.

A comparison between the various "standard" gear test rigs has recently been reported by a sub-panel of the Institute of Petroleum (19). Whilst the IAE 3¼" gear rig is in general use in the United Kingdom, the Ryder gear rig is preferred by research workers in the U.S.A. On the continent however the FZG rig developed by Professor Niemann is in use by academic and industrial organisations. The work of the IP/IAE Gear Rig Tests Sub-Panel is primarily to develop the IAE gear rig and standardise the testing procedure. To achieve this, it was realised that the repeatability and reproducibility of the results had to be examined and a comparison made with the results obtained from other rigs. From the thirteen IAE gear rigs employed in the investigation (20) considerable scatter in the scuffing loads for various operating conditions was observed. A statistical analysis of the results showed poor repeatability and reproducibility of scuffing loads and indicated a significant rig and test condition effect.

A further statistical analysis was employed to compare the IAE scuffing loads with the Ryder scuffing loads (21). Correlation coefficients were determined as .007, .471, .685, and .214 with the disappointing conclusion that there was no significant correlation between the IAE and Ryder gear rig results. It is noticeable that all the data is compared on a scuffing load basis with little reference made to the operating temperature of the gears in each machine. Although the oil inlet temperature is recorded in the IAE rig precision tests, and the IAE/Ryder correlation experiments, this need not be representative of the bulk temperature as shown by O'Donoghue

(14) in his tests on the 6" centres disc machine. At low load, the discs and shafts cool the oil supply but when the load is increased, the blank temperature rises well above the oil supply temperature. An example given by O'Donoghue is reproduced in Figure 2.2 where the bulk temperature rises to 200°F prior to scuffing compared to a constant oil inlet temperature of 95°F. One of the conclusions of the IP/IAE gear rig sub-panel was the significant interaction of the test conditions and machines on the results. This could possibly result from the different operating temperatures encountered in the various machines which would then produce a variation in the flash temperature required to cause scuffing and give rise to the apparent scatter in the scuffing loads. Regarding the scatter in the IAE/Ryder correlation tests, Cameron in the discussion to Reference 21 pointed out the differences in the gear housings of the two machines. The Ryder gear was enclosed in a smaller housing which would most certainly lower its heat transfer coefficient and raise the operating temperature.

Fowle (22) realised the importance of blank temperature and took this into account when comparing results obtained from the IAE and FZG rigs for a range of HVI mineral oils. The Niemann and Ohlendorf formula for bulk tooth temperature (23) was used although it was realised later that direct measurement would have been more accurate. Scuffing temperatures were obtained by adopting the same procedure as Hughes and Waight (24) who found in their tests that at constant speed but varying oil inlet temperature and load, the scuffing temperature was constant if the coefficient of friction at scuffing was assumed to be constant. With the same assumption Fowle applied the flash temperature and blank temperature equations to scuffing load tests on one oil at the same speed but at two

different oil inlet temperatures. The solution of the simultaneous equation so formed provided the scuffing temperature and the coefficient of friction. In this manner, the results of the IAE and FZG rigs were reasonably well correlated by the constant scuffing temperature concept.

The past thirty years has seen the production of a great deal of scuffing data and the development of different techniques to support the postulate of Blok that there is a constant scuffing temperature for a given lubricant. Little effort however has been directed towards providing an explanation of why scuffing should occur at an apparently constant temperature. If scuffing is associated with a lubricant failure then the series of events leading to the failure of the contact when its temperature reaches the critical scuffing value needs investigation.

Even if an explanation is found and the need for lengthy gear and disc tests reduced, the assistance of this lubricant rating to a gear designer will be limited by his ability to predict the temperatures occurring in the particular application. The thermal behaviour of the oil film between the mating surface will most certainly play an important role in determining both the temperature rise in the contact and the heat dissipated to the gear material. Heat transfer coefficients have been shown to influence the bulk temperature so the designer would require a knowledge of the heat transfer characteristics of his installation and the resulting behaviour of the bulk operating temperature.

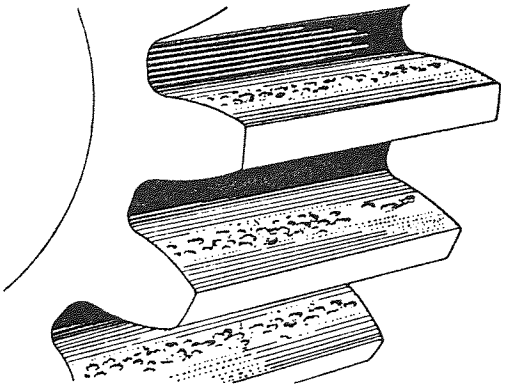

(a) Pitting

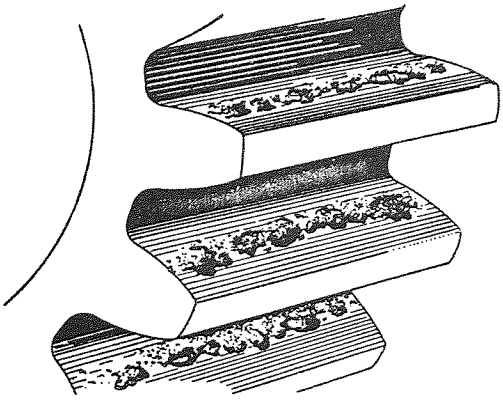

(b) Flaking

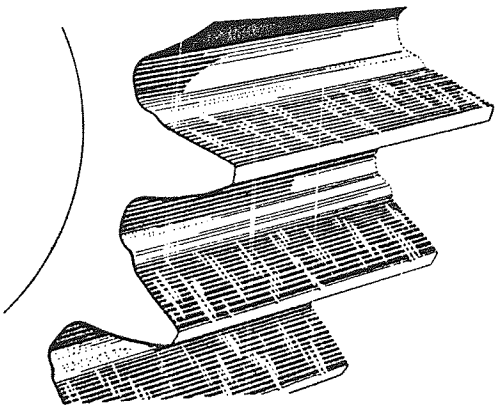

(c) Abrasion

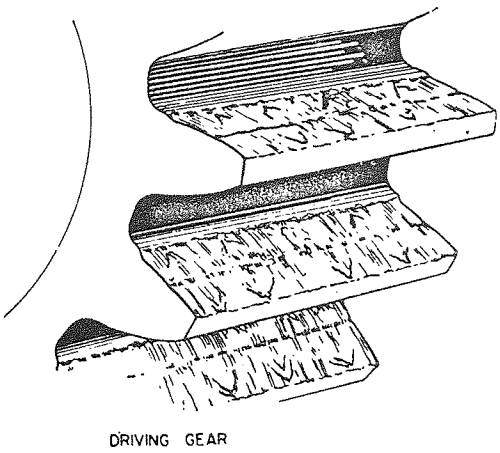

(d) Scuffing

Fig. 2.1. Types of Failure

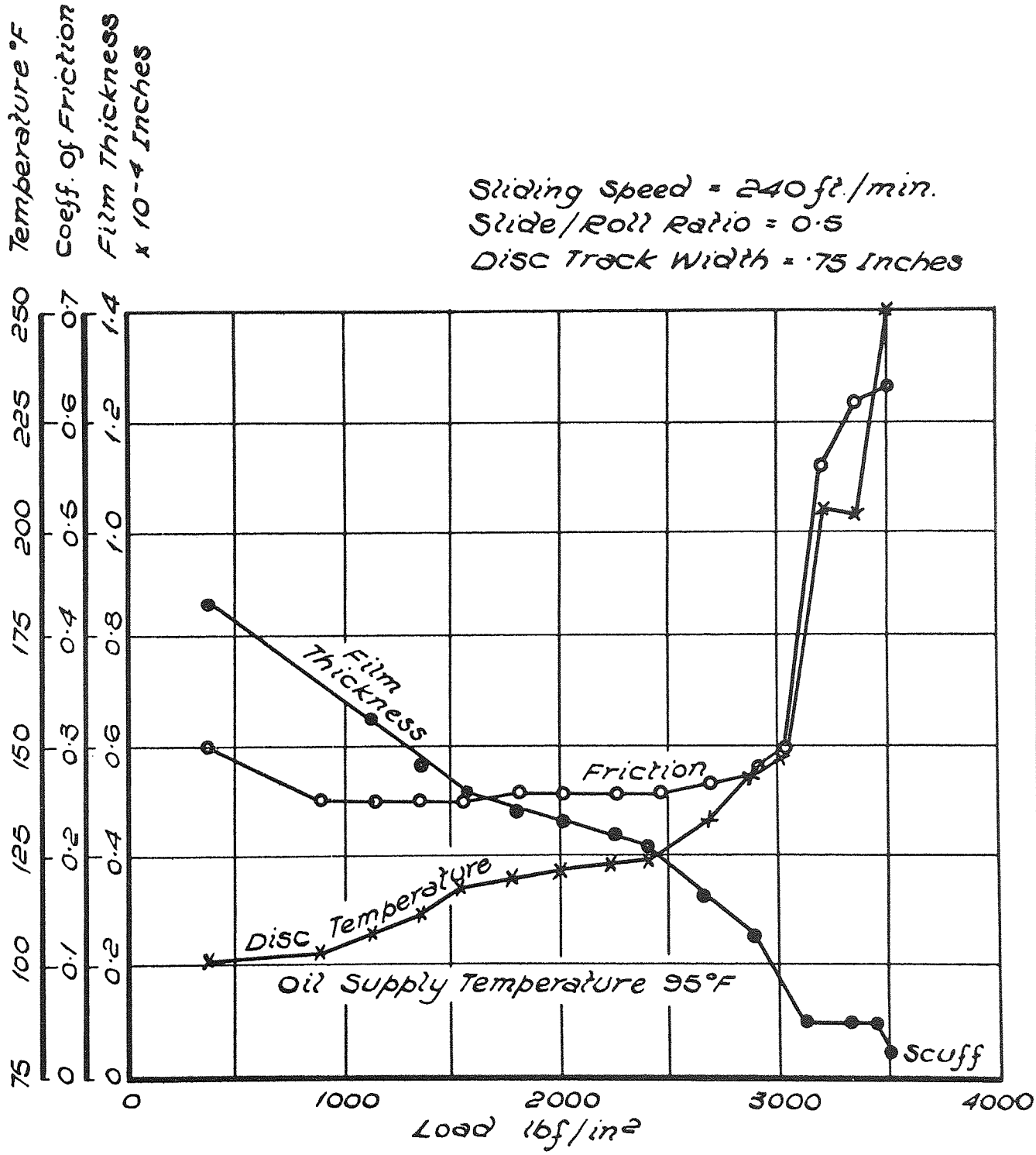

FIG. 2.2. SCUFFING TEST ON SIX-INCH CENTRES DISC MACHINE REPRODUCED FROM REF. (14) TO SHOW VARIATION OF DISC TEMPERATURE WITH LOAD.

3.0 THE MEASUREMENT OF CRITICAL TEMPERATURE

3.1 The Critical Temperature Hypothesis

It is thirty years since Blok presented his critical temperature hypothesis on the failure of lubricated rubbing surfaces. He defined the critical temperature as that temperature at which a lubricant loses its ability to lubricate the surfaces. The magnitude of load, speed, and coefficient of friction determined the peak temperature attained by the surfaces at the contact and if this temperature reached the critical value, direct contact between the rubbing surfaces was not prevented and scuffing resulted. Although the hypothesis referred to the boundary lubricated condition of rubbing surfaces, that is, where the lubricant was present on the surfaces but did not separate them by a hydrodynamic film, much evidence has been produced to support its application to the seizure of surfaces separated by a lubricant film, as shown in the previous section of this thesis.

The peak temperature attained by a lubricated rolling/sliding contact will consist of the operating temperature of the mechanical parts near to the contact zone, onto which is superimposed the momentary temperature rise of the surfaces in contact.

Simply,

$$T_t = T_b + T_f.$$

At Scuffing $T_t = T_c$

Blok (7) developed a general equation for the flash temperature at the contact between two surfaces moving at different velocities, by treating the contact area as a heat source, the intensity being a function of the dissipated frictional energy. The equation involves the mean coefficient of friction in the contact and, since this cannot in many cases be

conveniently assessed, unknown degrees of error can be introduced into the calculation. In most testing machines and gear applications the flash temperature forms the major part of the total contact temperature and there is a tendency to overlook the importance of the operating temperature, henceforth called the blank temperature. This has resulted in poor correlation between the scuffing temperatures calculated from conventional disc and gear machines (19 - 22).

Matveevsky (25) was the first to measure critical temperature directly as a property of the lubricant. He achieved this by operating a four ball machine at low load and speed, thus reducing the flash temperature component to a negligible part of the total contact temperature. The critical temperature was taken as the temperature to which the surrounding lubricant was heated to effect scuffing of the balls. A sketch of Matveevsky's KT2 machine is given in fig. 3.1(a). The top ball is rotated at 1 rev/min producing a sliding velocity of .4 mm/sec and the load is kept constant at 2 Kg, equivalent to a contact pressure of 200 $Kg/_{mm}2$ and the frictional force of rotation recorded. The technique consisted of bringing the apparatus to the desired temperature, running the test for one minute, and then stopping the machine. The balls were turned about or changed for new ones, the oil replaced, and the cycle repeated at a higher oil bath temperature. After each test, the diameter of the wear spots on the stationary lower balls were measured. At the critical temperature there was a sharp rise in friction accompanied by increased wear of the balls. Examples of the results obtained by Matveevsky are shown in fig. 3.1(b).

With this machine, Matveevsky was able to correlate most of the scuffing data obtained on various other types of machine, the only discrepancies occurring where low hardness

specimens had been employed. This lead Matveevsky to investigate the effect of specimen hardness on the measured critical temperature. The standard KT2 test employed hardened steel balls (normally chromium steel) but an adaption of the machine enabled the top ball to run against a washer on which a rubbing track on the inner rim had been formed; the arrangement had been justified earlier by comparison of results for steel. The material combinations tested and the critical temperatures obtained for these, over a range of contact pressures are given in fig. 3.2.

Matveevsky concluded that heavy plastic deformation was taking place at high loads in the relatively softer materials, displacing the lubricant from the contact zone as the surface metal was pushed aside in the deformation process and exposing underlying layers not yet covered by the lubricant. The condition where plastic deformation occurred at the asperities of the surfaces and failure of the lubricant was due to temperature effects alone, held for only a limited range of load. Beyond this there was a joint influence of temperature and plastic flow, and the measured critical temperatures were lower. This work showed that when determining critical temperatures by rubbing soft materials together, the pressure at the contact had to be chosen so that plastic deformation was not present.

From the low contact pressure results where the lubricant failure has been established as a thermal effect only, the critical temperature is seen to be dependent upon the material of the rubbing surfaces. The observation is in general agreement with the work of Bowden and Tabor (27) on boundary lubrication.

Referring to the hardened steel results of Matveevsky for a range of lubricants, Fein (28) pointed out the apparent increase in critical temperature with viscosity. Fein had found the converse to be true, that critical temperature

decreased with increased viscosity and from his extensive tests on disc and high-speed four-ball machine (29) observed that measurements tended to be a function of the investigator-machine combination as well as the lubricant-metal combination.

Fein (30) subsequently investigated the operating procedure effects on the measurement of critical temperatures and reported that the results depended upon the entire history of the test specimens and likened the effects to those experienced with extreme pressure additives. With extensive "running-in" the discs acquired a varnish-like film on their surfaces, specially prepared extracts of which indicated that they contained so-called "friction polymer" and iron oxides. Fein was convinced that these products of chemical reaction were responsible for the variation in the measured critical temperatures and that the procedure adopted by different investigators altered the specimen history and therefore the degree of interaction from the products of chemical reaction.

3.2 Lubricant Surface Films

In their work on boundary lubrication, Bowden and Tabor (27) show that when sliding metal surfaces are heated in the presence of a lubricant, a temperature is reached at which the adsorbed layer of lubricant softens. Areas of clean metal are exposed and a marked rise in friction and stick-slip motion is observed. The temperature at which this occurs depends on the material composition and the nature of the lubricant.

For straight chain paraffins and saturated fatty acids on steel surfaces, the coefficient of friction between sliding steel surfaces on the Bowden - Leben machine (31) reduced with increasing molecular chain length of lubricant. In this

apparatus the sliding speed was low and the pressure high, to ensure that conditions were well into the boundary lubrication region where the load is carried by contact of surface asperities and not by a hydrodynamic film. With increase in temperature however the friction rose sharply at temperatures between 40 to 50°C for the pureparaffins; the temperatures corresponding to their respective melting points.

The observations were explained on the basis of layers of molecules of the polar compounds physically adsorbed onto the surfaces. The transition temperature represented the melting point of these films at which the lateral adhesion between the molecules diminished. This then permitted increased metallic contact between surface asperities leading to increased friction and surface damage.

The behaviour of the fatty acids was however significantly different. The transition temperature from low to high friction occurred at temperatures very much higher than the bulk melting point of the fatty acid. The results are reproduced in Fig. 3.3.

It was discovered that with reactive metal surfaces, the fatty acids were reacting to form metal soaps and lubrication was effected not by the fatty acid itself but by adsorption of the metallic soap formed as a result of chemical reaction. Experiments with lauric acid showed that on unreactive surfaces such as nickel, chromium, platinum, silver and glass, the fatty acid was barely more effective as a boundary lubricant than paraffin oil itself. Applied to reactive surfaces like copper, cadmium, and zinc as a 1% solution of lauric acid in paraffin oil, the fatty acid provided a reduction in room temperature friction by 4 to 8 times. The metallic soap formed by introducing lauric acid into the lubricant for the copper

surfaces for instance, produced copper laurate as the metallic soap. By depositing this onto copper surfaces and non-reactive platinum surfaces, the same reduction in friction was obtained. Transition temperatures were also identical, occurring at the melting point of copper laurate.

There was, however, a marked difference between soap films produced on the surfaces by reaction between the fatty acid and the metal, and soap films deposited any other way. With soap films deposited on metal surfaces, in the presence of excess paraffin oil, breakdown could occur at a temperature lower than the melting point due to increased solubility of the soap in the liquid. On the other hand, soap films formed by chemical reaction at the interface between metal and liquid were firmly linked to the metal surface and even if covered in excess paraffin oil, lubricated up to the softening point.

Bowden and Tabor give an account of the examination of lubricant layers by electron beam diffraction reported by other investigators. It is found that for paraffins exceeding a certain chain length, the surface layers are arranged so that the carbon chains are normal to the solid surface. The structure remains unchanged whatever the thickness of the film. Fatty acids however, exhibit a well oriented first layer of molecules with layers on top of this monolayer taking the standard crystalline form of the fatty acid, with hydrocarbon chains inclined at an appreciable angle to the surface. The upper layers may be disturbed by rubbing with a degreased cloth, but the first monolayer remains unaffected, suggesting firm attachment to the surface. It has been suggested that when the orientation of the fatty acid on the metal substrate is very well defined, then it is likely that the chemical reaction has occurred at the surface with the formation of a soap.

By raising the temperatures of films deposited on non-reactive surfaces and viewing the diffraction pattern, the temperature at which the orientation of the monolayer disappears can be detected. Disorientation occurs at temperatures below the melting point of the acid and on heating to a temperature a little higher than the melting point, all the molecules are removed by evaporation. The temperatures at which the films on zinc, cadmium, and mild steel lose their orientation corresponds approximately to the melting point of the metallic soap formed by chemical reaction with the metal surface. This temperature corresponds very closely to that at which lubrication ceases to be effective, as will be seen by comparing the results shown in fig. 3.3(a) with those in fig. 3.3(b). With these metals it has been found very difficult to remove the molecules by evaporation, indicating that the soap film remains well adsorbed even after disorientation.

A further interesting result obtained by Tingle (32) concerns the effects of oxide layers on the chemical reactions between fatty acids and the substrate metal. The Bowden - Leben machine was adapted so that a cutting tool produced a smooth shallow track on the lower metal surface immediately before its passage under the loaded hemispherical slider. The cutting operation was performed under the applied lubricant of 1% solution lauric acid in paraffin oils so that fresh metal surfaces came into contact with the slider. The result was the complete absence of metal soap formation, detectable by the high order of friction recorded. This substantiated an earlier view that fatty acids would not react with an electropositive metal if metal oxide and oxygen were completely excluded.

It is interesting to see that here is further evidence

to support the findings of Matveevsky (26) regarding the lower critical temperatures measured when plastic flow of the metal surface is present. The remarks concerning the exposure of fresh metal surfaces within the contact are confirmed by the fact that the fresh metal will not have been in contact with oxygen or water and formed the necessary oxide film for the chemical reaction with the lubricant to take place. A lower critical temperature is therefore detected.

This comparison of course implies that the transition temperatures reported by Bowden and Tabor and other workers refer to the critical temperatures recorded by Matveevsky and furthermore to the scuffing temperatures obtained in disc and gear machines. In hydrodynamic lubrication as the load is increased and the speed of sliding reduced, the fluid film reduces in thickness and the number of surface asperity contacts increases. At the tips of these asperities the lubrication is of the boundary type described in the foregoing paragraphs, so that the amount of boundary lubrication increases whilst the hydrodynamic lubrication decreases. Whilst gears and discs seldom operate in the boundary lubrication region but develop a load carrying film of lubricant separating the surfaces, the conditions of Matveevsky's tests of low load and speed would certainly result in asperity contact. The critical temperatures measured by Matveevsky can be considered therefore to comply with the transition temperatures of the adsorbed layers of metal soaps on the surfaces, provided surface active compounds are present in the oils tested. Under fluid film conditions however the situation is not so clear. O'Donoghue (14) has put forward the suggestion that scuffing is a runaway process whereby chance contact occurs by debris passing through

the fluid film and bridging the distance between asperities. At the transition temperature of the surface films, there will be seizure between the surfaces which on subsequent passes of the damaged areas will cause further metallic contact, progressing eventually to severe welding and tearing of the surfaces.

Measurements of film thickness in gears by Ibrahim and Cameron (33) and later by O'Donoghue (14) have shown that a substantial film thickness is maintained up to the point of incipient scuffing where the blank temperature rises abruptly with a consequent reduction in film thickness. The failure of contacts separated by a fluid would therefore seem to depend upon the breakdown of the metal soap layer when the surfaces attain the transition temperature of the layer. The surfaces then continue their operation with a disoriented layer until such time as there is chance contact between asperities or with debris passing through the contact. The increase in friction then gives rise to a higher blank temperature which reduces the film thickness and increases the contact between asperities which are then at temperatures well in excess of the transition temperature. Failure by increased friction and scuffing then follows.

Work by Askwith, Cameron, and Crouch (34) showed that better lubrication was obtained by matching the chain length of the fatty acid to the carrier fluid. The results were obtained by recording scuffing load on the slow-running four-ball machine and the dwell-time on the disc and rider machine (i.e. the time to reach given value of friction).

Confirmation of the findings was later achieved on a Bowden-Leben machine (35) using stainless steel specimens, where a higher transition temperature was obtained by matching

the chain length of the fatty acid to the chain length of the paraffin oil to which it had been added.

Askwith, Cameron and Crouch (34) noticed a significant influence of boundary additive on the film thickness in the four ball tests. The method of measurement was by the voltage discharge technique (36) but calibration was not possible and the recordings were only comparative. The effect was further investigated by adopting the postulate that the molecules attached to the surfaces presented a surface film of much larger viscosity than the bulk fluid. Then, by setting up a simple squeeze film apparatus, it was possible to determine the viscosity distribution as the film thickness reduced. Details of the experimental method are given in the reference but briefly, it consisted of allowing an upper steel plate to fall a given distance onto a fixed bottom plate over which had been flooded the test fluid. By measuring the time taken for the plate to move successive 10^{-4} inch steps, the Stefan-Reynolds equation (37) could be used to derive the effective viscosity over that distance.

The equation is:-

$$\Delta t = \frac{3\pi R^4 \eta}{4w} \left(\frac{1}{h_1^2} - \frac{1}{h_2^2} \right)$$

where Δt is the time taken for the plate of radius R and weight w to move from film thickness h_2 to film thickness h_1.

The viscosity distribution so obtained for different acids in hexadecane are reproduced in fig. 3.4(a). The increase in surface viscosity is greatest when the additive and carrier are matched in chain length but the final separation of 3.5×10^{-4} inches was common to all fluids.

A more intensive study of these surface film effects is

given by Fuks (38). Using apparatus consisting primarily of two plane parallel discs, it was possible to measure the "thinning resistance" and the shear resistance of a liquid film.

In the thinning tests, Fuks found that a residual layer existed for each fluid-acid combination and that the layer could be further reduced by increasing the load between the discs. The results are shown in figure 3.4(b). The resistance to thinning however rose rapidly as the thickness diminished and the action was partially reversible. The loading - unloading curves suggested to Fuks that the thickness of the residual film was fixed by a combination of equilibrium and non-equilibrium forces. The first of these could be identified with the disjoining pressure between the molecules at the surface and the second was probably a plasticity effect. Fuks summarised his results as on Fig. 3.5(a).

The shear tests confirmed the results reported by Bowden and Tabor, that the shear resistance (or frictional force) reduced with increased chain length of fatty acid for a given contact load Fig. 3.5(b). Fuks' thinning resistance results had however shown that at constant load, the residual layer increased with acid molecule chainlength. Consequently by adjusting the load to give constant residual film thickness throughout the test, the shear resistance was found to be constant for all fatty acids Fig. 3.5(c). This lead directly to the conclusion that the increased lubricating action of fatty acids with higher molecular chainlength at constant contact load is due to the accompanying rise in the disjoining pressure and the increased gap between the rubbing surfaces. A further conclusion was drawn from the results of Fig. 3.5(c) which showed that although the shear resistance was not

affected by the length of the fatty acid molecule when the residual layer was kept constant, the effect of the base fluid became quite significant. The only explanation Fuks could offer was that the solvent molecules were located between the ends of the molecules oriented at the surface and reduced the interaction between them. The interaction was greater with benzene than with iso-octane, for instance, as shown in fig. 3.5(d).

It is interesting to compare the findings of Fuks with the theory of boundary lubrication proposed by Bowden and Tabor. Bowden and Tabor report a mono layer of molecules of the fatty acid at a surface, or if the surface is reactive, a layer of metal soap molecules. Now, stearic acid has a molecular length of 21.4 A^{o} (= .00214 microns) and so one would expect the thickness of the film to be of this order. Fuks shows that the surface films are considerably larger than this, suggesting multi-molecular residual layers with the solvent molecules interfering in the orientation of the outer-attached acid molecules. The residual film thickness is dependent on the load applied and the nature of the solvent-acid combination. Reference to the residual film results of Fuks shows how stearic acid performs in different fluids at different contact loads. The residual film varying in thickness from .11 to .36 microns compared to the molecular length of .00214 microns.

Figure 3.4(b) may be replotted to compare with the similar results given by Askwith, Cameron and Crouch. Fuks reduced the Stefan-Reynolds equation to

$$t = \frac{c}{h^2}$$

where c is a constant, by abandoning the postulate of variable

viscosity. Taking h_2 to be much greater than h_1 and therefore $\frac{1}{h_2^2}$ to be negligible, and R, W, and η to be constant for any test, the results could be plotted according to this reduced form of the equation as in fig. 3.4(b).

Reading off values of h at small increments in time, we may resubstitute into the original equation together with the values of R and W and obtain the variation in viscosity with film thickness. The results for two of Fuks examples are shown in fig. 3.6. It is seen that the results of Askwith et al do not go far enough. For some reason, possibly due to the presence of extraneous matter or alignment difficulties. (The apparatus was very simple and parallel approach of the plates relied on simultaneous removal of two strips on which the plate was supported.) the film thickness stops at 3.4 x 10^{-4} inches, without the infinite rise in viscosity that must be present to establish a residual film. Although reference has been made to the "plastic" layer of Fuks, the thickness is well above that determined by Fuks.

As a final note it is worth mentioning the effect of temperature on residual films observed by Fuks. A softening of the layer was experienced at about 10°C below the respective melting points but the layer could not be removed altogether below 100°C. This would seem to be in agreement with the observations made by electron diffraction on platinum surfaces, where disorientation of the mono molecular layer occurred at 10°C below the melting point of the acid. It required heating to 40°C above the melting point to remove the molecules completely. It is conceivable therefore that the residual films persisting on the surfaces at temperature of 100°C are layers of metal soap molecules some 50 - 200 rows deep and will

require heating to the melting point of the metal soap before removal.

3.3 The mechanism of Scuffing

With the vast amount of evidence to suggest that the critical temperature at which gears and discs scuff is a similar mechanism to the transition temperature of fatty acids adsorbed to metal surfaces, the question is to first determine whether such polar compounds exist in mineral-oils and whether the transition temperatures can be as high as is suggested by the critical temperature tests, usually in the region 150 - 200°C.

Bowden and Tabor give transition temperatures for pure paraffins in the region of 40 - 50°C and with stearic acid on steel, the transition temperature of 140°C has been obtained. However Frewing (39) has shown that solutions of 1% stearic acid in white oil exhibit stick-slip motion at 55°C.

Working on the Bowden-Leben machine, Frewing found that transition temperatures of white oil containing different additives could be correlated on the Von't Hoff isochore. This consisted of plotting log concentration against the reciprocal of the absolute temperature and straight lines were obtained, the slope of which gave the heat of adsorption. He found the heat of adsorption for the straight chain acids to be constant and equal to 13500 cal/mole.

O'Donoghue and Cameron (40) extended the concept to consider the findings of Groszek and Palmer (41). The basic thermodynamic equations were as derived in standard text books on physical chemistry (42).

The Gibbs free energy equation is:-

$$\Delta G = \Delta H - T\Delta S$$

where ΔG is the change in the Gibbs free energy,

ΔH the change in enthalpy, ΔS the change in entropy, and T the absolute temperature.

For equilibrium between the adsorption of polar molecules onto the surface and back again, the equilibrium constant is:-

$$K = \frac{\text{(covered surface sites)}}{\text{(clean sites) x (polar molecules in solution)}}$$

For a system obeying a Langmuir isotherm

$$K = \frac{\alpha}{1-\alpha} \cdot \frac{1}{C}.$$

where $\alpha/1-\alpha$ is the ratio of covered sites to clean sites. C denotes the concentration. The standard free energy change is $\Delta G^{o} = -RT \log_e K$

$$\therefore \; -\frac{\Delta H^{o}}{T} + \Delta S^{o} = R\left(\log_e \frac{\alpha}{1-\alpha} - \log_e C\right)$$

Following Frewing's assumption that transition occurred when a definite fraction α_t of sites are covered and also that ΔS^{o} and ΔH^{o} are not greatly influenced by temperature, O'Donoghue and Cameron put $\alpha = \frac{1}{2}$ from the results of referenced work.

$$\therefore \; \Delta S^{o} = \frac{\Delta H^{o}}{T} - R \log_e C$$

Substituting Frewing's values for heat of adsorption of acids (- 13,500 cal/mole, the minus sign indicating the process to be exothermic), it was possible to find the standard entropy change ΔS^{o}. The gas constant R is 2 cal/mole and T is the absolute temperature of transition. The concentration C is given as (10% wt/wt) per mol.wt, taking the standard state

for the free solute as 1 mole per 1000 gram of solvent.

The results are given below.

Acid	Mol. Wt.	$-\Delta S^{o}$ cal/mole
Capric C_{10}	172	43.3
Myristic C_{14}	228	37.6
Stearic C_{18}	284	34.5

Groszek and Palmer found that nominally neutral mineral oils had a much larger fraction of active material than commonly supposed. Averaged over eight samples of SAE 50 oil, 0.4 per cent wt/wt of acidic material was detected of comparatively high molecular weight (about 1000).

O'Donoghue and Cameron showed that assuming the compounds to have the same heats of adsorption as the other acids, a value for $-\Delta S^{o}$ of 22.2 cal/mole was required to give a transition temperature of 150°C. By plotting $-\Delta S^{o}$ against molecular weight for the acids already tabulated, the value of 22 cal/mole fell quite reasonably on an extrapolation of the graph, at the molecular weight of the active material.

Grew and Cameron (35) recently reported that they had dissolved the surface active material isolated by Groszek and Palmer into three solvents and plotted the $\log_{10}$ concentration - reciprocal transition temperature curves and obtained transition temperatures in the range 120 - 180°C, Fig. 3.7.

These results give support to the suggestion that the critical temperatures experienced by lubricated systems such as gears are identifiable with the transition temperatures of the adsorbed layers of polar compounds. The knowledge that now exists about the action of these molecular layers will

assist in the further investigation of failure by scuffing of lubricated rolling/sliding contacts.

3.4 The development of a disc machine for direct measurement of critical temperatures of lubricants

This section presents details of the construction and development of a machine for direct measurement of critical temperatures. The basic principles of operation are the same as those of Matveevsky's four ball machine but replace the point contact by the line contact of two discs.

Much greater accuracy in the determination of critical temperatures can be achieved by maintaining a small flash temperature and providing an accurate method of controlling the blank temperature. The error involved in calculating the flash temperature, arising from the assumptions concerning the contact conditions, is reduced to a small percentage of the total contact temperature.

Fig. 3.8 shows the two-disc machine, in which these conditions have been obtained. The 2.5 inch diameter discs were arranged to rotate totally immersed in a bath of the lubricant to be tested. They were lightly loaded through the lever mechanism shown in more detail in fig. 3.9 and geared to rotate at low speed in the same direction. This produced one hundred per cent sliding at the contact with a negligible amount of hydrodynamic effect. The temperature of the oil bath was controlled by the power supply to a 1 KW emersion heater and recorded continuously by a copper-constantan thermocouple. A stirrerensured even distribution of temperature during the heating cycle, and so the recorded oil temperature could be taken as the blank temperature of the discs.

The driving torque from a $\frac{1}{4}$ HP, 3-phase motor fitted with a Kopp variator and through a 2 : 1 reduction belt drive was measured by a torque tube that had been previously calibrated. The amplified signal from the torque tube was displayed on the same chart as the temperature trace so that the friction at any temperature in the heating cycle could be read directly. The true contact temperature at any instant was obtained by calculating the flash temperature for the known load, speed, and friction and adding this to the recorded blank temperature. This was seldom more than a few degrees and in effect represented a correction term to the measured temperature. With this apparatus it would be possible to detect a sudden rise in friction when the critical temperature of the lubricant was reached.

Preliminary tests showed that with hardened steel S.106 discs, no increase in friction could be obtained with temperatures up to 230°C, the maximum attainable by the apparatus. At this time, Grew and Cameron (35) reported a similar experience with their four-ball machine and pointed-out the need to use stainless steel specimens in this type of test. It was also noted that Matveevsky had used chromium steel in his investigations. On changing to stainless steel discs (18% Cr. 8% Ni) a sudden increase in coefficient of friction from about .18 to .50 was detected at temperatures between 180 and 200°C, depending on the lubricant. Typical traces are given in figs. 3.10, 3.11, and 3.12. It may be reasoned that at the sustained high temperatures experienced by this machine, chemical reactions may have modified the S106 disc surfaces. Inspection of the discs showed a discolouration to be present with a lacquer-like texture. Similar effects were later observed by Fein (28) as stated earlier, and his findings give support to this

explanation for the absence of transition with hardened steel discs. Using stainless steel specimens the chemical reactions presumably do not occur. With conventional gear test machines, and in practical applications the peak temperature is reached only for the instant of time the surfaces pass through the contact and this is insufficient for the chemical reactions to take place. Thus, when the lubricant film breaks down and metal to metal contact occurs there is no protective film on the surfaces to prevent scuffing.

The mean traces for the S.106 and the stainless steel discs are compared in fig. 3.13. In all subsequent tests, stainless steel discs were used and replaced after each test by new ones that had been previously washed in benzene. The surface finish of the discs was approximately 15μ-inches CLA. A running-in procedure was adopted at 5 rev/min at 2 lbf load for 15 minutes to remove high spots and flashes after machining. The tests were then conducted at a speed of 26 rev/min and 5 lbf load. These conditions were determined as the most suitable for obtaining a clear friction trace but the effects of running at other combinations of load and speed are shown on fig. 3.14 where the repeatability of the critical temperature reading is quite evident, once the necessary correction for flash temperature has been made. A sample calculation of the critical temperature is given in Appendix II.

At the onset of friction rise, the scuffing was quite audible and it was found that the friction rise could be arrested at any point by maintaining a particular temperature. Further heating resulted in a continuation of the friction rise to the maximum after which, on cooling, the process could be reversed. The blank temperature at which the decrease in

friction commenced was lower than the corresponding increasing friction temperature. This sequence is shown in the sketch on fig. 3.15.

3.5 Critical temperature results for a range of nominally plain mineral oils

A range of plain mineral oils were rated on the critical temperature machine described above and there emerged an apparent dependence of critical temperature on viscosity. The viscosities of the four lubricants are given in Appendix I, and the mean critical temperature traces in fig. 3.16. On the I.A.E. gear machine Blok (12) obtained confidence limits for critical temperature which increased with viscosity. Redrawing this chart and adding the results of de Gruchy and Harrison (13), O'Donoghue and Cameron (40), Shipley (3), Matveevsky (26), Fein (29), Leach and Kelley (17), Meng (15), Ghenkin et al (16), Ali and Thomas (18), and the results of these tests, the general rise is still evident but the limits require to be increased, Fig. 3.17. The result is that, as pointed out by Fein (28), critical temperature may reduce with viscosity for one range of oils but increase with viscosity for another. It is much more convenient to consider critical temperature as an additional property of the lubricant depending upon the nature of the surface active compounds, the surface in contact with the lubricant, and the base fluid itself. This is far less misleading than attempting to relate critical temperature to the viscous properties of the lubricant.

3.6 Critical temperatures measured for oils used by Ali and Thomas (18)

Having established the characteristics of the two-disc

machine in measuring critical temperatures, it is important to determine the accuracy of the results in predicting scuffing. For the purposes of this investigation, Ali and Thomas were able to supply samples of oils 'B' and 'C' used in their extensive disc machine tests. The results are replotted in fig. 3.18, superimposed with the two critical temperatures measured on the two-disc critical temperature machine. Good agreement with the calculated scuffing temperatures is achieved.

3.7 The gear machine

The Thornton gear tester used in this work was that used by Ibrahim and Cameron (33) and later by O'Donoghue (14). A photograph of the machine and a schematic layout of the loading system are given in figs. 3.19 and 3.20 respectively.

The drive is supplied by a 5 HP, 3 phase, synchronous motor running at 1470 rev/min and fitted with a Kopp variator to give a speed range of 200 - 1800 rev/min. The output shaft is coupled to one shaft of the slave gear box that houses the power-return gears. The slave gear box is supported in the lever arm and suspends between two support blocks which are bolted to the frame of the machine. This allows the complete assembly of slave gear box, lever arm, 0 - 600 lbf spring balance, and balance weight, to pivot about the drive shaft. An extension of the drive shaft couples with one of the shafts of the second gear box, this one housing the test gears and being firmly bolted to the machine frame. The remaining two gears are connected by a Hardy Spicer telescopic shaft with universal joints. These joints permit the lever arm and the power return gearbox to rotate about the main shaft pivot in the support blocks. The machine is loaded by applying a load

to the end of the lever arm by means of the handwheel connected to the springbalance. This tends to rotate the power return gear box, but the test gears restrain the slave gears from any motion other than taking up the backlash and tooth deflection. The two shafts therefore carry a torque that is supplied by the lever arm and not by the drive shaft. When the gears are rotated, the "locked-in" torque causes the test gears to effectively carry a load, but the power transmitted by them is returned by the power-return gears, so that the motor has only to supply the friction losses. The machine is therefore capable of simulating very high loading conditions, but only requires a relatively small driving motor.

Replacement of the test gears is a lengthy procedure owing to the necessity for dismantling the circulating shafts. In scuffing tests this can occupy a considerable amount of the total testing time. The test gears are consequently manufactured with the working faces divided into two by a central groove. Four tests are then possible from the same set of gears. The face width of each gear is 0.437 inches whilst that of the slave gears is 2 inches. The test gears are subjected therefore to a higher load per inch width than the slave gears and may be subjected to failure loads without risk to the permanently installed slave gears. The slave gears are supplied with E.P. 90 transmission oil applied by splash and jet. The test gears were separately lubricated with the test lubricants applied by a jet directed towards the entry zone of the meshing gears. The oil inlet and outlet temperatures were measured by mercury-in-glass thermometers. The test gear blank temperature was measured by the method to be described in section 3.9 of this thesis.

The test gears were made from EN 32 plain free cutting carbon steel case hardened to a depth of .025 inches (750 V.P.N.). The gear forms conform to BS. 436 : 1940 with a tip relief of 0.6×10^{-3} inches the surface finish was about 15μ inches CLA. Full details of the gears are given in Appendix III.

3.8 The Disc Machine

In reviewing the published work on scuffing, attention was drawn to the fact that disc machines could be used to simulate the contact conditions of gear teeth. Reference to fig. 3.21 will show how the kinematic conditions of the rolling and sliding of gear teeth in mesh can be represented by two discs. A different pair of discs are required for simulation of each point along the contact path of the gears. The advantages of using a disc machine are:-

(i) The disc specimens can be manufactured accurately, using standard equipment. With gears the precision required to eliminate profile and spacing errors make testing a costly and timely procedure.

(ii) Instrumentation is aided considerably, with any instant of engagement along the contact path easily studied under steady-state conditions.

Unfortunately, the dynamic effects encountered in gear teeth where the radii of contact are continually changing and the sliding/rolling speeds are varying are not reproduced. With the differences in heat transfer and energy dissipation between discs and gears it is important to take account of the blank temperatures when measuring scuffing loads.

Several types of disc machine have been constructed by

the Oil Industry and Gear Manufacturers, details of which are given in the literature on scuffing.

The disc machine used in this investigation was the standard Amsler Wear Machine with a fixed 10% difference in speed of rotation between the two shafts. With discs of equal diameter, the slide/roll ratio is fixed at this, and so combinations of differing diameters have to be selected to give other sliding speeds. A photograph of the machine and a schematic layout of the discs are given in figs. 3.22 and 3.23 respectively.

The machine is driven by a $\frac{1}{4}$ HP two speed motor equipped with a variator giving a speed range of 60 to 500 rev/min. The lower disc is driven by an epicyclic gear train and the friction torque obtained by observing the deflection of a pendulum attached to the planet gear shaft. Torques of 0 - 100 Kg. cm could be read from a graduated scale or recorded on a rotating drum. The upper disc was driven through a back-shaft geared to rotate at the reduced speed. There is also provision for reversing the direction of rotation of the upper disc. A load of 0 - 200 Kg is applied to the discs by a calibrated spring attachable to the loading bracket carrying the upper disc.

The machine is designed principally for wear studies and the loads and speeds are insufficient for conducting scuffing tests. The machine was consequently operated with the reverse gear engaged to produce a higher flash temperature component. The oil tank was modified by attaching a heating element beneath the oil container. The discs rotate with one lower half dipping into the lubricant. The blank temperature could consequently be adjusted to any desirable value and the test

carried out at increasing load and speed until scuffing occurred. Measurement of blank temperature was achieved by the method described in the following section. The disc specimens were 5.71 cms in diameter and 1 cm wide.

3.9 Surface Thermocouples

In both the Thornton gear tester and the Amsler Wear Machine the total temperature of contact was derived by addition of the calculated flash temperature to the measured blank temperature.

Two methods of blank temperature measurement are available for the disc machine. These consist of either thermocouples trailing on the working surfaces of the discs or a thermocouple embedded in one of the surfaces. Blank temperature measurement in gears necessitates the use of an embedded thermocouple or some thermocouple attached to the surface and rotating with the gear, the output being transmitted via a slip-ring assembly.

3.9.1 The Embedded Thermocouple

The embedded thermocouple used in the gear tests was of the type used by O'Donoghue and Cameron (40). With extreme care in the assembly of these thermocouples, high response times are possible and measurement of rapid changes in temperatures, such as the flash temperature at the contact between gear teeth can be detected. In this instance however very high response times were not required as it was the intention to record operating blank temperatures only. The thermocouples could be located at the working faces of the gear teeth without interfering with the engagement of the tooth flanks.

The finish ground gear is electro-spark machined to give

a hole .012 inches in diameter, penetrating from the side of the gear to the desired position on the surface. The positions chosen were at the tooth tip, the pitch point, and in the root of the gear. Into the hole is inserted a 0.010 inch external diameter stainless steel tube, the end of which is shaped to the contour of the tooth face. It was found in practice that the needle must be insulated from the gear by epoxy resin in order to prevent noise pick up on the thermocouple output. An enamelled constantan wire is next placed into the tube and secured by epoxy resin. The protuding wire is then smoothed down to conform to the surface profile. At this stage the thermocouple appears as shown in fig. 3.24(a).

The next part of the procedure has been developed by Davies and Forrester (44) from experience in a number of applications. The thermocouple tip and a small surrounding area of the surface are lightly recessed with a very localised sand blast. The roughened surface is then etched for 5 seconds in a solution of concentrated nitric acid (20 ml), ferric chloride (5 gm), concentrated hydrochloric acid (200 ml), cuprous chloride (5 gm) and water (200 ml). To assist subsequent plating, a copper rod, cleaned in a solution of 35% ammonia (50 cc) and 100 volumes of hydrogen peroxide (200 cc), is rubbed over the rough surface. The surface is then rapidly rinsed with acetone and a small etectroplating cell is formed by placing a short length of soft $\frac{1}{4}$" bore plastic tube filled with commercial cyanide plating solution on the surface. A plating current of 30 mA/cm^2 is then passed and the solution agitated by an air stream blown through a very thin glass capillary to prevent the evolved gas surrounding the plating electrode. This produces copper plating 0.001 inch in thickness

which may then be reduced in thickness by smoothing down with emery to blend into the surface and so increase the time response of the thermocouple junction. Leads from the constantan wire and the stainless steel tube were then taken to an IDM slip ring assembly, consisting of silver rings with silver brushes. Figure 3.24(b) shows the general arrangement of the coaxial thermocouple described above.

3.9.2 The Trailing Thermocouple

For simplicity in the Amsler disc machine tests, a thermocouple of the trailing type was used. The thermocouple junction is mounted on the end of a leaf spring fixed to the frame of the machine and is loaded against the disc surface. This type of thermocouple is reported elsewhere (17) (14). Leach and Kelley (17) found that recorded temperatures were lower than the actual surface temperature when oil supply temperatures were below 180^{o}F. This was attributed to the influence of the thermal separation of the thermocouple probe and the disc at the higher viscosities and large temperature gradients throughout the thermocouple junction. The relationship reproduced in fig. 3.25(a) was not affected by speed.

O'Donoghue (14) further demonstrated the influence of spring load on the recorded temperatures. Higher loads produced frictional heating at the junction and correct thermocouple readings were only obtained when the tendency to read lower than the surface temperature was counteracted by the frictional heat.

A comparison between the findings of O'Donoghue and Leach and Kelley shows that the position of the thermocouple relative to the oil supply affects the recorded temperature.

The disc experiments of O'Donoghue were carried out with the thermocouple making contact with the upper disc of the Amsler machine near the inlet to the contact. From the experience in running the same machine during the work for this thesis it was observed that in placing the thermocouple in this position only a thin film of lubricant was present on the surface in contact with the thermocouple junction, once the discs had completed a few revolutions. The oil was being carried to the contact zone by the lower disc from the oil bath into which it was dipping and only part of the oil passing through the contact was being carried away by the upper disc. This oil would attain the surface temperature of the disc before passing the thermocouple and re-entering the contact.

In reference (17) however the thermocouples were placed at the inlet to the contact but the surfaces had already been coated by the fresh lubricant from the supply jet at the outlet of the contact zone. The thermocouples were consequently flooded in fresh oil and when the oil supply temperature was considerably lower than the disc surface temperatures, the trailing thermocouples would register a mean value of the two temperatures. Only a small percentage of the oil enters the contact and this will consist of the oil adjacent to the metal surface. It is therefore essential to record the true surface temperature and the thermocouple arrangement proposed by O'Donoghue is to be preferred.

3.10 Scuffing results on the gear and disc machine

Scuffing tests to assess the accuracy of the critical temperature machine were conducted on the Thornton gear tester and the modified Amsler machine. Since time would not allow

extensive scuffing tests on the full range of oils under a range of various operating conditions, it was decided to obtain as many results as possible for the SAE 30 plain mineral oil. The results are shown in fig. 3.26 together with the test details.

Both gear and disc results exhibit the scatter usually associated with these conventional scuffing tests. The Amsler test gives a direct reading of the coefficient of friction at the contact whereas the Benedict and Kelley formula had to be used to give the coefficient of friction at the tip of the 5" gears. The low order of flash temperature in the Amsler machine necessitated higher than normal blank temperatures which although attaining 120°C in one case did not produce the same modification of the metal surfaces as had been experienced in the critical temperature machine.

The scuffing temperatures so obtained agree with the directly measured critical temperatures using stainless steel specimens, which would consequently provide a reasonable value on which to base design against scuffing. Within the limits of experimental accuracy it is a further observation that there is little variation of critical temperature with steel specification (details given in Appendix IV).

3.11 Discussion of Critical Temperature results

From the comparison of the scuffing temperatures obtained on the conventional disc and gear machine with critical temperatures measured on the two-disc machine, the use of stainless steel specimens appears to be justified.

In view of the findings of Bowden and Tabor concerning the importance of the metal surfaces as well as the lubricant

in determining the transition temperatures of adsorbed films, the chromium content of the metal might be expected to interact in the chemical reactions between the surface active compounds and the steel. The experimental results however do not indicate that any significant interaction is occurring.

One consideration however is the effect of plastic deformation of softer materials on the critical temperatures measured, as shown by Matveevsky. The stainless steel from which the discs were manufactured for the critical temperature machine is considerably softer than the hardened steels used in the gear and disc tests. The loads and speeds are however quite low. A contact pressure of only 90 Kg/cm^2 is produced between the discs. This compares favourably with the maximum allowable stress of 12500 Kg/cm^2 for mild steel on mild steel; 250 Kg/cm^2 for hard steel on copper; and 40 Kg/cm^2 for copper on copper. These figures were determined by Matveevsky as the stress below which there would be little plastic deformation of the contacting surfaces. The measured critical temperatures would consequently not be affected by the hardness of the material. With the agreement between the stainless steel and hardened steel results and the low order of the contact pressure, the method appears to produce valid results of critical temperatures of lubricants.

The time taken for each test is about one hour, which is somewhat longer than a four-ball test but much shorter than a conventional gear or disc machine test. The simplicity of the apparatus, the test specimens, and the procedure make the proposed technique ideal for the industrial rating of oils.

If scuffing is to be taken as a function of the critical temperature of the lubricant in contact with the materials of the contacting surfaces, the lubricant should be rated on

this temperature rather than on load capacity for a particular application. Providing an engineer is able to assess the temperatures attained at the contact between the surfaces of the machine element, then design against scuffing should be possible provided critical temperature ratings of oils are available. Calculation of the temperature generated in a contact will depend on a knowledge of the heat generation in the lubricant film separating the contacting surfaces and the way in which this heat is dissipated to the surroundings from the machine surfaces.

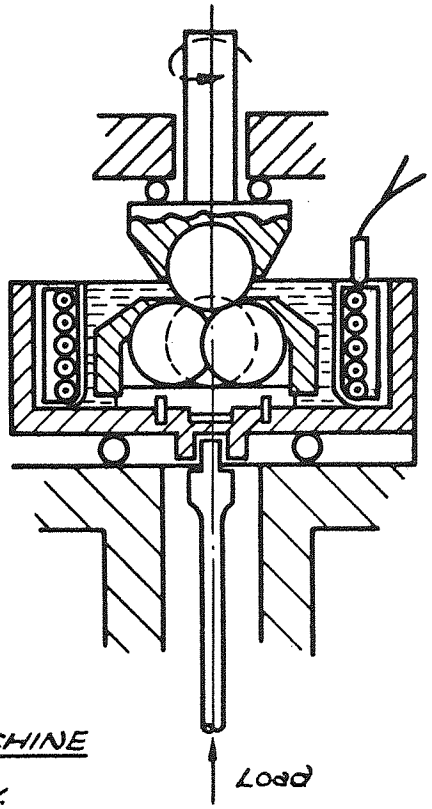

FIG. 3.1.(a)
FOUR BALL KT-2 MACHINE
USED BY MATVEEVSKY.

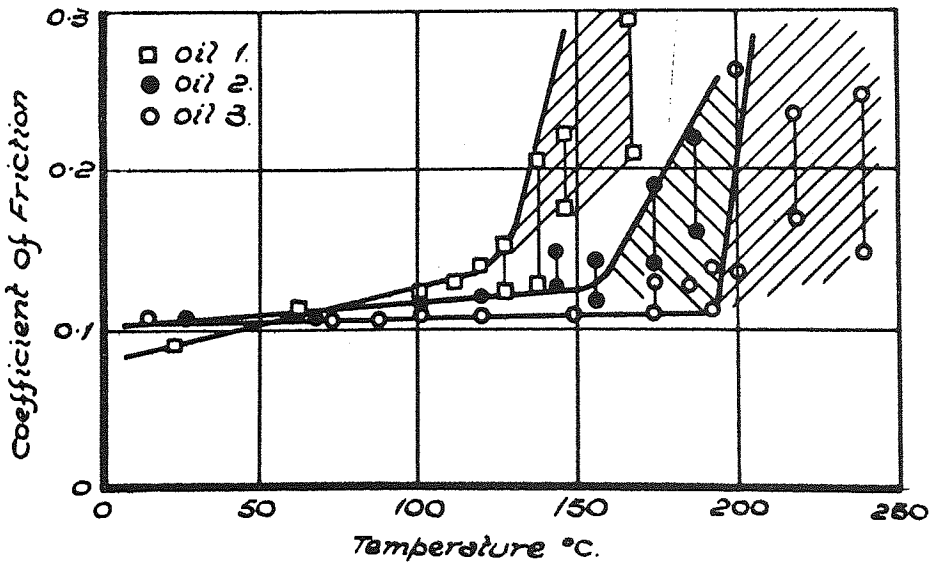

FIG.3.1.(b) FRICTION AS FUNCTION OF TEMPERATURE FOR MINERAL OILS OBTAINED BY MATVEEVSKY (25) ON KT-2 MACHINE.

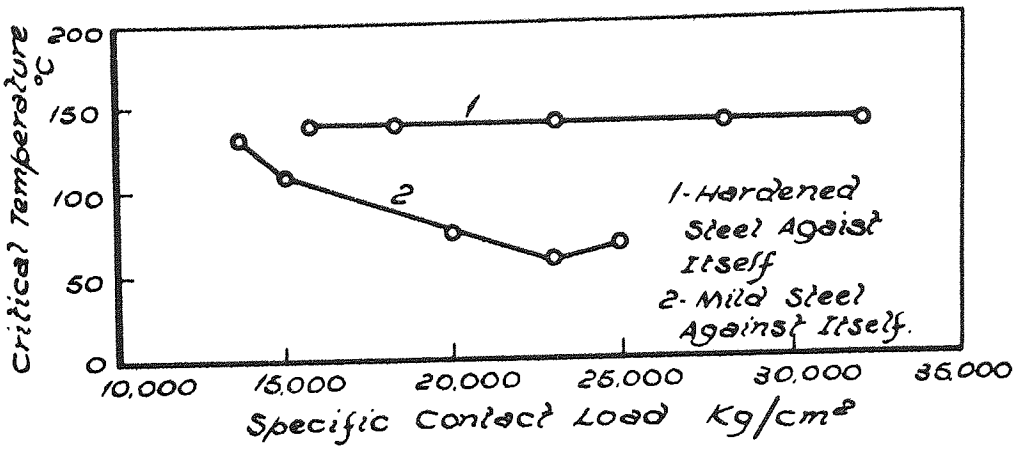

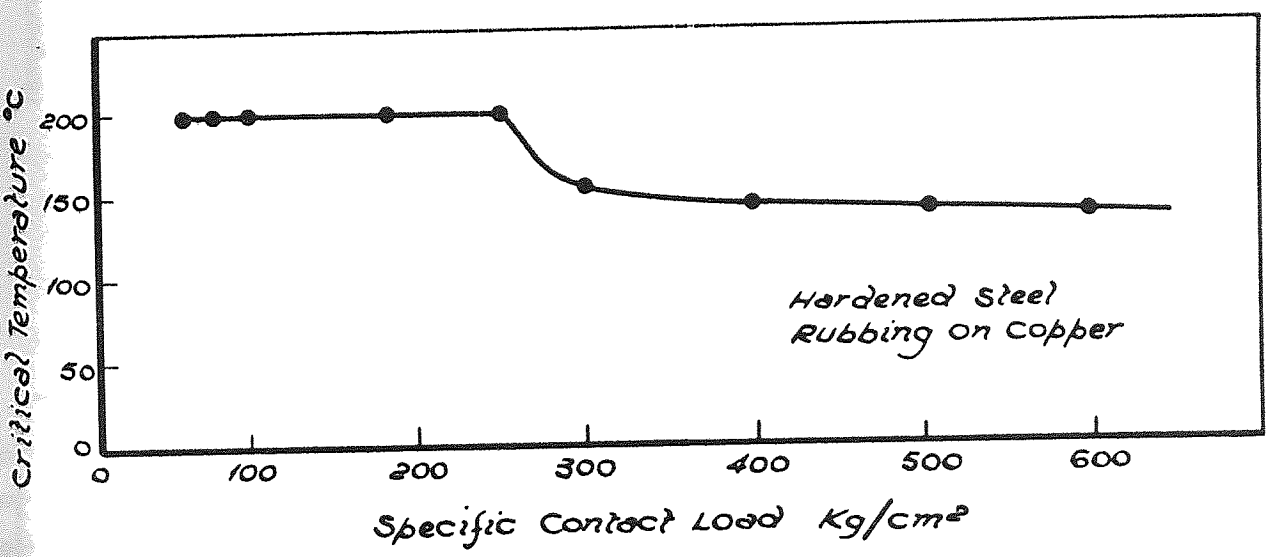

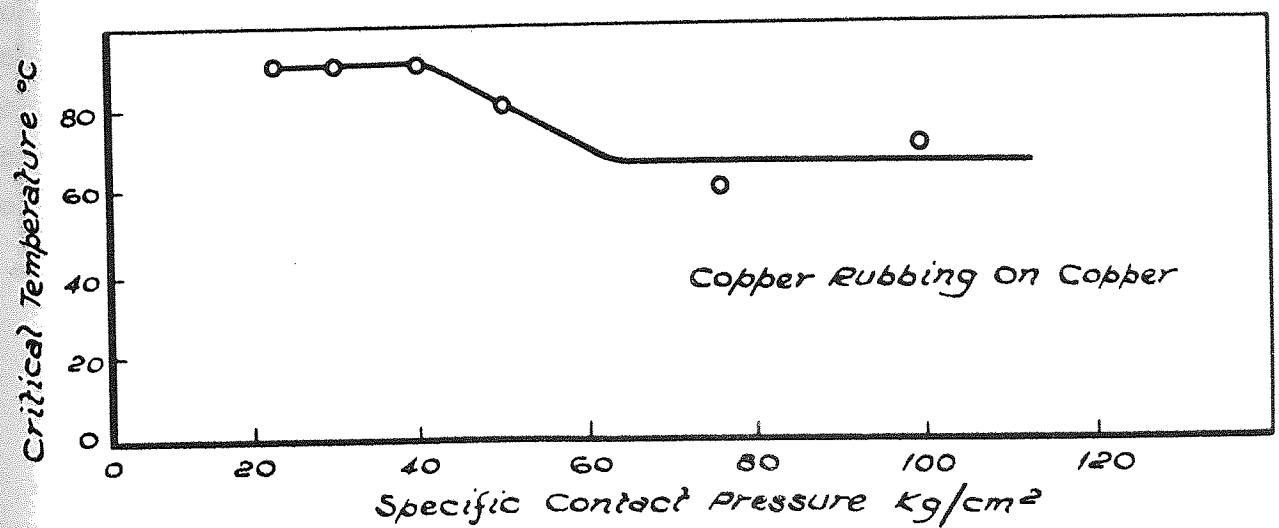

FIG. 3.2. CRITICAL TEMPERATURE AS FUNCTION OF CONTACT PRESSURE FOR VASELINE OIL CONTAINING 0·1 % STEARIC ACID FOR DIFFERENT MATERIAL COMBINATIONS AS OBTAINED BY MATVEEVSKY.

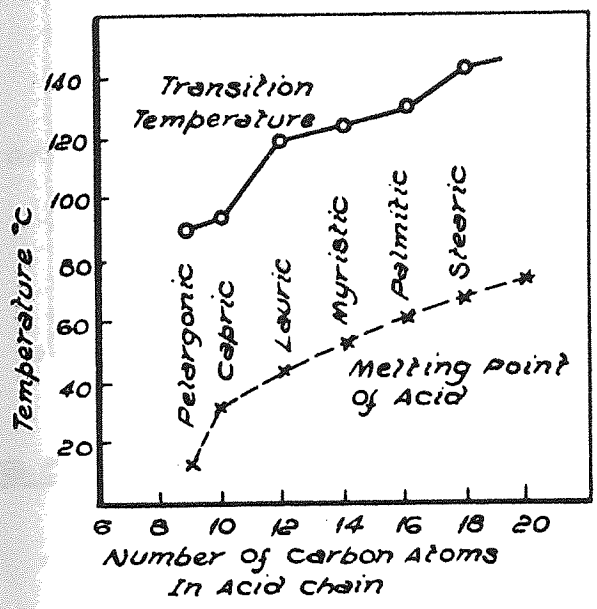

FIG. 3.3.(a) BREAKDOWN OR TRANSITION TEMPERATURE OF FATTY ACIDS ON STEEL SURFACES AS A FUNCTION OF CHAIN LENGTH FROM FRICTION TESTS ON BOWDEN-LEBEN MACHINE, REF. (27)

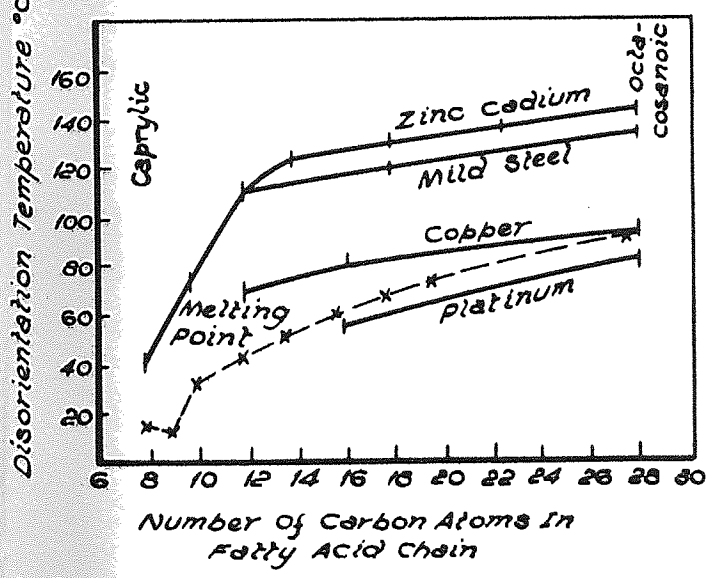

FIG 3.3(b) DISORIENTATION TEMPERATURES OF FATTY ACIDS FILMS ON SUBSTRATES OF Zn, Cd, MILD STEEL, Cu & Pt. AS FUNCTION OF CHAIN LENGTH AS OBTAINED BY ELECTRON DIFFRACTION METHODS REPORTED BY BOWDEN AND TABOR. (27) THE DISORIENTATION TEMPERATURE CORRESPONDS APPROXIMATELY TO SOFTENING POINT OF METALLIC SOAPS FORMED BY CHEMICAL REACTION ON THE SURFACE.

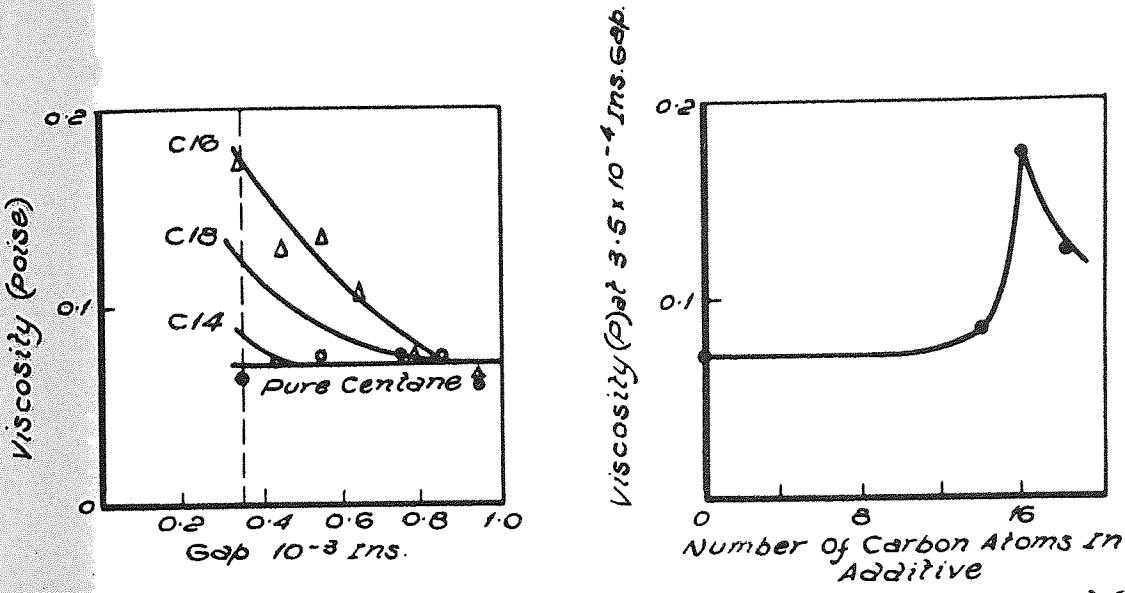

FIG. 3.4.(a) SURFACE VISCOSITY EFFECTS FROM ASKWITH et al (34)

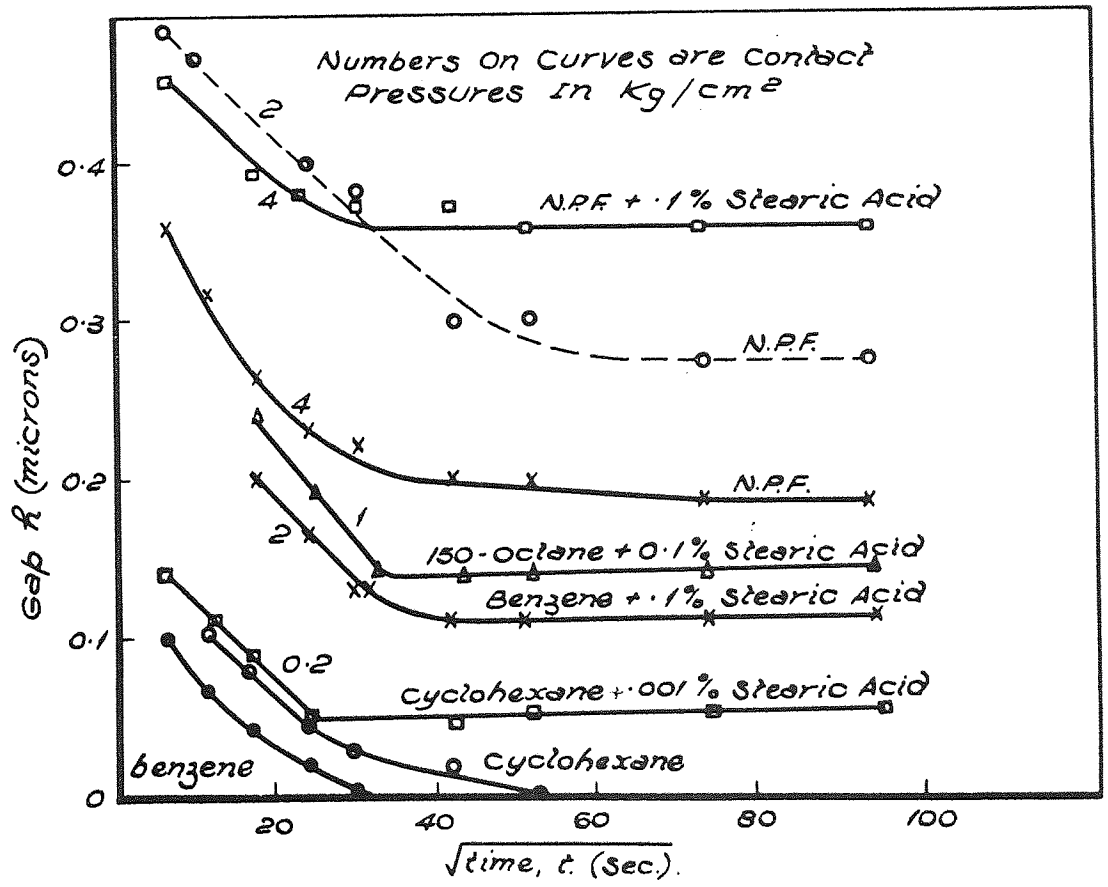

FIG. 3.4 (b) DEPTH OF LIQUID FILM BETWEEN DISCS AND TIME OF CONTACT OBTAINED BY FUKS.(38)

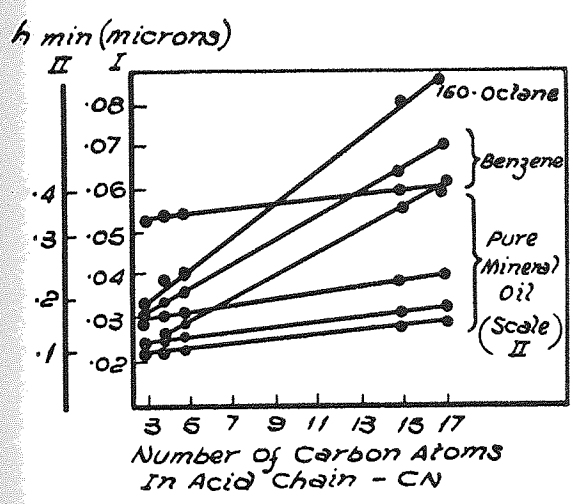

(a)

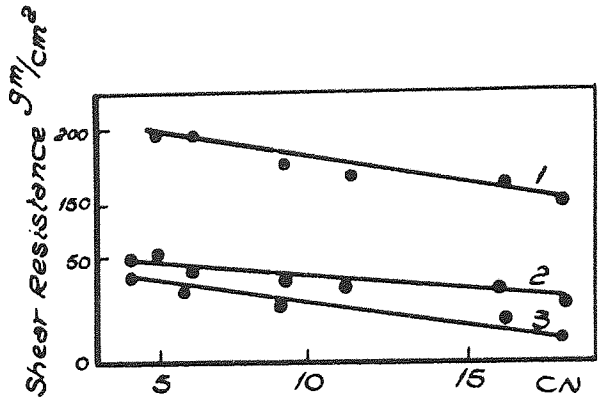

(b)

1) N.P.F. + ·1% Acid σ = 22 kg/cm²
2) N.P.F. + ·1% Acid σ = 6 kg/cm²
3) 160 - Octane + ·1% Acid σ = 4 kg/cm²

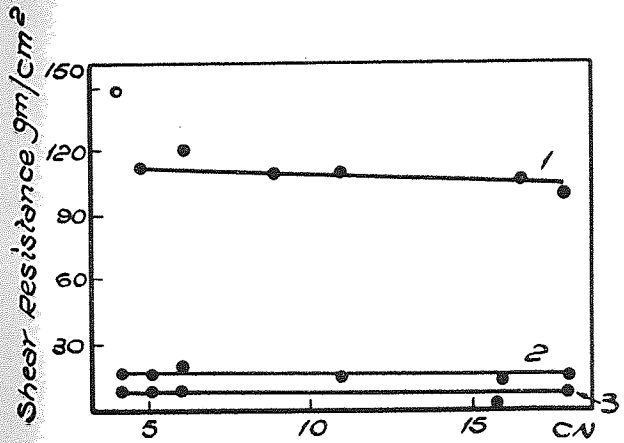

(c)

1) 150 - Octane + ·1% Acid h = ·1μ
2) NPF + ·1% Acid h = ·3μ
3) NPF + ·1% Acid h = ·1μ

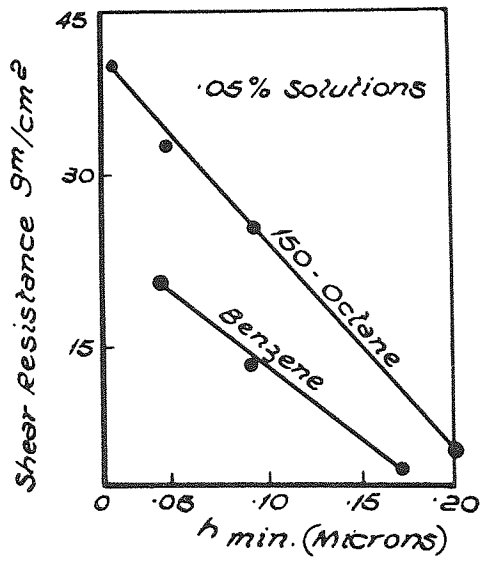

(d)

FIG. 3.5 THE RELATIONSHIP BETWEEN h Min. SHEAR RESISTANCE & CHAIN LENGTH OF ACID ACCORDING TO FUKS(38)

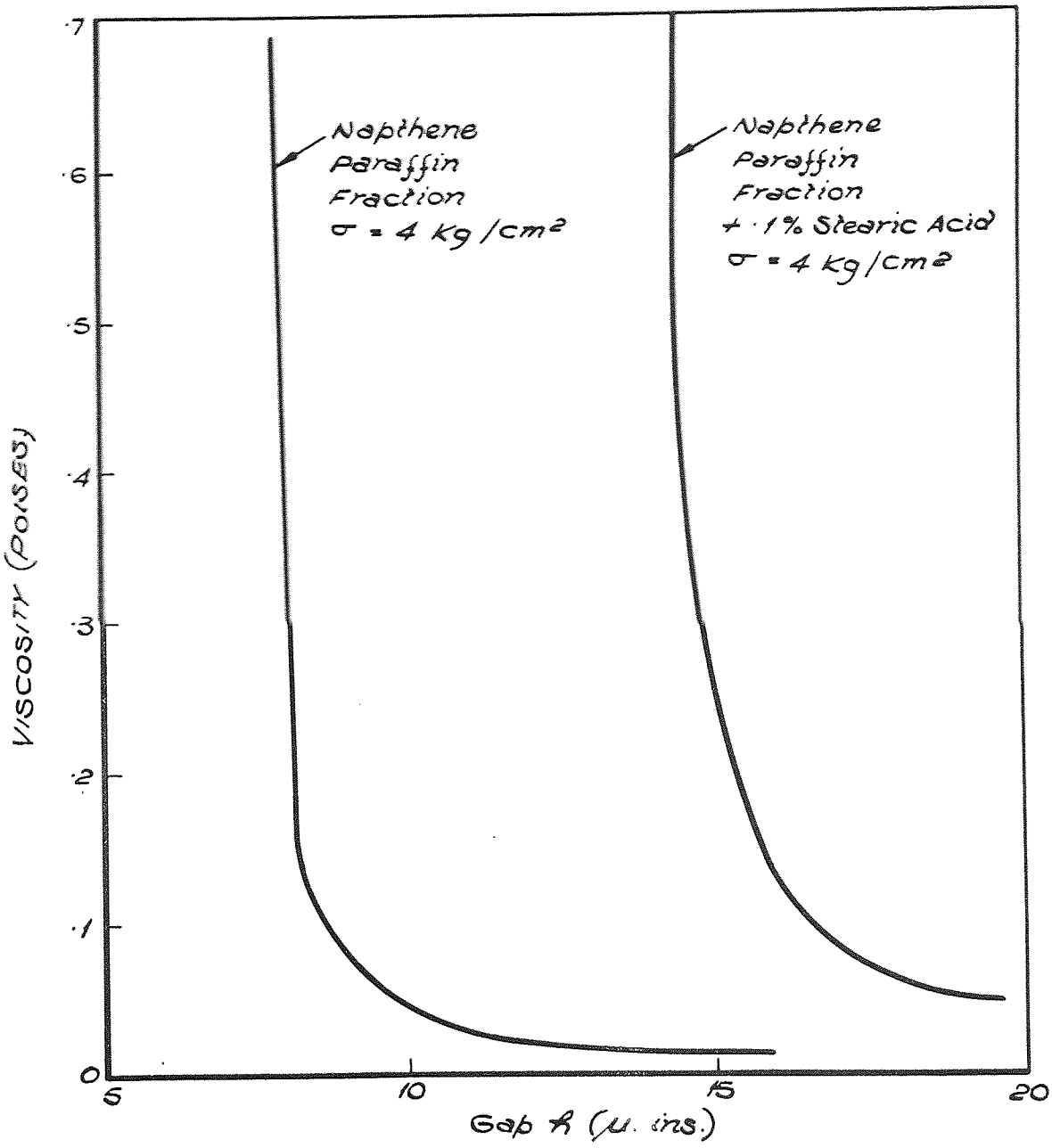

FIG. 3.6. EXAMPLES OF CONVERSION OF THE RESULTS OF FUKS TO VISCOSITY VARIATION WITH GAP THICKNESS USING STEFAN - REYNOLDS EQUATION

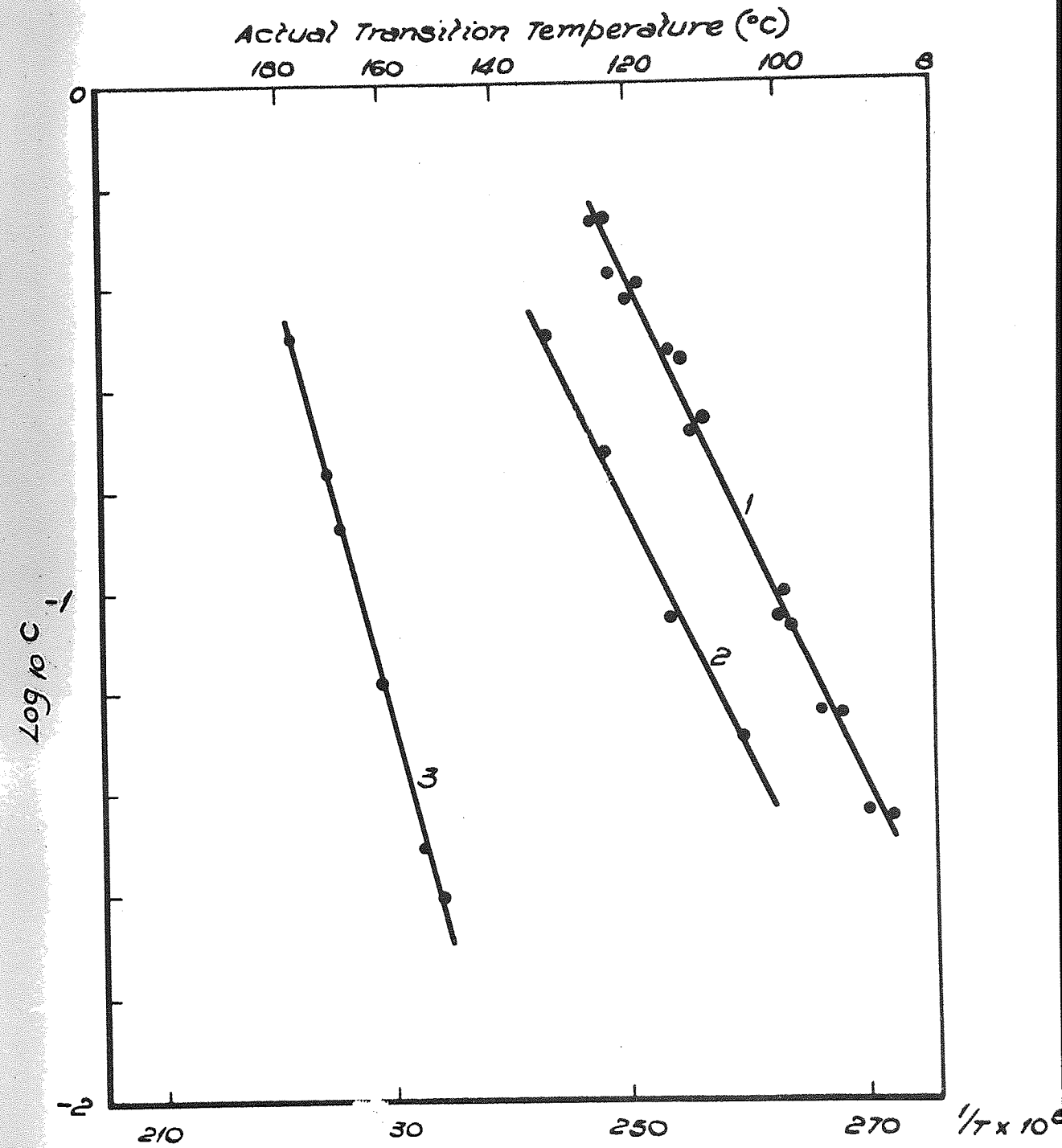

FIG. 3.7. LOG_{10} CONCENTRATION (Wt/100g SOLVENT) - RECIPROCAL TRANSITION TEMPERATURE °K FROM GREW & CAMERON (35) FOR NATURALLY OCCURRING SURFACE ACTIVE COMPOUNDS IN 1) CETANE 2) DEKALIN 3) WHITE OIL

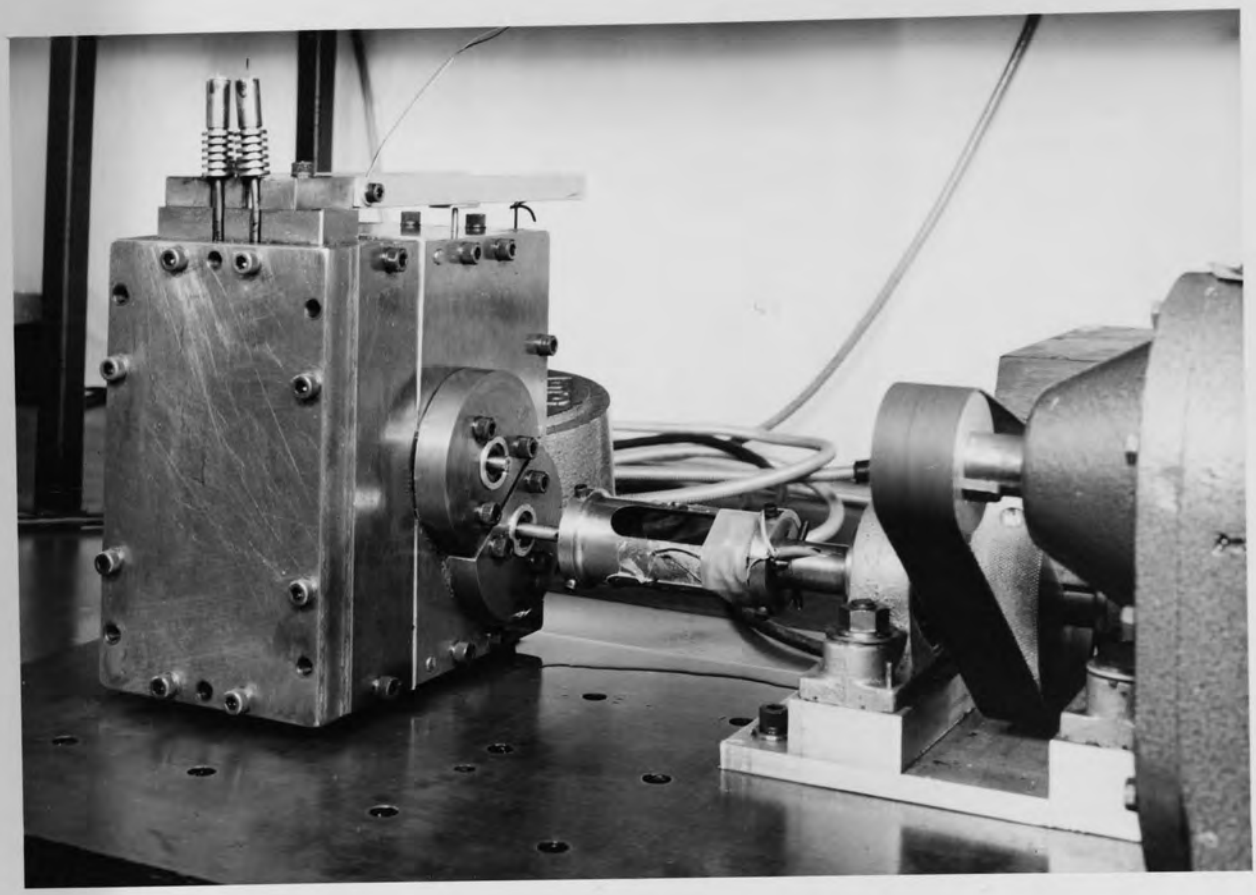

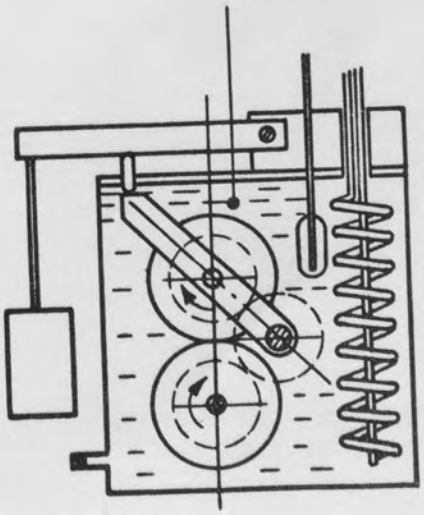

Dia of Disc. 2.500 ins.
Width of Disc. 0·250 ins. (0·1875 Track
Load 5 lbf.
Speed 26 rev/min.

FIG. 3.8 THE CRITICAL TEMPERATURE MACHINE

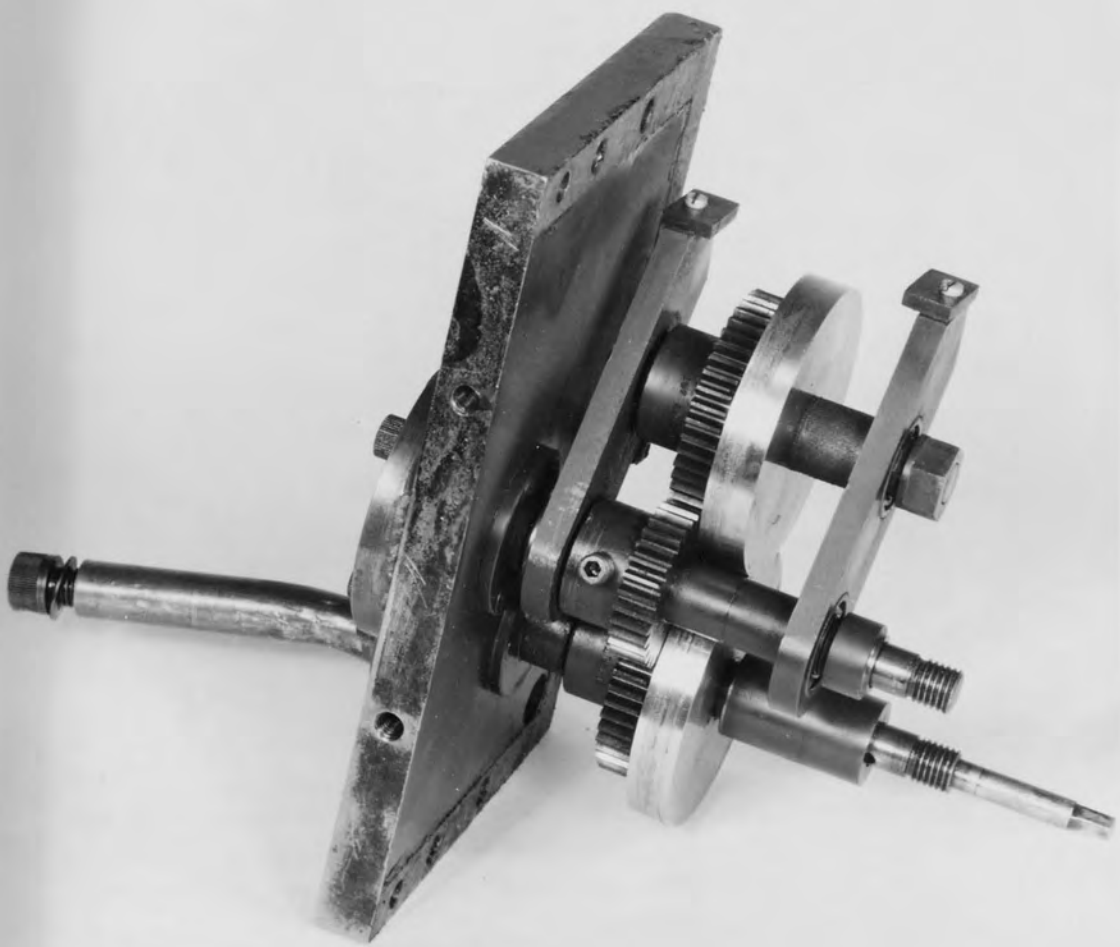

Fig. 3.9 The loading mechanism of
the critical temperature machine

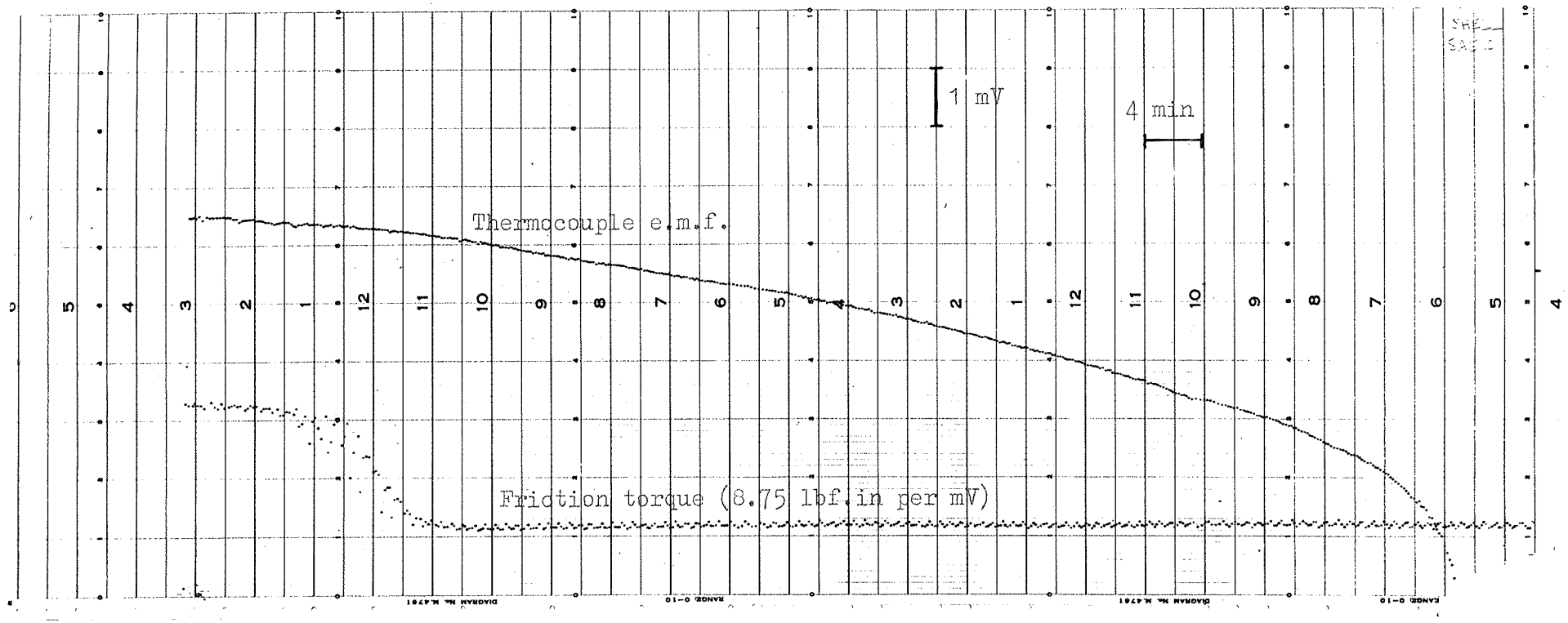

Fig. 3.10 Output trace from critical temperature machine for SAE 10 oil

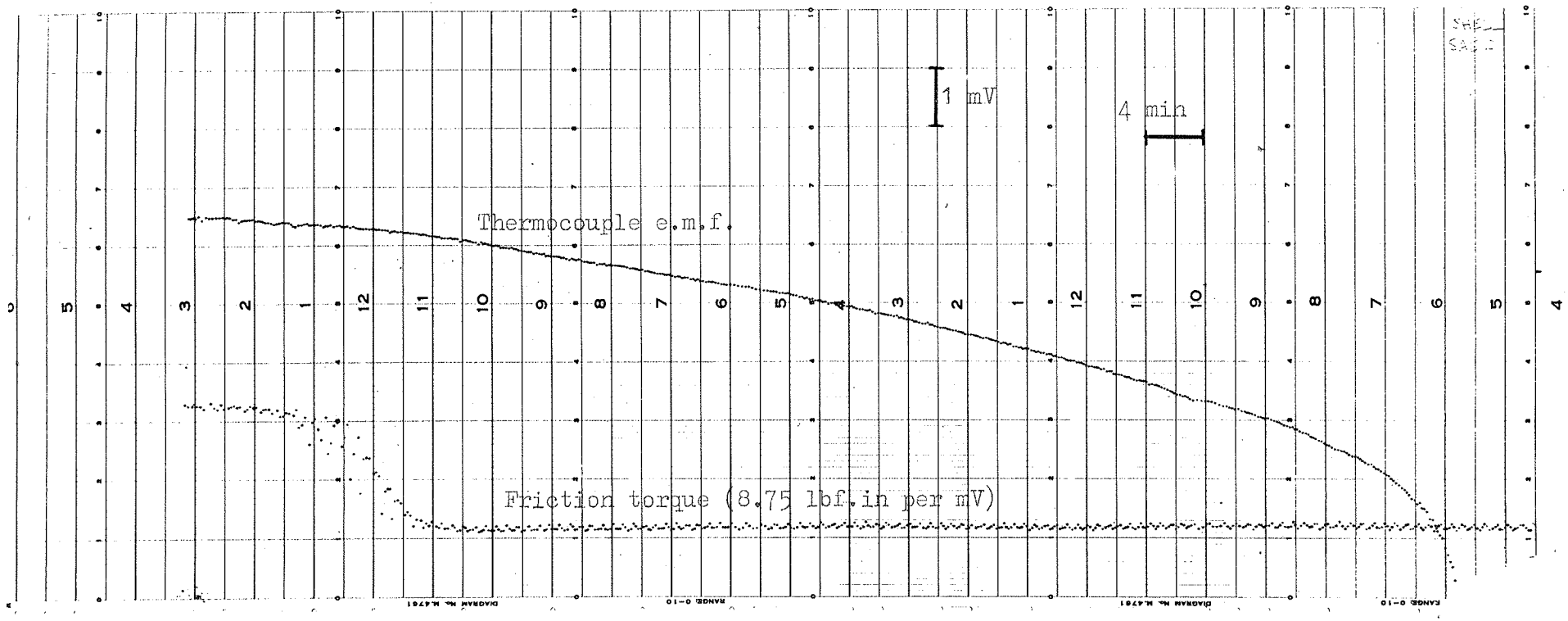

Fig. 3.10 Output trace from critical temperature machine for SAE 10 oil

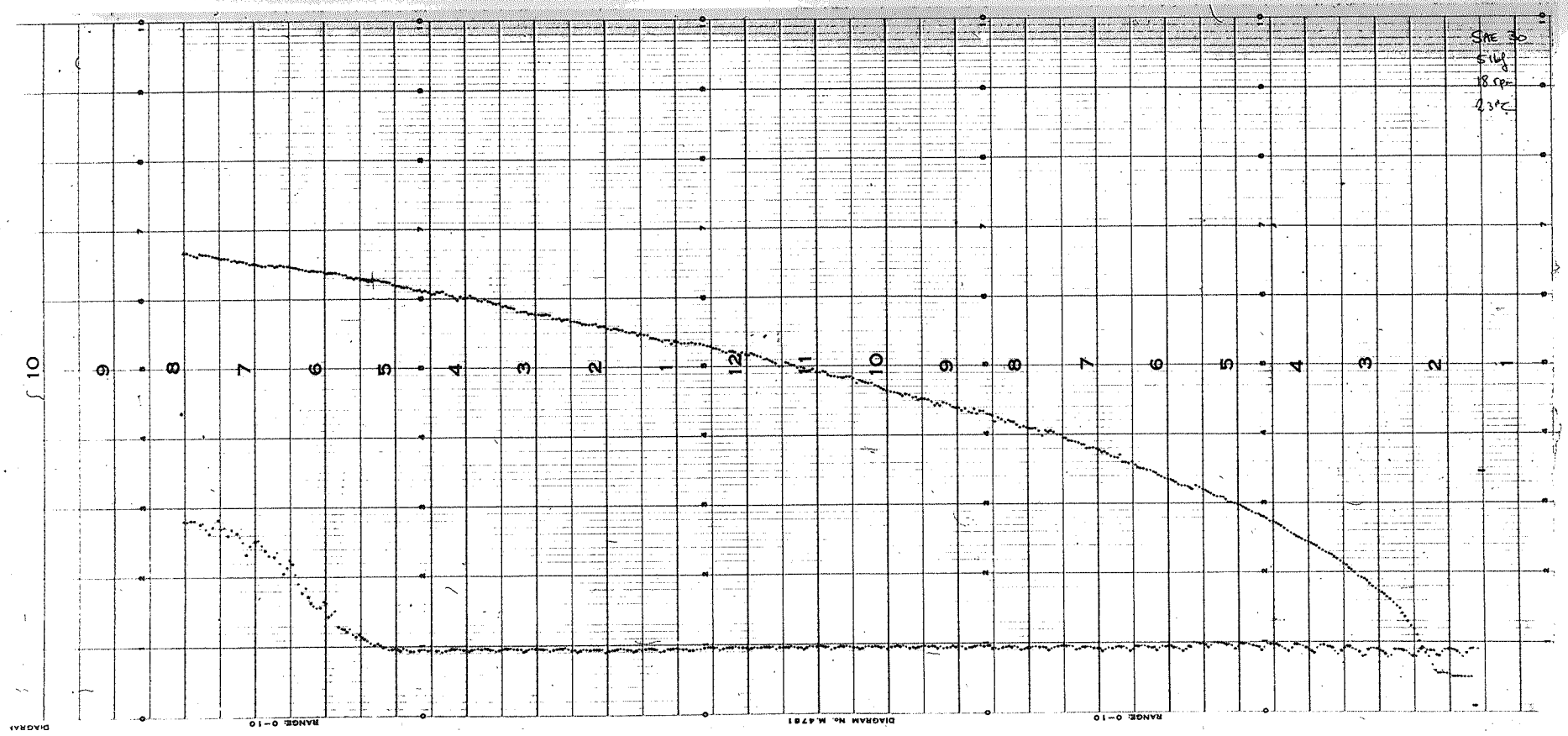

Fig. 3.11 Output trace from critical temperature machine for SAE 30 oil

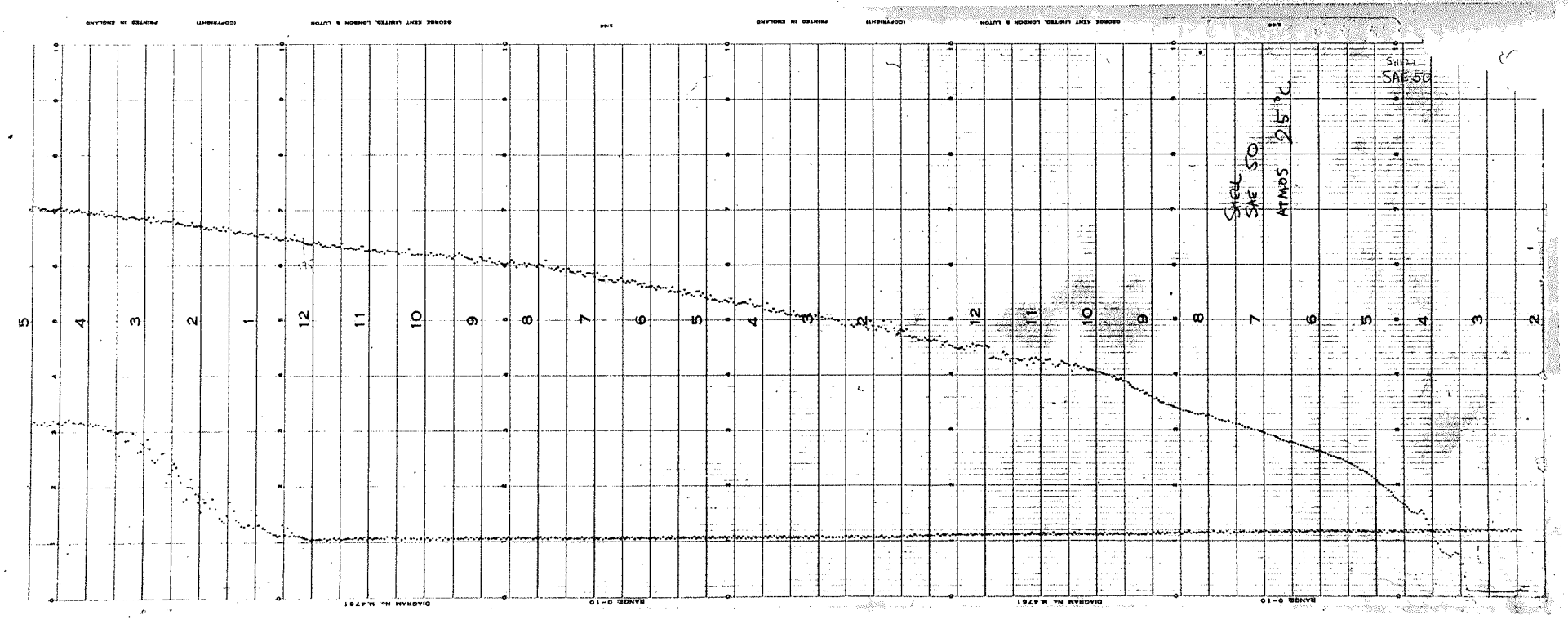

Fig. 3.12 Output trace from critical temperature machine for SAE 50 oil

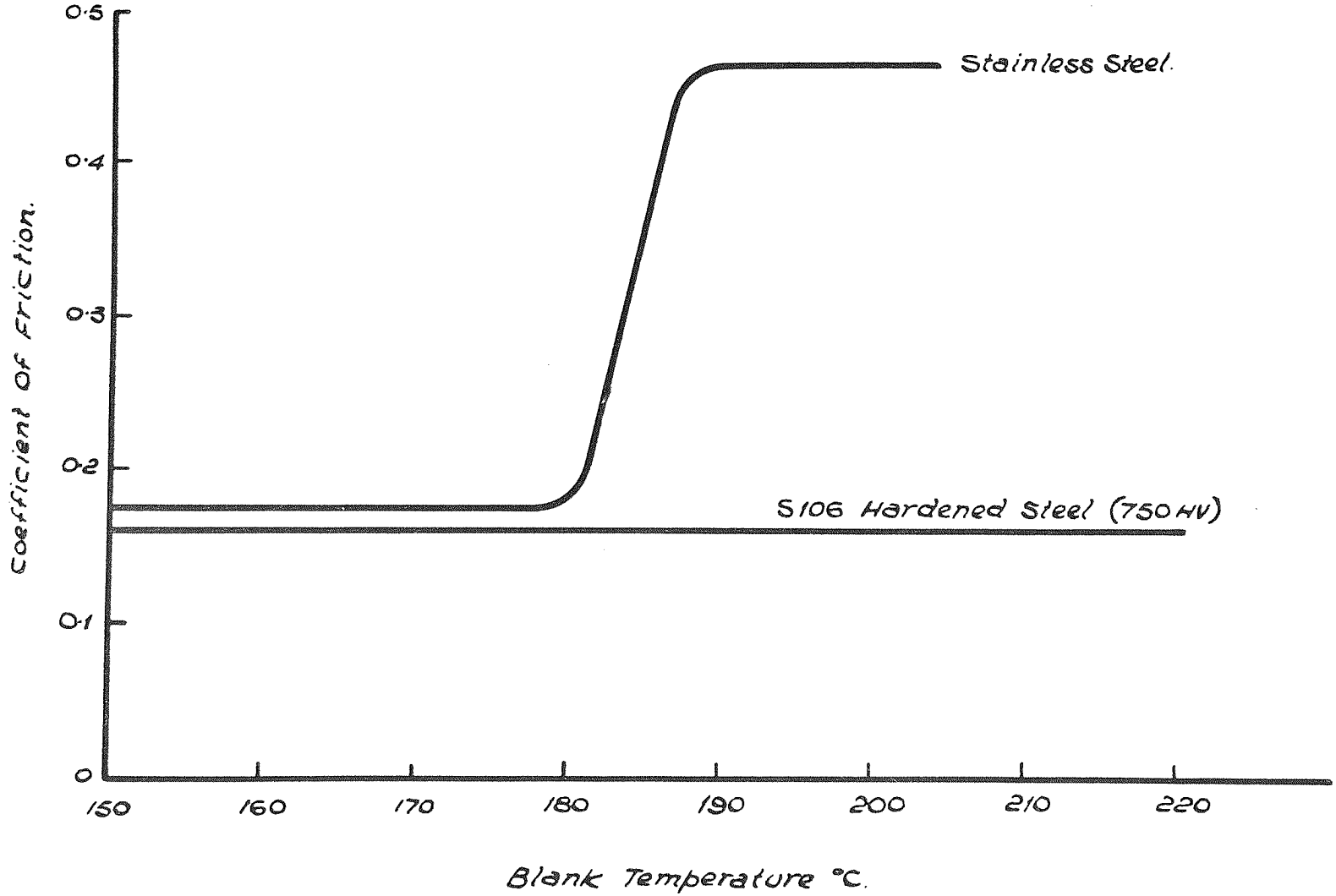

FIG. 3.13 COMPARISON OF FRICTION - TEMPERATURE TRACES AT 26 REV/MIN & 17.5/16f.

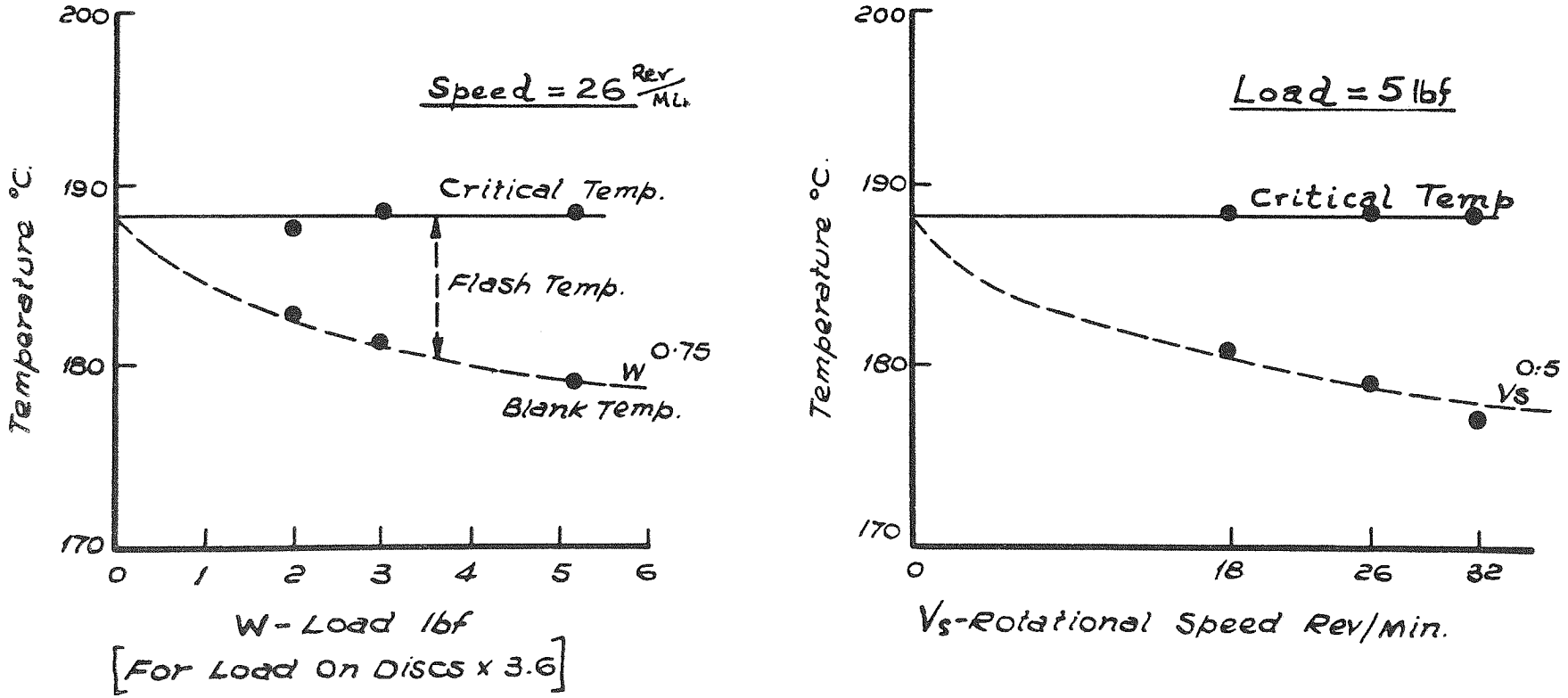

FIG. 3.14. EFFECTS OF SPEED AND LOAD ON TEMPERATURES MEASURED.

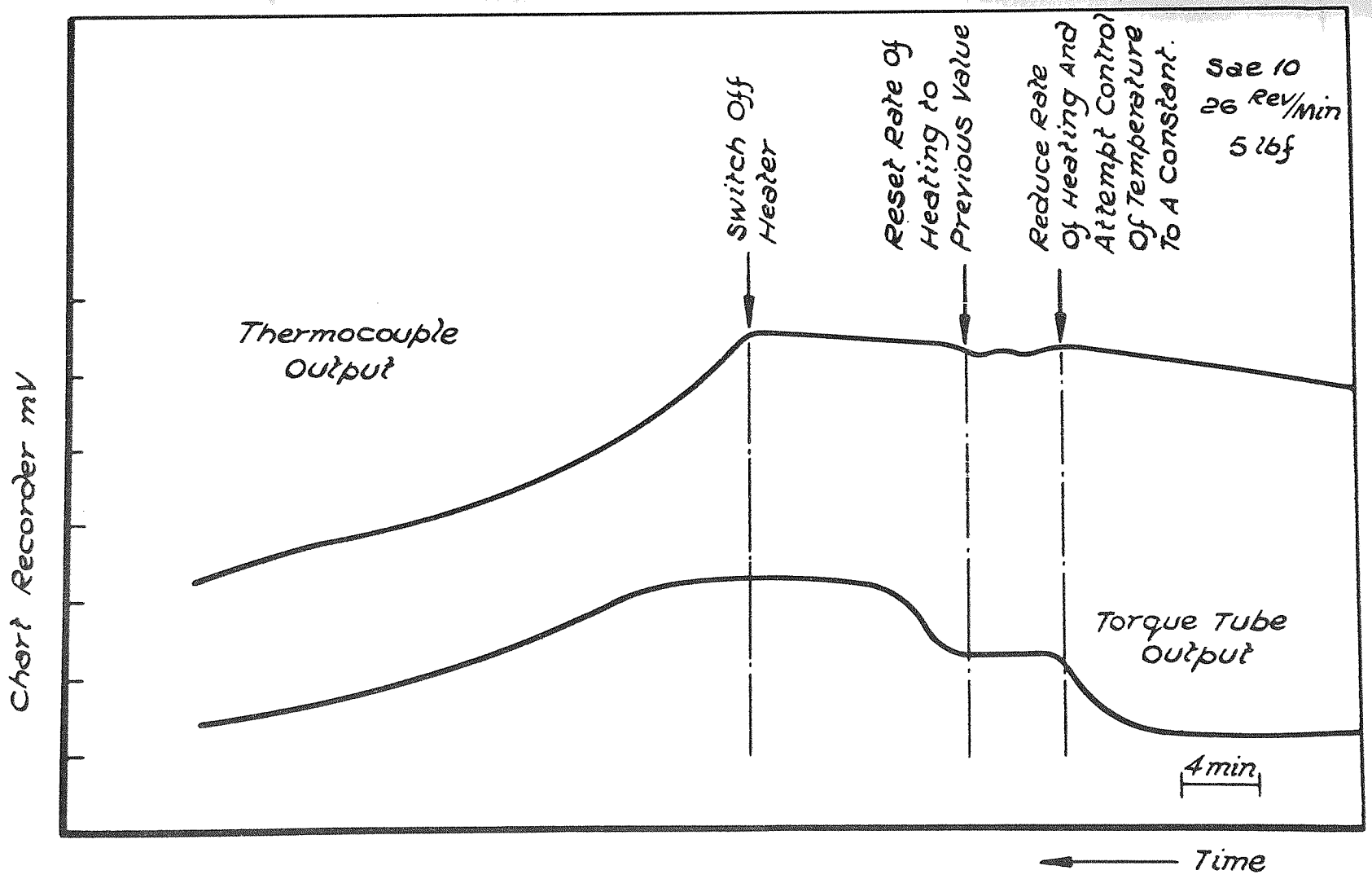

FIG. 3.15. MEAN TRACE OF TEMPERATURE CYCLE EFFECT ON FRICTION.

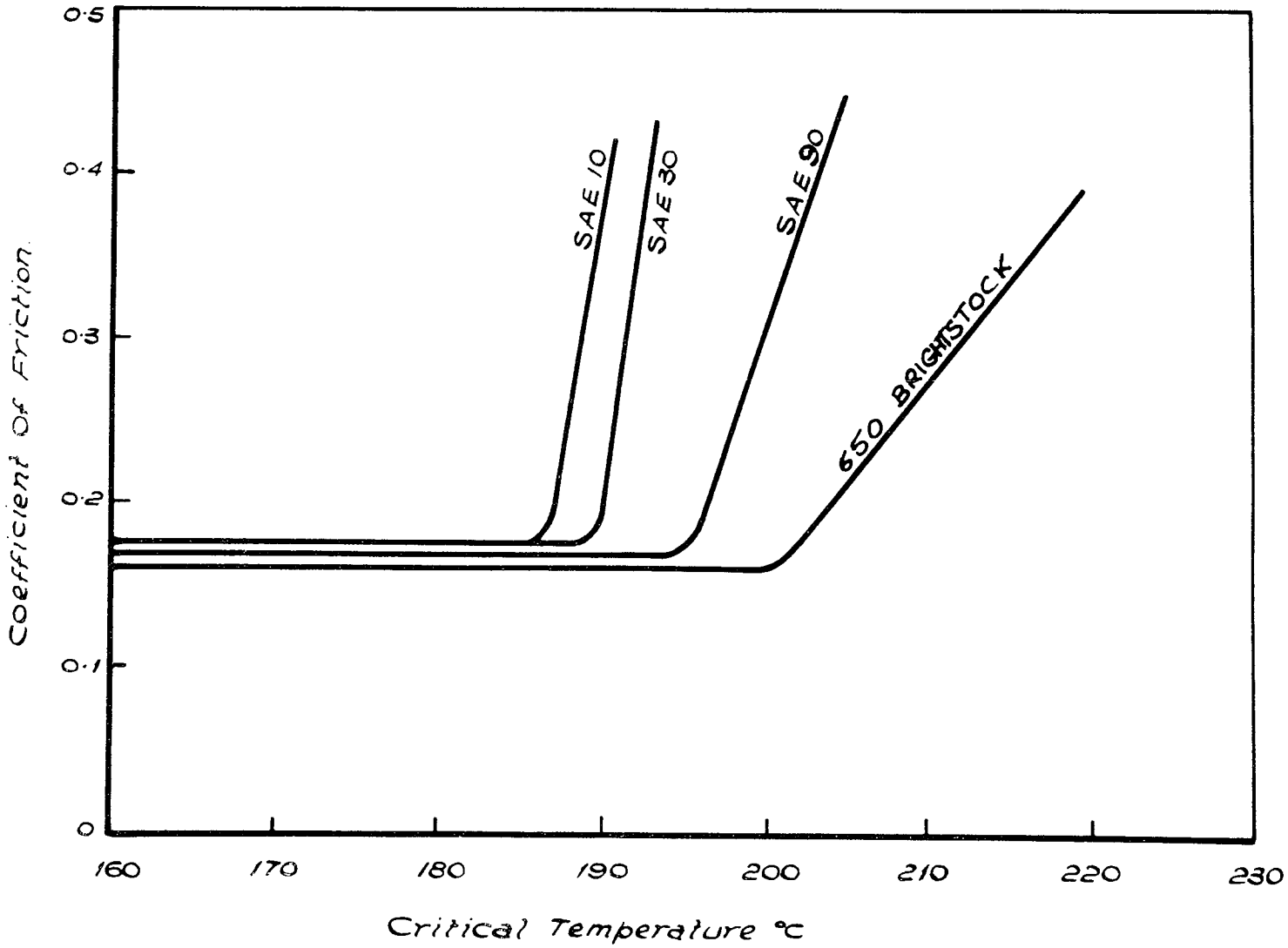

FIG 3.16.

CRITICAL TEMPERATURE TRACES FOR VARIOUS SHELL OILS, NOMINALLY NEUTRAL MINERAL OILS WITHOUT ADDITIVES.

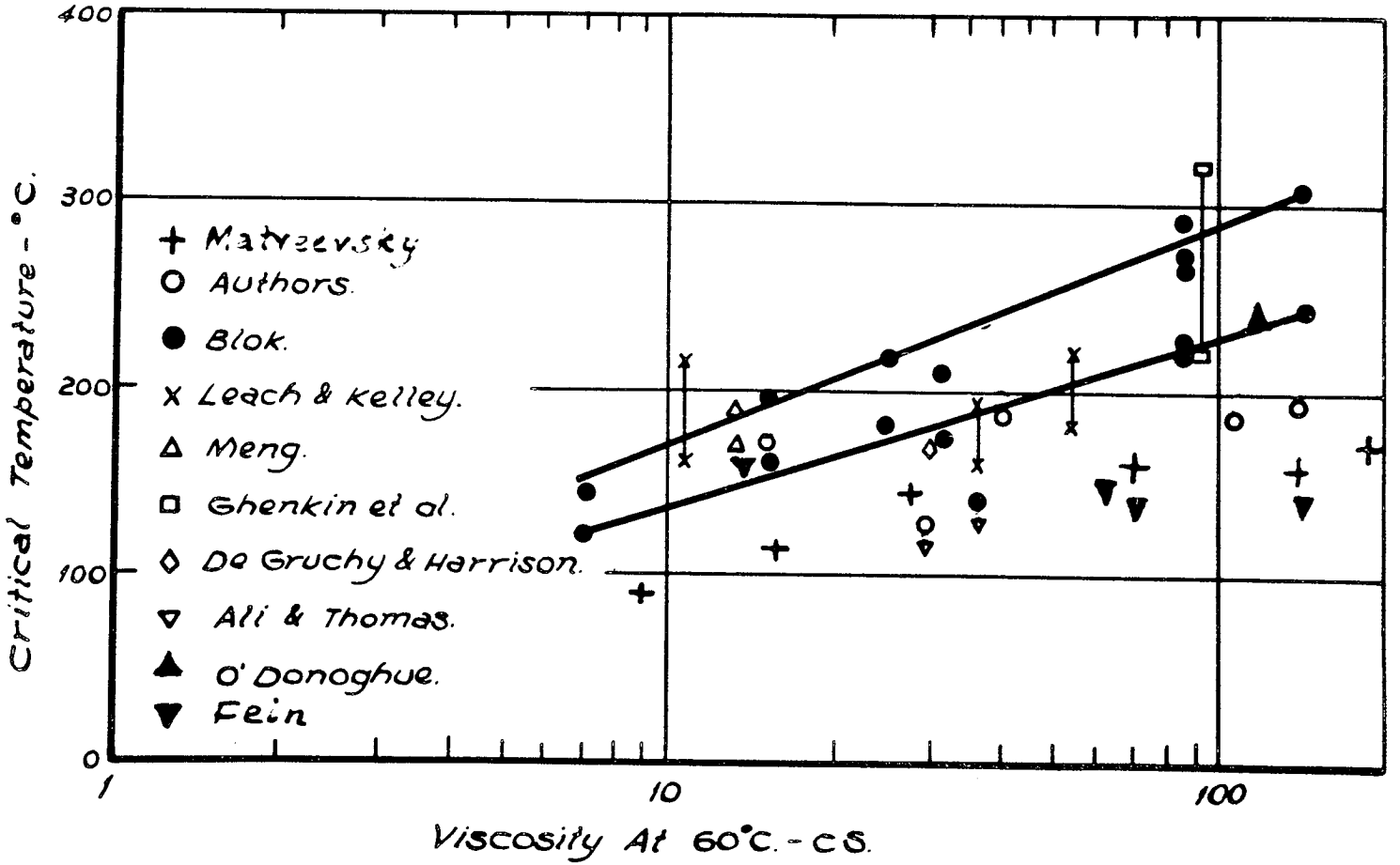

FIG 3.17 Variation of Tc with Viscosity

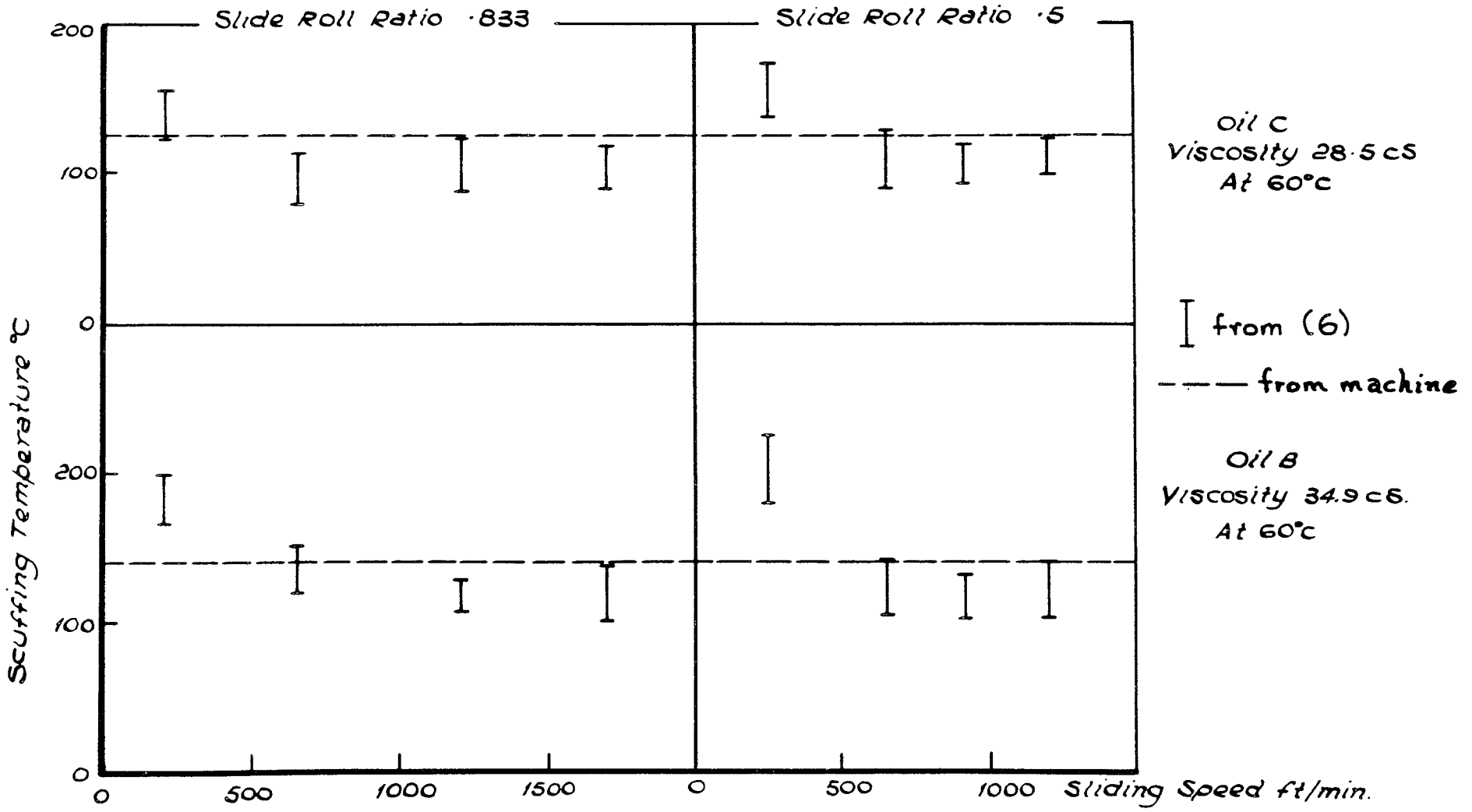

FIG. 3.18 SCUFFING TEMPERATURE RESULTS OF ALI & THOMAS[18] COMPARED WITH THE CRITICAL TEMPERATURES DETERMINED FOR EACH OIL.

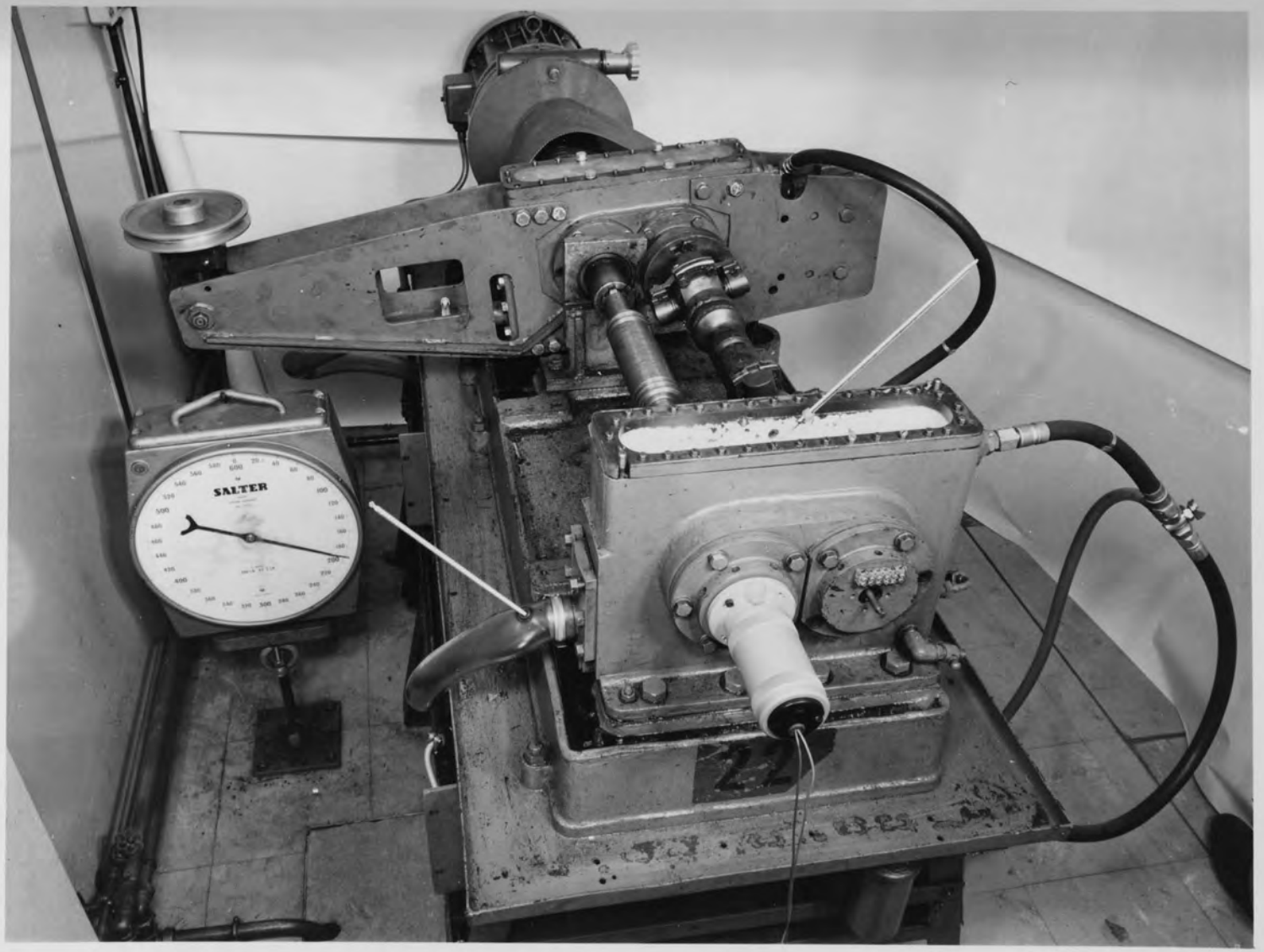

Fig. 3.19 The Thornton gear tester

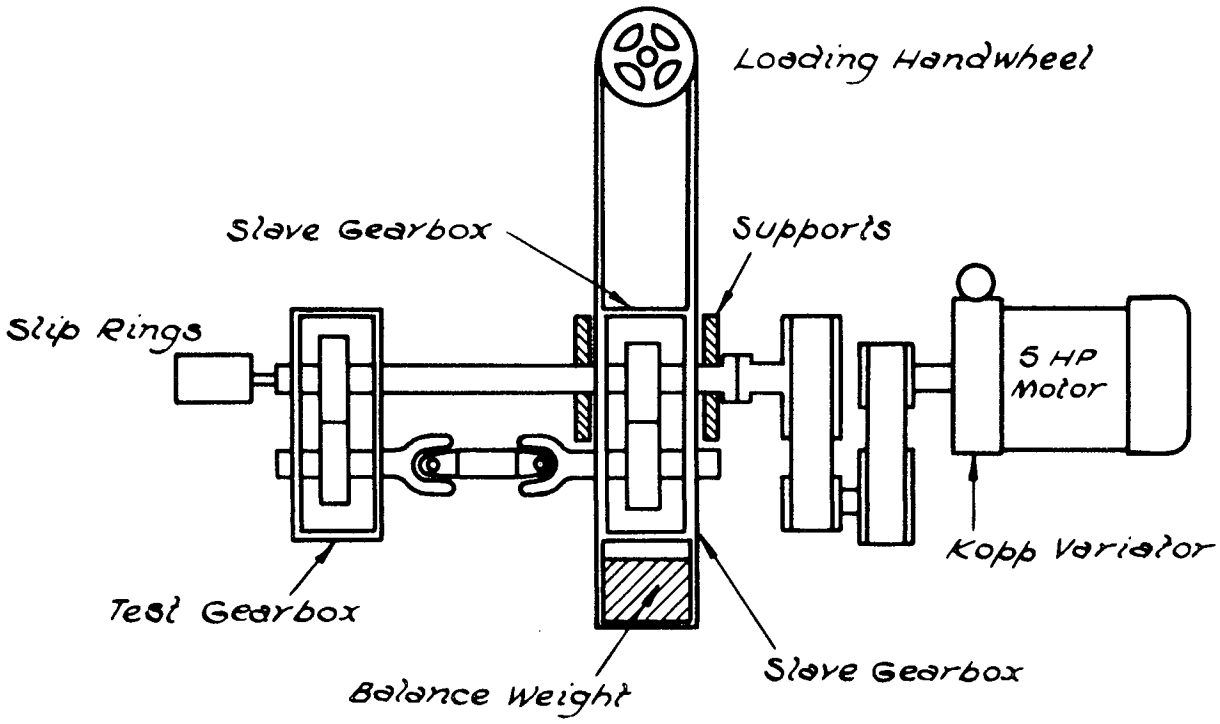

FIG. 3.20. LAYOUT OF THORNTON GEAR TESTER.

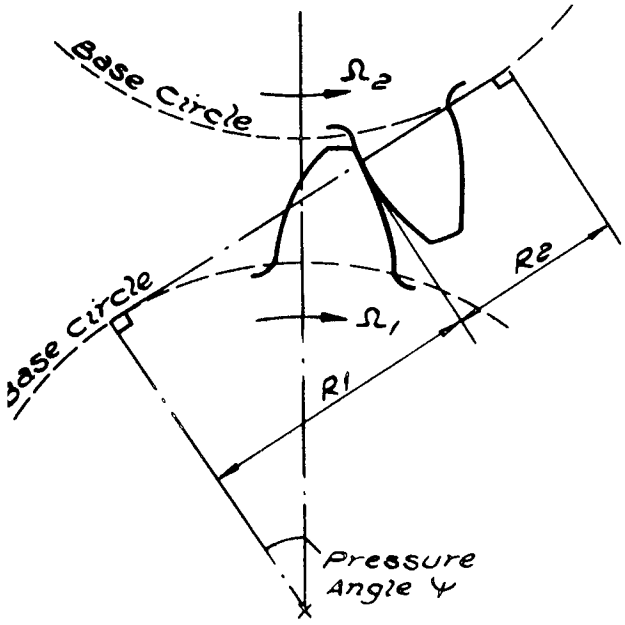

Gears In Contact.

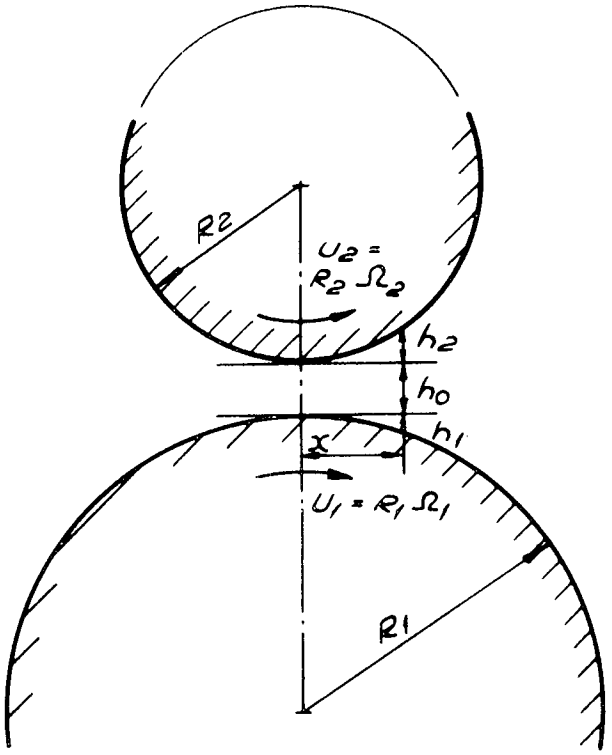

Equivalent Cylinders Representing Given Point on Contact Path of Gears Including Film Thickness ho

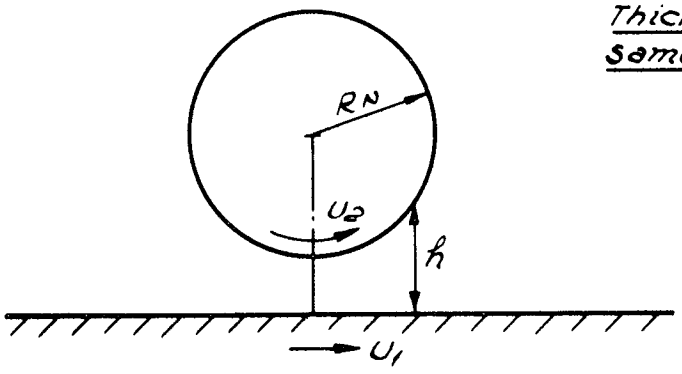

Equivalent Cylinder & Plane.

R_N is determined so that film thickness variation with x is the same.

$$\therefore h = h_1 + h_o + h_2$$

$$\simeq \frac{x^2}{2R_1} + h_o + \frac{x^2}{2R_2}$$

$$\simeq h_o + \frac{x^2}{2}\left(\frac{1}{R_1} + \frac{1}{R_2}\right)$$

$$\therefore \frac{1}{R_N} = \frac{1}{R_1} + \frac{1}{R_2}$$

FIG. 3.21. EQUIVALENT CYLINDERS.

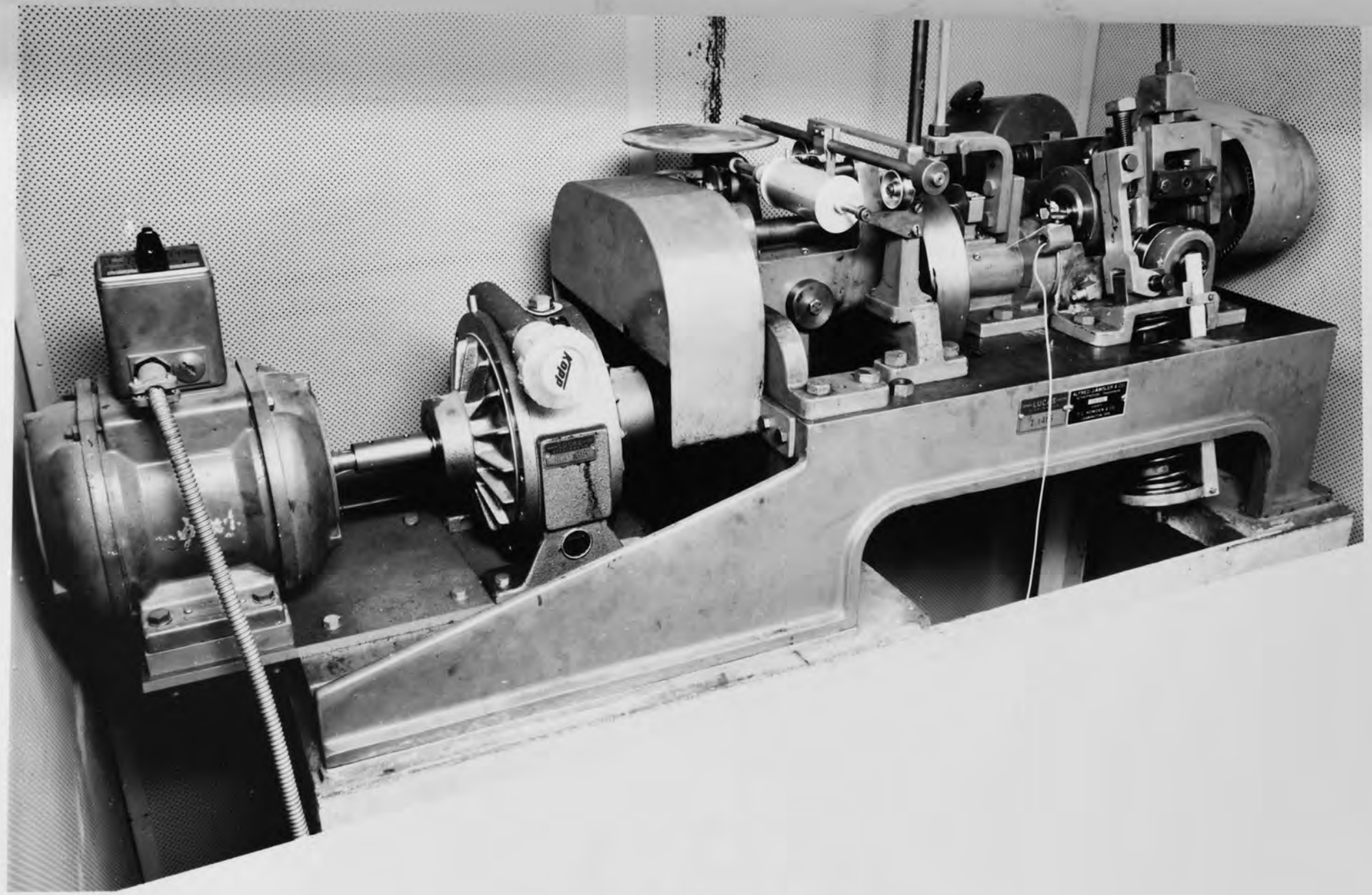

Fig. 3.22 The Amsler disc machine

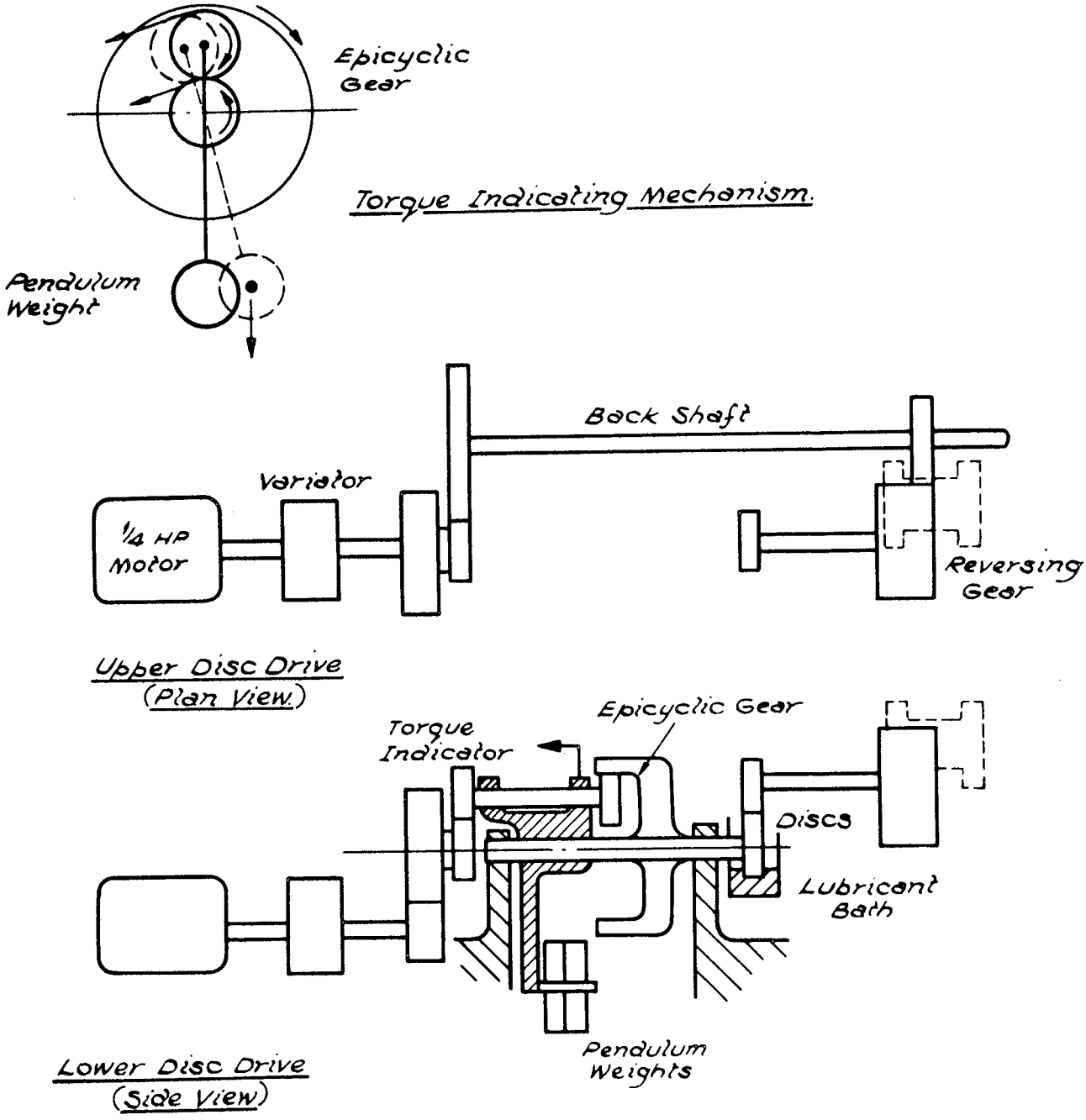

FIG. 3.23. SCHEMATIC LAYOUT OF DISCS AND PENDULUM IN AMSLER WEAR MACHINE.

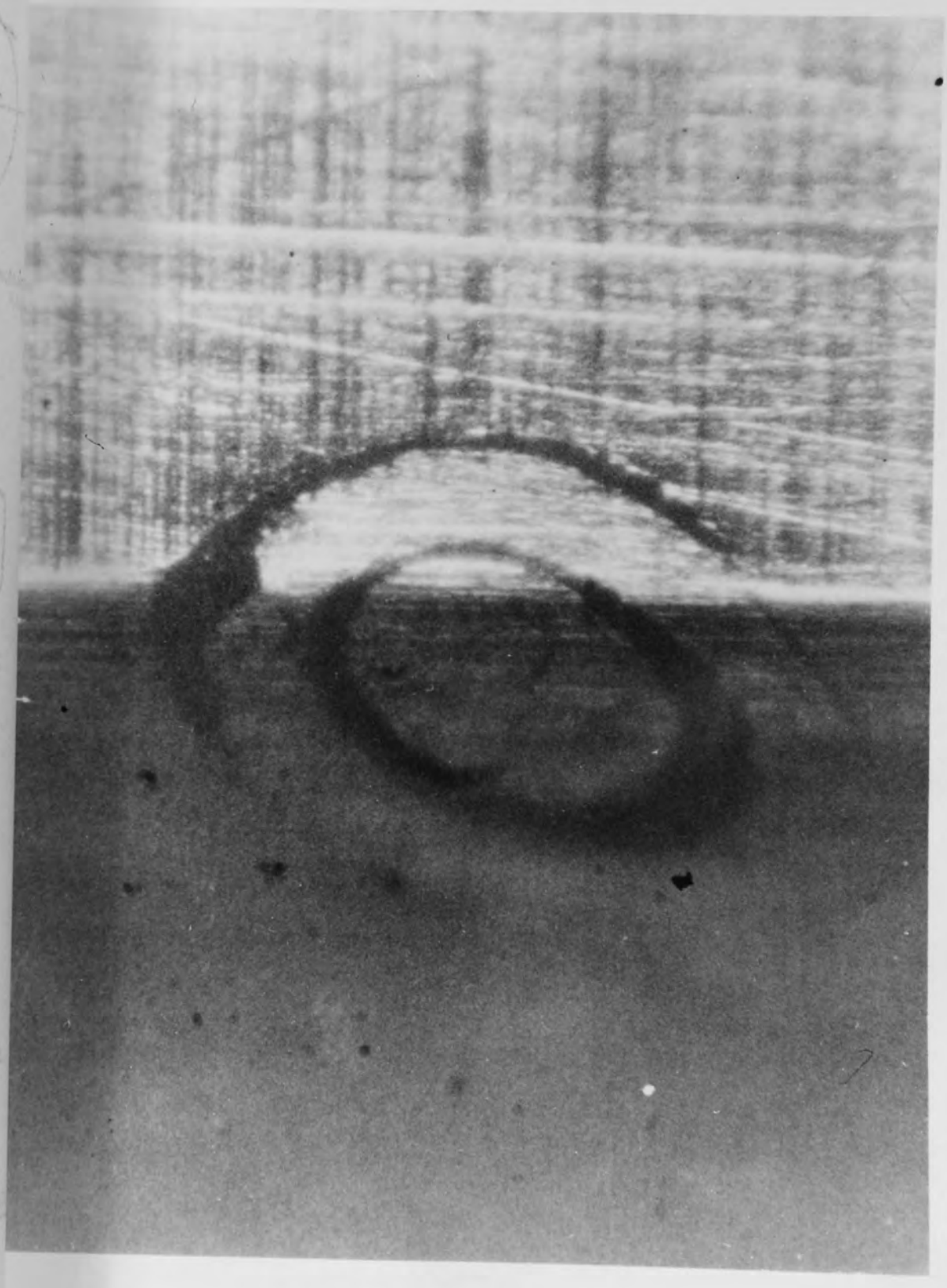

Fig. 3.24(a) Surface thermocouple
at tip of test gear

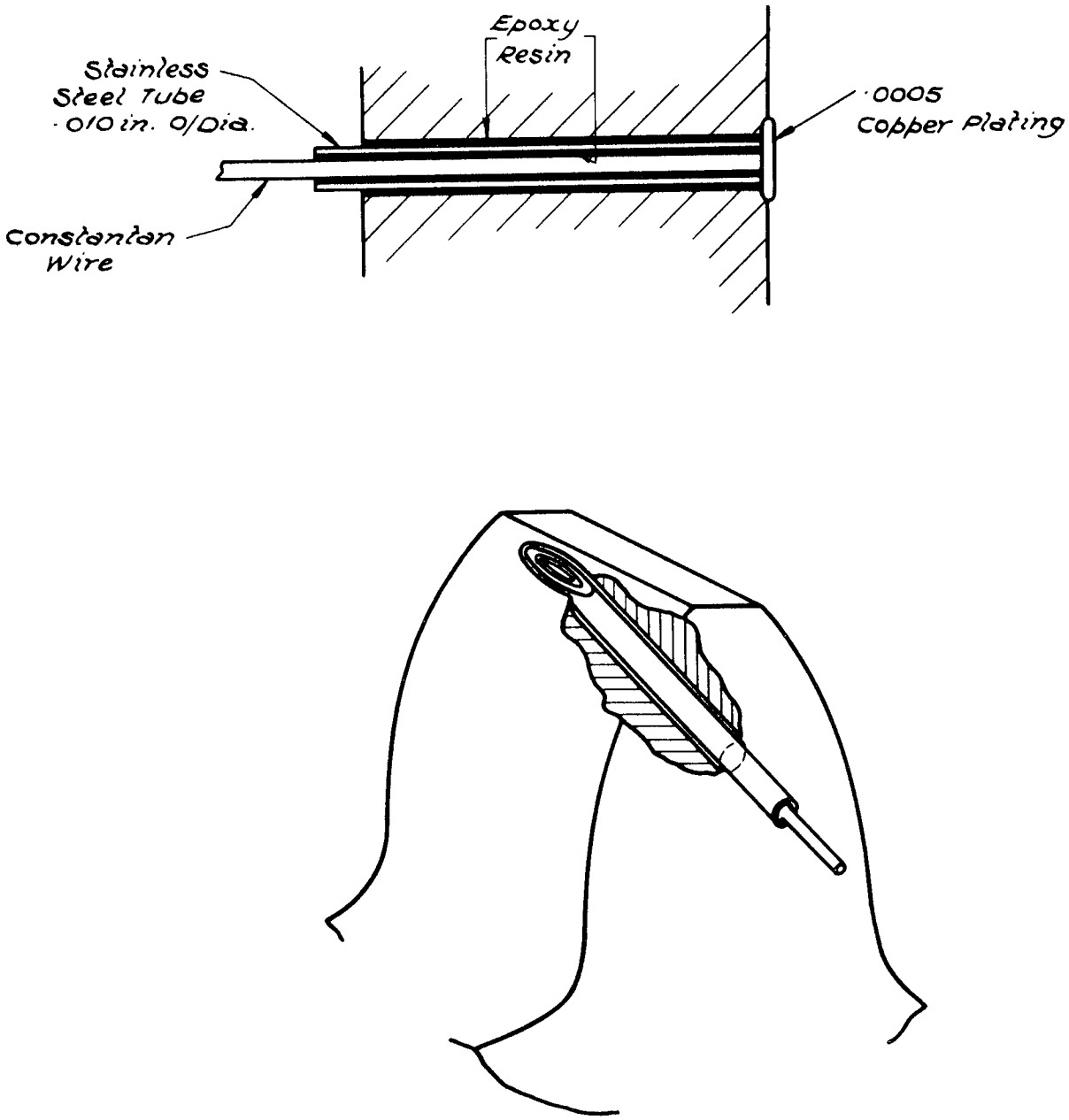

FIG. 3·24 (b) DIAGRAMMATIC VIEW OF EMBEDDED COAXIAL THERMOCOUPLE.

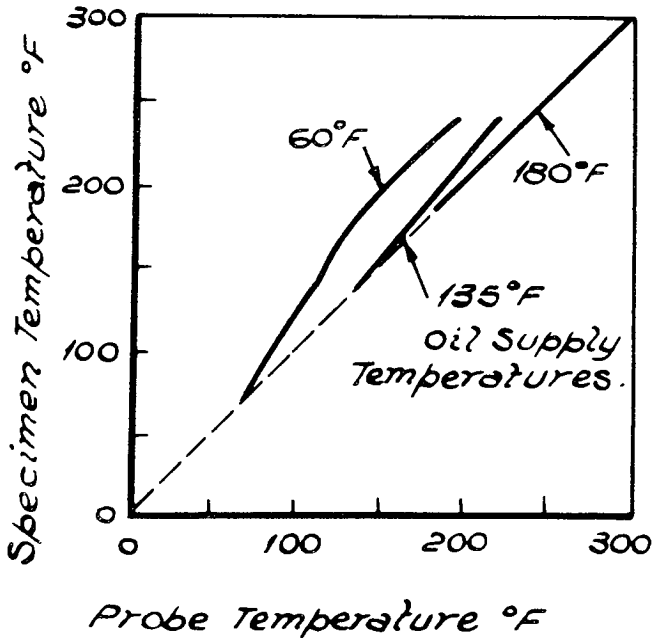

(a) Reference (17)

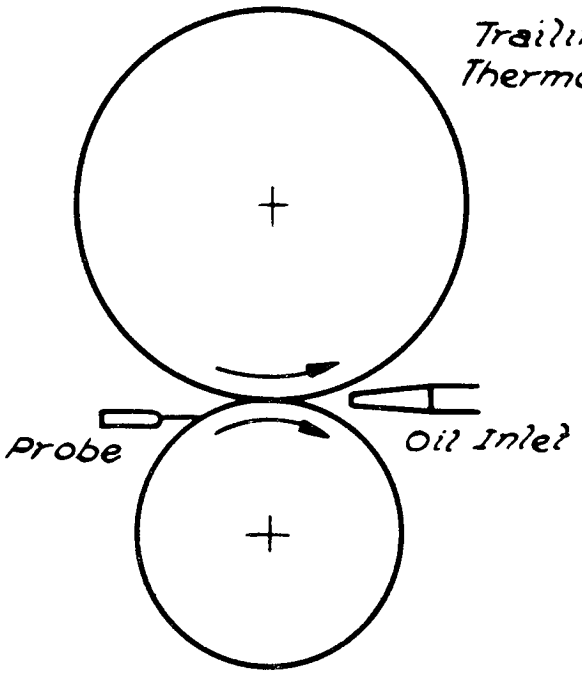

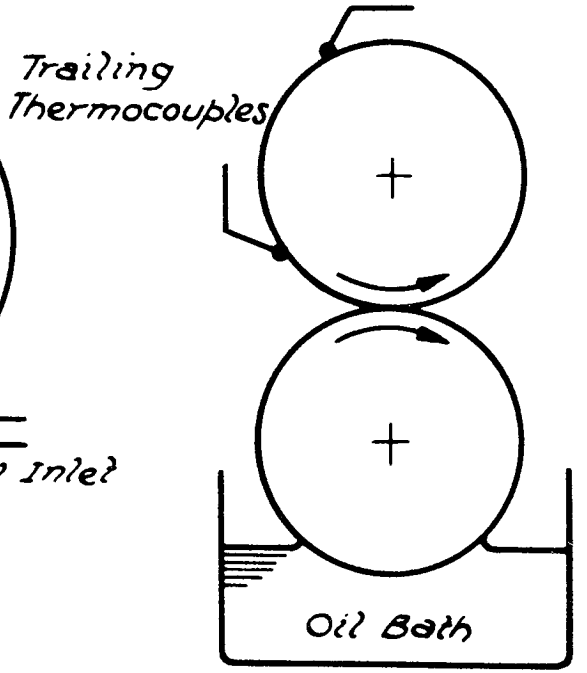

Agreement Between Trailing & Embedded Thermocouples.

(b) Reference (14)

FIG. 3.25 TRAILING THERMOCOUPLE PERFORMANCE FROM REFERENCES (17 & 14)

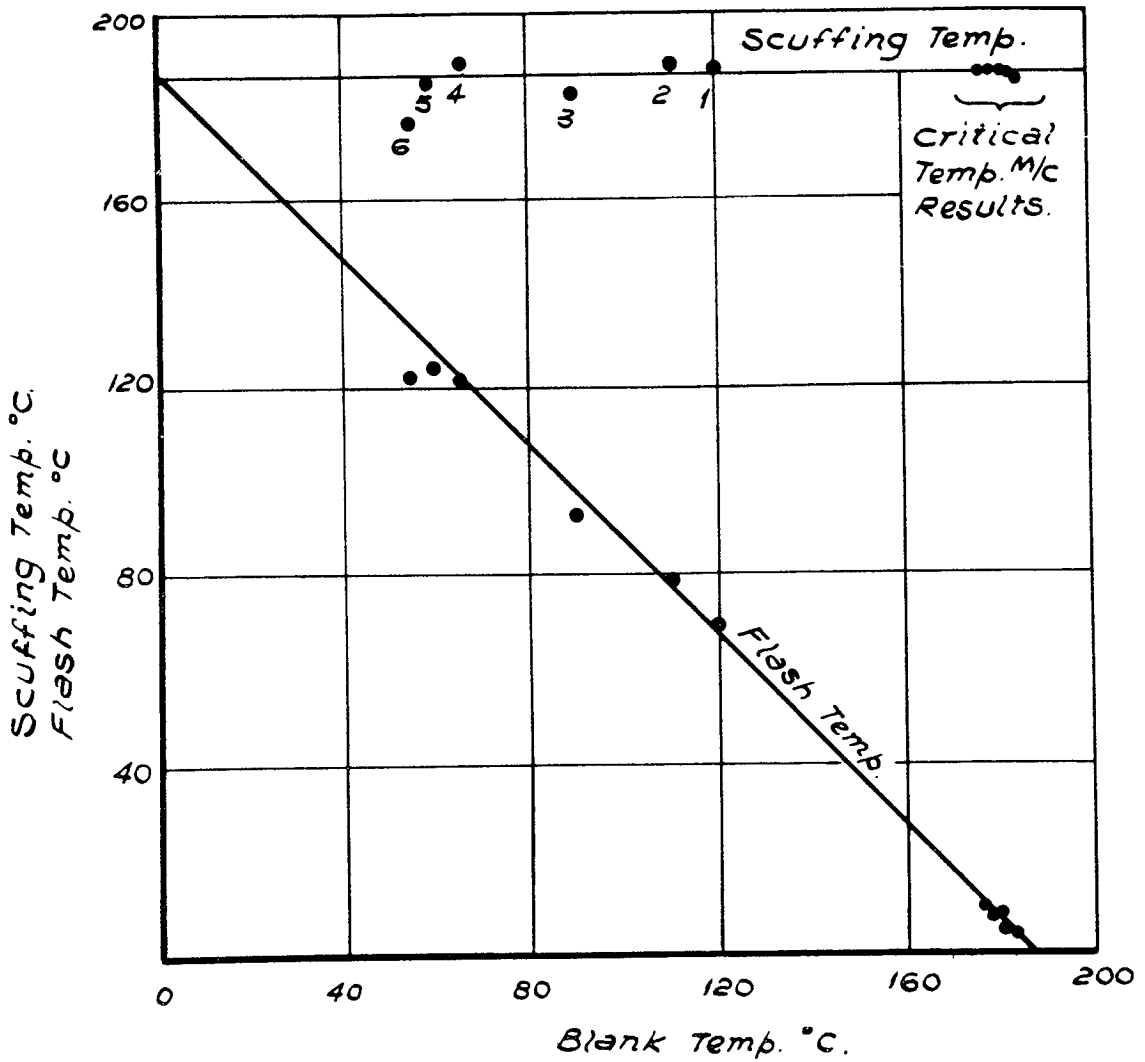

Amsler Disc M/c Tests.	
1	KE 961 Discs 122 Kg 100 r.p.m.
2	KE 839 Discs 145 Kg 70 r.p.m.
3	KE 961 Discs 200 Kg 70 r.p.m.

5" CTRS Gear M/c Tests.	
4	En 31. Gears 550 lbf. 1000 r.p.m.
5	520 lbf. 800 r.p.m.
6	480 lbf. 500 r.p.m.

FIG. 3.26. SCUFFING TESTS FOR SAE 30. PLAIN MINERAL OIL.

4.0 BLANK TEMPERATURES

4.1 Temperatures due to heat sources moving through infinite media

It is well known that in the operation of gears and discs, there is heat input from the zone of contact between sliding surfaces and that this heat has to be dissipated by conduction and convection. In so doing, the blank temperature of the surfaces rises to an equilibrium value above that of the surroundings so that convection takes place according to the expression:-

$$T_b = \frac{Q}{h_c} \qquad \ldots\ldots (4.1)$$

where Q is the heat injected into the metal and h_c the convection heat transfer coefficient from the surface.

The problem of determining the heat injected into the metal at the contact has concerned research workers for some time. Blok (43) gave the first solution by solving the equations for a band source moving along the surface of a semi-infinite conducting medium and injecting heat into it. The surface outside the heat source was considered to be insulated. A later development of this solution by Jaeger is reported by Carslaw and Jaeger (45).

The starting point is the solution to the equation for conduction of heat in a fixed medium,

$$\frac{\partial^2 T}{\partial x^2} + \frac{\partial^2 T}{\partial y^2} + \frac{\partial^2 T}{\partial z^2} = \frac{1}{\kappa}\frac{\partial T}{\partial t}$$

of the form

$$T = \frac{Q^1}{8(\pi \kappa t)^{3/2}} e^{-\left\{(x-x^1)^2 + (y-y^1)^2 + (z-z^1)^2\right\}/4\kappa t}$$

Q^1 being the source strength, i.e. the temperature to which unit ~~mass~~ volume would be heated by the instantaneous heat $\varrho\rho' c$ at $(x^1\ y^1\ z^1)$.

By considering a heat source passing through the fixed medium and injecting q units of heat per unit time, the temperature at time t at a point P, due to the (qdt^1) heat units emitted at time t^1, will be

$$dT = \frac{qdt^1}{8\rho c\left(\pi\kappa(t-t^1)\right)^{3/2}} \exp\left(-\frac{[x - U(t-t^1)]^2 + y^2 + z^2}{4\kappa(t-t^1)}\right)$$

Point P has coordinates (x, y, z) referred to the heat source and moving with it.

∴ The total temperature at point P at time t due to the heat emitted by the heat source O is obtained by integration from time zero to t. At $t = \infty$, a steady thermal regime is established and

$$T = \frac{q}{4\pi k\ (x^2 + y^2 + z^2)^{\frac{1}{2}}} e^{-\frac{U}{2\kappa}\left[(x^2+y^2+z^2)^{\frac{1}{2}} - x\right]}$$

It is required to know surface temperatures only and so z is put equal to zero. Also for a line source along the y axis where q is now in heat units/unit time/unit length the temperature at point P becomes:

$$T = \frac{q}{2\pi k} e^{\frac{Ux}{2\kappa}} Ko[\beta x] \qquad \ldots\ldots (4.2)$$

where $\beta = \frac{U}{2\kappa}$ and $Ko[\beta x]$ is the Modified Bessel function of the 2nd kind of order zero.

$$Ko[\beta x] = \frac{1}{2}\int_{-\infty}^{\infty} \frac{e^{-\left(\frac{U}{2k}\sqrt{x^2+y^2}\right)}}{(x^2+y^2)^{\frac{1}{2}}}\, dy$$

Equation 4.2 is recognised as the standard solution of this problem, tabular values of $Ko(\beta x)$ being obtained from the British Association Mathematical Tables Vol. VI.

Cameron, Gordon, and Symm (46) extended this work to consider the contact of two bodies with heat flow into both due to the friction between them. For a band of heat sources from $x = 0$ to $x = 1$.

$$T = \frac{1}{2\pi k}\int_0^1 q\, e^{\beta(x-\xi)}\, Ko\{[\beta(x-\xi)]\}\, d\xi \qquad \ldots\ldots (4.3)$$

However this solution is for a band of heat source passing through a fixed infinite medium. For two moving media, however, passing in contact with a band of sources q per unit length, the heat partition will depend on the relative conductivities and surface velocities (i.e. β). Cameron et al produced the following relationships:-

$$T_1 = \frac{q}{\pi(k_1+k_2)}\int_0^1 \left\{1 + \frac{f(\xi)}{k_1}\right\} e^{\beta_1(x-\xi)}\, Ko([\beta_1(x-\xi)])\, d\xi$$

$$T_2 = \frac{q}{\pi(k_1+k_2)}\int_0^1 \left\{1 - \frac{f(\xi)}{k_2}\right\} e^{\beta_2(x-\xi)}\, Ko([\beta_2(x-\xi)])\, d\xi$$

The introduction of the heat source $f(\xi)/k_1$ was necessary in order to satisfy the condition $T_1 = T_2$ at the contact, although the temperature could vary outside the contact. This condition would arise if there was no coherent hydrodynamic film i.e. the conditions of lubrication were in the "boundary" region. The solution of these equations was achieved by numerical

analysis for $K_1 = K_2 = K$, $q/2\pi k$ taken as 10; $\beta_2 = 10$; and β_1 varying from -10 to 10 in steps of 1. The results were represented as non-dimensional temperatures defined as $T\ (\pi KJ/2k_1)$ and are reproduced in fig. 4.1.

Further results were given by Cameron et al for the simple case of equal partition of heat between two media moving at the same speed past the source. This involved the numerical solution of equation (4.3) for a range of values of βL from 2 to 1000. Values of $e^u\ Ko(u)$ are not plotted for $u > 20$. Therefore, the asymptotic expansion was used:-

$$e^u\ Ko(u) \simeq \sqrt{\frac{\pi}{2u}} \left(1 - \frac{1}{8u} + \frac{1^2\ 3^2}{2!(8u)^2} - \frac{1^2\ 3^2\ 5^2}{3!(8u)^3} + \ldots\ \right) \quad \ldots\ (4.4)$$

This integrates to

$$\int_{z_1}^{z_2} e^u\ Ko(u)du = \left[\sqrt{2\pi u}\left\{1 + \frac{1}{8u} - \frac{1^2\ 3}{2!(8u)^2} + \frac{1^2\ 3^2\ 5}{3!(8u)^3} + \ldots\ \right\}\right]_1^2$$

where $u = \beta (x - \xi)$ $\quad \ldots\ (4.5)$

For $u < 0$ $\quad e^u\ Ko(|u|)\ du = -\int e^{-u}\ Ko(u)\ du$

Noting that $e^{-u}\ Ko(u)\ du \to 0$ for $z_2 > z_1 > 20$ $\quad \ldots\ (4.6)$

Cameron et al calculated the temperatures at the extended range of speeds by numerically solving the above equations and comparing them with the asymptotic solution derived analytically.

The asymptotic solutions for $\beta \to \infty$ are

$T = 0$ for $x < 0$

$$T \simeq \frac{q}{k}\sqrt{\frac{\kappa l}{\pi U}}\left[\sqrt{\frac{x}{l}} - \sqrt{\frac{x-1}{l}}\right] \quad \text{for } 0 < x < 1$$

$$T \simeq \frac{q}{k}\sqrt{\frac{\kappa l}{\pi U}}\left[\frac{x}{l} + C\right] \quad \text{for } x > 1$$

This agrees with the asymptotic solution predicted by Blok for the peak temperature T at the rear of a band source of strength q^1 moving over a semi-infinite plane and injecting all the heat into the one body.

$$T = \frac{2q^1}{k}\sqrt{\frac{\kappa l}{\pi U}}$$

where $x = 1$ at rear edge of heat source and $q^1 = \frac{q}{2}$

The shape of the temperature profile is given in fig. 4.2(a).

A further case to be studied in the same work was that where the surfaces were no longer insulated. The heat was lost by convection to the surroundings according to Newton's law of cooling.

This imposed the condition at the surface that:

$$K\left(\frac{\partial T}{\partial z}\right)_{z=0} = hc\,T$$

Previously hc was put equal to zero to give a fully insulated surface. The required solution was found to be

$$T = \frac{q}{2\pi k} e^{\beta x}\left[\,Ko\,(\beta x) - \lambda \int_0^\infty e^{-\lambda V}\, Ko\left\{\beta\sqrt{x^2+V^2}\right\}\, dV\right.$$

where $\lambda = \frac{hc}{k}$ and reduced to the former expression (4.2)

when $\lambda = 0$.

By subsequent transformation and solving for the steady state temperature after an infinite number of repeated contacts

distance L apart the following integral was obtained:-

$$T_{(\text{steady state})} = \frac{q}{2\pi k} \int_0^{\infty} \frac{e^{-\beta LV} - 1\sqrt{V^2 + 2V}}{1-e^{-\beta LV}} \frac{}{V^2+2V+\alpha^2} dV$$

where $\alpha = \lambda/\beta$

This could then be used to represent the contact between discs or gears where the band heat source moved over the entire surface once each revolution. The integral was evaluated over a large range of α and β L and found for all practical purposes to equal $\pi/\beta L_{\alpha}$

Hence $$T = \frac{q}{2\pi k} \frac{\pi}{\beta L \alpha} = \frac{q}{2Lh_c}$$

which agreed with the well known expression (4.1). Here q is the heat per unit band width shared equally between the two surfaces.

Figures for the build-up of temperature to the steady state as the number of contacts increased were tabulated, with temperature expressed in the non-dimensional form $I = \frac{2\pi kT}{q}$

The computed results for temperature are plotted against n, the number of contacts in fig. 4.3. It is seen that almost up to the equilibrium value, the heat transfer coefficient has very little effect on the build-up of temperature and the temperature increases with $n^{\frac{1}{2}}$, once a few hundred contacts have been made.

4.2 A simplified theory for predicting blank temperatures

The following simplified version of the theory derived in reference (46) was supplied by Gordon and Cameron (47):-

When a point on the surface of a rotating disc makes its first contact with the other disc, its temperature is T(0). After one revolution the same point is about to come into contact for the second time with its temperature now reduced to T(L). The quantity of heat associated with this critical contact may be considered to decay in the manner indicated in fig. 4.2(b). The second contact, however, produces an additional temperature rise of T(0) and after the second revolution this temperature has also reduced to T(L) so that after the second revolution, the temperature of that part of the surface considered is T(L) + T(2L), where T(2L) is the temperature corresponding to the initial contact after two revolutions. This process is repeated for subsequent revolutions so that after n revolutions prior to the (n + 1)th contact, the temperature Tn at the surface is

$$Tn = T(L) + T(2L) + T(3L) + \ldots\ldots T(nL)$$

In Ref. (46) this sum was considered when the source of heat was both conducted and convected away and that after an infinite number of contacts $T_\infty = q/2Lh_c$. From the plotted computer values of Tn (fig. 4.3 and 4.4) it is seen that over the range $10^2 < n < 10^5$ they are to a large degree independent of the convection. If convection can be ommitted, the determination of Tn, the surface temperature after n revolutions is obtained from the following simplified version of the theory derived in Ref. (46) and kindly provided by Gordon and Cameron (47).

Restating equation (4.2) as

$$T = \frac{q}{2\pi k} e^{\beta L} Ko(\beta L)$$

where $\beta = U/2\kappa$

and L = distance between heat source and point at which T is required to be known.

For large values of βL i.e $\beta L > 10$,

$$T = \frac{q}{2\pi k} e^{\beta L} \left(\frac{\pi}{2\beta L}\right)^{\frac{1}{2}} e^{-\beta L}$$

from equation (4.4)

For n repeated sources,

$$T \simeq \frac{q}{2\pi k}\left(\frac{\pi}{2\beta L}\right)^{\frac{1}{2}} + \left(\frac{\pi}{2\beta 2L}\right)^{\frac{1}{2}} + \ldots\ldots\left(\frac{\pi}{2\beta nL}\right)^{\frac{1}{2}}$$

If n is large it is sufficient to replace

$$\frac{1}{(1)^{\frac{1}{2}}} + \frac{1}{(2)^{\frac{1}{2}}} + \frac{1}{(3)^{\frac{1}{2}}} + \ldots\ldots \frac{1}{(n)^{\frac{1}{2}}} \text{ by } \int_1^n \frac{dx}{(x)^{\frac{1}{2}}}$$

$$= 2\,(n)^{\frac{1}{2}}$$

Hence $$Tn = \frac{q}{k}\left(\frac{n}{2\pi\beta L}\right)^{\frac{1}{2}}$$

$$= \frac{q}{kL}\left(\frac{\kappa}{\pi}\right)^{\frac{1}{2}}\left(\frac{nL}{U}\right)^{\frac{1}{2}}$$

Now U, the surface speed = NL where N = rev/sec, L = π D, ($^{n}/_{N}$ = t, time in seconds and $^{q}/_{L}$ is the strength of the heat source per unit area of the disc surface to be shared equally between the two bodies).

Hence $$Tn = \frac{q}{kL}\left(\frac{\kappa t}{\pi}\right)^{\frac{1}{2}} \qquad \ldots\ldots (4.6)$$

The asymptotic temperature derived in Eq. (4.6) is plotted in fig. 4.3 and 4.4 in the form:-

$$I = \frac{2\pi T k}{q} = \left(\frac{2\pi n}{\beta L}\right)^{\frac{1}{2}}$$

which can be compared directly with the computed values. The temperature calculated from the simple theory of course goes on increasing with the number of contacts whereas the actual temperature approaches the steady state. Here there is equilibrium between the heat injected into the medium and the heat lost by convection from the surfaces. The simple theory already stated ignores the heat convection.

Agreement between the full computed values and the two asymptotic lines is very good. The two lines meet when $Tn = T\infty$ i.e.

$$\frac{q}{kL}\left(\frac{\kappa t}{\pi}\right)^{\frac{1}{2}} = \frac{q}{2Lh_c}$$

or $$h_c = \frac{k}{2}\left(\frac{\pi}{\kappa t}\right)^{\frac{1}{2}} \qquad \ldots\ldots (4.7)$$

Hence according to this equation it should be possible to obtain the heat transfer coefficient by plotting the increase in temperature and determining where the two asymptotic lines intersect.

4.3 Measurement of blank temperature in gears and discs

Experiments to record the behaviour of blank temperatures of actual gears and discs were conducted on the gear machine described in section 3.7 and the Amsler disc machine, section 3.8. In the case of the disc machine, surface temperatures of the discs were recorded by a trailing thermocouple of the type detailed in section 3.9.2. The disc material was case hardened EN 34 steel with a thermal conductivity of 25 Btu/ft^{o}Fhr and a

diffusity of .5 ft^2/hr. Simultaneous measurement of the friction torque was possible on the disc machine as previously mentioned.

A surface thermocouple of the type detailed in section 3.9.1 was used to measure the blank temperature of the gears. Although the transmitted torque in the gear machine was known this was not representative of the friction force at the sliding teeth in mesh and so an estimation of coefficient of friction was made using one of the empirical equations quoted in section 2.2 of this thesis.

By displaying all the temperatures on a timed chart recorder, the behaviour of the blank temperature with time could be examined. A typical trace, for the disc machine is shown in fig. 4.5 with the frictional torque superimposed upon it.

A rapid rise in blank temperature is observed in the first few minutes followed by a gradual increase after two or three hours of running. With this variation in blank temperature, it would be reasonable to expect a set of gears that may have been running satisfactorily for up to one hour, to scuff after prolonged operation at the same load and speed. O'Donoghue (14) reported the scuffing results of Fowle, where a noticeable dependence of scuffing load with time of test was noticed.

The measurement of blank temperature is often overlooked but its importance is once more indicated. With the blank temperature increasing with testing time, a lower flash temperature is required to raise the total contact temperature to equal the critical temperature of the lubricant.

4.4 Application of theory to the blank temperature results

Replotting the temperature rise against time on a log-log scale in fig. 4.6 for the disc machine and in fig. 4.7 for

the gear machine, produces curves resembling those predicted by Cameron, Gordon, and Symm (46). Temperature rise above ambient is plotted in preference to actual surface temperature, so that a comparison may be made with theory, where the non-dimensional temperature referred to that above ambient.

From Eq. (4.6) an asymptote having a gradient of $\frac{1}{2}$ may be drawn to the curves and made to intersect with the asymptote representing the steady state temperature previously described.

By substituting in Eq. (4.6) for the temperature rise in a given time along the asymptote, a value for the heat injected into one body per unit area (i.e. $2\frac{q}{L}$) is determined. This is half the energy dissipated at the contact since equal partition of heat is assumed.

Substituting the values of time t at the points of intersection of the asymptotes into Eq. (4.7) produces values of the heat transfer coefficient, hc.

It is interesting to note that Eq. (4.6) suggests that $T/t^{\frac{1}{2}}$ is constant for the asymptote and that by plotting the temperature against the square root of time, the position of the asymptote would be determined by that part of the curve having a constant slope. Redrawing the temperature curves to the base of $\sqrt{t}$ produces a series of curves fig. 4.8 and 4.9, each with three linear portions. It is difficult to decide which straight portion relates to the asymptote given by Eq. (4.6). The asymptote to the initial slope of the curve, where the convection has little or no effect on the build-up of temperature, passes through the origin. The theoretical asymptotes however show maximum agreement with the full theory at points removed from the origin.

If the second slope is chosen, the agreement between the

curve and the asymptote is obtained almost up to the steady state condition, where the convection plays an active role in the temperature behaviour and Eq. (4.6) cannot apply. The advantage, therefore, in viewing the results on a log - log scale is that the curves bear a resemblence to the theoretical curves and only one straight line satisfies Eq. (4.6).

The results so obtained for the disc machine can be checked directly from the measured torque and sliding velocity. The value of $q/2L$ is calculated from the expression:-

$$\frac{q}{2L} = \frac{\text{(Friction torque) (Sliding velocity)}}{2\,\pi(\text{disc diam.})^2\,\text{(disc width)}}$$

The sliding speed between the discs is built-in as 10% of the lower disc speed.

The heat transfer coefficient corresponding to both the heat input and the measured steady operating temperature of the disc is obtained by applying Newton's law of cooling Eq. (4.1). The results so obtained are listed in Table 4.I where they compare well with the corresponding values from the experiments.

Table 4.I

Experimental results for the disc machine

N (rev/min)	tn (secs)	$Tn/t^{\frac{1}{2}}$ ($^{o}C/sec^{\frac{1}{2}}$)	hc ($Btu/ft^2.hr.^{o}F$)	$q/2L$ ($Btu/ft^2.hr.$)
500	600	.596	76.9 (55)*	2020 (1850)
325	1600	.155	43 (39)	525 (545)
250	2500	.104	39 (35)	352 (400)

* Values in brackets are those calculated from frictional torque readings.

The gear results fig. 4.7 show that whilst following the same trend as the disc results fig. 4.6 there is a slight deviation from the slope of the theoretical temperature - time curves. The theory cannot really be expected to hold for gears as the source strength is in no way constant over one tooth, due to variations in sliding speeds, and also the path of the heat flow is interrupted from tooth to tooth.

In the absence of a measure of the frictional force at the contact of gear teeth, it is not possible to perform the simple calculation to estimate the heat generated at the contact and the surface heat transfer coefficients, as it is for discs. The values obtained from the temperature - time curves may however be compared with approximate calculations based on the O'Donoghue and Cameron (9) expression for friction. The estimated coefficient of friction is then used to calculate the heat generation in a similar way to that with the discs. Subsequently, by further approximating the gear to a disc of outside diameter equal to the pitch circle diameter of the gear, an estimate of the heat transfer coefficient can be

obtained. The values are listed in Table 4.II for comparison with the experimental values.

Table 4.II

Experimental results for gear machine

N (rev/min)	Load (lbf/in)	t_n (secs)	f	$T/t^{\frac{1}{2}}$ ($^oC/sec^{\frac{1}{2}}$)	$q/2L$ ($Btu/ft^2.{}^oF.hr$)	($Btu/ft^2.hr$)
500	2338	110	.026	.58	1,960 (2,310)*	180 (200)
1000	2338	65	.019	.94	3,180 (3,250)	232 (210)
500	4676	37	.026	1.47	5,000 (4,620)	308 (230)
750	4676	25	.022	2.45	8,460 (5,760)	376 (215)

* Values in brackets are those calculated from assumed coefficient of friction f.

The difference in the values of heat transfer may be attributed to the assumptions on which the calculations are based and also to the fact that one gear tooth face never comes into contact with the mating gear.

A further consideration which applies to both gears and discs, but does not affect the comparison between theory and experiment, is the reference of the heat transfer coefficient to the rubbing surface of gear or disc. Included in this coefficient is the contribution to the overall heat loss, of the convection from the side faces of the gears or discs and the conduction of heat to other surfaces from which there is also convection.

No measure of the contributions of the respective heat transfer coefficients to the temperature of the surface entering the contact is indicated.

In conclusion, the thermal theory advanced in reference (46) may be used to predict the blank temperatures of discs and to some extent gears, provided the heat generation at the contact and the overall heat transfer coefficient referred to the rubbing surfaces are known. The approximate theory reported in this thesis shows that the converse is also true, that having a record of the blank temperature behaviour, the heat generation and the heat transfer coefficient may be determined.

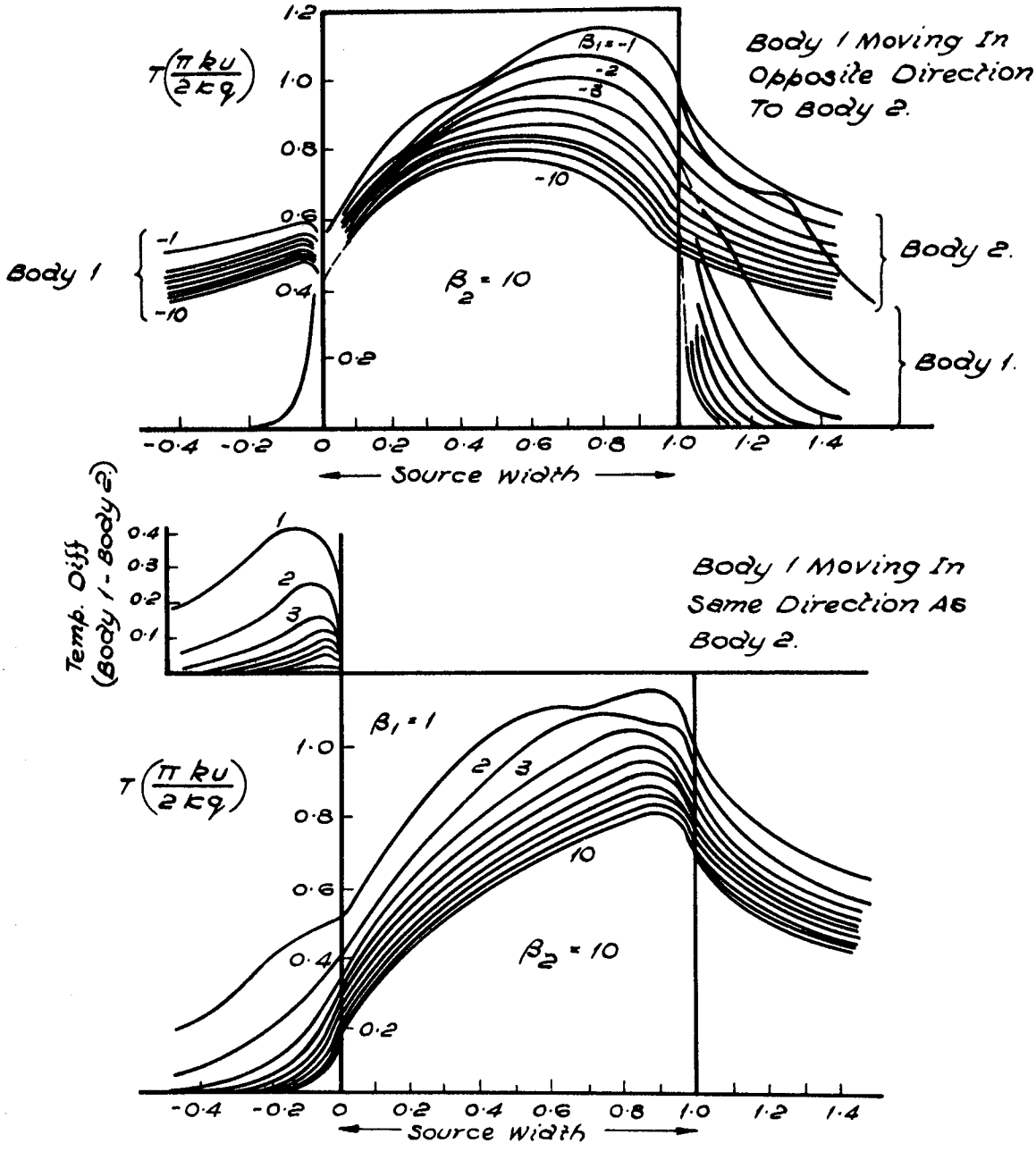

FIG. 4.1. SURFACE TEMPERATURES FROM REF. (46)

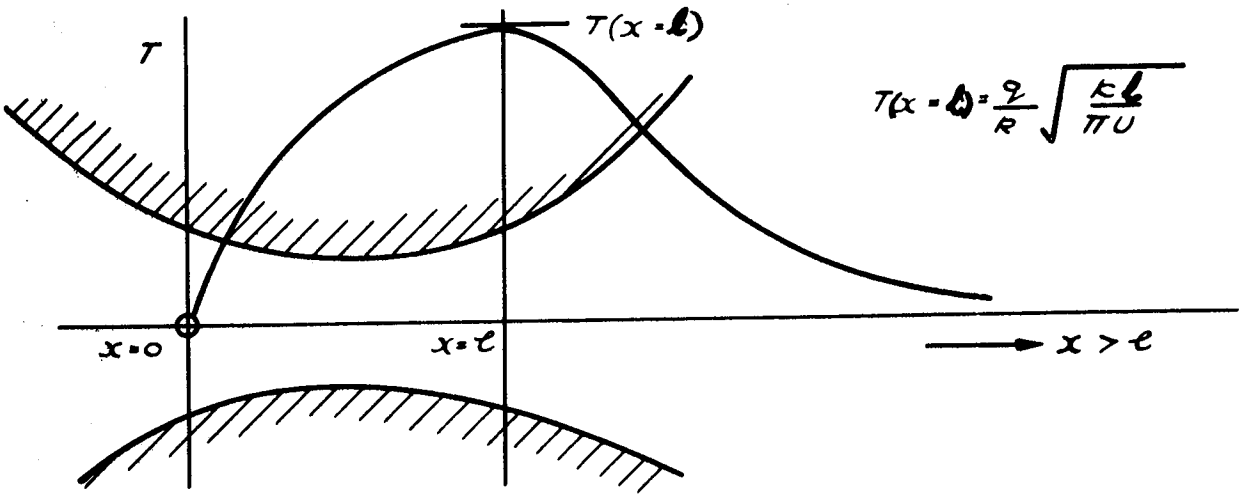

FIG. 4.2 (a) TEMPERATURE FOR ASYMPTOTIC SOLUTION FOR EQUAL PARTITION OF HEAT FROM REF. (46.)

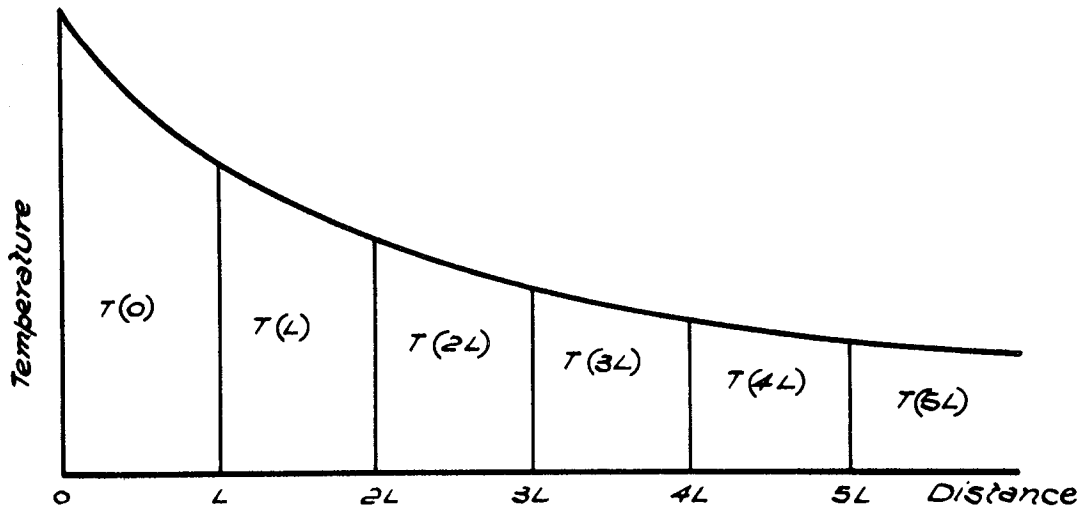

FIG. 4.2 (b) DECAY OF TEMPERATURE

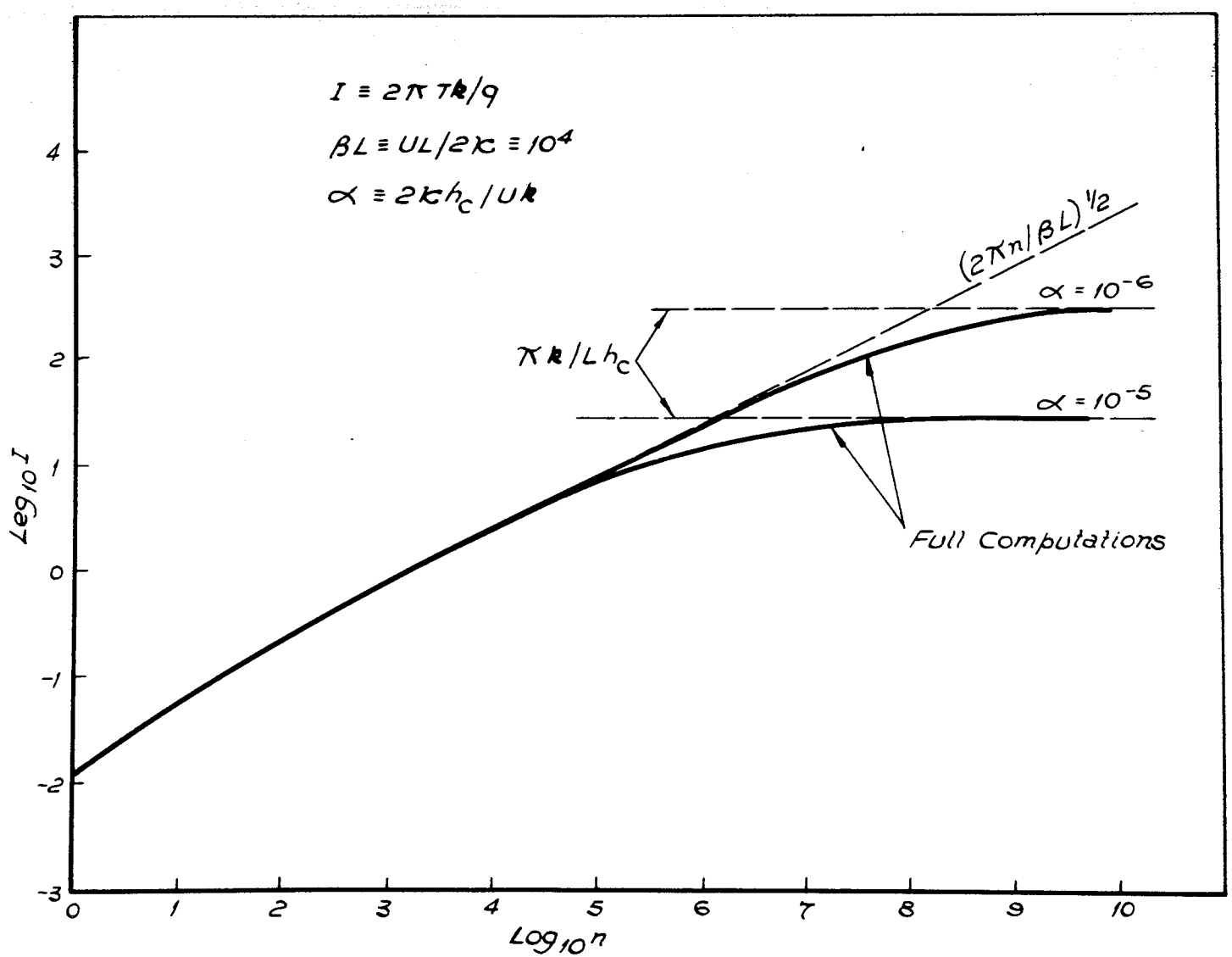

FIG. 4.3 COMPARISON OF ACCURATE & ASYMPTOTIC TEMPERATURES.

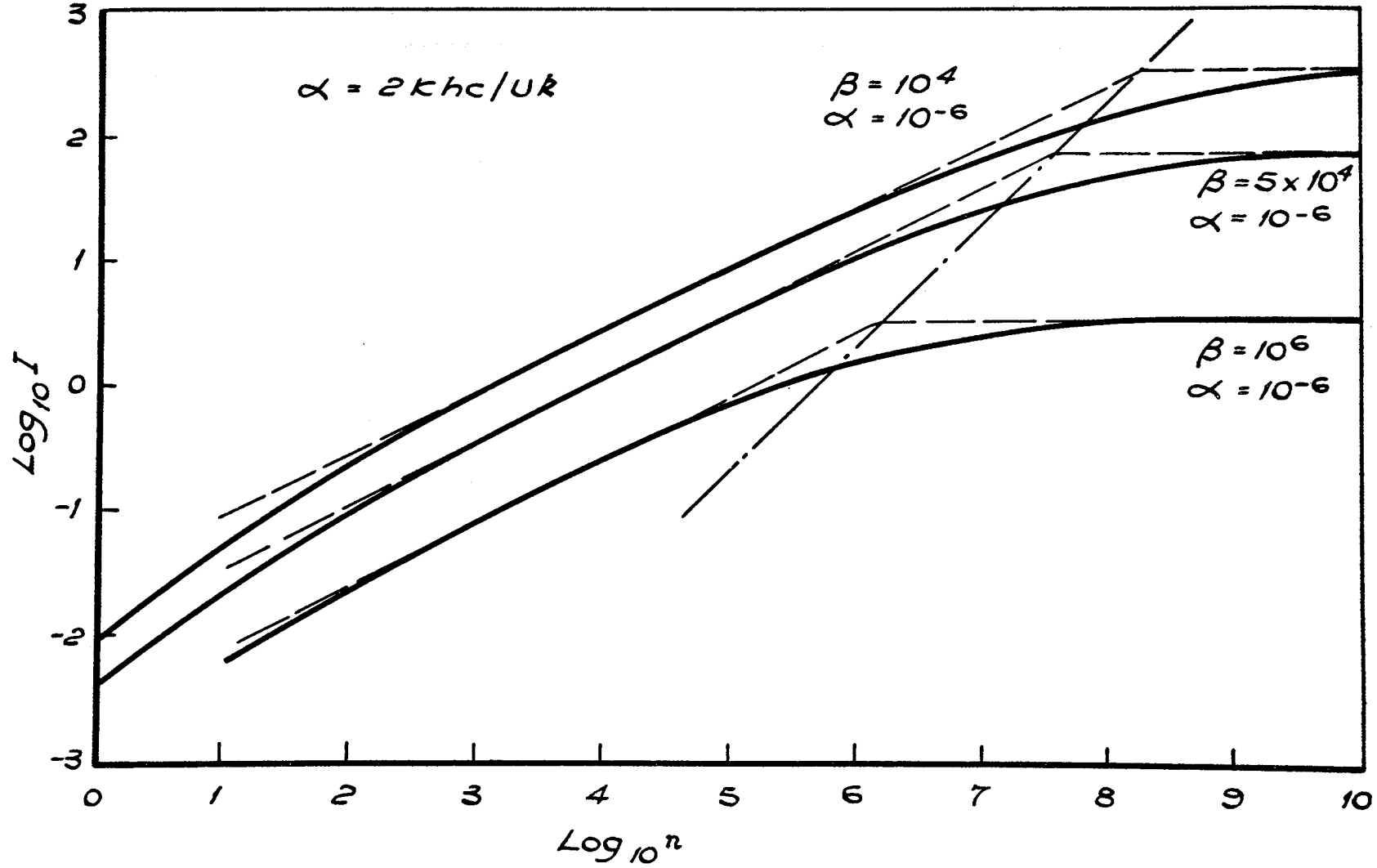

FIG. 4.4 THEORETICAL RESULTS OF CAMERON, GORDON, & SYMM (46)

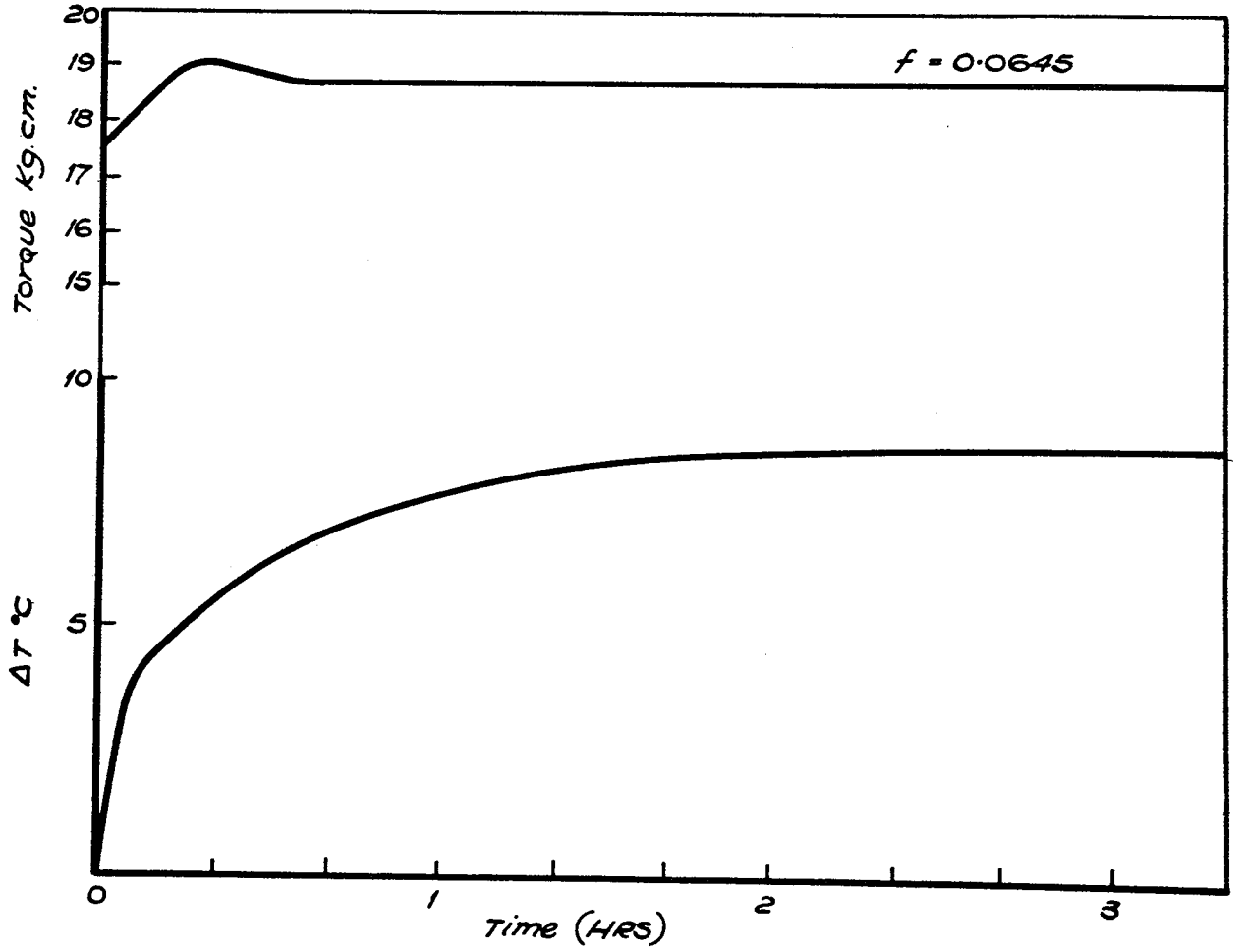

FIG 45 FRICTION FORCE MEASURED FOR DISC AT 325 REV/MIN.

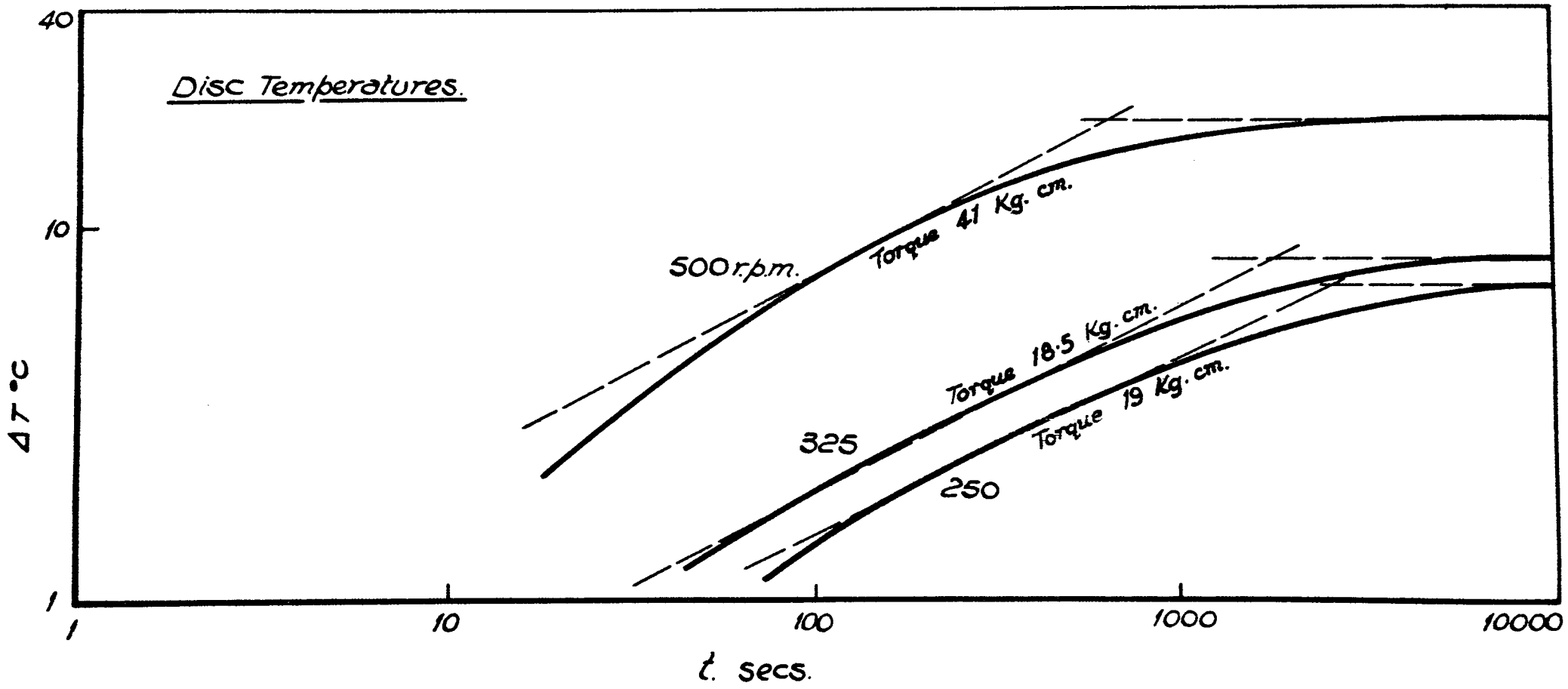

FIG. 4.6 TEMPERATURE RISE FOR DISCS AT VARIOUS SPEEDS.

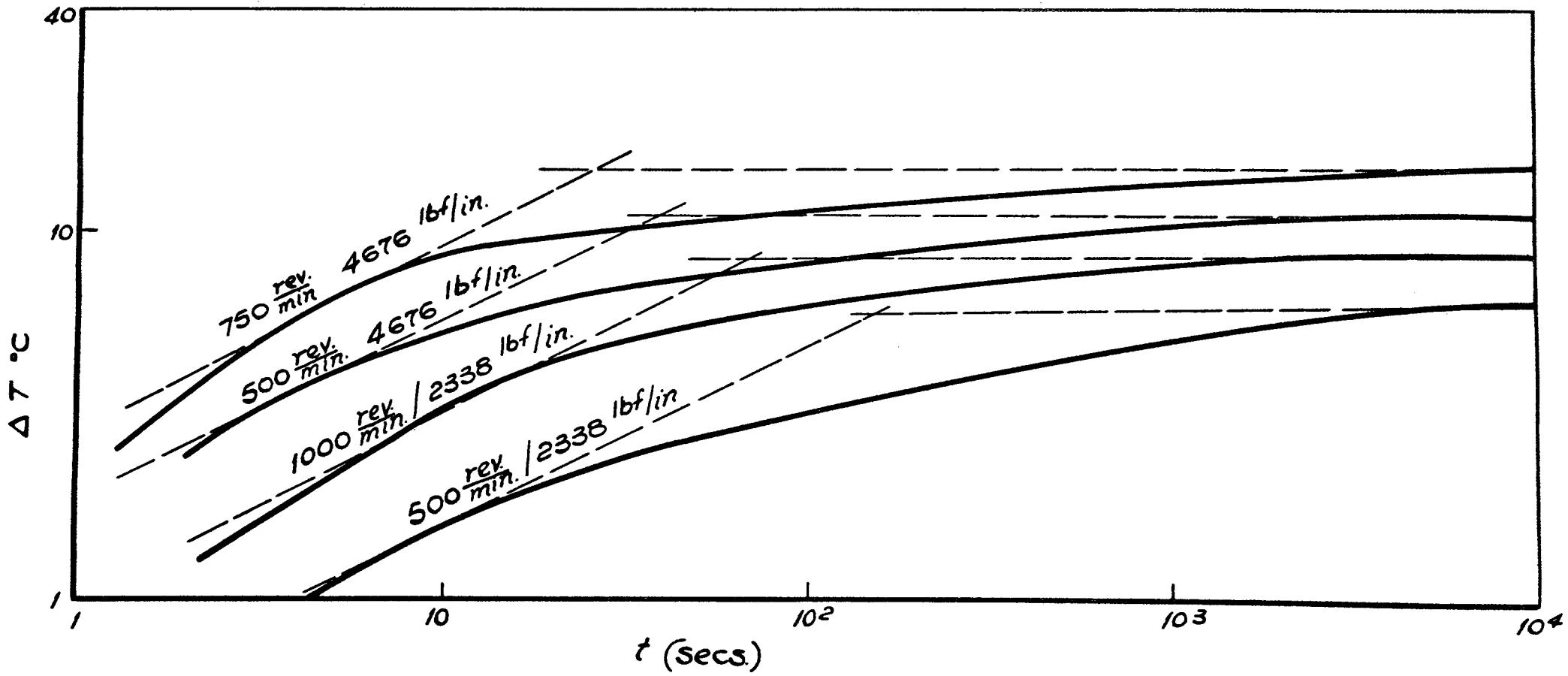

FIG. 4.7. GEAR MACHINE RESULTS.

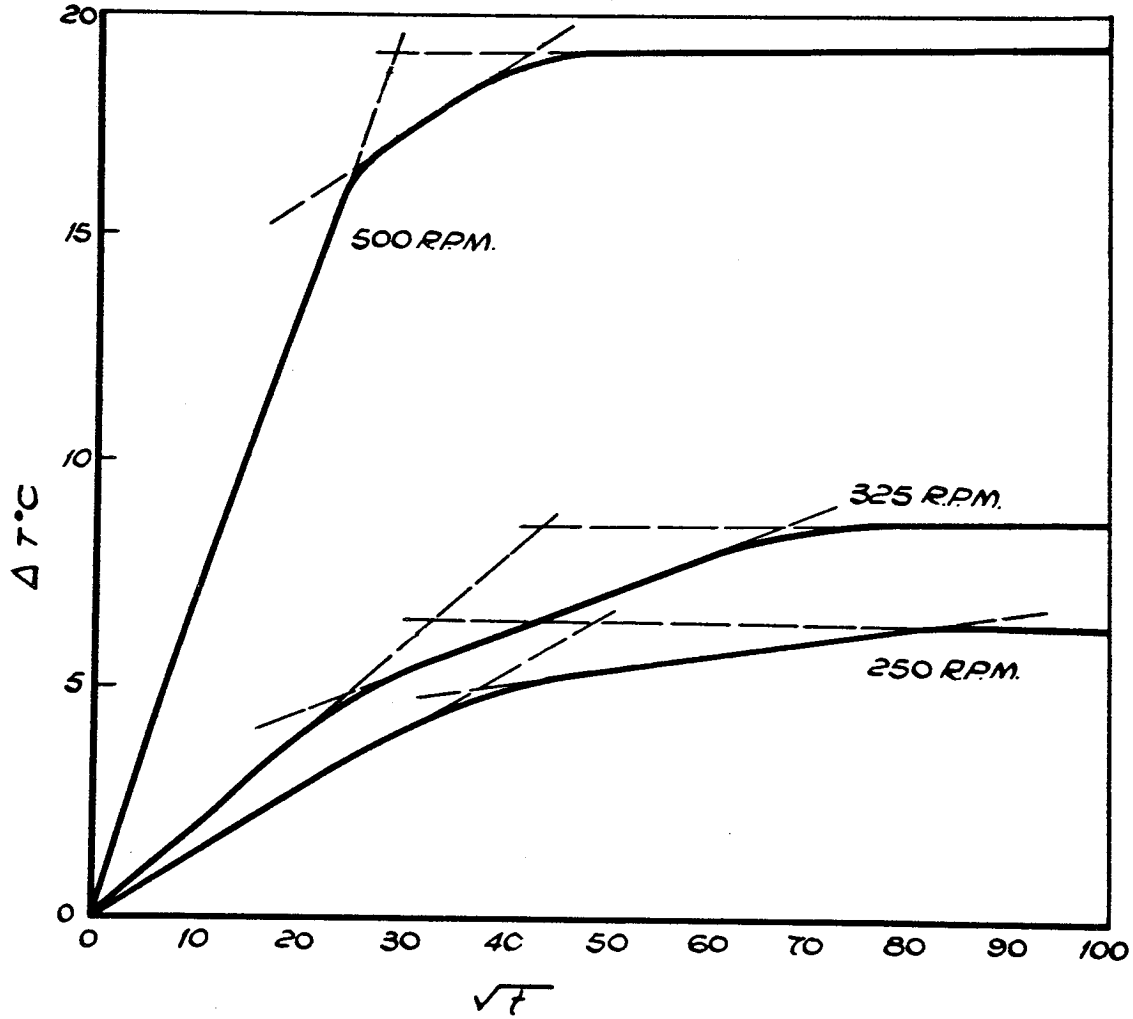

FIG.4.8 DISC TEMPERATURES AGAINST THE SQUARE ROOT OF TIME.

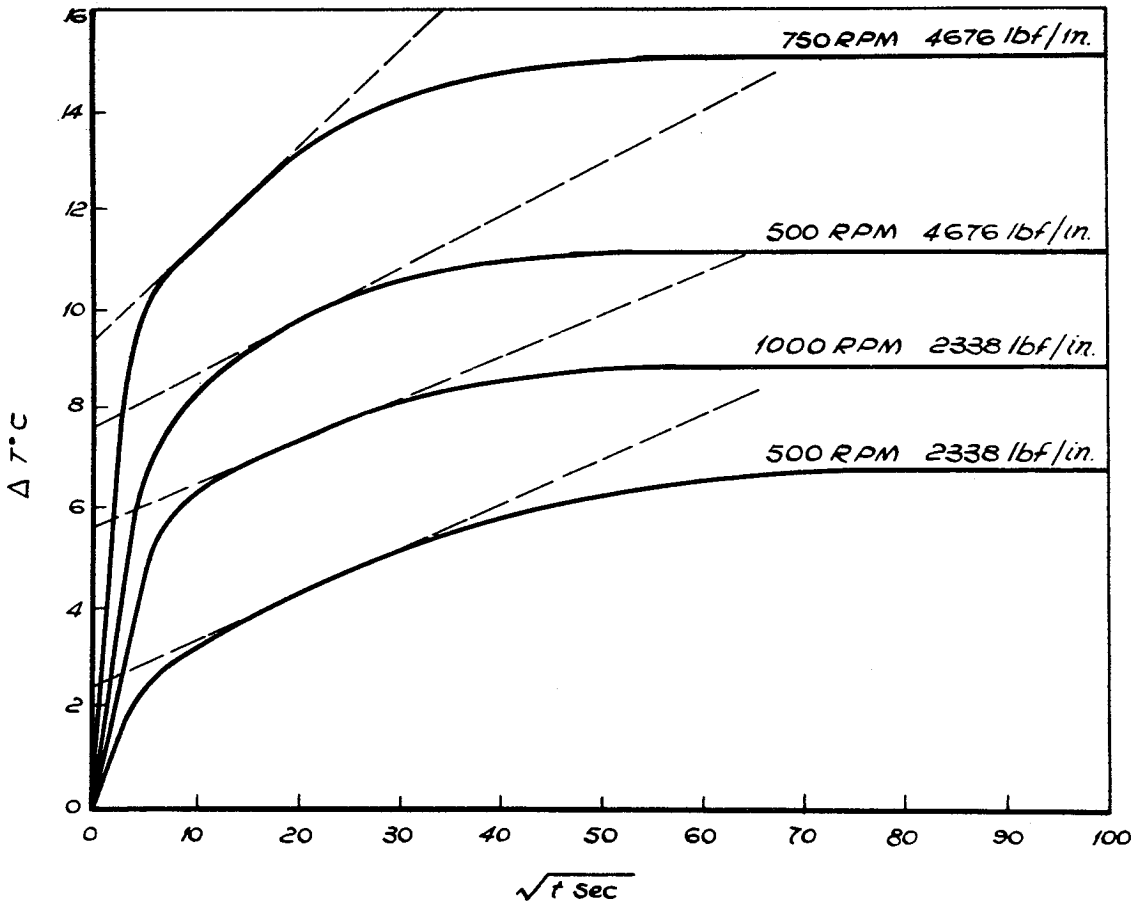

FIG 4.9 GEAR TEMPERATURES PLOTTED AGAINST SQUAREROOT OF TIME.

5.0 HEAT TRANSFER COEFFICIENTS

For the seizure of loaded machine elements having relative motion in the presence of a lubricant, it has been shown that the combination of load and speed to cause failure by scuffing is such that a critical temperature is attained at the contact. This temperature is the combined effect of the steady operating temperature of the machine components, referred to as the blank temperature, and the instantaneous rise within the contact, referred to as the flash temperature. If either of these temperatures can be reduced, the total contact temperature will be below the critical value and seizure prevented. Alternatively, since the flash temperature is dependent upon load and speed, a reduction in the blank temperature will enable a higher flash temperature to be endured before seizure occurs. This in turn means that the machine elements may carry greater loads or operate at higher speeds.

The blank temperature has been shown to depend on the heat injected into the contacting surfaces and also upon the heat transfer coefficient from the surfaces of the machine component. In the case of gears and discs the surfaces consist primarily of discs and cylinders, very often enclosed in a casing and either immersed in or sprayed with a lubricant.

In order to assess the blank temperature of a gear or disc it is necessary to know the heat transfer coefficient pertaining to the particular operational conditions.

A considerable amount of well established heat transfer expressions for discs and cylinders are available although the overall problem of heat injection, conduction, and convection is not yet solved for the particular case of lubricated gears or discs.

5.1 Heat Transfer Coefficients from Isolated Cylinders

For a stationary cylinder in an infinite environment of homogeneous fluid, the relationship between Nusselt Number and the product of Grashof and Prandtl Numbers is given as

$$Nu = 0.53\ (Gr.\ Pr)^{0.25}$$

after McAdams (48) where Nusselt Number represents the convective heat transfer coefficient referred to the diameter of the cylinder and the Grashof and Prandtl Numbers are calculated from the properties of the fluid taken at the mean temperature of the cylinder surface and the surrounding fluid. A further relationship was later given by Etemad (49) as

$$Nu = 0.456\ (Gr.\ Pr)^{0.25}$$

For a rotating cylinder, Anderson and Saunders (50) show that there is little change in the heat transfer coefficient as the rotational Reynolds Number of the cylinder is increased to a value of 10^3. At this value a transition occurs whereupon a further increase in Reynolds Number produces an increase in Nusselt number according to the expression:-

$$Nu = 0.1\ Re^{0.67}$$

This result is reproduced in fig. 5.1(a) Etemad produced a similar relationship,

$Nu = 0.076\ Re^{0.7}$ and also illustrated how the Grashof Number influenced the nature of the transition from the free convection to the second regime of continuous boundary layer around the cylinder. Although transition commenced at about $Re = 10^3$ for all Grashaf Numbers, it was not complete until a Reynolds Number of about 10^4 had been reached. The resulting expression, taking into account the Grashof Number is as follows:-

$$Nu = 0.11 \left\{ (\tfrac{1}{2}Re^2 + Gr)\ Pr \right\}^{0.35}$$

for $Re > 10^3$. The results of Etemad are summarised in fig. 5.1(b).

Kays and Bjorklund (51) derived an empirical relationship for the case of an isolated cylinder rotating in a cross-flow. At low rotational Reynolds Numbers the results agreed with the expression given by McAdams for a crossflow on a stationary cylinder, i.e. $Nu = 0.24\ Re_c^{0.6}$ for $10^3 < Re_c < 5 \times 10^4$. Transition from the free convection regime again commenced at $Re = 10^3$ and extended to somewhere between $Re = 10^4$ and $Re = 5 \times 10^4$, depending upon the crossflow Reynolds Number. The transition zone terminated and the continuous boundary layer formed at a rotational Reynolds Number of about twice the crossflow Reynolds Number. This coincided with the potential flow solution for circulation, for the point where the circulation was sufficiently strong for the two stagnation points to meet and become detached from the cylinder. The curves are reproduced in fig. 5.2 where the results are correlated by

$$Nu = 0.135 \left\{ \left(\tfrac{1}{2} Re^2 + Re_c^2 + Gr\right) Pr \right\}^{1/3}$$

5.2 Heat Transfer Coefficients from Isolated Discs

For a stationary disc with its axis in the horizontal position McAdams (52) gives the following relationship:-

$$Nu = 0.59\ (Gr.\ Pr)^{\frac{1}{4}}$$

for $10^4 < Gr.\ Pr < 10^9$

where the convection flow is laminar, and

$$Nu = 0.13\ (Gr.\ Pr)^{1/3}$$

for tubulent flow $10^9 < Gr.\ Pr < 10^{12}$

The Grashof Number is based on the diameter of the disc and transition from laminar convection to turbulent flow occurs

at $Gr = 4 \times 10^8$.

Richardson and Saunders (53) give the expression

$$Nu = 0.4 (Gr. + Re^2)^{\frac{1}{4}}$$

to represent the heat transfer from a rotating disc for the range $10^6 < (Gr. + Re^2) < 10^9$, the laminar region. Cobb and Saunders (54) derived the following empirical relationship for the turbulent region:-

$$Nu = 0.015 Re^{0.8}$$

which agrees quite well with the Von Karmann analogy between temperature and tangential velocity within the boundary layer (55). These results are given in fig. 5.3.

5.3 The Effect of Nearby Stationary Plates and Enclosures

Richardson and Saunders (53) investigated the effect of a nearby stationary plate on the heat transfer from the side of a disc. It was found that a stationary plate of diameter smaller than that of the disc had no significant effect upon the heat transfer, merely affecting the axial inflow towards the disc. Measurements on a disc rotating near a stationary plate having a diameter equal to or greater than that of the disc showed that the heat transfer was affected only when the distance of separation was reduced to less than one disc diameter.

As the stationary plate was brought from infinity towards the rotating disc, the flow required for continuity of flow over the disc surface had to enter via a progressively narrowing gap. Eventually, the resulting reduction in pressure in the space between the disc and plate caused the disc outflow to attach itself to the plate and produce a recirculatory pattern. This is illustrated in fig. 5.4(a).

Richardson and Saunders observed that the heat transfer coefficient from the disc-plate combination was reduced by a reduction in the separation distance, fig. 5.4(b). This represented the overall heat transfer dependent upon the heat transfer from the disc to the air flowing over its surface and also upon the heat transfer from the recirculating flow to the stationary plate followed by convection to the surroundings from the other side of the plate. It was observed that the temperature of the axial inflow to the disc was higher in the presence of a stationary plate and just as Cobb and Saunders' results (54) were corrected by taking account of the temperature within the large enclosure rather than the room temperature (53), the inflow temperature to the disc may be used to estimate the heat transfer from the disc.

The actual temperatures are not published but the effect of including this factor would be to produce a relationship between the disc heat transfer and the separation lying above the curve on fig. 5.4(b) and possibly showing an increase in heat transfer with separation distance.

A very important point emerges from these considerations in that the two heat transfer coefficients may be considered separately in order to assess the effect of any change in the physical conditions of either the disc or the plate.

O'Donoghue (14) in his heat transfer of gears studies observed a higher heat transfer coefficient for a cylindrical surface rotating in an enclosure.

At low rotational Reynolds Numbers, the expression

$Nu = 10.8\ Re^{0.25}$ gave greater heat transfer coefficients than the McAdams expression for an isolated stationary cylinder but above $Re = 10^5$, the behaviour agreed

with the Anderson and Saunders relationships for the continuous boundary layer regime of a rotating cylinder.

The cylinder diameter was 5" and enclosed in an 8" sided box. By varying the box size a dependence of heat transfer coefficient on box size was detected and by flow visualisation techniques, a flow pattern within the enclosure was observed. varying with the rotational Reynolds Number.All heat transfer coefficients were calculated for the cylindrical surfaces by reference to the mean air flow temperatures within the box.

O'Donoghue (14) also produced an expression for the heat transfer from a gear surface. The surface represented a 5" P.C.D. 6 DP gear in an enclosure and exhibited higher heat transfer coefficients than the equivalent diameter disc.

$$Nu = 12\ Re^{\frac{1}{4}} \quad \text{for } 2.5 \times 10^3 < Re < 4.5 \times 10^4$$

Above $Re = 4.5 \times 10^3$, $Nu = 0.145\ Re^{2/3}$.

The results are summarised in fig. 5.5.

The higher coefficients for the gears were explained on the grounds of increased turbulence in the tooth spaces.

The one inch face-width specimens used by O'Donoghue were flanked by asbestos plates either side. Whilst this confined the convection to the "cylindrical" surfaces of the specimens, distortions of the temperature profiles in the air were experienced due to the air flow over the asbestos side plates. A further comment made by O'Donoghue was that whilst the heat transfer coefficient was increasing with reduction in box size, the surface temperatures were increasing. This implied that the overall heat transfer coefficient was reducing, so a reduction in the box temperatures was necessary in order to gain an overall heat transfer improvement. This could possibly be effected by forced cooling to the outside of the box.

A further implication of the rising air temperatures however is made apparent by reference to fig. 5.1(b) where Etemad showed an increase in heat transfer for higher Grashof Numbers. With the higher surface temperatures it is likely that the Grashaf Number is varying and affecting the flow of air inside the box, and consequently the heat transfer coefficient from the cylinder.

If an experiment is aimed at producing information for the idealised infinite cylinder then a large length to diameter ratio specimen is necessary so that temperature measurements are uniform in the axial direction. Secondly if the Nusselt Number - Reynolds Number characteristic is to be investigated for the effect of different enclosure sizes, then all other parameters such as Grashof Number and Prandtl Number should be maintained at a constant value.

5.4 The Heat Transfer Apparatus

The apparatus shown in fig. 5.6 consists of a 1.5 inch diameter shaft passing through a perspex enclosure such that the shaft can be rotated within the enclosure whilst supported as shown. The length of the shaft inside the perspex box is maintained at 9 inches for each box size of 15 inches, 6 inches and 2 inches. A micrometer head and a setting screw mounted on sliding panels in the perspex walls enabled thermocouples to be adjusted to any position inside the enclosure. Two thermocouples embedded in the surface of the shaft, fig. 5.7 gave readings of surface temperature via a slip-ring assembly of the silver contact type and mounted at the driven end of the shaft.

The belt drive from a $\frac{1}{4}$ HP motor and Kopp variator via a series of pulleys gave a speed range of 50 - 1,000 rev/min

representing a maximum Reynolds Number of 6,000. Details of the shaft are given in fig. 5.8 where the construction of the heater between the asbestos insulating pieces is shown. The power to the heater was supplied via copper slip-rings built into an araldite end on the brass shaft.

.5 Preliminary Measurements of temperatures

With the 15 inch enclosure mounted onto the shaft, preliminary temperature measurements were made for a heat input of 18.8 watts. It was found necessary to allow one or two hours for conditions to stabilise after setting up the required conditions, particularly at the higher speeds where initial fluctuations in the air temperatures were experienced. The air temperatures around the cylindrical surface were uniform in the axial direction, except for a slight temperature gradient thought to be due to variations in the coil spacing of the internal heater and a certain amount of "end-effect" near and owing to the side-walls. Figs. 5.9(a), (b), (c), and (d) give the boundary layer temperatures extending up to 1.5 inches away from the top and sides of the cylinder at various speeds.

For free convection, the air temperatures at the sides of the cylinder resemble the typical boundary layer temperature distribution of air accelerated over a surface by the buoyancy forces produced as a result of the change in density on heating. At the top surface, there is separation of the boundary layers and the formation of a convection chimney. This is indicated by the temperature measurements, fig. 5.9(a). Rotation of the cylinder aids the upward flow of air at the upward moving side of the cylinder and decreases the rate of growth of the boundary layer there. The resistance to heat

flow is thereby reduced and the temperature gradient increased. On the downward-moving side, the peripheral speed of the cylinder is opposing the free convection flow and producing an increase in the boundary layer thickness. Here there is an increase in the heat flow resistance and a reduction in the temperature gradient. These features are confirmed by comparing fig. 5.9(a) with fig. 5.9(b) and are in agreement with the findings of Anderson and Saunders (5).

A further consequence of the changes in velocities of the two boundary layers is that the stagnation points and hence the convection chimney or wake is moved in the direction of rotation so that the top side temperature traverse does not detect a convection chimney. At increased rotational speeds, the convection chimney is carried further round the cylinder until a speed is reached at which it becomes coincident with the side of the cylinder. Meanwhile, the top of the cylinder has shown the same reduction in boundary layer with subsequently higher temperature gradients fig. 5.9(c). Above this critical speed, the stagnation point is moved away from the cylinder and a continuous boundary layer is formed around the cylinder which although increasing in thickness, experiences a reduction in the thickness of the laminar sub layer with increase in speed and hence reduces the resistance to heat flow.

Various authors (49, 50, 51) have observed the same behaviour and of particular interest are the conclusions drawn by Kays and Bjorklund (51) for the case of cylinder rotation in a crossflow. Under these conditions separation of the boundary layer occurred nearer the sides of the cylinder than in the free convection case. Two equal vortices were produced, one of which was strengthened by rotation of the cylinder

whilst the other weakened. At a rotational speed producing a peripheral cylinder velocity equal to about twice the crossflow velocity, the weaker vortex disappeared completely and the stagnation point reached the 90 degree position to the direction of cross-flow. Further increase in rotational speed produced a continuous boundary layer around the cylinder with resulting increases in heat transfer due to reductions in thickness of the laminar sub-layer.

Having thus established the behaviour of the air temperatures around the cylinder within the enclosure, the equipment was used to assess heat transfer coefficients from the cylinder for various conditions of rotational speed, cylinder surface temperature, and box size.

.6 Discussion of Heat Transfer Results

Fig. 5.10 gives the variation of Nusselt Number with Reynolds Number for different Grashof Numbers. The Grashof Number is varied by adjusting the heat input to the shaft, thereby varying the surface temperature of the shaft and the local properties of the air. Upon rotation of the cylinder there is eventually an increase in the heat transfer coefficient which lowers the Grashof Number slightly, as shown in the sample results given in Appendix V. Henceforth, Grashof Number will refer to the zero or low-rotational value.

For each Grashof Number the curves follow the same trend, at first showing a slight reduction in Nusselt Number, as the Reynolds Number is increased up to 1,000, followed by an increase in Nullelt Number proportional to Reynolds Number to the power of one quarter. For higher Grashof Numbers, the curves lie above those for lower Grashof Numbers

but indicate that eventually they meet the Anderson and Saunders line shown in the figure. This line is the relationship between Nusselt Number and Reynolds Number for a cylinder possessing a continuous boundary layer. The Nusselt Number increases as Reynolds Number to the power of two thirds and whatever the Grashof Number, the cylinder exhibits the same Nusselt Number once the transition from free convection to a continuous boundary layer is complete.

The higher Nusselt Numbers resulting from increased Grashof Numbers at low Reynolds Numbers are however to be expected when the nature of the convection is considered. With increased Grashof Number, there will be an increased rate of flow past the cylinder which although increasing the turbulent boundary layer thickness reduces the thickness of the laminar sublayer and hence the thermal resistance. This problem has been investigated by McAdams (48) and Etemad (49) who have produced empirical relationships between Nusselt Number and the product of Grashof and Prandtl Numbers. A comparison of the free convection results in the 15 inch enclosure and the expressions for isolated cylinders is given in fig. 5.11. The points lie above the $^{B}/_{D} = \infty$ line and further free convection results for $^{B}/_{D} = 4$ and $^{B}/_{D} = {}^{4}/_{3}$ are also included. A family of curves are produced that show an increase in Nusselt Number with (Gr x Pr) for each $^{B}/_{D}$ ratio, with lower $^{B}/_{D}$ ratios producing higher Nusselt Numbers at the same Grashof Number.

Figs. 5.12 and 5.13 give the Nusselt Number versus Reynolds Number relationship for different $^{B}/_{D}$ ratios at approximately the same Grashof Number. There emerges a marked dependence upon the enclosure size which suggests the

formation of a self-induced flow pattern whereby part of the kinetic energy imparted to the convection chimney leaving the cylinder is retained. Whereas the kinetic energy of the convection flow from a cylinder in an infinite environment will be dissipated to the atmosphere, an enclosure will conserve part of the velocity by deflecting the upward convection flow into two streams passing down the enclosure walls to the bottom wall. The flow is then deflected upwards to the cylinder with a retained velocity. This produces an effective crossflow to the cylinder, with a velocity depending upon the buoyancy forces at the cylinder, the buoyancy forces at the enclosure walls and the skin friction of the walls.

For larger Grashof Numbers the acceleration of the convection flow is greater, resulting in an increase in the retained velocity of effective crossflow. Stable conditions are attained when the acceleration of the flow due to buoyancy forces equalises the deceleration due to skin friction. A reduction in enclosure size has the effect of reducing the amount of skin friction by reducing the length of the flow path at the enclosure walls. The retained kinetic energy is thus much greater and hence a larger crossflow velocity is experienced. This in turn re-establishes a higher skin-friction and retains equilibrium. The reduced area of the enclosure also has the effect of reducing the heat transfer to the atmosphere, with a consequent increase in cylinder and air temperatures within the enclosure. This affects the mean properties of the enclosed air and the Grashof Number reduces thereby reducing the extent of the increase in crossflow velocity.

The proposed flow pattern of reference 14 is reproduced in fig. 5.14, where the convection flow is developed into fully

rotational flow.

At one side of the cylinder, where the surface is moving upwards, the natural velocity is increased by the surface velocity, whilst on the other side, where the surface is moving downwards, the natural velocity is decreased so that the total flow pattern is distorted. The distortion increases with surface velocity until the stagnation point moves to the downward side of the cylinder, after which Couette type motion occurs. In this condition, a continuous boundary layer at the cylinder is formed and the enclosure size will have little or no effect on the heat transfer from the cylinder. Moreover, the heat transfer would be expected to be the same as for the isolated cylinder and hence agree with the Anderson and Saunders relationship. The enclosure size does however affect the nature of the flow in the intermediate transitional zone where the heat transfer coefficient has reached a minimum at Re = 10^3 and increases with Reynolds Number to the power of one quarter up to the point of formation of a continuous boundary layer.

If the hypothesis that there exists an effective cross-flow to the cylinder due to the convection flow and the enclosure walls is to be accepted, then it should be possible to estimate the crossflow velocity from the Nu vs. Re curves. The present curves resemble those of Kays and Bjorklund where the crossflow Reynolds Number was raised at known Grashof Numbers. At the point where the transitional zone met the Anderson and Saunders line, the rotational Reynolds Number equalled about twice the crossflow Reynolds Number (referred to the cylinder diameter). Reading off the points from the present curves, the free convection Nusselt numbers are

plotted against the estimated crossflow Reynolds Number and agreement obtained with the McAdams equation for crossflow fig. 5.15. All the experimental points above the critical Reynolds number, including the transitional zone, are included in the Kays and Bjorklund relationship

$$Nu = 0.135 \left\{ (\tfrac{1}{2}Re^2 + Re_c^2 + Gr)\ Pr \right\}^{1/3}$$

There is good agreement over the entire range of results, Fig. 5.16 and an indication that considerable crossflow is present as a result of the enclosure, thus confirming the hypothesis of O'Donoghue.

5.7 Application of heat transfer expressions to lubricated gears and discs

The existing expressions for the heat transfer from discs and cylinders have been extended to include the special case of cylinders rotating in enclosures.

The heat transfer coefficient from a disc or gear is seen to depend upon the fluid properties surrounding the disc, the rotational speed of the disc, and the amount of crossflow whether forced or self-induced by an enclosure.

A disc or gear consists of a cylindrical surface (in the case of a gear this may be considered to be corrugated) and two disc surfaces. The overall heat transfer problem consists of determining the amount of heat injected into the contact of each disc and then solving for the heat conduction to the disc and cylindrical surface. The heat flow to the respective surfaces will depend on the heat transfer coefficients at the various points on the surfaces and the solution for the surface temperatures appears to be complex. Elsewhere in this thesis a solution for the surface temperatures and heat flow into

the contacting surfaces is presented. Combining this with the heat transfer coefficients at the cylindrical and disc surfaces determined by the parameters listed above, it should be possible to obtain a temperature distribution for the whole disc. The temperature of the surface as it just enters the contact could then be obtained.

It should be noted that the heat transfer coefficients derived by the experiments detailed in this section have been obtained with air as the surrounding fluid. The results are presented as non-dimensional quantities which enable the prediction of heat transfer coefficients for discs and cylinders surrounded by other homogeneous fluids such as lubricating oils.

The results are valid for discs rotating fully immersed in a lubricant. Very often discs or gears rotate in casings in which the lubricant is drip-fed or sprayed onto the surfaces. The heat transfer from the surfaces then consists of the heat carried away by the oil flow and the heat convected from the surfaces to the surrounding air. The blank temperature results obtained on the gear machine were used to estimate the heat transfer coefficients of gears which were lubricated by drip-feed. It is interesting to compare these results with the heat transfer coefficients due to air only, as given in this section of the thesis.

Appendix VI provides the calculation of coefficients from the heat transfer equations, with the result that the air convection coefficient referred to the working surface of the gear is 6.8 Btu/ft^2.hr.$^\circ$F compared to the much larger measured value of 230 - 308 Btu/ft^2.hr.$^\circ$F. The difference arises from the heat carried away by the oil flow over the surface, effectively increasing the heat transfer coefficient.

This particular test was repeated with a known oil flow

and the oil inlet and outlet temperatures measured (there was a difference of about 2.5°F with the oil leaving at the same temperature as the gear surface). A heat balance shows that of the 227.5 Btu/hr, 14.7 Btu/hr is convected to the air whilst the remainder is carried away by the oil flow. In this drip-feed arrangement therefore, the oil flow (1.26 in^3/sec) provides the most important means of heat transfer.

Heat transfer coefficients, whether measured directly or by the blank temperature method, are a useful method by which to assess different methods of lubrication, including perhaps the recently introduced method of aerosol lubrication, and give a direct assessment of any means for reducing the operating temperature of machine components.

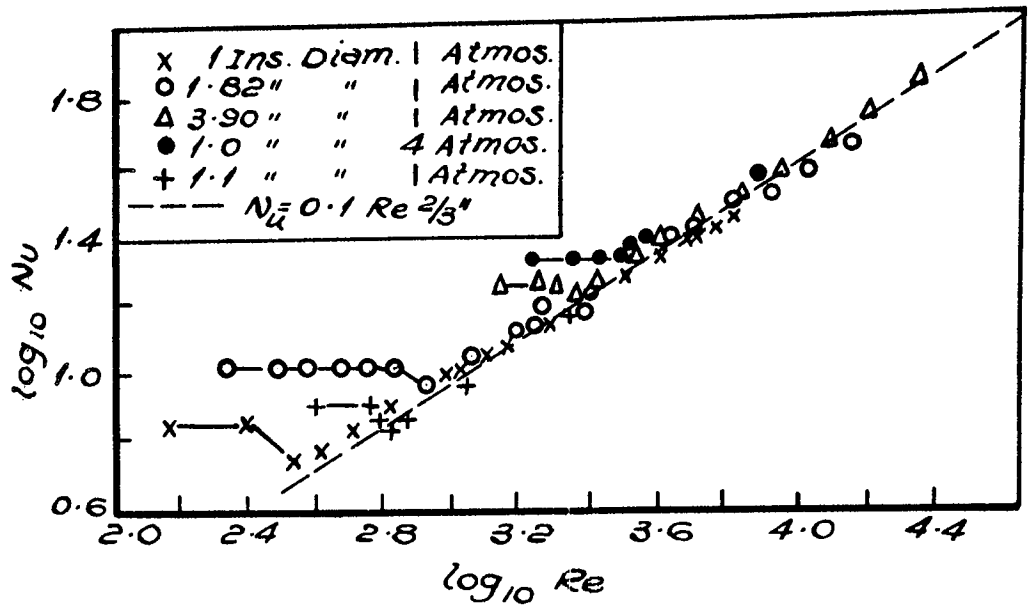

FIG. 5.1 (a) THE RESULTS OF ANDERSON & SAUNDERS (50)

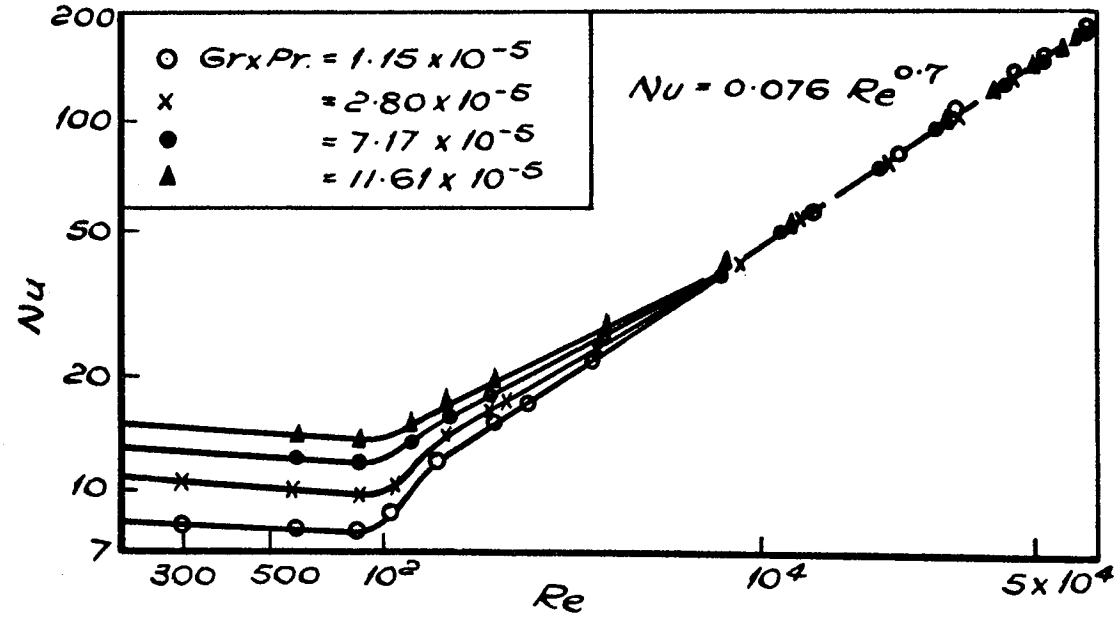

FIG. 5.1 (b) THE RESULTS OF ETEMAD (49)

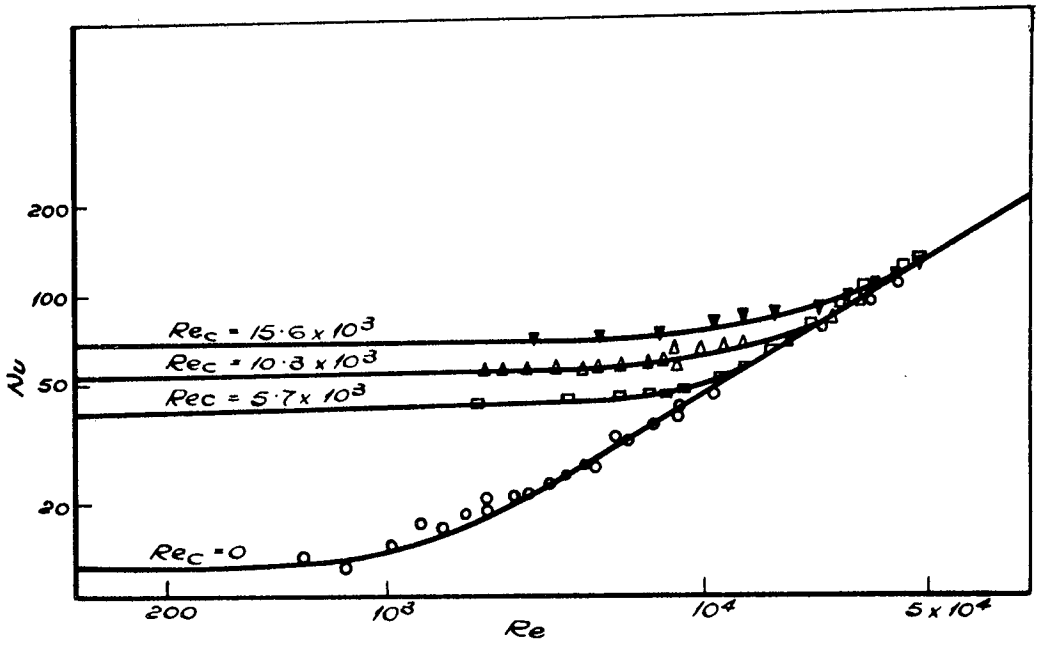

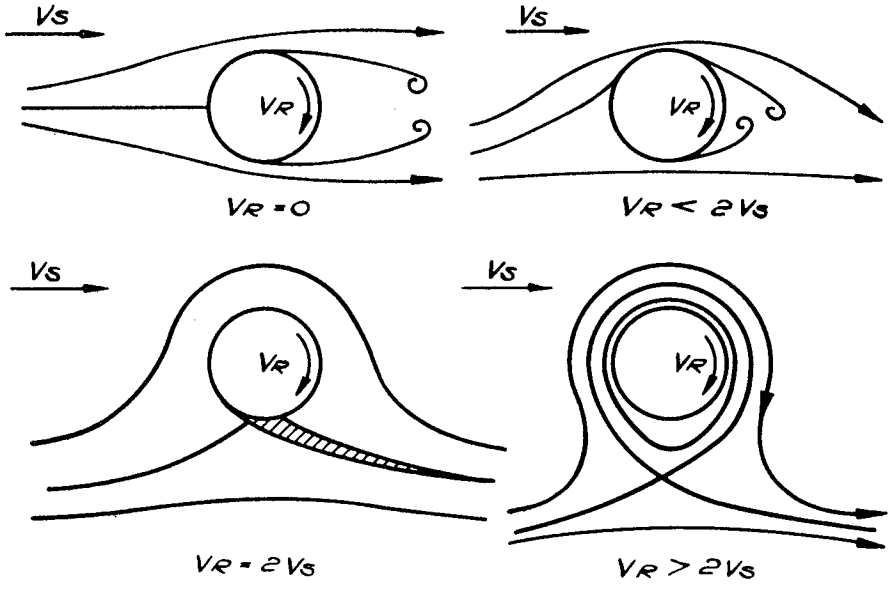

Probable Flow Patterns According to Ref. 51.

FIG. 5.2 SUMMARISED RESULTS OF KAYS & BJORKLUND

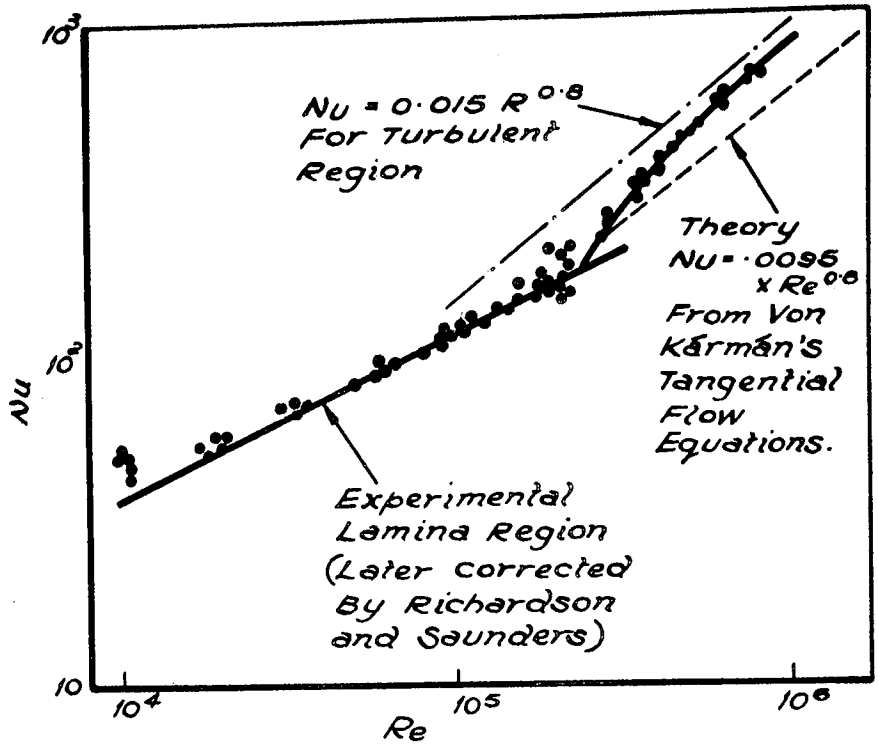

FIG 5.3(a) RESULTS OF COBB & SAUNDERS (54)

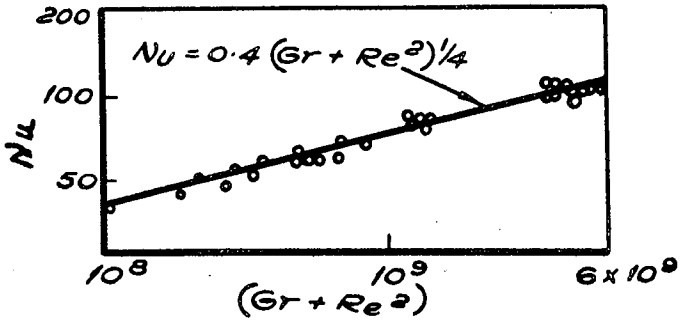

FIG 5.3(b) RESULTS OF RICHARDSON & SAUNDERS (53) INCLUDING CORRECTED POINTS OF REF (54)

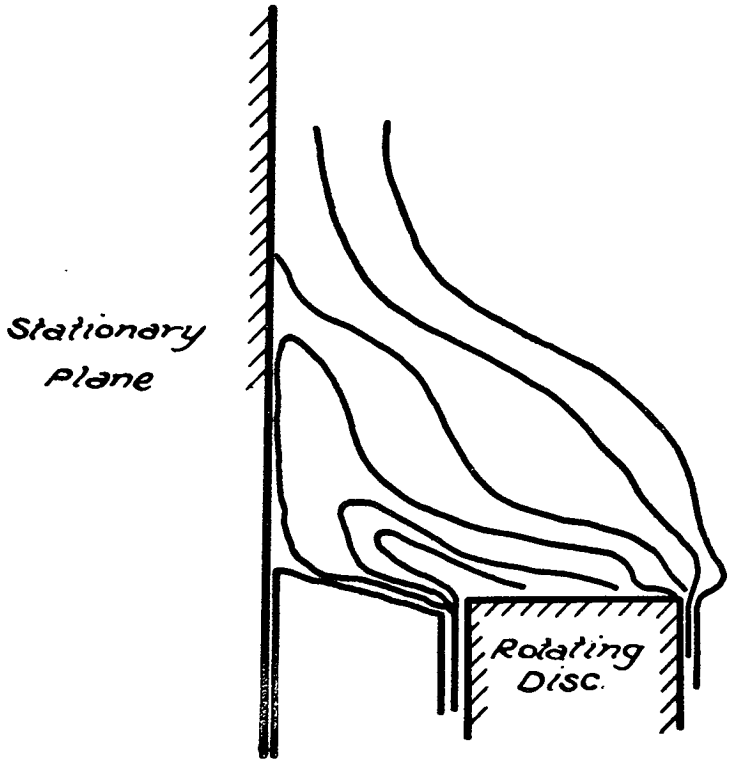

FIG. 54a ISOTHERMS OF FLOW IN VICINITY OF THE EDGE OF AN ISOTHERMAL HEATED DISC NEAR A PLANE REF. 53.

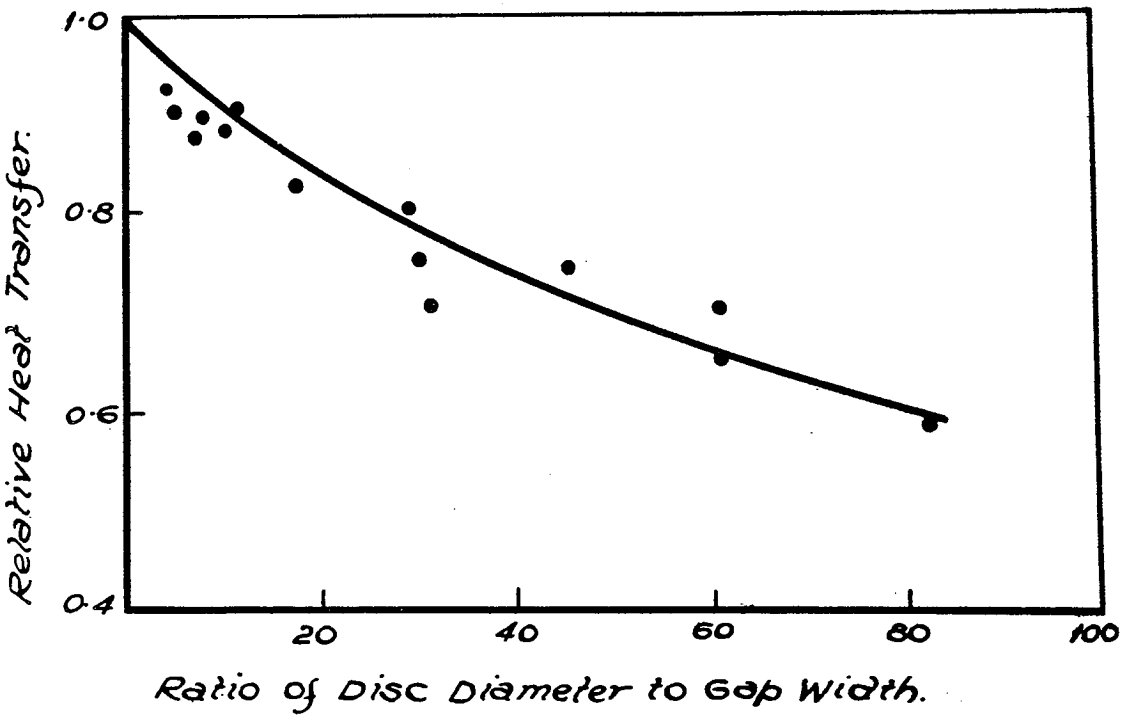

FIG. 54b THE HEAT TRANSFER FROM A SHROUDED SIDE OF A ROTATING DISC ACCORDING TO RICHARDSON & SAUNDERS 53.

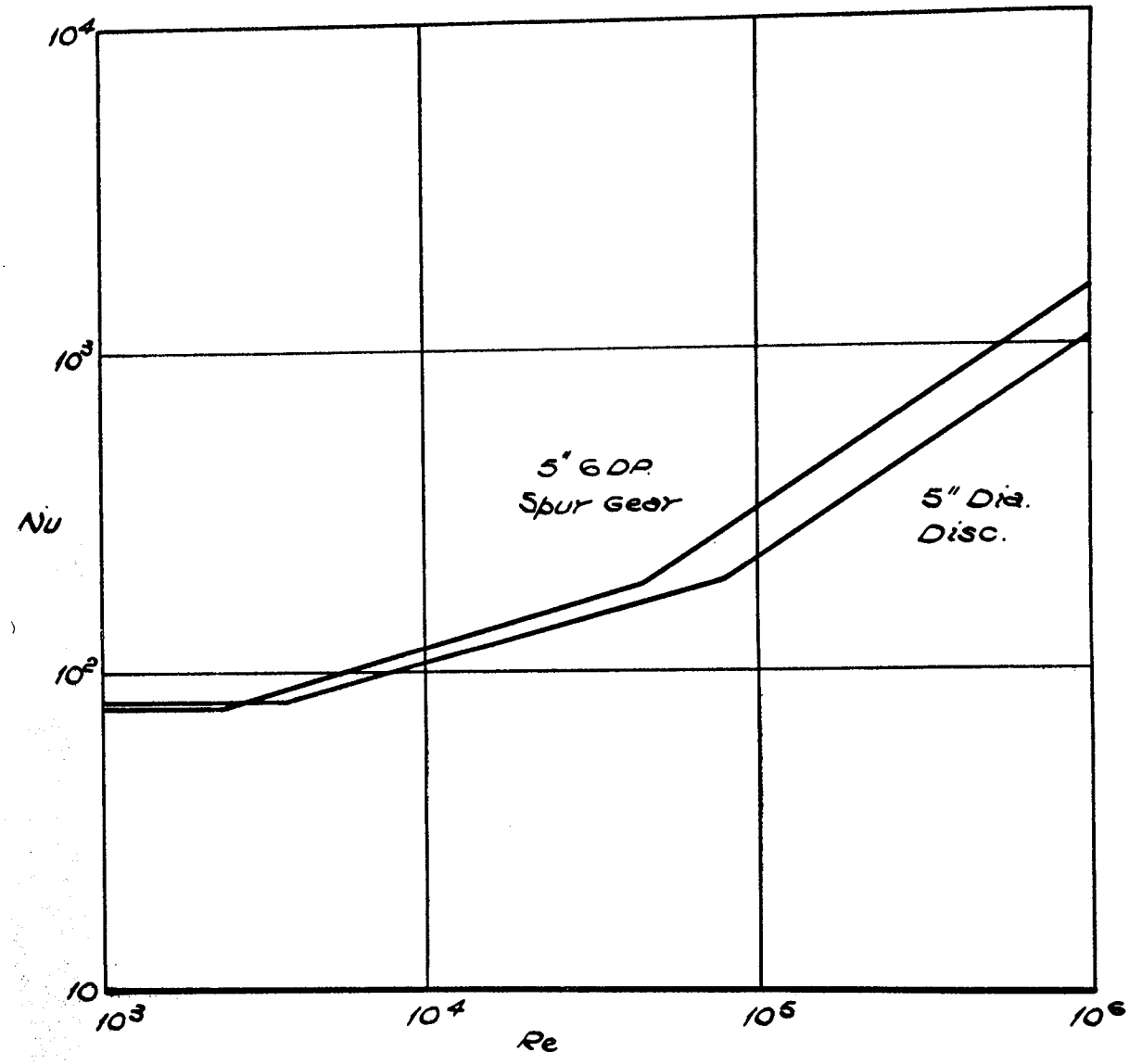

FIG. 6.5 THE SUMMARISED RESULTS OF O'DONOGHUE (14) FOR 5" DISCS AND GEARS IN 8" BOX.

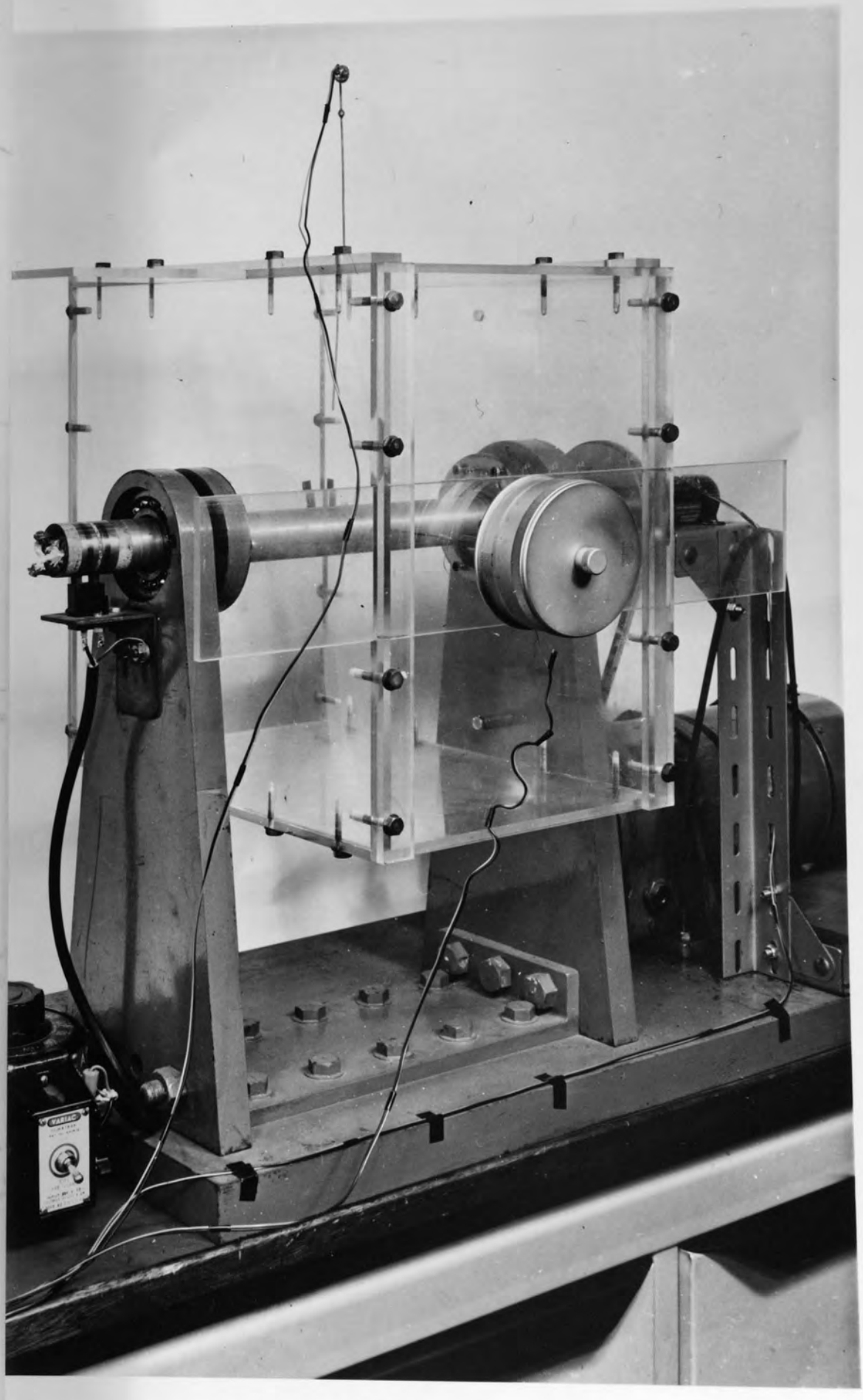

Fig. 5.6 The heat transfer apparatus

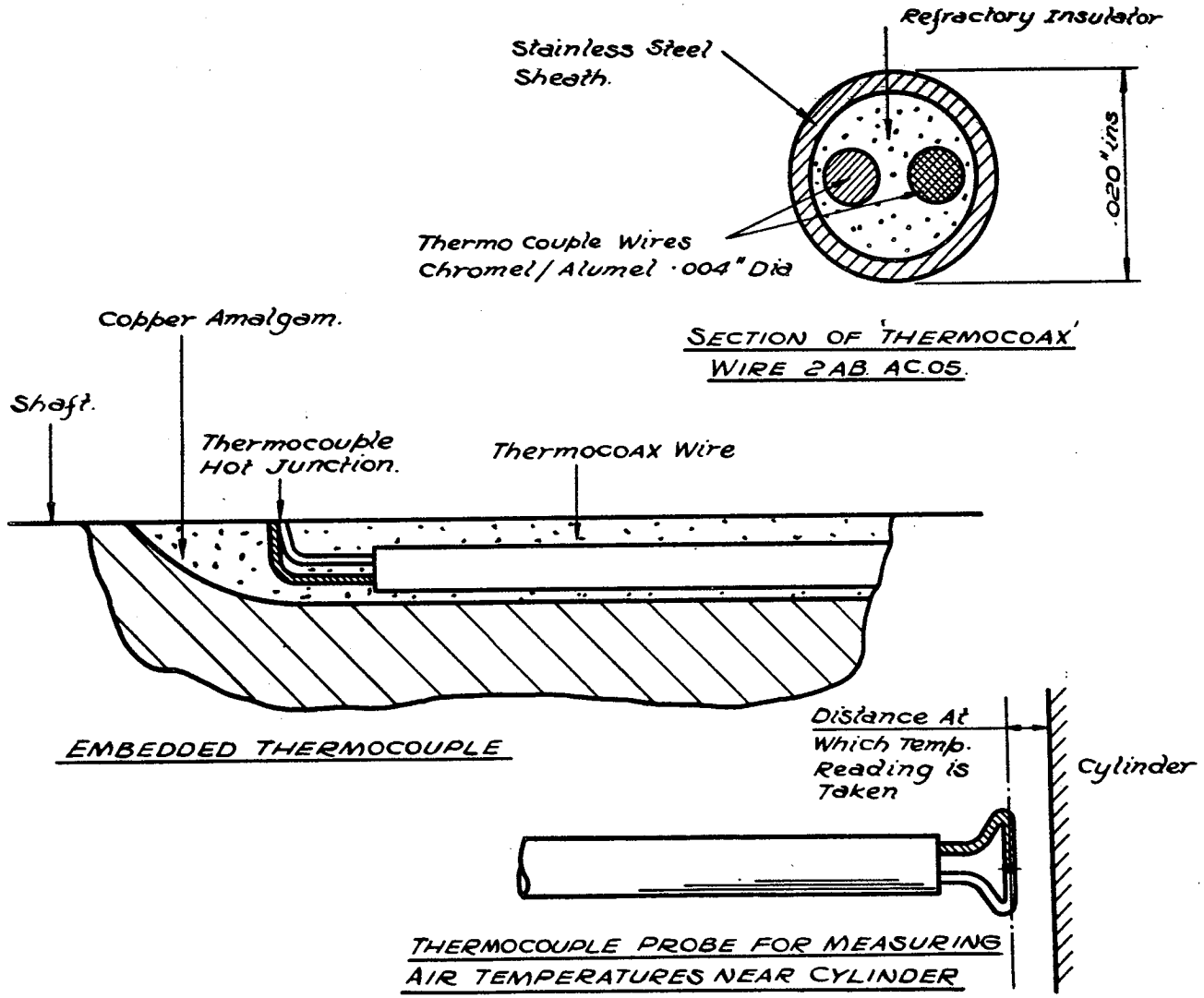

FIG.5.7. THERMOCOUPLE DETAILS.

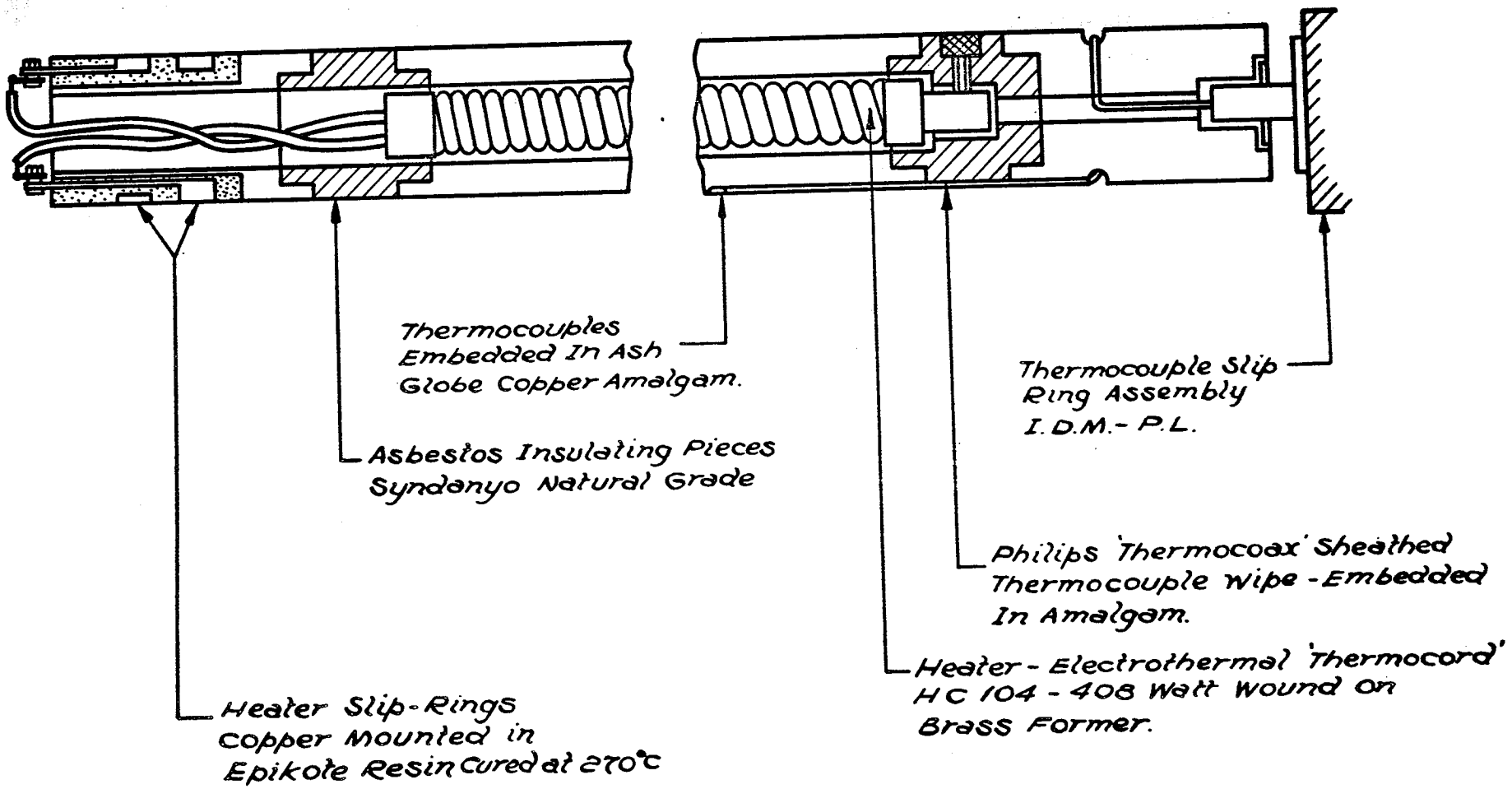

FIG.5.8. DETAILS OF SHAFT.

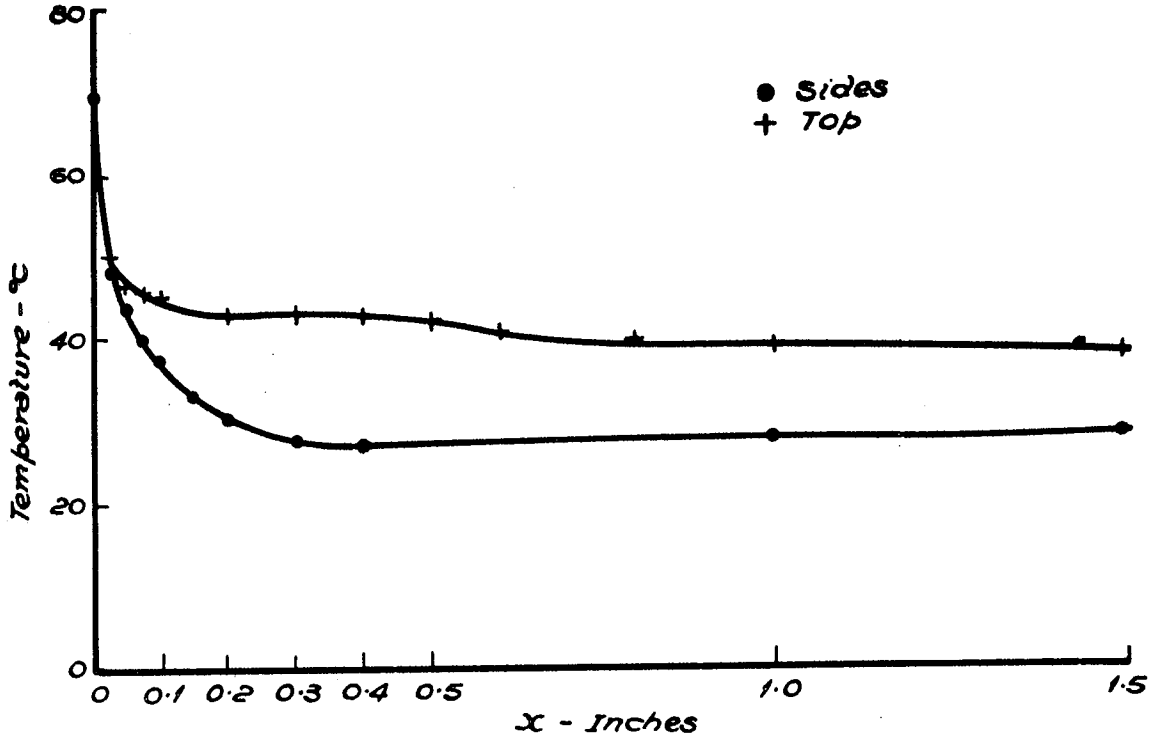

(a) STATIONARY CYLINDER

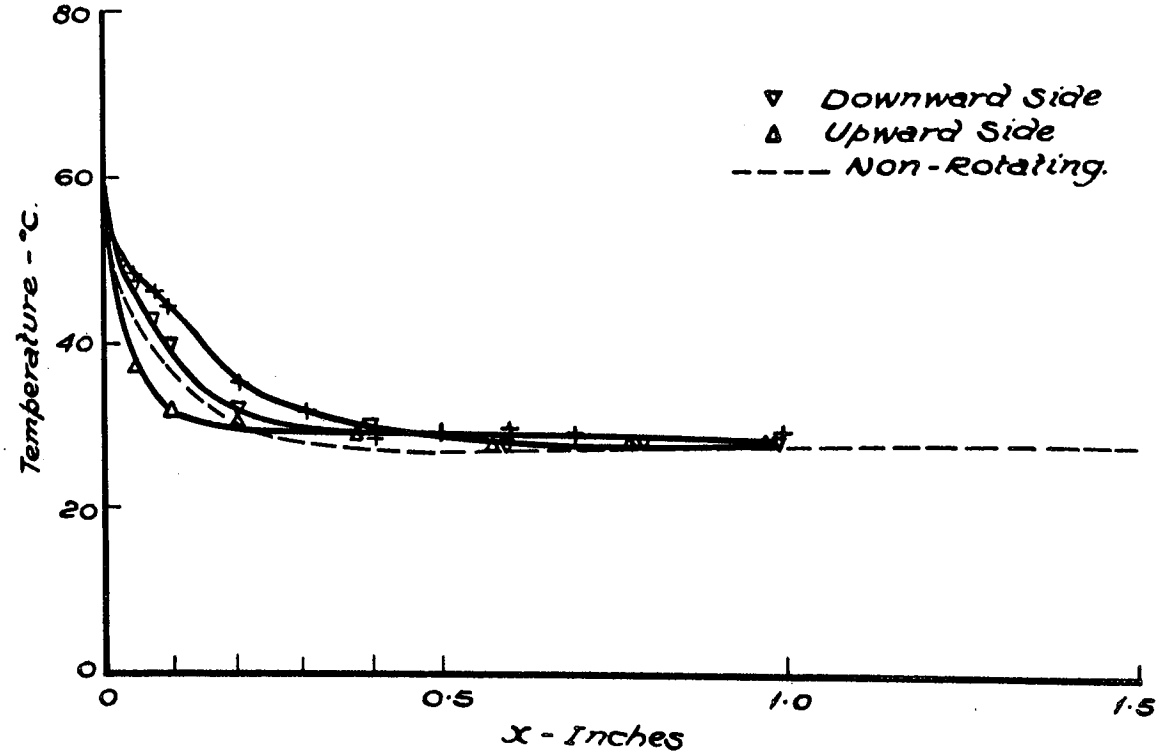

(b) SPEED 50 REV/MIN.

FIG 5.9.(a)&(b) TEMPERATURE PROFILES AT TOP & SIDES OF CYLINDER.

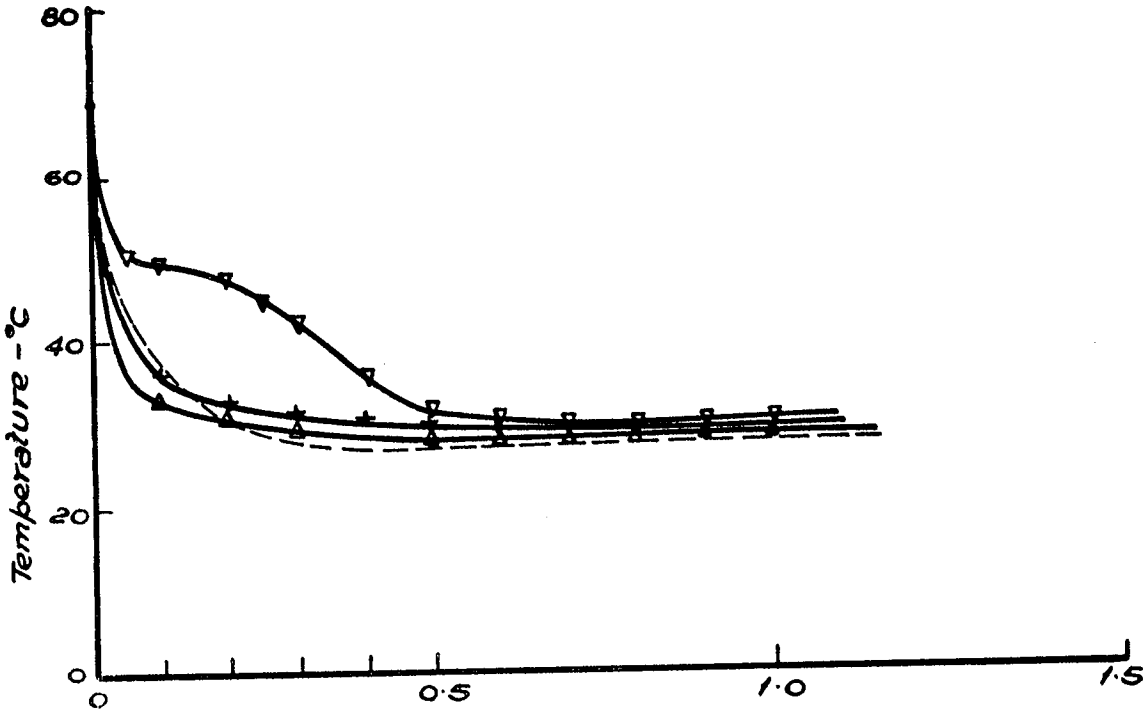

(c) Speed 160 Rev/Min.

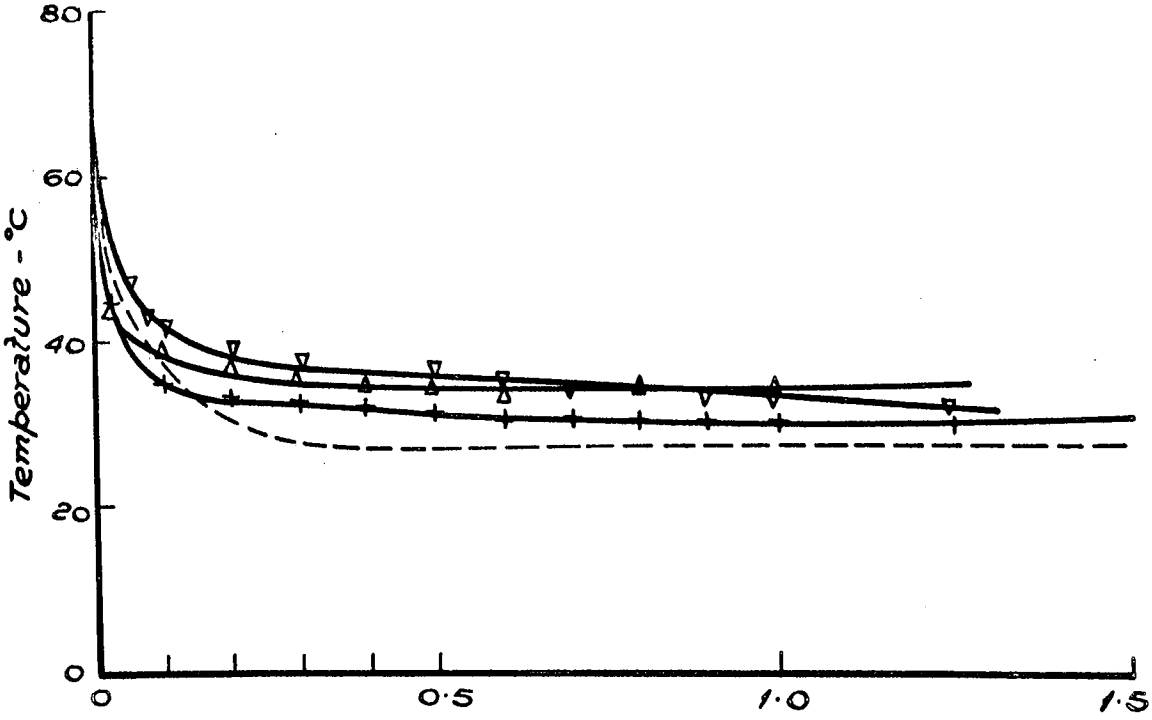

(d) Speed 310 Rev/Min.

FIG 5.9.(c) & (d) TEMPERATURE PROFILES AT THE TOP AND SIDES OF CYLINDER.

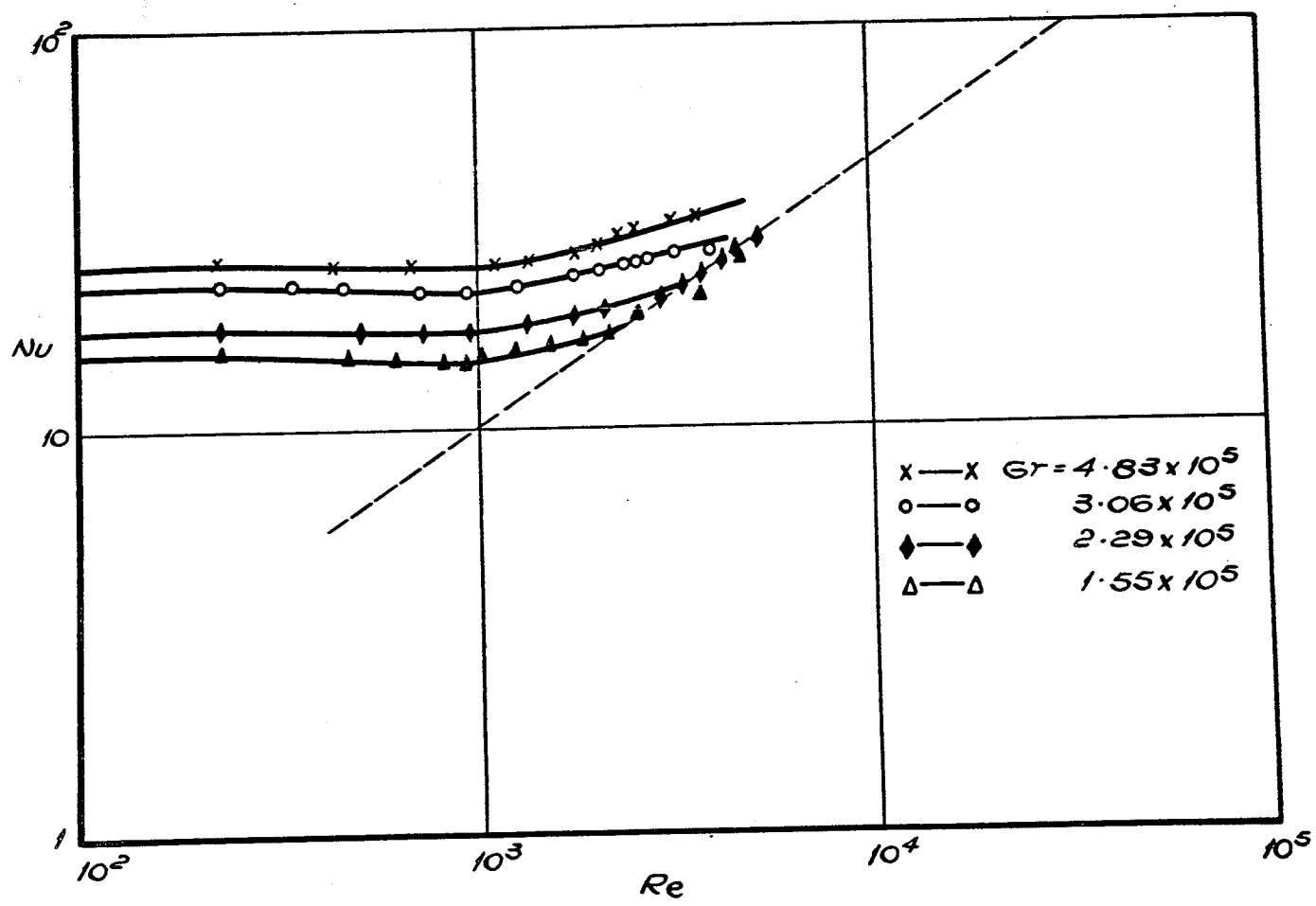

FIG. 5.10 HEAT TRANSFER RESULTS FOR CYLINDER ROTATING IN ENCLOSURE [B/D = 10] AT VARIOUS GRASHOF NUMBERS.

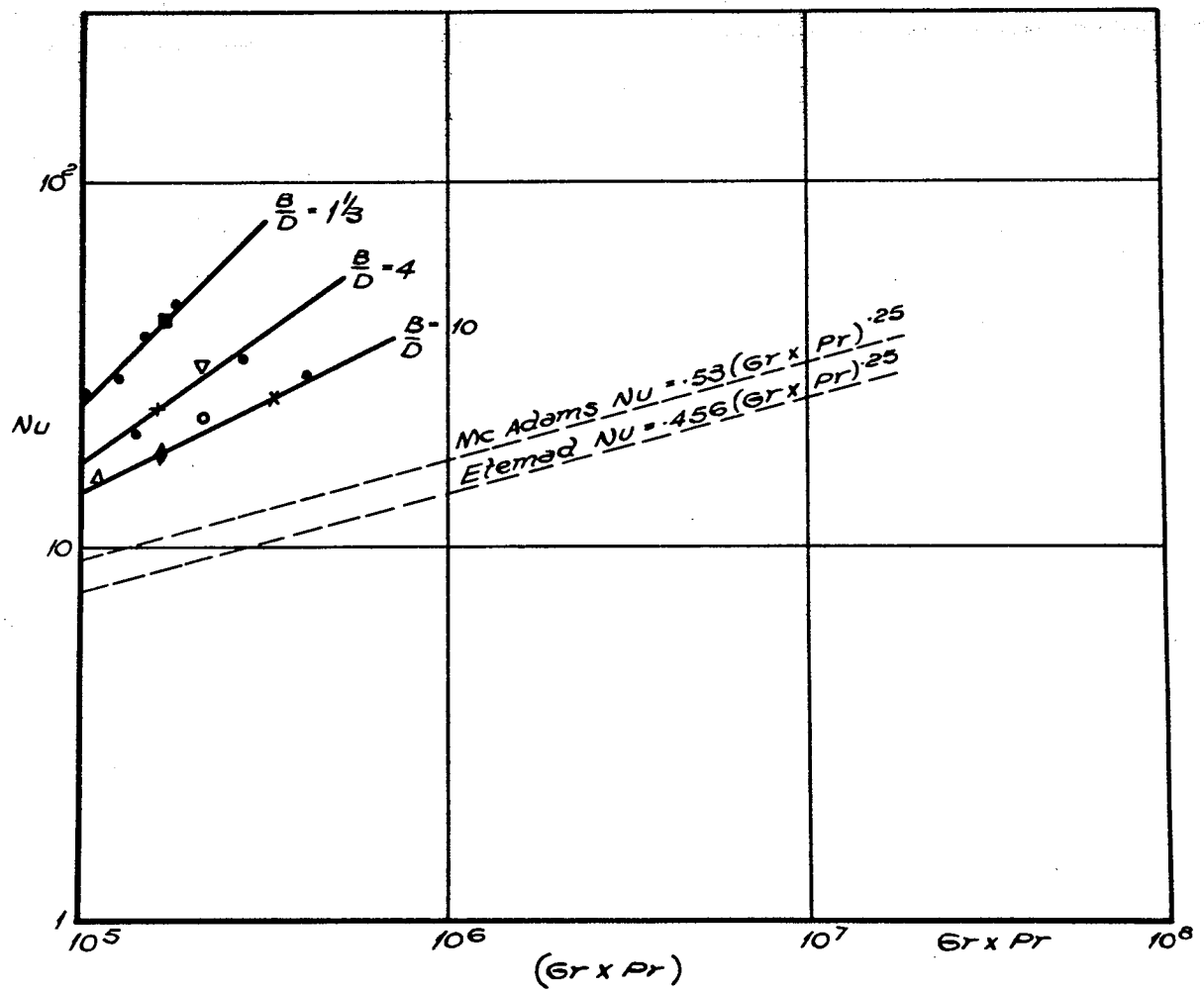

FIG. 5.11 SUMMARISED RESULTS FOR NON-ROTATING CYLINDER IN VARIOUS ENCLOSURES.

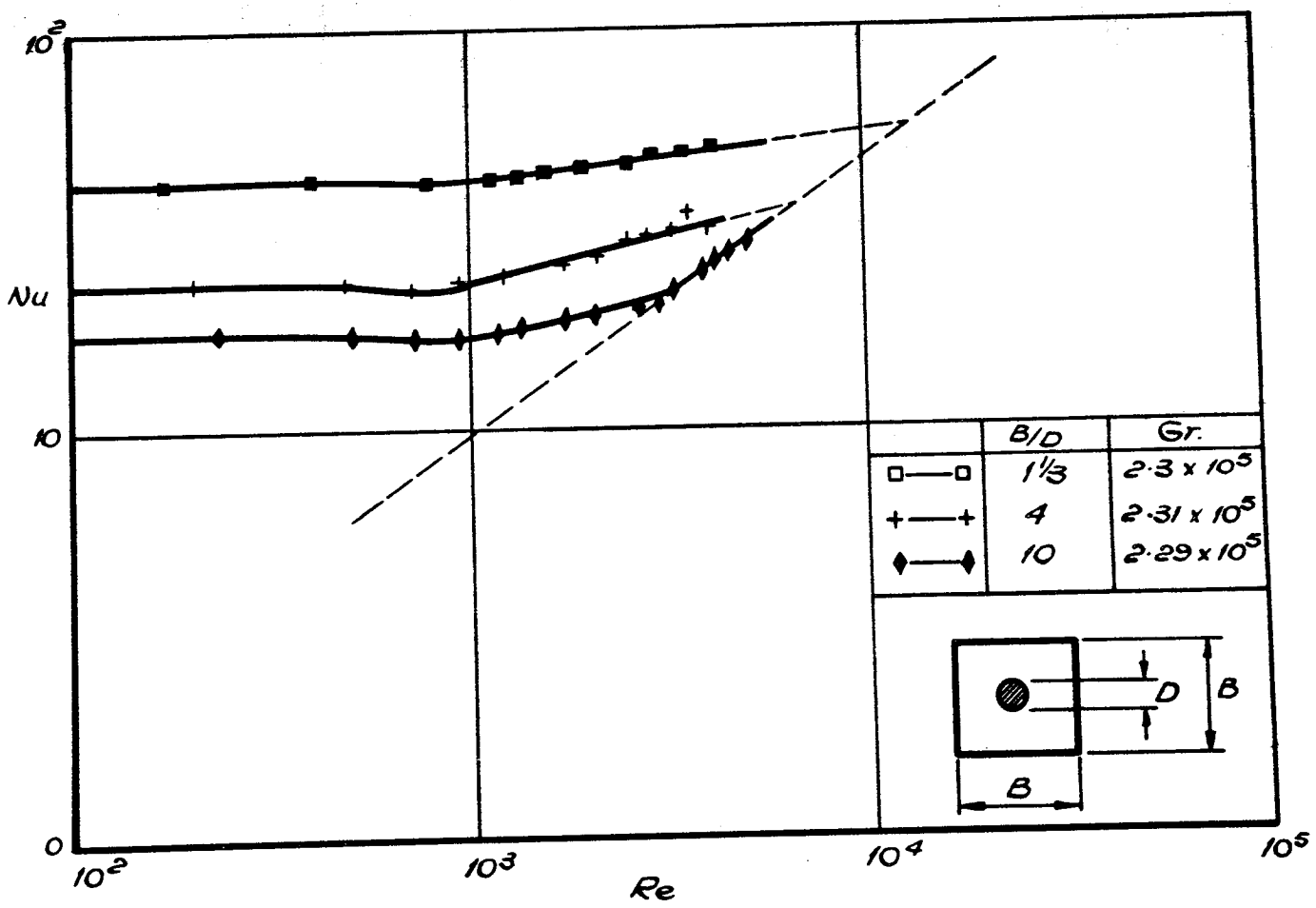

FIG.5.12 THE EFFECT OF ENCLOSURES ON THE HEAT TRANSFER FROM A ROTATING CYLINDER AT GRASHOF No ≃ 2·3 x 10^5

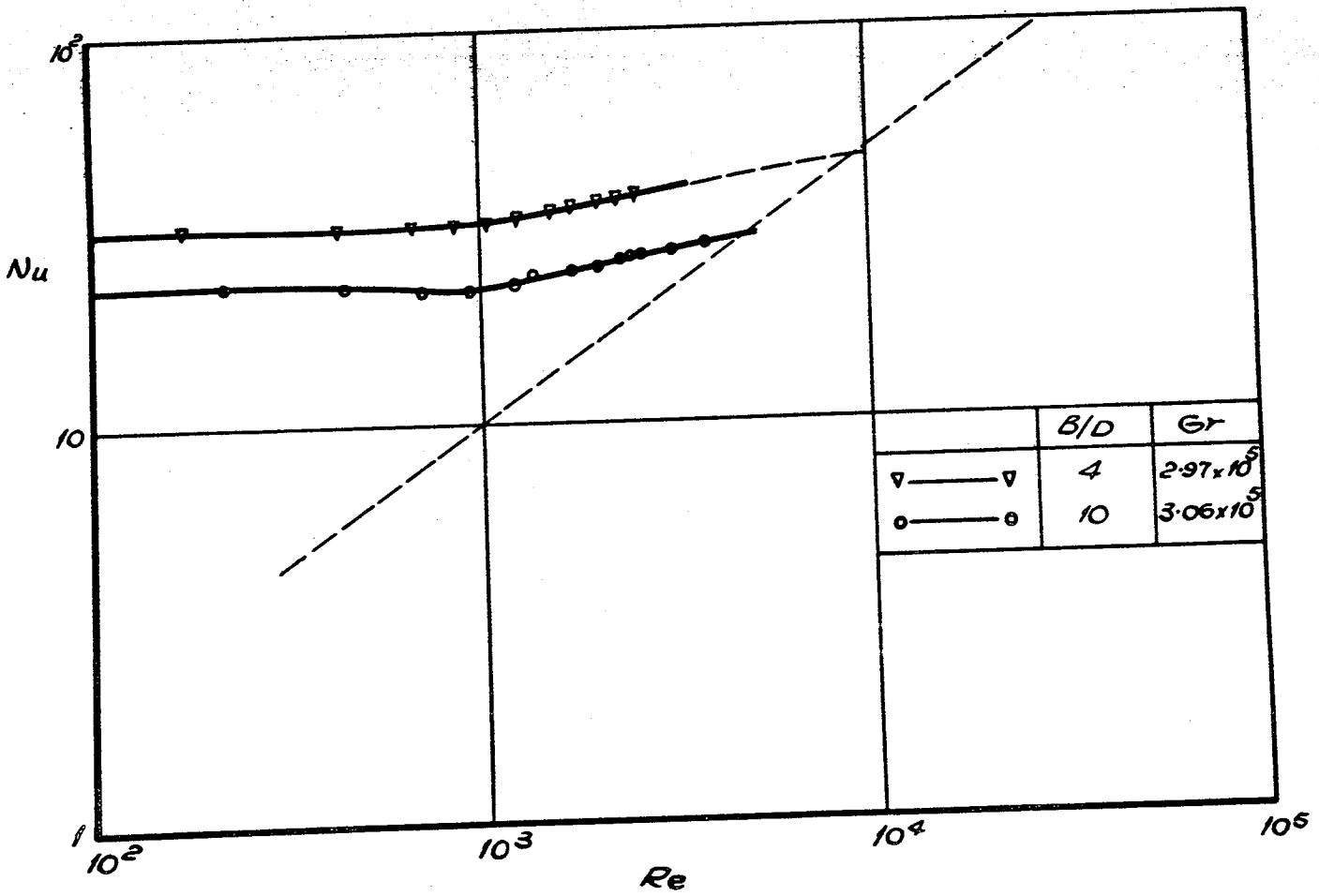

FIG 5.13. FURTHER RESULTS TO SHOW EFFECT OF ENCLOSURES ON THE HEAT TRANSFER FROM A ROTATING CYLINDER (GRASHOF No. $\simeq 3.0 \times 10^5$)

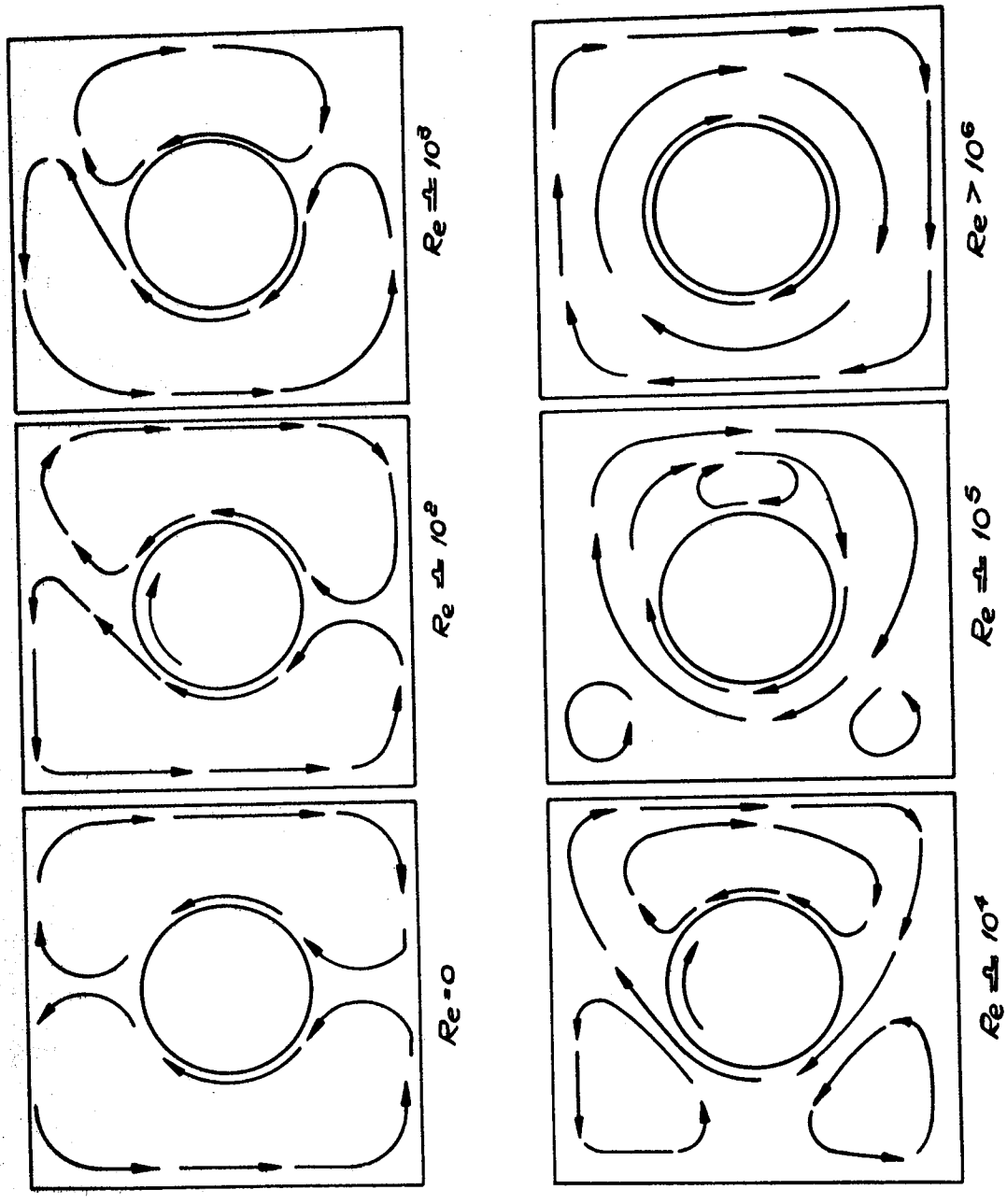

FIG.5.14 PROBABLE FLOWPATTERNS OF ROTATING CYLINDER FROM REF. (14.)

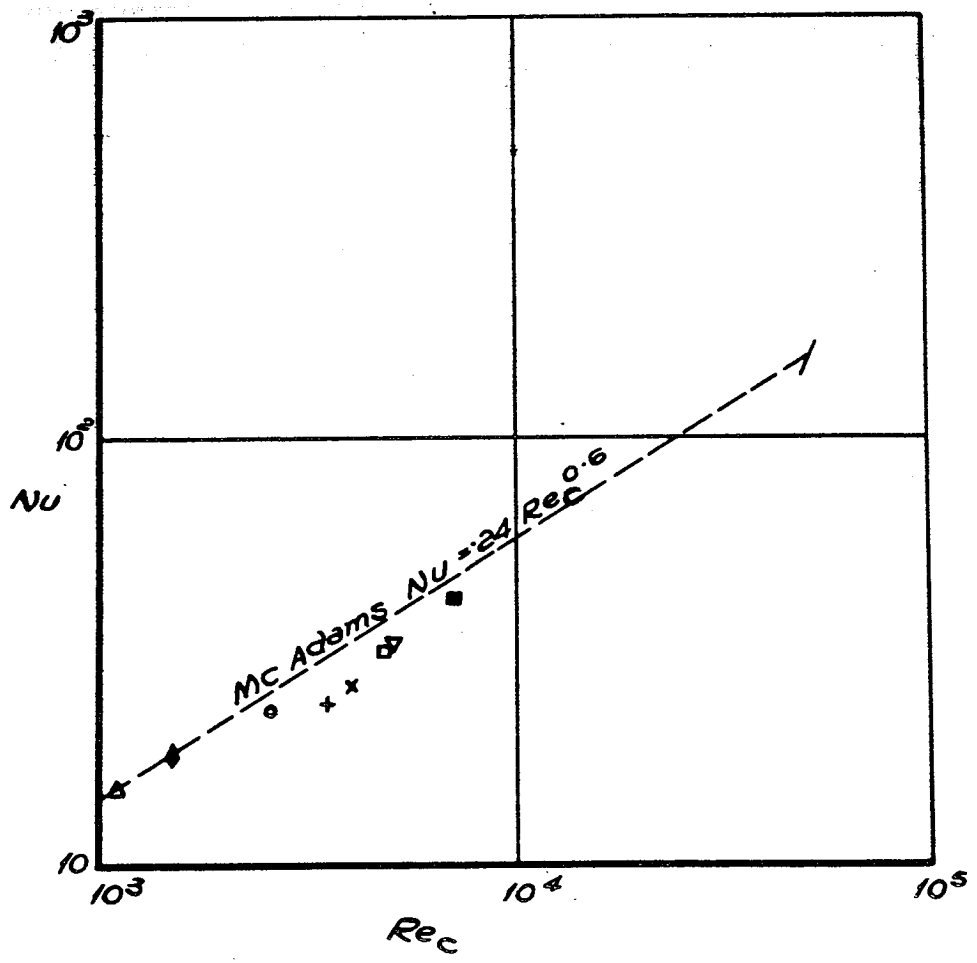

FIG. 5.15. NON-ROTATING RESULTS WITH INDUCED CROSSFLOW

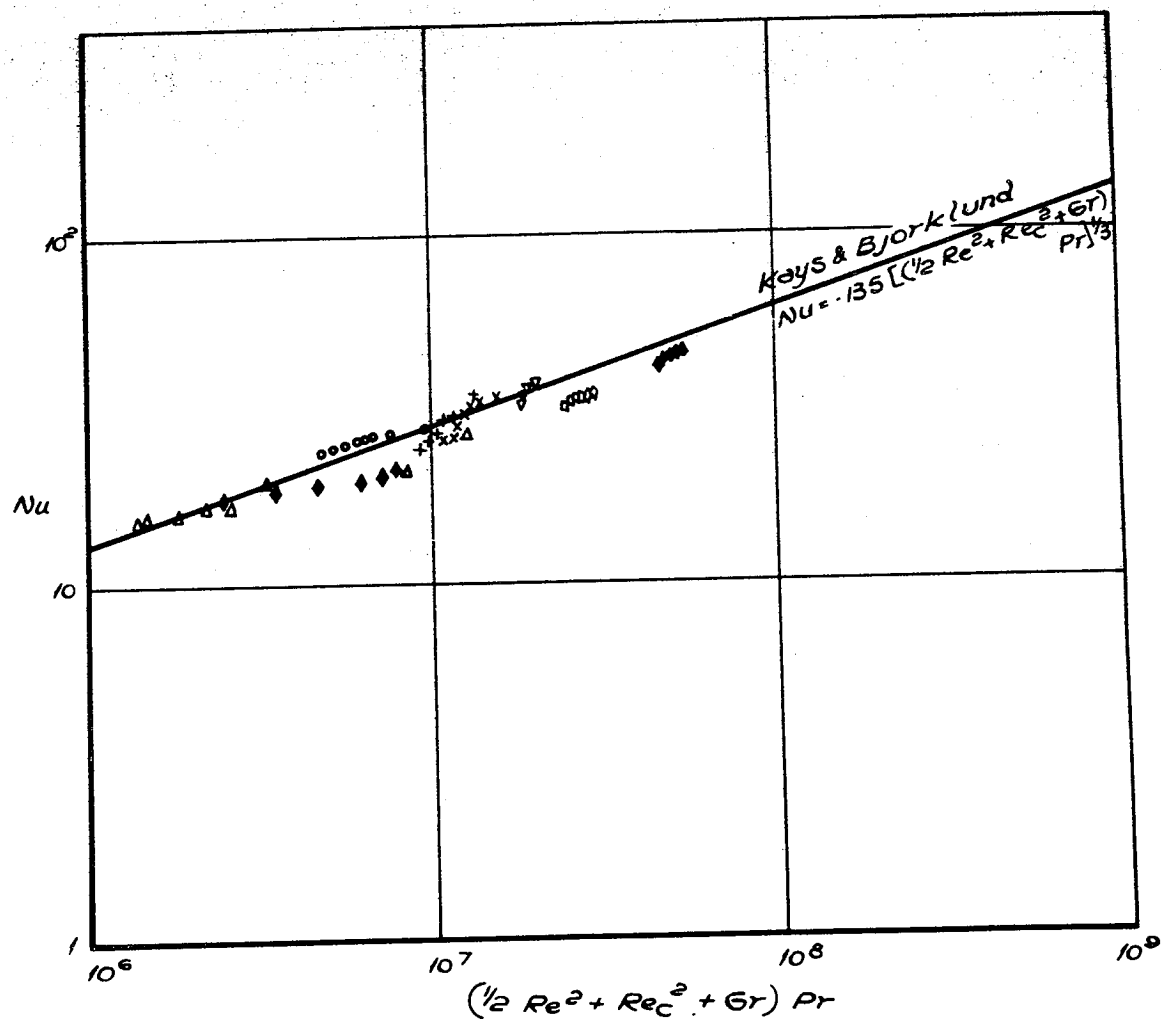

FIG. 5.16. SUMMARISED RESULTS ABOVE THE CRITICAL REYNOLDS NUMBER.

.0 TEMPERATURES AT LUBRICATED ROLLING/SLIDING CONTACTS

.1 Approximate Solutions

Solutions for the temperature distribution produced by a heat source passing through an infinite medium are given in Section 4.1. In these derivations, Blok (7), Carslaw (45), and Cameron et al (46) assumed the contact between discs to represent a heat source of finite length and the discs themselves to represent two semi-infinite solids. With the discs rotating at the same speed, the asymptotic solution for a heat source passing through an infinite medium applied. If the discs possessed different speeds, however, Cameron et al (46) modified the amount of heat injected into each solid, in order to maintain equal surface temperatures of the two discs throughout the contact.

Blok (43) in his original analysis showed that the solution for the peak temperature reached at the rear of a heat source passing over a semi-infinite solid

$$T = \frac{2q^1}{k}\sqrt{\frac{\kappa l}{\pi U}}$$

could be employed where the surface velocities, U were different. Letting a fraction α^1 of the total heat q generated by the friction at the contact, flow into one body and $(1 - \alpha^1)$ into the other, then

$$T_1 = \frac{2\alpha^1 q}{k}\sqrt{\left(\frac{\kappa l}{\pi U}\right)} \qquad (q_1{}^1 = \alpha^1 q)$$

$$T_2 = \frac{2(1 - \alpha^1)}{k} q\sqrt{\left(\frac{\kappa l}{\pi U}\right)} \qquad (q_2{}^1 = (1 - \alpha^1) q$$

Using the condition of equal surface temperatures throughout the contact $T_1 = T_2$, the ratio α^1 could be determined and consequently the peak contact temperature. This solution was subsequently transformed into the well known Blok Flash Temperature equation for the contact between discs,

$$Tf = \frac{1.11\ f\ w\ (U_1^{\frac{1}{2}} - U_2^{\frac{1}{2}})}{Kb^{\frac{1}{2}}}$$

The above solutions are based on the assumption that surface temperatures are equal. This implies that the lubrication conditions are boundary in nature and that no fluid film exists between the discs.

Recent developments in the theory of lubrication of discs and rollers have confirmed the formation of substantial oil-films between the contacting surfaces. The metal surfaces are consequently not in direct contact and need not experience the same temperature rise. The above equations should therefore only be used in cases where the amount of heat flowing into each surface is known. In many tests however, this is not readily assessed and an approximate calculation of the peak temperature using the Blok equation is accepted. With the information now available concerning the mechanism of fluid film formation between highly loaded rolling/sliding contacts, it should be possible to investigate the heat generation within the film, its dissipation to the metal surfaces and their resulting temperature rise.

.2 Theories for the lubrication of rollers

For many years the possibility of fluid film lubrication in highly loaded contacts has attracted much attention. Operating experience has shown that very often there is little

evidence of metallic contact between the sliding surfaces and the original grinding marks are still present after prolonged operation at service conditions.

An early solution to the lubrication problem was given by Martin (56) who applied the standard Reynold's equation (57) to the case of a cylinder near a plane. As shown in fig. 3.21 this arrangement may be used to represent the contact between discs, which may further be considered to represent the contact between gear teeth at a given point on the contact path. The radius of the cylinder is chosen to give distances of separation from the plane equal to those between the two discs. In Martin's analysis, the boundaries were considered to be rigid and the lubricant to be incompressible and isoviscous. The predicted loads were however much lower than those actually carried by gears and the oil film thicknesses quite insignificant compared with the surface irregularities.

This theory was later extended by Peppler (58) and then Mendahl (59) who both considered the elastic distortions of the contacting bodies, but the increase in the predicted load capacity was still below that required to support the argument that a continuous fluid film existed between loaded gear teeth.

Gatcombe (60) obtained predicted film thicknesses of the same order as the surface irregularities. He achieved this by solving the Reynolds equation for a lubricant having pressure-dependent viscosity and situated between rigid boundaries, but the load capacities were still inadequate. Further extensions of this approach were carried out by Cameron (61) and McEwen (62) where increases in load capacity by factors of 2.8 above the Martin prediction were obtained.

About this time, Grubin (63) presented a study of the

contact between lubricated machine components. The effects of both the elastic distortions and the increases in viscosity due to pressure were taken into account and although no complete solution of the elasticity and lubrication equations was given, the results indicated the nature of the full solution to be achieved in later investigations. An outline of Grubin's analysis is presented here as the results will be used in the development of a thermal theory.

Grubin first assumed that the shape of the surfaces would be similar to those given by Hertzian theory for dry contacts. The generation of pressure in the inlet region could then be examined and the required separation of the surfaces within the Hertzian zone determined.

Reynolds equation is:

$$\frac{dp}{dx} = 6 (U_1 + U_2) \eta \frac{h - h_o}{h^3}$$

here h_o is thickness of film at $\frac{dp}{dx} = 0$.

Assumptions are p is constant in y direction (i.e. no side leakage).

Taking the pressure viscosity relationship as:-

$$\eta = \eta_o e^{\delta p}$$

for constant $\eta = \eta_o$, denote pressure by po and,

$$dp_o = 12 \eta_o U_e \frac{(h - h_o)}{h^3} dx \qquad \ldots\ldots 6.1$$

where $U_e = \frac{U_1 + U_2}{2}$

If viscosity varies then,

$$dp\, e^{-\delta p} = 12\, U_e \eta_o \left(\frac{h - h_o}{h^3}\right) dx$$

$$\therefore \quad dp\, e^{-\delta p} = dp_o$$

Integrating between 0 and p

$$\frac{1 - e^{-\delta p}}{\delta} = p_o$$

for large p, $e^{-\delta p} \to 0$

$$\therefore \quad p_o = \frac{1}{\delta} \qquad \ldots\ldots 6.2$$

Resubstitution in equation 6.1

$$-\frac{1}{\delta} \frac{d(e^{-\delta p})}{dx} = 12\, U_e \eta_o \frac{h - h_o}{h^3} \qquad \ldots\ldots 6.3$$

The Hertzian pressure distribution is elliptic given by:-

$$P_H = P_{H(MAX)} \left(1 - \left(\frac{x}{b/2}\right)^2\right)^{\frac{1}{2}}$$

Grubin showed that over the range $-.98 < \frac{x}{(b/2)} < .98$

$e^{-\delta P_H}$ varied only slightly for typical values of

$P_{H_{MAX}}$ = 1.5 to 5 x 10^5 lbf/in^2 and δ = .00016 in^2/lbf.

Hence $\frac{d(e^{-\delta P_H})}{dx} \to 0$

This implied from Eq. (6.3) that $h - h_o \to 0$ and consequently for $-.98 < \frac{x}{(b/2)} < .98$ the film thickness is constant. The net result is a Hertzian-type contact with the surfaces

separated by an oil film of constant thickness h_o and a semi-elliptic pressure distribution.

Grubin further showed how the value of h_o could be calculated together with the pressure distribution at the inlet to the contact zone.

Outside the contact zone, the Hertzian expression for the shape of the surfaces is

$$\delta^1(R) = 2\left\{\frac{x}{(b/2)}\sqrt{\frac{x^2}{(b/2)^2} - 1} - \log_e\left(\frac{x^2}{(b/2)^2} + \sqrt{\frac{x^2}{(b/2)^2} - 1}\right)\right\}$$

The Grubin contact therefore gives:

$$h = \delta^1(R) + h_o = \delta(R)$$

Letting $Ho = \dfrac{h_o}{w/E^1}$ $\qquad H^1 = \dfrac{\delta^1(R) + ho}{w/E^1}$

$$\therefore \frac{dp_o}{dx} = 12\,\eta_o\,\frac{U_e\,\delta^1(R)}{(\delta^1(R) + ho)^3} \qquad \ldots\ldots 6.4$$

outside the contact zone.

By integrating this expression from $x = -\infty$ to a point on the inlet side of the contact ($x < -b/2$), the reduced pressure Po at that point was calculated. Grubin found it necessary to solve the integrand numerically and results are shown in fig. 6.1 for Po and corresponding pressures as a ratio of $P_{H_{MAX}}$ for different assumed values of Ho.

Ibrahim (82) computed the values of Po at $x = -1.2\,(\frac{b}{2})$, $-1.4\,(\frac{b}{2})$ and $-1.6\,(\frac{b}{2})$ thus enabling the inlet pressure curve to be traced as in fig. 6.1. Over the range $-\infty < x < -b/2$, the numerical results were correlated by the expression,

$$Po = .0986\ Ho^{-1.375}\ \frac{12\,\eta_o\,U_e(b/2)}{(w/E^1)^2} \qquad \ldots\ldots 6.5$$

Further at $x = -b/2$, Po is known to equal $\frac{1}{\delta}$ from Equa. 6.2.

$$\therefore \quad ho = \frac{1.95\,(\eta_o U_e \delta)^{8/11}}{(w/E^1)^{1/11}\,(\frac{1}{R_N})^{4/11}} \qquad \ldots\ldots 6.6$$

The film thicknesses given by this equation are several orders of magnitude greater than the corresponding predictions of the Martin theory and the pressure distributions are consistent with the loads carried.

Grubin was also able to make further conclusions regarding the pressure profile. In the inlet region, the actual pressures would lie beneath the Hertzian, to balance the added load carried by the hydrodynamic pressure in the inlet sweep. At the outlet, it was observed that large pressure gradients would be required to reduce the pressure to zero at the end of the contact zone and that a consequent local reduction in film thickness would be required for continuity of flow. ($\frac{dp}{dx} = p = 0$ at outlet).

An outstanding contribution to the study of elastohydrodynamic lubrication was made by Crook (64) who reported the direct measurement of film thickness by a capacitance method. The disc machine results supported the Martin theory at low loads but at high loads indicated film thicknesses of about 40 μ- inches, supporting the theory for continuous fluid films.

Further results over a range of conditions showed that the viscosity of the oil at the temperature of the disc surfaces was the viscosity which determined the oil film thickness (65). The introduction of sliding between the discs did not significantly affect the film thickness despite the accompanying rise in frictional heating. The magnitudes of the film thicknesses

compared favourably with those predicted by the Grubin equation but there was a discrepancy in the dependence of film thickness on the product of rolling velocity ($= \frac{U_1 + U_2}{2}$) and inlet viscosity. Theory predicted a relationship to the power of 0.7 whereas experiment gave an exponent of about 0.5. In order to seek an explanation for this discrepancy, Crook conducted further investigations into the behaviour of the fluid film.

.3 Crook's solution for oil film temperatures

In order to determine the physical conditions met by an oil film in its passage through the contact between discs, Crook (66) developed an analytical solution for the temperatures generated within the oil film.

The starting point for the solution was the simplified form of the Navier Stokes equation:-

$$-\frac{\partial p}{\partial x} = \frac{\partial}{\partial z}\left(\eta \frac{\partial U}{\partial z}\right)$$

For viscosity independent of z this reduced to the familiar Reynold's equation in one dimension but in contacts where temperatures existed across the oil-film, viscosity had to be treated as a function of x and z (x is direction of sliding and z is direction across film).

By successive integrations with the appropriate boundary conditions (taking z = 0 at the surface with velocity U_2) Crook further reduced this equation to

$$\frac{\partial U}{\partial z} = -\frac{1}{\eta}\frac{\partial p}{\partial x}\left(z - \frac{h}{m}\right) + \frac{\eta_m}{\eta}\left(\frac{U_1 - U_2}{h}\right) \quad \ldots\ldots 6.7$$

where η_m is the viscosity at position $z = h/m$ at which

$$\frac{\partial U}{\partial z} = \frac{U_1 - U_2}{h}$$

In order to solve the above equations for Θ Crook considered the viscosity at the boundaries. If θ_s was the surface temperature on the entry side, the viscosity of the oil as it entered the contact was η_s. Within the contact it was assumed that the surface temperatures remained constant at θ_s and that the oil viscosity at the surfaces (η_x) which differed from η_s because of the rise in pressure was given by $\eta_x = \eta_s e^{\delta p}$ Away from the surfaces of the discs, because of the heating in the oil, the temperature exceeded θ_s. The excess was denoted by θ rising to θ_c on the median plane of the film. The local viscosity was therefore given by:-

$$\eta = \eta_x e^{-\gamma \theta}$$

$$\eta = \eta_s e^{(\delta p - \gamma \theta)}$$

Crook was only able to provide a solution for θ if η was expressed as

$$\eta = \eta_s e^{(\delta p - \gamma \theta_c)}$$

which resulted in overestimates of θ.

The second term on the right hand side of Eq. 6.7 disappears when pure rolling is considered ($U_2 = U_1$). The first term was therefore taken as the velocity profile in pure rolling and the second in sliding.

Each of these terms were introduced into the energy balance given by:-

$$pcU \frac{\partial \theta}{\partial x} + k \frac{\partial 2\, \theta}{\partial z\, 2} = - q$$

The heat generated per unit volume q was given by the product of stress and rate of strain.

$$q = \eta \left(\frac{\partial U}{\partial z} \right)^2$$

The first term related to the transport of heat by the oil (convection) and the second to conduction of heat across the oil film. Conduction in the x direction was ignored by considering the film thickness to be very small compared to the length of the contact and consequently temperature gradients across the film were much larger than those in the x direction.

Crook showed that in pure rolling, the temperatures arising from friction were confined to the entry side of the contact region and that for the range of conditions considered, the temperatures were too low to influence the inlet viscosity and film thickness.

With the introduction of sliding Eq. 6.7 reduced to:

$$\frac{\partial U}{\partial z} = \frac{\eta_m}{\eta} \frac{(U_1 - U_2)}{h}$$

which by integration across the film produced a definition for η_m in terms of local viscosity η.

$$\frac{1}{\eta_m} = \frac{1}{h} \int_0^h \frac{\partial z}{\eta} \qquad \ldots\ldots 6.8$$

Assuming conduction across the oil film to be dominant, the energy balance became,

$$k \frac{\partial^2 T}{\partial z^2} = - \eta_m^2 \frac{(U_1 - U_2)^2}{\eta \, h^2}$$

By subsequent integration and use of the relationship

$$\eta = \eta_x \exp(-\gamma\theta)$$

$$\frac{\partial \theta}{\partial z} = \pm \left[2\omega \left(1 - \frac{\Lambda}{\gamma\omega} \exp(\gamma\theta) \right) \right]^{\frac{1}{2}} \qquad \ldots\ldots 6.9$$

where $$\Lambda = \frac{\eta_m^2}{k \eta_x} \frac{(U_1 - U_2)^2}{h^2}$$

and $$\omega = \frac{8\,\eta m^2\,\psi\,(\psi + 1)}{\eta_x^2\, h^2\, \psi^2}$$

where $$\psi = \frac{\eta_x \Upsilon (U_1 - U_2)^2}{8k}$$

Maximum θ occurred on the medium plane where

$$\exp(\Upsilon \theta_c) = \frac{\partial \omega}{A} = \left(\frac{\eta_x \Upsilon (U_1 - U_2)^2}{8k} + 1 \right)$$

Integration of equation 6.9 with respect to z with the boundary conditions $z = 0$, $\Theta = 0$ gave

$$\ln \left[\frac{1 - \sqrt{(1 - \exp(\Upsilon\theta)/\exp(\Upsilon\theta_c)}}{1 + \sqrt{(1 - \exp(\Upsilon\theta)/\exp(\Upsilon\theta_c)}} \right]$$

$$-\ln \left[\frac{1 - \sqrt{(1 - \exp(-\Upsilon\theta_c)}}{1 + \sqrt{(1 - \exp(-\Upsilon\theta_c)}} \right] = z\Upsilon\sqrt{2\omega} \quad \ldots\ 6.10$$

With the condition that $\theta = \theta_c$ at $z = \frac{1}{2}h$ this reduced to an expression for

$$\omega = \frac{2}{h^2 \Upsilon^2} \left[\ln \left\{ \frac{1 - \sqrt{(1 - \exp(-\Upsilon\theta_c)}}{1 + \sqrt{(1 + \exp(-\Upsilon\theta_c)}} \right\} \right]^2$$

Hence

$$\left[1 - \frac{2z}{h}\right] \ln \left[\frac{1 - \sqrt{1 - \eta_c'/\eta_x}}{1 + \sqrt{1 - \eta_c/\eta_x}} \right]$$

$$= \ln \left[\frac{1 - \sqrt{1 - \eta_c/\eta}}{1 + \sqrt{1 + \eta_c/\eta}} \right]$$

which gives the temperatures expressed in terms of the viscosities.

The numerical results obtained by Crook for temperature and viscosity distribution are reproduced in fig. 6.2 where sliding is seen to generate temperatures of up to 200°C in the pressure zone but not significantly affect the temperatures in the inlet region.

The analysis so far had considered constant temperatures at the disc surfaces which clearly, by virtue of the heat conducted to them would experience a temperature rise. Crook took this into account by including a heat flow equation of the type mentioned in section 6.1. The strength of the heat source was taken as

$$q = \frac{\eta m}{2h} (U_1 - U_2)^2$$

The results showed that even when the rise in surface temperature was as high as 50°C, the maximum temperatures in the oil film were unchanged.

The results of the analysis were to prove very useful to Crook in interpreting his frictional traction results between discs on the basis of effective viscosities in the contact. This will be dealt with later.

A direct application of the above solution was made by Dowson and Longfield (67). Measurements of pressure and temperature were made over the surface of a phosphor bronze shoe running against a steel disc in the presence of a lubricant. By assuming the disc surface to maintain constant temperature throughout the contact zone, Dowson and Longfield were able to predict the variation of temperature and viscosity throughout the whole oil film.

Because the shoe temperature was not constant, a slight

modification to Equa. 6.10 was necessary. The equation became:-

$$\ln\left[\frac{1-\sqrt{(1-\exp^{(\Upsilon\theta)}/\exp(\Upsilon\theta_c)}}{1+\sqrt{1-\exp(\Upsilon\theta)/\exp(\Upsilon\theta_c)}}\right] - \ln\left[\frac{1-\sqrt{1-\exp(\Upsilon\theta_1)/\exp(\Upsilon\theta_c)}}{1+\sqrt{1-\exp(\Upsilon\theta_1)/\exp(\Upsilon\theta_c)}}\right] = z\Upsilon\sqrt{2\omega}$$

where z was the distance from the shoe. Owing to the differences in the surface temperatures of the disc and shoe the temperature profile could no longer be assumed symmetrical as in the examples given by Crook. A similar expression for θ was therefore given in terms of distance from the disc surface at $z = 0$ for locations in the oil film between the disc and the point of maximum temperature θ_c.

By solving the equations for ω in a similar way to Crook, Dowson and Longfield were able to determine θ_c and hence the distribution of θ at any point through the contact. An example of the temperatures and corresponding viscosities calculated by Dowson and Longfield is given in fig. 6.3.

4 The full elasto-hydrodynamic solution

A complete solution to the elasticity and lubrication equations was given by Dowson and Higginson (68). Initial calculations were obtained for lightly loaded contact between bronze discs that related to the geometry of the apparatus reported by Dowson and Longfield (67). The notable differences between the pressure profiles calculated and those predicted by previous workers was the absence of a second pressure peak.

By extension of the method of solution to cover a range of loads, speeds, and material properties, a pressure peak was

detected together with a local constriction in the film shape (69). The existence and form of the pressure peak was found to be a function of the variables and the initial calculations were in fact related to conditions not conducive to its formation.

The method of solution involved an iterative process whereby a pressure profile was found that produced agreement in the predicted film shapes from both the Reynolds equation and the elastic surface displacement equation. An inverse form of the Reynolds equation speeded up the process and solutions were obtained after only a small number of cycles.

The standard Reynolds equation,

$$\frac{dP}{dx} = 12 \eta U_e \left(\frac{h - h_m}{h^3} \right)$$

may be written,

$$K \bar{h}^3 + \bar{h} - 1 = 0$$

$$\text{where } K = \frac{h_m^3}{12 \eta U_e} \frac{\partial P}{\partial x}$$

$$\bar{h} = h/h_m$$

At any point in the contact therefore, for a given pressure profile, the above equation could be solved for h. The viscosity was adjusted for pressure effects according to the pressure-viscosity characteristics of an actual lubricant.

In the calculation, Dowson and Higginson divided the pressure curve into four regions as shown in fig. 6.4(a). The pressure at the boundary between (1) and (2) was fixed at the start of the calculation by integrating Reynolds equation assuming a value for h_m and an isoviscous lubricant. The

The boundary was determined as the point at which the pressure effect on viscosity could no longer be ignored. By initially assuming a Hertzian pressure distribution in regions (2), (3), and (4), Dowson and Higginson calculated the corresponding elastic displacements by suitable equations derived from the Boussinesq function for stresses in a semi-infinite solid due to a normal line load on the surface. The pressure profile was divided into small blocks and represented by a series of polynominal expressions for substitution in the displacement equations.

In region (2) the pressure curve was then recalculated by integration of the Reynolds equation for values of h derived from the elastic displacements. At the point of inflexion in the pressure profile, a new value for h_m was determined, which would be used in the next cycle.

In region (3), the film shapes calculated by the elastic and the inverse hydrodynamic equations were compared and the differences taken as a measure of the error in the pressure curve. Adjustment of the pressure curve before commencing the next cycle in the process was a question of experience in the manipulation of the technique.

The tip of the pressure spike formed the boundary between regions (3) and (4). The pressure gradient was recognised as being equal to zero at the tip of the spike and was determined by interpolation. In region (4) the Reynolds equation was integrated to find the pressure curve.

A useful assessment of the relative importance of the pressure dependence of viscosity and the elastic distortion of the rollers was also provided in reference (68). Fig. 6.4(b) reproduces these results and demonstrates the very significant

influence of these two additions to the simple Martin theory of isoviscous lubricant and rigid rollers. Separately the two factors have only a modest effect on the pressure distribution, but combined they explain the load capacity of elastohydrodynamic contacts.

Typical results obtained by Dowson and Higginson (69) and taking into account the combined effect of pressure-viscosity and elasticity are reproduced in fig. 6.5. The film thicknesses of 10 - 20 μ inches are comparable with the surface irregularities normally obtained in practice. Whilst load was found to have very little effect on the film thickness, the film thickness increased considerably with increased rolling speed or inlet viscosity. Modifications to the pressure curves were also experienced, fig. 6.6. At high speeds, the film thickness was shown to approach the claimed Martin theory owing to the relatively lower pressures in the actual contact zone (70).

The prediction of film thickness is an important feature in assessing the performance of rolling contacts and Dowson and Higginson (71) from a survey of their solutions produced a convenient dimensionless formula for minimum film thickness.

$$H^* = \frac{1.6\, G^{*0.6}\, U_D^{0.7}}{W^{0.13}}$$

where $H^* = \frac{h_{min}}{R}$

$$G^* = \alpha E^1$$

$$U_D = \frac{\eta_s U_e}{E^1 R}$$

$$W = \frac{w}{E^1 R}$$

Also, $$V = \frac{\eta_s (U_1 - U_2)}{E^1 R} \qquad \text{(see later)}$$

A comparison of this formula with that obtained by Grubin, expressed in the same dimensionless group, has shown that the discrepancy between the two does not exceed 20 per cent.

From Equa. 6.6, the Grubin equation is:

$$H = \frac{1.95 (\overset{*}{G} U_D)^{0.73}}{W^{0.091}}$$

where $$H = \frac{h}{R}$$

With the agreement between the theoretical film thicknesses and the experimental results of Crook (65) and Sibley and Orcutt (72), obtained in reference (70), film thicknesses can now be predicted with confidence for pure rolling elements, where the isothermal conditions assumed in the theory may be considered to apply (fig. 6.7). The results were also in agreement with the findings of Archard, Gair, and Hirst (73) who confirmed the overall shape of the film and pressure profiles.

The theory was subsequently applied to the analysis of real contacts. Dowson and Higginson (74) carried out an analysis of roller bearing performance and later, an analysis of gear lubrication (75). This provided designers with charts from which to assess the variation of film thickness through the meshing cycle of a gear pair. In this work it was assumed that sliding did not affect the film thickness, a reasonable inference from the results of Crooks experiments. Nevertheless, the effect

of sliding and other aspects of the problem, such as the rheological behaviour of the fluid and the frictional behaviour of the contact were to come under close examination. These considerations are the subject of the following sections.

Thermal-Elastohydrodynamic Solutions for rolling/sliding contacts

The introduction of the energy equation into the elasto-hydrodynamic solution, considerably complicates the numerical method. Sternlicht, Lewis, and Flyn (76) assumed that all the heat produced by viscous dissipation was carried away by the lubricant and produced excessively high film temperatures. Cheng and Sternlicht (77) however, produced a re-iterative method for the simultaneous solution of the Reynolds, elasticity, and energy equations. At the metal surfaces the boundary conditions for temperature were taken as the temperatures given by the Carslaw and Jaeger (45) expression with the injected heat calculated as a function of the temperature gradient in the oil adjacent to the surface. The lubricant was assumed to be Newtonian as in the previous solutions, and exponential relationships for viscosity with pressure and temperature were adopted. The method involved locating the position of the secondary pressure peak and then relaxing the solution to give the corresponding rolling speed with a predetermined sliding/rolling speed ratio.

The results indicated that the basic features of the elasto-hydrodynamic contact given by isothermal theory also applied to contacts possessing sliding. Of particular interest was the result that film thickness remained appreciably unaffected by the oil film temperatures generated in sliding (fig. 6.7).

A comparison of the film thickness predictions from the various thermal and isothermal theories and also the experimental data of Sibley and Orcutt and Crook is given in fig. 6.7.

A typical temperature profile produced by Cheng and Sternlicht is reproduced in fig. 6.8 where the oil temperatures are expressed as mean values across the film. This is a direct consequence of an initial approximation in the theory that a mean viscosity existed across the film. This restriction was later removed by Cheng (78). In order to assess the validity of his theory, Cheng compared his calculated frictional forces with those measured by Crook (91) on the disc machine. The oil film temperatures were found to have a major influence upon the friction force, and the general behaviour of the friction with sliding speed observed experimentally was confirmed by the results of the analysis, fig. 6.10(a). Cheng at that time remarked on the absence of experimentally measured pressure profiles with which to compare his predicted pressures, and later (79) reported the measurement of pressure profiles using platinum transducers on glass discs. Agreement between theory and experiment was considered to be fair but the second pressure peak was not detected. An excellent review of the developments in experimental techniques for the measurement of film thickness, film shape, temperature distribution, and frictional traction was given by Archard (80), which included the work of Crook and Sibley and Orcutt.

An alternative numerical procedure for the thermal elasto-hydrodynamic problem was developed by Dowson and Whitaker (81) as an extension of the earlier work on isothermal conditions. A Newtonian fluid was once more assumed and pressure profiles, film shapes, and temperature distribution obtained for a range

of sliding/rolling speeds fig. 6.9.

The results were in qualitative agreement with the features of Cheng and Sternlicht's analysis. Film thickness reduced by about 1% for a change in sliding/rolling speed ratio from 0 to 50%. The height of the pressure spike was reduced by sliding and its location moved towards the centre of the contact zone. With higher film temperatures, the spike became more rounded. This differed from the results of Cheng and Sternlicht where the height increased with sliding. A further discrepancy may be observed between the two solutions by comparing the magnitudes of the film temperatures. Dowson and Whitaker produce maximum film temperature rises of between 1 and 14°C whereas Cheng and Sternlicht's temperature rises are in the region of 10 - 50°C. This may be a result of the slight differences in numerical procedure or simply the different range of conditions considered and pressure viscosity relationships employed.

The frictional force variation with sliding speed given by Dowson and Whitaker however, does not agree with the general behaviour of Crook's experimental results. The disc machine tests showed that a maximum frictional force is reached at a sliding/rolling speed ratio of 5 to 15% beyond which the friction falls continuously with increasing sliding. Cheng supported his method of solution by obtaining similar behaviour of his predicted frictional forces. In Dowson and Whitaker's solution, the frictional force continued to rise, even at a sliding/rolling speed ratio of 50%, fig. 6.10(b).

More support is therefore given to the higher temperatures obtained by Cheng and Sternlicht and it is interesting at this point, to recall the temperatures calculated by Crook in his analysis outlined in section 6.3. Although film thicknesses

and pressure profiles were assumed from the Grubin theory, the calculated temperatures were in the order of 100 to 200°C.

Clearly, if the failure of rolling/sliding contacts is to be examined in the light of the critical temperature theory, then it is important to be able to assess the temperatures generated in the oil film and particularly the temperature rises at the metal surfaces. Whilst the heat generation does not appear to significantly affect the main features of the elasto-hydrodynamic solution, it will be responsible for the peak temperatures attained by the metal surfaces in their passage through the contact.

In the present investigation, a numerical procedure for the application of the energy equation to an elastohydrodynamic contact of given shape and pressure profile is developed. The thermal diffusivity of the metal surfaces is considered and the usual approximations to semi-infinite solids are dispensed with. A method of calculating the temperature distribution in the contact zone is provided and interesting and useful characteristics of the heat flow are discovered.

The Energy Equation

The full energy equation for an arbitrarily chosen elemental volume of fluid is given by (83):-

$$\frac{\partial Q}{\partial t} + \frac{\partial}{\partial x_j}(U_i \tau_{ij}) - \frac{\partial}{\partial x_j}(E_t \rho U_j) + \frac{\partial}{\partial x_j}\left(k \frac{\partial T}{\partial x_j}\right) - \frac{\partial E_t \rho}{\partial t} = 0 \qquad \ldots\ldots (6.11)$$

where $\frac{\partial Q}{\partial t}$ is the rate of heat produced per unit volume by

external agencies and Et is the total energy of the system per unit mass, i.e. $E_t = \frac{1}{2} Ui\ Ui + Pe + Ee$ (6.12). Pe is the potential energy, and $\frac{1}{2} Ui\ Ui$ is the kinetic energy per unit mass. Ee is the internal energy.

The first term involving the total energy represents the energy loss by convection and the last term gives the rate of change of total energy with time.

The second term is the rate at which heat is produced by viscous stresses, τij representing the components of viscous stress and Ui the i-th component of velocity. The $\frac{\partial}{\partial xj}\left(k \frac{\partial T}{\partial xj}\right)$ term gives the energy loss by heat conduction from the volume. The symbols i and j assume the values 1, 2, and 3.

The two total energy terms may be combined to give:-

$$\frac{\partial Et \rho Uj}{\partial xj} + \frac{\partial Et \cdot \rho}{\partial t} = Et\left(\frac{\partial \rho}{\partial t} + \frac{\partial Uj \rho}{\partial xj}\right)$$

$$+ \rho\left(\frac{\partial Et}{\partial t} + Uj \frac{\partial Et}{\partial xj}\right) = \rho \frac{DEt}{Dt}$$

Since $\frac{\partial \rho}{\partial t} + \frac{\partial(\rho Uj)}{\partial xj} = 0$ by continuity of flow ..... (6.13)

From Eq. (6.12), $\rho \frac{DEt}{Dt} = \rho\left(Ui \frac{DUi}{Dt} + Uj \frac{\partial Pe}{\partial xj} + \frac{DEe}{Dt}\right)$

Since $\frac{\partial Pe}{\partial t} = 0$ ..... (6.14)

Also, $\frac{\partial(Ui\ \tau ij)}{\partial xj} = Ui \frac{\partial \tau ij}{\partial xj} + \tau ij \frac{\partial Ui}{\partial xj}$

From Newton's second law of motion the total force acting on a compressible fluid mass enclosed in an arbitrary volume fixed in space is equal to the time rate of change of momentum, i.e.

$$\rho \frac{DUi}{Dt} = X + \frac{\partial \tau ij}{\partial xj} \qquad \ldots\ldots(6.15)$$

where X is the i-th component of the body forces per unit volume and equal to $- \rho \frac{\partial Pe}{\partial xi}$

It is found that a convenient approximation for the stress - strain relationships of a viscous fluid (84) is,

$$\tau ij = - p + \lambda \left(\frac{\partial Uk}{\partial xk} \right) + 2 \eta \frac{\partial Ui}{\partial xi}$$

when $i = j$ and $k = 1, 2, 3$

and $$\tau ij = \eta \left(\frac{\partial Ui}{\partial xj} + \frac{\partial Uj}{\partial xi} \right)$$

when $i \neq j$ ..... (6.16)

η may be identified with the experimentally determined coefficient of shear viscosity, termed the "first coefficient of viscosity" (84). The quantity λ is in the nature of a viscosity and termed by various writers as the "second", the "dilational" or the "volume" coefficient of viscosity.

For an incompressible fluid the dilation $\left(\frac{\partial Uk}{\partial xk} \right)$ is zero from equation (6.13) and λ drops out of the equations and does not enter into the hydrodynamic phenomena generally experienced.

However, if the compressibility of the fluid is not ignored, then the term remains and some relevant value has to be

found. This is discussed later.

Substituting Eqs. (6.12), (6.14) and (6.15) into Eq. (6.11) produces,

$$\frac{\partial Q}{\partial t} + \tau_{ij}\frac{\partial U_i}{\partial x_j} + \frac{\partial}{\partial x_j}\left(k\frac{\partial T}{\partial x_i}\right) = \rho\frac{DEe}{Dt}$$

which may be rewritten from Eq. (6.16) as:-

$$\frac{\partial Q}{\partial t} + k\nabla^2 T + \phi = \rho\left\{\frac{DEe}{Dt} + p\left(\frac{\partial U}{\partial x} + \frac{\partial V}{\partial y} + \frac{\partial w}{\partial z}\right)\right\} \quad \ldots\ldots (6.17)$$

where $\nabla^2 = \frac{\partial^2}{\partial x^2} + \frac{\partial^2}{\partial y^2} + \frac{\partial^2}{\partial z^2}$ if $x = x_1$, $y = x_2$, $z = x_3$

and $\phi = \eta\left[2\left\{\left(\frac{\partial U}{\partial x}\right)^2 + \left(\frac{\partial V}{\partial y}\right)^2 + \left(\frac{\partial w}{\partial z}\right)^2\right\}\right.$

$\left. + \left\{\frac{\partial U}{\partial y} + \frac{\partial V}{\partial x}\right\}^2 + \left\{\frac{\partial V}{\partial z} + \frac{\partial w}{\partial y}\right\}^2 + \left\{\frac{\partial w}{\partial x} + \frac{\partial U}{\partial z}\right\}^2\right]$

$+ \lambda\Delta^2$

Δ is the dilation $= \frac{\partial U}{\partial x} + \frac{\partial V}{\partial y} + \frac{\partial w}{\partial z}$

Also $p\left(\frac{\partial U}{\partial x} + \frac{\partial V}{\partial y} + \frac{\partial w}{\partial z}\right) = -p\frac{1}{\rho}\frac{D\rho}{Dt} = +p.\rho\frac{D(1/\rho)}{Dt}$

In most texts, the $\rho\frac{DEe}{Dt}$ term is usually written $\rho\frac{D(CT)}{Dt}$, but as pointed out in reference (81) this is not correct for liquids. Instead, the internal energy may be derived from enthalpy considerations.

$$I_e = E_e + p\,V$$

and $$dI_e = C\,dT + \left[V - T \left(\frac{\partial V}{\partial T} \right)_p \right] dp \quad \text{from ref. (85)}$$

give $$dE_e = C\,dT - T \left(\frac{\partial V}{\partial T} \right)_p dp - p\,dV$$

$$= C\,dT - \epsilon\, TV\, dp - p\,dV$$

$$= C\,dT - \frac{\epsilon T}{\rho}\, dp - p\,d\left(1/\rho\right)$$

Hence Eq. (6.17) takes the form:-

$$\rho C \frac{DT}{Dt} - \epsilon T \frac{Dp}{Dt} = \frac{\partial Q}{\partial t} + k\nabla^2 T + \phi$$

with k assumed constant throughout the volume of fluid.

In considering the flow of oil between discs, the problem is simplified by taking the discs to be infinitely wide and running steadily. This implies that variations in the y direction can be neglected if the x direction is taken as that of the surface velocities of the discs, that V = w = 0, and conditions are steady with time.

Hence $$\phi = \eta \left\{ 2 \left(\frac{\partial U}{\partial x} \right)^2 + \left(\frac{\partial U}{\partial z} \right)^2 \right\} + \lambda \left(\frac{\partial U}{\partial x} \right)^2$$

and $$\rho C U \frac{\partial T}{\partial x} = \left(\frac{k \partial^2 T}{\partial x^2} \right) + \left(\frac{k \partial^2 T}{\partial z^2} \right)$$

$$+ \epsilon TU \frac{\partial p}{\partial x} + \phi$$

The $\frac{\partial Q}{\partial t}$ term is omitted as external heat sources are not usually present in the type of problem considered here.

In rolling contacts, the oil film is very thin compared to the length of the contact zone. As a first approximation therefore a solution to the above equation may be obtained for

$$\frac{\partial^2 T}{\partial z^2} >> \frac{\partial^2 T}{\partial x^2}$$

The energy equation is thus:-

$$\rho C U \frac{\partial T}{\partial x} = k \frac{\partial^2 T}{\partial z^2} + \epsilon T U \frac{\partial p}{\partial x} + \eta \left(\frac{\partial U}{\partial z} \right)^2 + (2\eta + \lambda) \left(\frac{\partial U}{\partial x} \right)^2$$

To obtain a first solution to the energy equation, the fluid will be considered incompresible; in which case the compressibility terms $\left(\epsilon T U \frac{\partial p}{\partial x}\right)$ and $(2\eta + \lambda)\left(\frac{\partial U}{\partial x}\right)^2$ disappear.

The latter term is associated with compressibility in that $\frac{\partial U}{\partial x}$ implies a change of velocity in the x direction.

The simplified energy equation therefore becomes:-

$$\rho C U \frac{\partial T}{\partial x} = k \frac{\partial^2 T}{\partial z^2} + \eta \left(\frac{\partial U}{\partial z} \right)^2 \qquad \ldots\ldots (6.18)$$

These restrictions are removed at a later stage to study the effects of compressibility.

6.7 Numerical Solution of the Energy Equation

The method of solution involves the application of the energy equation to the contact of lubricated gear teeth and discs, where the conditions are "Near - Hertzian" that is, where the full solutions for the pressure profiles approach very closely the Hertzian pressure profiles for dry contacts.

The object of the present work is not to perform a full thermal analysis of the elastohydrodynamic problem, as this is

presented elsewhere (77, 78, 81), but to provide a method by which to calculate the temperatures at lubricated rolling/sliding contacts.

In most cases, full pressure profiles and film shapes are not available and in order to assess the possibility of failure of the contact, the Grubin contact model has to be adopted. Under near - Hertzian conditions the film thickness given by the Grubin formula is in good agreement with the full solution of Dowson et al.

In the examples given here, a Grubin type contact is assumed but the method can be applied to a contact for which the full pressure profile and film shape is known. The method of solution presented here is one of utilising the results of the isothermal elastohydrodynamic solution and applying the energy equation to elements in the contact rather than providing simultaneous solution of the elasticity, lubrication, and energy equations. Such solutions have shown that the introduction of sliding and consequent temperature rise does not significantly alter the overall results for pressure and film thickness.

The geometry of the contact is therefore taken as represented by the Grubin model given in fig. 6.11.

The Hertzian solution (57) gives the width of the contact as,-

$$b = 3.193 \sqrt{\frac{w\, R_N}{E^1}}$$

and a maximum contact pressure of:-

$$Po = 0.399 \sqrt{\frac{E^1\, w}{R_N}}$$

with a pressure distribution of:-

$$Px = Po \left(1 - \left(1 - \frac{x}{(b/2)}\right)^2\right)^{\frac{1}{2}}$$

The Grubin model (63) gives a constant film thickness of

$$h = \frac{1.95\,(\eta_o\, U_e\, \delta)^{8/11}}{(w/E^1)^{1/11}\,(\frac{1}{R_N})^{4/11}}$$

Alternatively, the Dowson and Higginson (71) equation may be used although this applies to the minimum film thickness occurring at the constriction near the exit of the contact.

$$\text{i.e.} \quad h = 1.6\,\delta^{0.6}\,(\eta_s\, U_e)^{0.7}\,(E^1)^{0.03}\,R_N^{0.43}\,w^{-0.13}$$

The difference between the two expressions is about 10 to 20%.

U_1 and U_2, the surface velocities are determined by the angular velocities of the contacting members and their respective radii of contact. The slip between the two surfaces is defined as:-

$$S = \frac{U_1 - U_2}{U_1}$$

Finally, by assuming inlet surface temperatures and the viscosity characteristics of the lubricant, the starting conditions for the solution are complete.

The contact zone is divided by a grid into a number of elements at which the energy equation (Eq. 6.18) is applied in turn Fig. 6.12. Starting at the inlet, the first row of elements across the film and into the metal are set at the inlet temperatures and the oil viscosities determined from the relevant viscosity - temperature characteristic for the lubricant.

In the results given later for a series of plain mineral oils, the following equations from the Vogel viscosity relationship (57) were used:-

$\eta_s = .0088\, e^{1650/T+170}$ micro Reyns for SAE 10

$$\eta_s = .0073\, e^{2100/T+170} \quad \text{micro Reyns for SAE 30}$$

$$\eta_s = .0015\, e^{2700/T+170} \quad \text{micro Reyns for SAE 50}$$

The dissipation term is first calculated using this viscosity and assuming the shear stress to be transmitted through each element across the film.

In this case, $\tau = \eta_j \left(\frac{\partial U}{\partial z}\right)_j$

where j is location across film

$$\therefore \sum_{o}^{h} \Delta U_j = \sum \frac{\tau}{\eta_j} \Delta z$$

$$= U_2 - U_1$$

$$= S.\, U_1$$

$$\therefore \quad \tau = \frac{S.U_1}{\Delta z} \Big/ \int_{o}^{h} \frac{1}{\eta_j}$$

hence $\left(\frac{\partial U}{\partial z}\right)_j = \frac{\tau}{\eta_j} = \frac{SU_1}{\eta_j \Delta z} \Big/ \sum_{o}^{h} \frac{1}{\eta_j}$

which gives the dissipation term $\eta_j \left(\frac{\partial U}{\partial z}\right)_j^2$ and the velocity U_j.

The temperatures across the film are then set at the values equivalent to this heat dissipation given by the equation:-

$$\rho\, C U_j \frac{\Delta T_j}{\Delta x} = \eta_j \left(\frac{\Delta U_j}{\Delta z}\right)^2$$

expressed in finite difference form.

Before progressing to the next position on the grid, it is necessary to calculate the heat conducted to the metal by virtue of the temperature gradients so obtained.

Thus,

$$\rho\, C U_j \frac{\Delta T_j}{\Delta x} = \frac{2k}{\Delta z^2} \left[\frac{T_{j+1} + T_{j-1}}{2} - T_j \right]$$

where Δz, k, ρ, C have the relevant values for the lubricant or metal depending whether the element j is in the oil or in the metal.

The above diffusion equation may be used explicitly or implicitly (86). Used explicitly, the equation produces new values of Tj from the known values of T_{j+1} and T_{j-1} and requires a stability criterion to be satisfied.

The equation applies to the transient state, but a condition exists where $Tj = \frac{T_{j+1} + T_{j-1}}{2}$ at which the steady state is reached and the above equation does not apply. There is consequently a limiting value

$$\frac{2k \Delta x}{\rho \, CUj \, \Delta z^2} = 1 \qquad \text{(ref. 87)}$$

at which Tj assumes the steady state solution. A grid size Δz and Δx has to be chosen so that $\frac{2k\Delta x}{\rho \, CUj \, \Delta z^2} \leqslant 1$

If this condition is not met, then Tj exceeds $\frac{T_{j+1} + T_{j-1}}{2}$ and an instability in the calculation of Tj follows at subsequent grid positions. This criterion has to be satisfied for elements in both the oil and the metal. At the interface, the following diffusion equation applies as described in Appendix VII.

$$Uj \frac{\Delta Tj}{\Delta x} = \frac{2}{\rho \, m \, Cm \Delta z_m} \left[\frac{T_{j+1} - T_j}{\frac{\Delta z_o}{2ko} + \frac{\Delta z_m}{2km}} + \frac{T_{j-1} - T_j}{\frac{\Delta z_m}{km}} \right]$$

In this case j and j-1 are elements in the metal and (j+1) is in the oil. A similar stability criterion applies to this equation, but it was found that if the previous criterion is satisfied in both the oil and metal, then the interface equation

is also stable.

An implicit solution of the above diffusion equations does not involve the consideration of stability. Tj has to be calculated from the final calculated values of T_{j-1} and T_{j+1} which are initially unknown. A re-iteration over the grid is therefore required in order to find values of Tj satisfying the equations. It was considered that there would be little saving in computing time by adopting an implicit method of solution, although a smaller number of grid points would be needed.

Having determined the temperatures across the film and into the metal at the first row of elements in the contact, the elements are followed through into the next row of grid positions in the direction of sliding. This represents the convection term in the energy equation, which has now been solved for the preceding row of element grid positions. The heat convected from the grid position was provided by the viscous dissipation minus the net heat conducted to adjacent elements.

At the new position, the elements have acquired a new viscosity due to the new temperature and this is calculated by the equations used previously. There is also a local pressure rise at the new grid position, as the elements pass through the Hertzian pressure profile. In the examples given later, the Cameron and Chu (88) relationship for pressure - viscosity effects is used where

$$\eta = \eta_s (1 + C_1 . p)^{16} \qquad .4 + \frac{T^oF}{400}$$

$$C_1 = .062\ \eta_s^{-0.62}\ 10^{-(\quad)}$$

P = pressure in lbf/in x 10^3

η_s in cp

The whole process of dissipation using the new viscosity followed by diffusion is then repeated to produce a further temperature distribution that is then carried over to the next row of grid positions at a new local pressure and so on through the contact zone to the exit.

The numerical procedure was programmed for the Elliot 803 computer using AUTOCODE 803 language. A block diagram representing the main functions of the programme is given in Appendix VIII, and a copy of one of the programmes is included in Appendix IX.

6.8 Discussion of Results

The results given in the present work are for the case of 5" PCD 20° pressure angle gears, operating at speeds of 500 to 1500 rev/min and subjected to 1174 to 4676 lbf/inch width loading. These gears are those used in the Thornton gear tester for the scuffing tests and details of the tooth profile are given in Appendix III. The effective contact radius at the tip of the gear teeth is 0.330 inches and this contact model is used to investigate a range of slide ratios, although a slip of .64 applies to the actual case. Throughout the calculations, the oil properties of thermal conductivity, density, and specific heat are assumed constant except where stated otherwise.

The following constant properties have been assumed

Thermal diffusivity of oil	= .000178 in^2/S
Thermal diffusivity of metal (steel)	= .0168 in^2/S
Specific Gravity of oil	= .87
Density of metal	= .288 lb/in^3
Specific heat of oil	= .5 BTU/lb^oF
Specific heat of metal	= .115 BTU/lb^oF

6.8.1 The mid-oil and metal surface temperature

An assumption in the theory, that heat conduction in the direction of sliding is negligible compared to that across the film, enabled an explicit diffusion equation to be used. The assumption appears to be valid when the isotherms over the contact zone are examined (fig. 6.13). Remembering that the oil film thickness is drawn to a scale 50 times that of the contact width, the temperature gradients across the film are much larger than those in the sliding direction. Even in the inlet region the temperature gradient across the film is two orders higher than that in the negative sliding direction. A re-iteration of the numerical calculation, this time taking into account the heat conduction in the direction of motion, would result in little change in the temperature distribution, the main differences occurring at inlet and outlet. The peak temperatures would be only slightly affected, and these temperatures are the important ones when investigating the failure of elasto-hydrodynamic contacts.

Figs. 6.14, 6.15, 6.16, 6.19, 6.20 show the variation of temperatures for a range of entraining velocities, slip, load and viscosity. The oil film temperatures are much higher than the metal surface temperatures but at exit there is approximately a uniform temperature distribution. The maximum temperature attained by a metal surface depends upon the time of transit through the contact, consequently the slower speed surface attains the highest temperature of the two surfaces. It follows that at increased entraining velocities, the metal surface temperatures are reduced and the oil film temperatures increased. An overall increase in both oil and metal temperatures is achieved by a greater slip, the difference between the metal

surface temperatures increasing. The combined effects are shown in fig. 6.17.

In all these results, the temperature at inlet to the contact has been taken as uniform across the oil film and into the metal, implying that the two metal surfaces are able to attain the same blank temperature before re-engaging. No account has been taken of the small temperature rise due to the heat of compression in the oil film at entry or the heat conducted upstream of the oil flow from the contact zone. The theory therefore assumes that the temperatures at inlet, taking into account these factors, are known and that these are the starting points for the calculation. The controlling factor over the blank temperatures will be the ability of the machine elements to dissipate the heat to the surroundings and this will depend on the heat transfer coefficient of the particular component. A steady operating condition will be reached at which the blank temperatures will be known. The effect of differing blank temperatures between the two surfaces, owing to different heat flows and heat transfer coefficients, will be examined later. For uniform blank temperatures varying by twenty to thirty per cent, fig. 6.18 shows that the mid-oil temperature profile differs in the inlet and outlet regions only and that the temperature rise of the metal surfaces differ by not more than eight per cent.

6.8.2 Effect of Viscosity

The results so far have been concerned with a lubricant of SAE 10 rating, a relatively low viscosity lubricant for this type of contact. By increasing the viscosity grades to SAE 30 and SAE 50, the temperature profiles become modified. At low

slip, the SAE 30 oil results in a slightly higher mid-film temperature and lower surface temperatures. The SAE 50 again produces lower surface temperatures but the mid-film temperature does not rise to as high a value as the lower viscosity lubricants and produces a higher exit oil temperature. The same behaviour is observed for the SAE 30 lubricant when the slip is increased to 0.3 and a marked increase in the difference between the surface temperatures becomes apparent. This increase in surface temperature differences is more when viscosity and slide ratio are increased. Whereas the peak oil temperature for the SAE 10 oil always occurs at or near the mid-plane of the oil-film, the more viscous lubricants produce peak temperatures offset from the mid plane and under the conditions given, nearer the slower surface. This is illustrated more clearly by considering the transverse film temperature profiles in fig. 6.21. The velocity profiles of the fluid at three positions through the contact are shown in fig. 6.22, for each of the lubricants, the central profile in each case corresponding to the position of the temperature profiles in fig. 6.21(b). At any section across the oil film, the shear stress is constant and proportional to the product of viscosity and strain rate at any element in that section. The elements nearer the slower surface are consequently at a higher temperature and have lower viscosities than the corresponding elements on the other side of the mid-plane and nearer the faster surface. For the lower viscosity lubricant, the temperature differences do not produce as great a variation in viscosity as for the higher viscosity oils. Consequently, the strain rate is symmetrically distributed about the mid-plane of the film. With the larger percentage change in viscosity of the more viscous lubricants, there will be an increase in the strain rate wherever the viscosi-

is reduced due to higher temperatures on the slower side of the mid plane. In the energy equation, the viscous dissipation term is given as the product of viscosity and the square of the strain rate. The heat generation on the slower side is therefore a lot larger than that on the faster and lower temperature side, with the result that the temperatures near the slower surface are further increased. The overall effect is to move the heat source due to viscous dissipation nearer the slower surface, which consequently experiences a larger temperature rise than the other surface.

6.8.3 The heat partition ratio

From the foregoing analysis, it is possible to calculate the ratios of heat conducted to the metal surfaces. This can be computed by determining the thermal gradients at the oil-metal interface or more accurately, by a summation of the temperature rises of all elements in the metal after passing through the contact. The actual values are readily available from the computed temperature distributions of the contact. The results are shown in fig. 6.23 where the ratio of heat conducted to the slower surface over that to the fast surface increases with viscosity and slip, never being less than unity. Here, unity will represent equal partition of the heat dissipated at the contact.

A comparison may be made with the heat partition derived by Blok from the flash temperature concept.

Now, $$T_1 = \frac{2q_1}{k}\left(\frac{b}{\pi}\right)^{\frac{1}{2}}\left(\frac{\kappa}{U_1}\right)^{\frac{1}{2}} \quad \text{where } \kappa = \frac{k}{\rho C}$$

$$T_2 = \frac{2q_2}{k}\left(\frac{b}{\pi}\right)^{\frac{1}{2}}\left(\frac{\kappa}{U_2}\right)^{\frac{1}{2}}$$

partitions estimated from the above theory are shown as crosses. Once again the heat ratio approaches unity at low viscosity. Results are given later, where the heat partition attains values less than unity under certain conditions.

6.8.4 Experimental disc results reported by Merritt

Merritt (89) has reported some experimental work aimed at actually measuring the heat partition of two discs rotating under elastohydrodynamic conditions. It was found that the faster disc carried away more heat than the slower one and this was explained by a consideration of the temperature gradients within the oil film. A hypothetical curve, reprodocued in fig. 6.24 of the temperature distribution across the oil film was constructed on the assumption that there existed a uniform rate of heat generation per unit volume of the oil film. The resulting curve was therefore parabolic, and with the knowledge that more heat was to be conducted to the faster surface, the apex was displaced to a plane nearer the slow surface, so that the temperature of the slower surface was the higher although it received less heat than the other surface, by virtue of the temperature gradients at the boundaries. In fact, the faster surface was operating at a higher total contact temperature, with the conclusion that the opening assumptions were invalid and that some asymmetry in the mechanism of heat generation was present.

Such an asymmetry has been observed in the results of the present analysis. As suggested by Merritt, the heat generation is asymmetric but the temperature gradients at the surfaces do not correspond to those of a parabola; they are inverted, so that the higher temperature surface receives the greater part of the heat generated. The results so far have assumed that the

inlet temperatures are uniform. If the temperature of the faster metal surface is set higher than the other surface, to represent the conditions in Merritt's experiments, the effect on the heat partition is shown in fig. 6.25. As the temperature of the faster metal surface increases, the peak oil temperature moves nearer that side and increases the heat flow into it. The heat partition ratio then becomes less than one (fig. 6.25(b)) and the condition where the faster surface is the hotter and receives more heat is satisfied. It may seem from this that the situation becomes unstable, with the hotter surface becoming still hotter after successive passes through the contact. It has to be remembered however that in an actual application where all the heat is lost by surface convection outside the contact zone, steady operating conditions have been established and the surface will re-enter the contact at the same blank temperature.

6.8.5 Viscosity variation through the contact and tangential stresses

Merritt also predicted the variation of viscosity in the direction of sliding at the mid plane of the oil film and at the two surfaces, the latter operating at differing temperatures. The distributions obtained in the present work fig. (6.26 and 6.27) confirm the predictions of Merritt, with the added effect of the much higher oil film temperatures overriding the pressure effects and producing a large reduction in viscosity. With higher viscosity lubricants the presence of a sharp rise in viscosity at entry to the contact is associated with the pressure rise before the temperature has risen sufficiently high enough to cancel this effect. The tangential stresses are shown in fig. 6.28 where again there is agreement with the stress distributions predicted by Merritt.

6.8.6 The heat of compression

The theory has neglected the heat of compression terms $\left(\epsilon \, TUj \, \frac{dp}{dx} \right)$ and $(2\eta + \lambda) \left(\frac{\partial U}{\partial x} \right)^2$, the latter occurring as the second term in the dissipation function. The first term is readily considered by taking the appropriate value for the thermal expansion coefficient, ϵ and including the term in the step by step numerical procedure. (A typical relationship is (57) $\epsilon = \left[5.5 - \log_{10} \eta \text{ cp} \right] \times 10^{-4}$ per ^{o}F) In the first half of the contact the heat of compression is positive, since $\frac{dp}{dx}$ is positive and slightly higher oil film temperatures result. In the second half of the contact $\frac{dp}{dx}$ is negative and a cooling effect is produced. This behaviour is followed by each plane across the oil film, but is more pronounced where the velocity is higher at points in the oil film nearer the fast surface. The results show that although the magnitudes of the temperature increments due to the heat of compression term are small, the differences in magnitude across the film are sufficient to render more symmetrical a temperature distribution which would otherwise have its peak markedly nearer the ~~faster~~ slower surface than the ~~slower~~ faster.

When considering the second term in the dissipation function, the value of the second coefficient of viscosity is uncertain. In most standard texts, λ is replaced by $-\frac{2}{3}$, (57) according to the classical theory, but for liquids it has been found that λ may have a positive value. Taskoprulu, Barlow and Lamb (90) have carried out measurements of λ for oil, and determined a value of $\frac{4}{3}$; the range of validity of this result is however not known. The effect of including these different values is shown in fig. ~~81(a)~~ 6.29 where the $\lambda = -2\eta$ case represents a second

term of the dissipation function equal to zero. The change in the asymmetry of the temperature profile is again apparent, this time due to the variation in $\left(\frac{\partial U}{\partial x}\right)$ across the film. As previously determined, the peak oil temperature occurs at the plane where $\frac{\partial U}{\partial z}$ is a maximum with the effect of increasing the oil film velocities of elements nearer the fast surface and reducing the velocities nearer the slow surface. The net effect is a larger change in velocities nearer the fast surface as progress is made through the oil film (Reference to fig. 6.22 clarifies this observation). Any change in the asymmetry of a temperature profile will result in a change in the surface temperature rises and consequently the heat partition, as indicated by fig. 6.29(a) and (b). The computed results showed that besides the heat partition being reduced, the total heat dissipated at the contact reduced by as much as 10% due to the increased temperatures and reduced viscosities in the first half of contact.

When compression is being considered, the variation in density of the lubricant should be taken into account. The relationships used were those given in Ref. 81 for the effects of pressure i.e.

$$\rho = \rho_o \left(1 + \frac{.C09\ p}{1 + .02\ p}\right)$$

where $\rho o = \rho_{\substack{60^oF \\ 14.7\ lbf/in^2}} \left(1 - \epsilon\ (T - 60^oF)\right)$ from (57)

The second coefficient of viscosity is seen to be important in the determination of the surface temperature rises and heat partition and further analysis will be possible when more

definite information is available regarding the value of λ for lubricants.

6.8.7 Variable lubricant properties

Except in the analysis involving the effect of heat of compression, the lubricant properties of thermal conductivity, density, and specific heat have been assumed constant for all temperatures and pressures.

Whilst expressions exist for the effect of pressure and temperature on ρ there is little data available that relates thermal conductivity and specific heat to pressure changes. Relationships for the effect of temperature on these properties, determined at atmospheric pressure are however generally available. These are quoted in ref. 57 and given below;

$$k = \frac{.813}{\text{sp gr}} \left\{ 1 - .0003\,(T^{\circ}F - 32) \right\} \frac{\text{B Th U}}{\text{hr.ft}^{2\circ}\text{F/in}}$$

$$(\text{at } 60^{\circ}F)$$

$$C = (0.388 + .00045 \times T^{\circ}F) \times (\text{sp gr})^{-\frac{1}{2}} \frac{\text{BtU}}{\text{lb}^{\circ}\text{F}}$$

$$\text{at } 60^{\circ}F$$

These expressions were written into the computer programme so that the numerical procedure adjusted the values of density, thermal conductivity, and specific heat as the element progressed through the contact.

Examples of the effect of variable lubricant properties are given in figs. 6.30 and 6.31. The heat of compression term is ignored in both cases. Only slight adjustments to the temperature profiles occur as a result of these considerations. The mid-plane temperature profiles differ over the second half of

the contact where the temperatures are highest and the thermal diffusivities low. The net result is a reduction in the amount of heat conducted across the film to the metal surfaces, which consequently experience temperature rises about 1 to 3°F below the original predictions.

Although only small changes in temperature profile have been obtained by the above consideration, the lubricant properties of thermal conductivity, coefficient of thermal expansion, density, specific heat, and the second coefficient of viscosity, should be included in the thermal analysis wherever the relevant values at the local temperatures and pressures have been established. The numerical method presented here is readily adaptable to include these quantities as and when they become available.

6.8.8 Comparison of present method of solution with others

The oil film temperatures obtained in the present solution are of the same order as those obtained by Crook (66) but greater than those produced by the thermal elastohydrodynamic solutions of Cheng (79) and Dowson and Whitaker (81).

The treatment of the energy equation presented in this thesis differs from the previous solutions in that the energy equation is applied to both metal and lubricant and no assumption is made regarding the temperature rise of the metal surfaces. Exact heat conduction and convection equations are employed at the metal-lubricant interface and the ratios of heat partition of the contacting bodies obtained directly.

Because of this, the results show that the heat partition calculations of Blok (43) based upon the assumption of zero temperature gradients at the conjunction need to be modified.

Although Crook produced oil film temperatures, shear rates,

and viscosities having the same basic characteristics as those obtained here, the method relied upon either prior knowledge of the surface temperatures or an approximation by the Blok flash temperature equation. Consequently, Crook's method is useful in predicting phenomena that rely upon the lubricant film behaviour, such as sliding friction, but offers no additional or alternative method of calculating the surface temperature rise, which is the important factor in the prediction of scuffing. The main objection to the use of the Blok flash temperature equation is that calculated temperature rises depend so much upon the assumptions regarding the heat injected into the surfaces. The present solution has shown that the simple expression given by Blok is invalid and the actual heat partition ratio is determined by the lubricant properties and by the surface temperatures themselves.

The temperature profiles obtained in the thermal solutions of the elastohydrodynamic problem were also dependent upon the approximate heat flow equation but with the quantity of injected heat given by the thermal gradients at the edge of the oil film. The introduction of the energy equation into the elastohydrodynamic solution has shown conclusively that the major characteristics of the pressure profile and film shape are changed very little by thermal effects. Although the resulting temperature distributions assist in the further understanding of elastohydrodynamic lubrication, the method of calculating the surface temperatures is not a convenient one for gear designers.

The thermal solution proposed in the present investigation provides a method for estimating the surface temperatures at the contact between lubricated rolling/sliding surfaces and in addition enables a closer study of the oil film behaviour. It

has been found that the magnitudes of the temperatures and the heat sharing between the surfaces depend to a large extent upon the physical properties of the lubricant. The step-by-step method is however completely adaptable to take account of any specified variation of these properties through the contact and may be extended to consider the behaviour of Non-Newtonian liquids. To the authors knowledge, all published literature on thermal solutions of the elastohydrodynamic contact have been confined to the assumption of a Newtonian fluid, a theory which has proved inadequate in explaining the observed frictional behaviour of lubricant films.

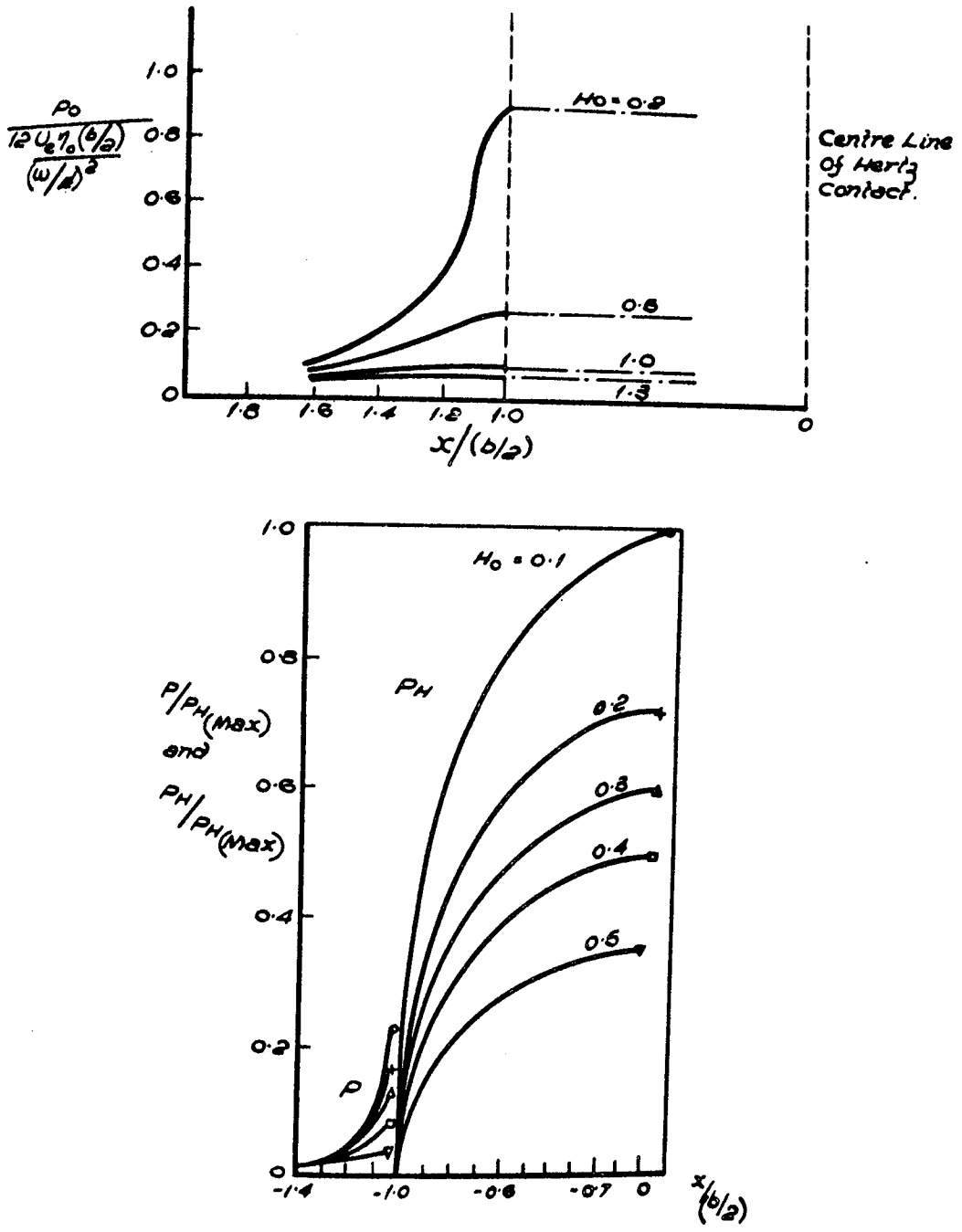

FIG. 6.1 REDUCED PRESSURE P_0 AND ACTUAL PRESSURE P IN INLET REGION TO GRUBIN (GS) CONTACT.

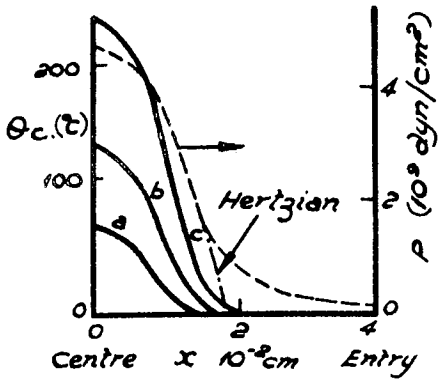

Temperature rise on medianplane for steel discs 7·6 cm. dia. $\eta_s = 0{\cdot}4$ P. $\delta = 1{\cdot}6 \times 10^{-9}$ dyn.$^{-1}$ cm^2, $u_e = 460$ cm/s, $u_1 - u_2$ = (a) 500 (b) 200 (c) 100 cm/s. $h = 0{\cdot}6 \times 10^{-4}$ cm.

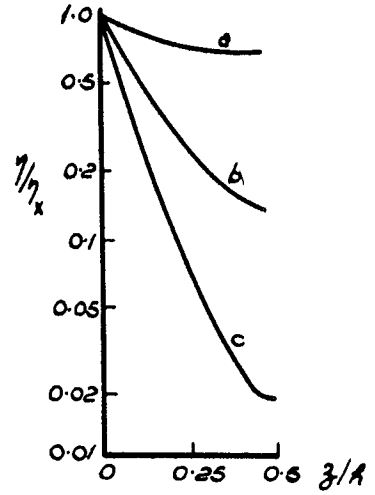

Viscosity Profile Across Film for θ_c = (a) 20°C (b) 100°C (c) 200°C.

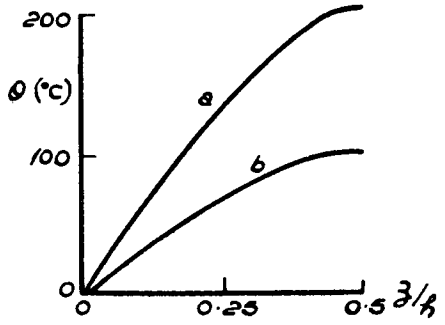

Oil Temperature Across Film for θ_c = (a) 200°C (b) 100°C

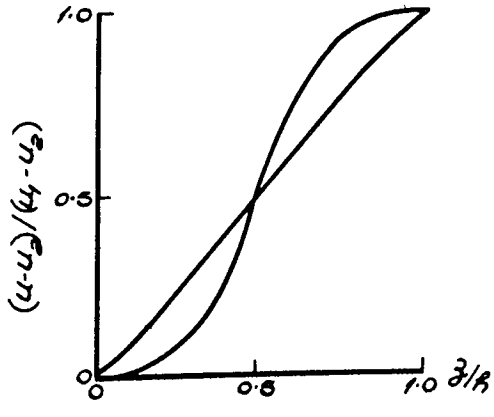

Velosity Profile Across Film for θ_c = (a) 10°C (b) 200°C.

FIG. 6.2 TEMPERATURE, VISCOSITY, AND VELOCITY PROFILES FROM CROOK'S ANALYSIS (66)

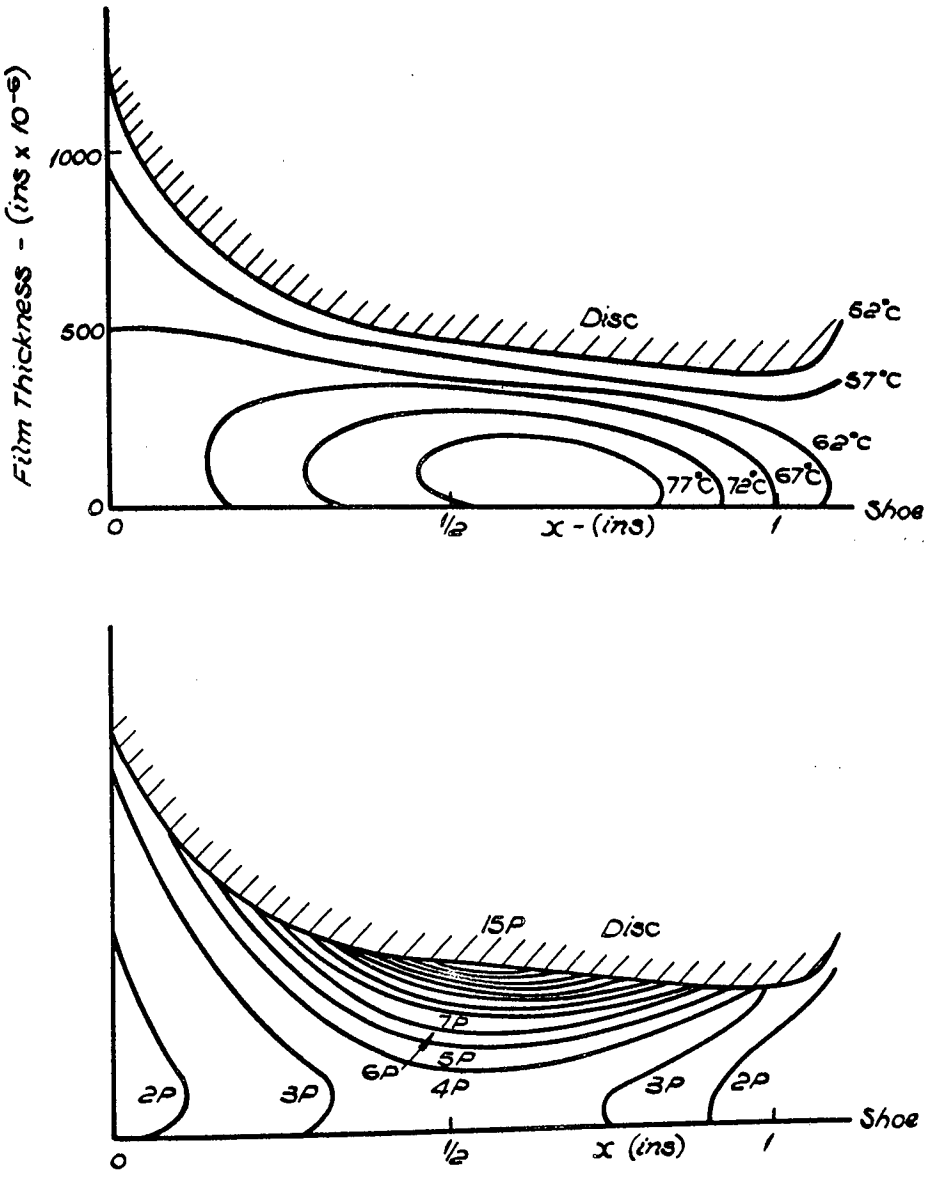

FIG. 6.3. TEMPERATURE AND VISCOSITY DISTRIBUTIONS IN OIL FILM CALCULATED FROM MEASURED SHOE TEMPERATURES IN REF. (67.)

ω = 3000 lb/inch width
Disc Dia. = 11·908 ins.
Shoe Rad. = 6·473 ins.
Speed = 300 rev/min.
Oil Viscosity 1·37P at 60°C.

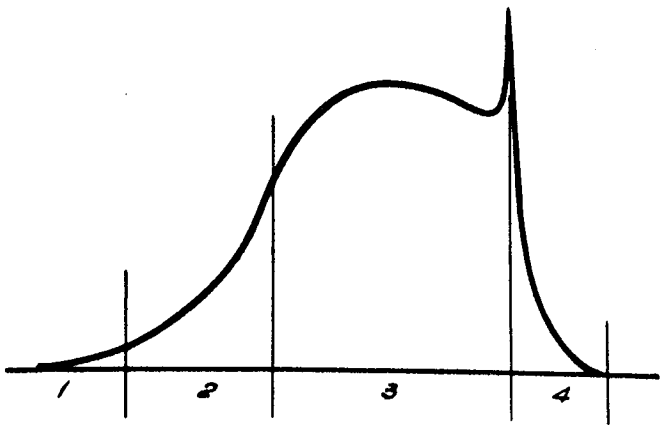

FIG. 6.4. (a) THE COMPUTING ZONES OF THE PRESSURE PROFILE USED IN REFERENCES 68, 69, 70, 80.

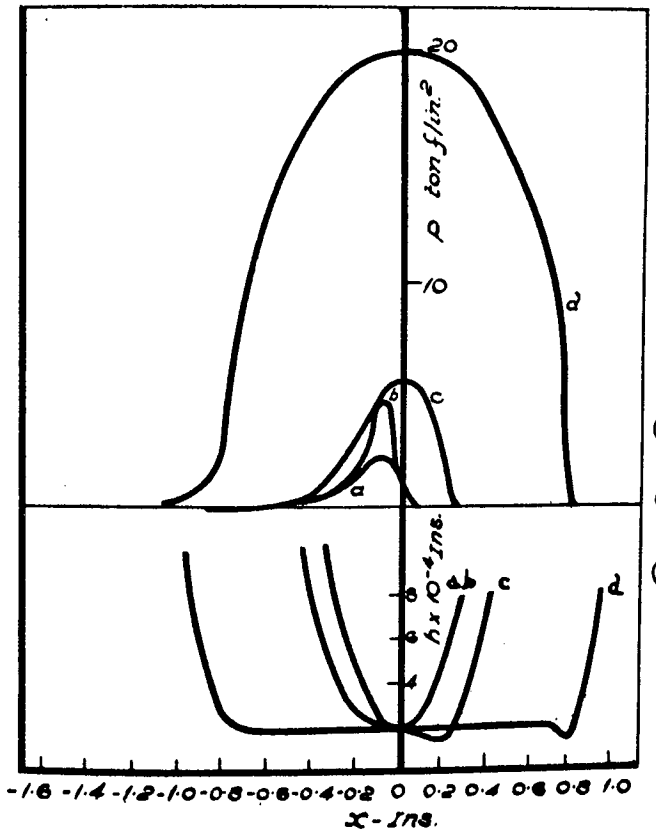

FIG. 6.4 (b)

PRESSURE DISTRIBUTIONS & FILM SHAPES FOR SAME FILM THICKNESS FROM REF. 68.

(a) Constant Viscosity, Rigid Cylinder
(b) Pressure-Dependent Viscosity, Rigid Cylinder
(c) Constant Viscosity, Elastic Cylinder
(d) Pressure Dependent Viscosity, Elastic Cylinder.

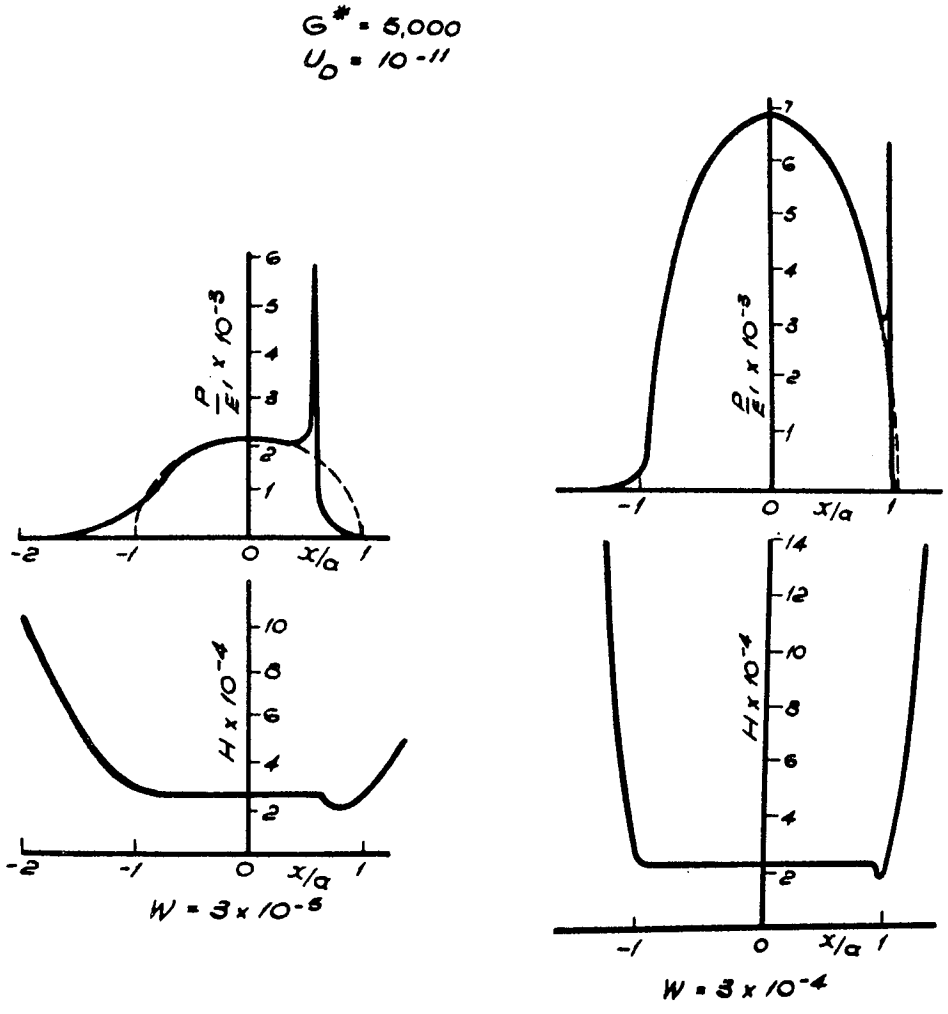

FIG. 6.5 TYPICAL RESULTS OBTAINED BY DOWSON & HIGGINSON (69) FOR PRESSURE PROFILE & FILM SHAPE IN ELASTO-HYDRODYNAMIC CONTACTS.

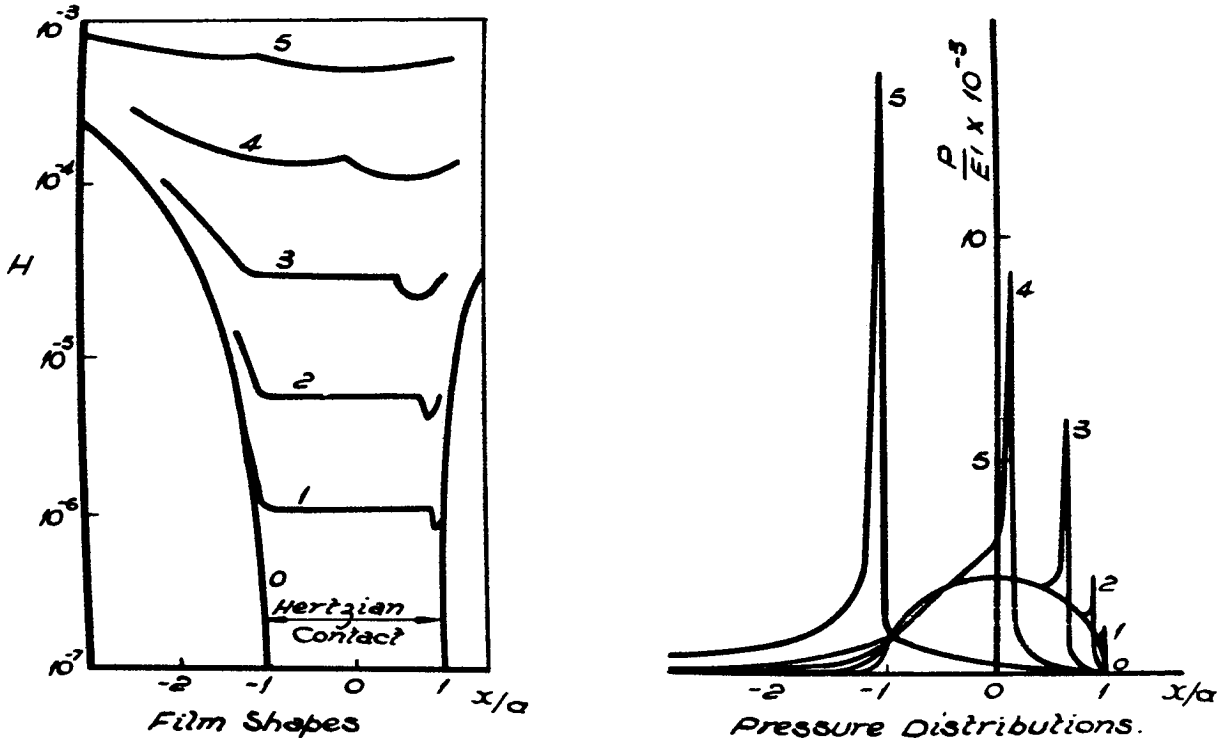

FIG. 6.6. FILM SHAPES AND PRESSURE PROFILES FOR DIFFERENT SPEEDS FROM REF. (70)

$W = 3 \times 10^{-6}$; $G^* = 5000$. U_D = (0) 0, (1) 10^{-13}, (2) 10^{-12}, (3) 10^{-11} (4) 10^{-10}, (5) 10^{-9}

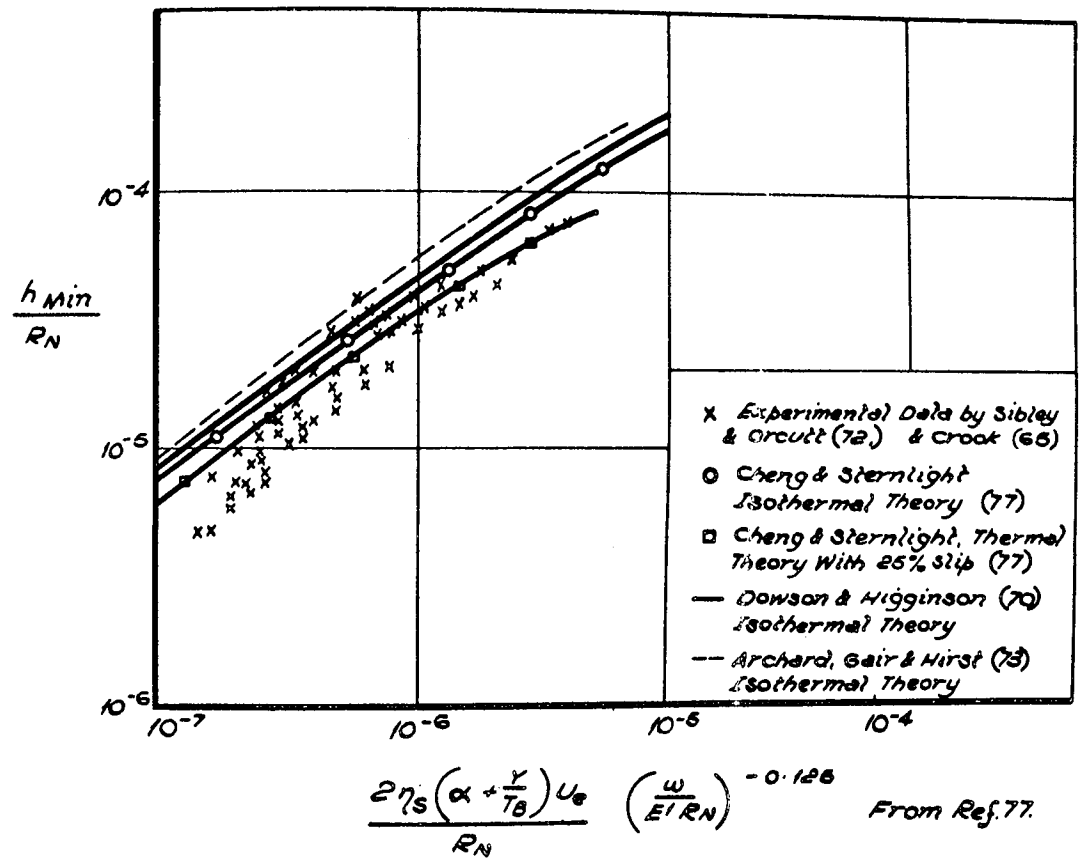

FIG. 6.7. COMPARISON OF FILM THICKNESS PREDICTIONS.

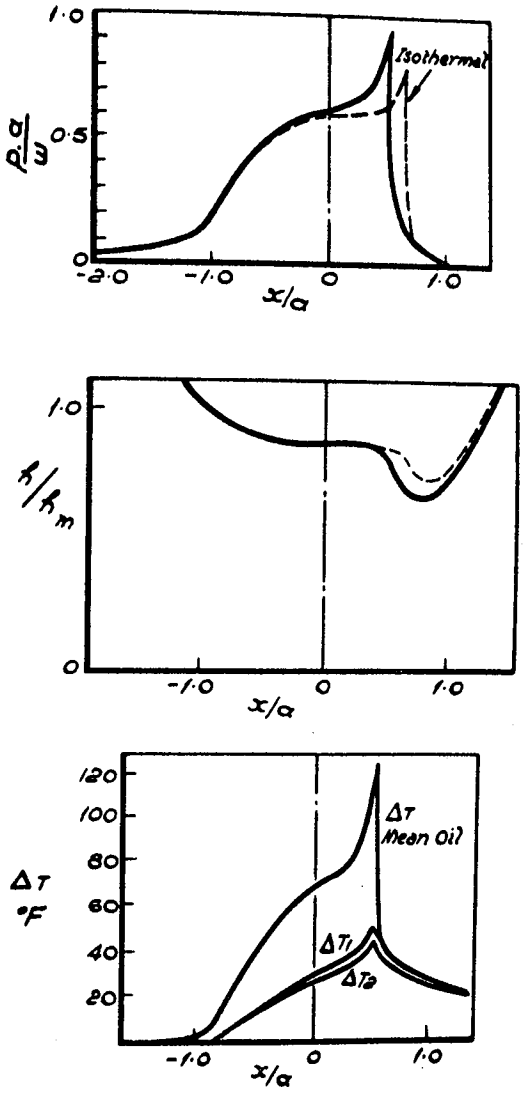

FIG. 6.8 THE THERMAL - ELASTOHYDRODYNAMIC RESULTS OF CHENG & STERNLIGHT (77)

U_e = 79·26 in/s, $\frac{U_1 - U_2}{U_1}$ = ·25. Roller Dia. = 3 ins.

T_B = 100°F.

$G^* = 3737$, $W = 3.19 \times 10^{-5}$

$T_B = 50°C$, Roller Dia = 3 ins.

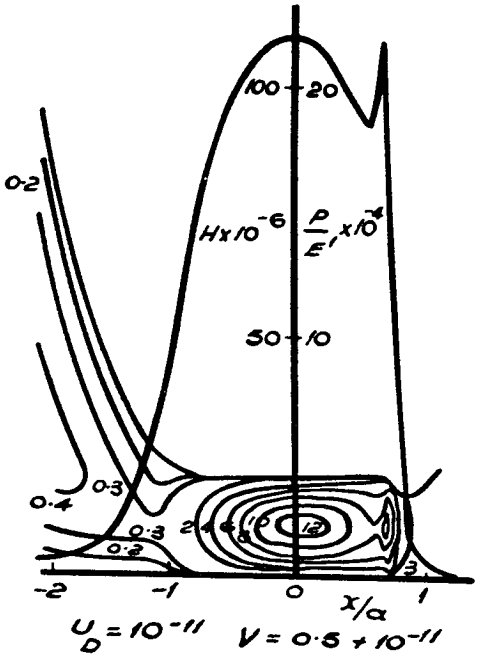

Temperature rise at EHL Contact (ΔT °C)

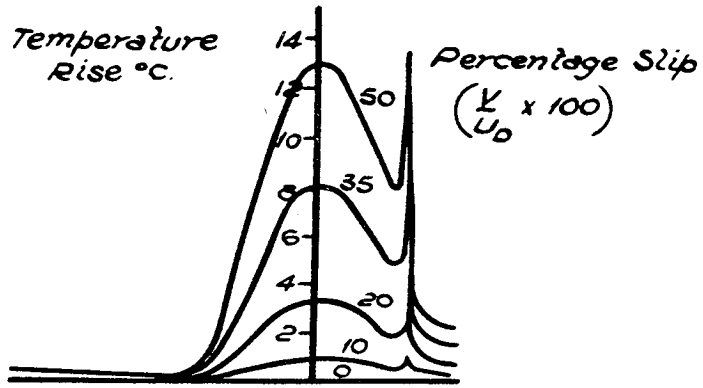

The range of mid film temperature distributions (ΔT °C)

FIG. 6.9. THE CALCULATED TEMPERATURE RISE DISTRIBUTIONS FROM REF. (81)

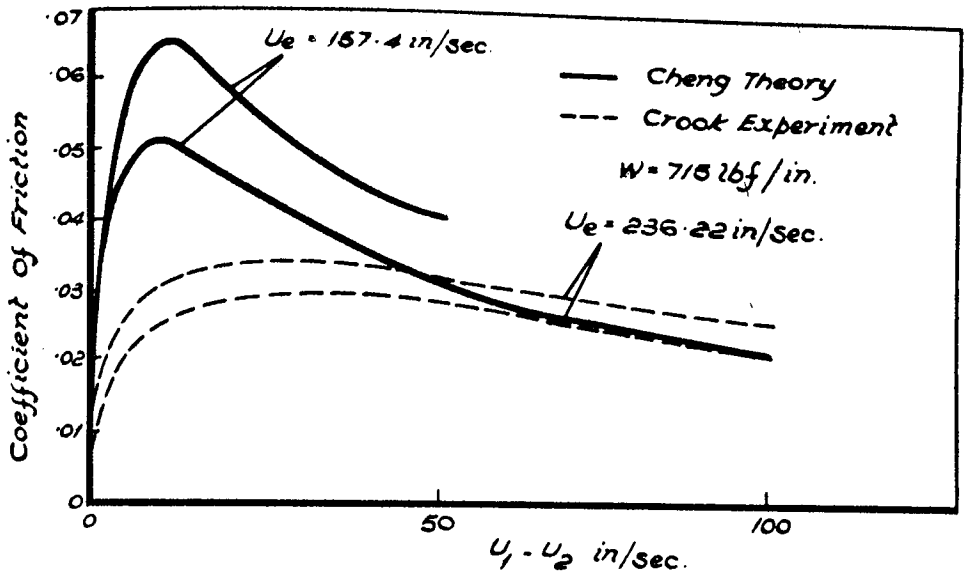

FIG. 6.10 (a) FRICTIONAL FORCE RESULTS FROM REF. (78) COMPARED WITH EXPERIMENT.

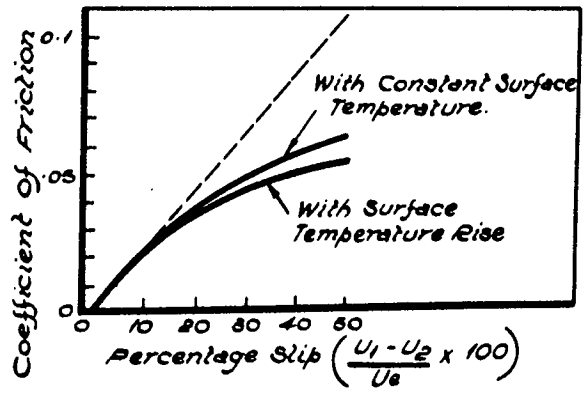

FIG. 6.10(b) THE FRICTIONAL FORCE RESULTS FROM REF. (81.)

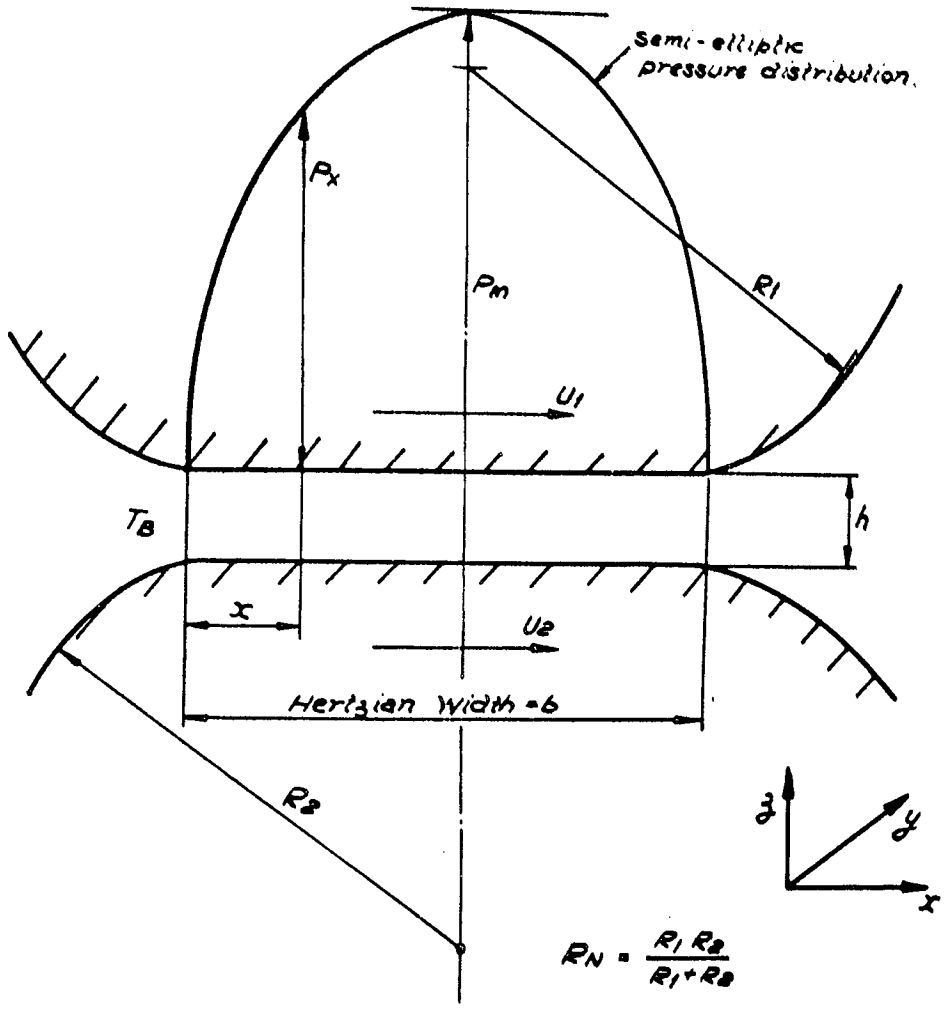

FIG. 6.11. THEORETICAL MODEL OF CONTACT.

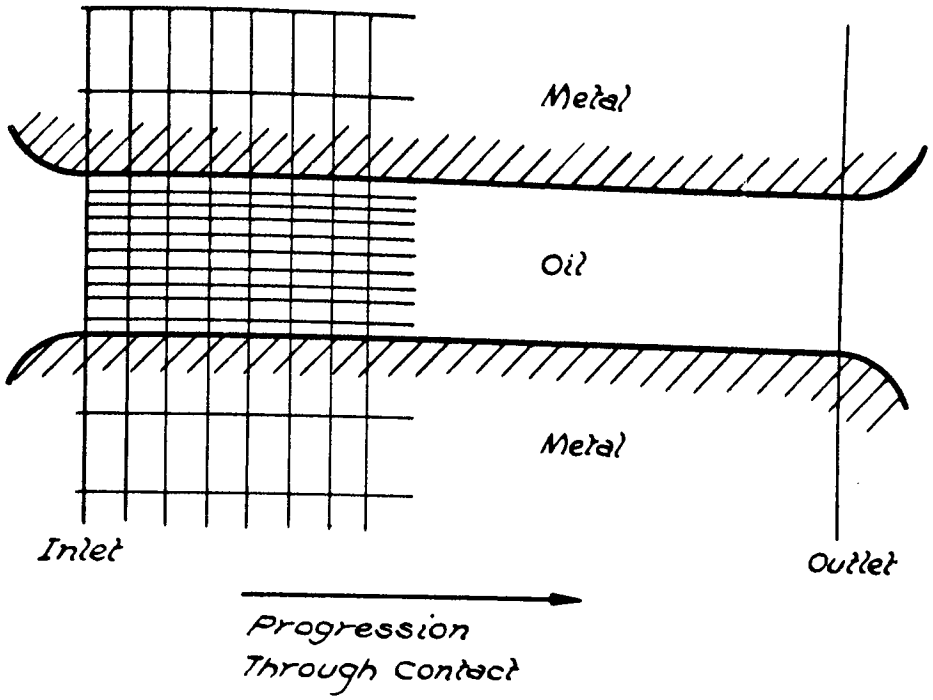

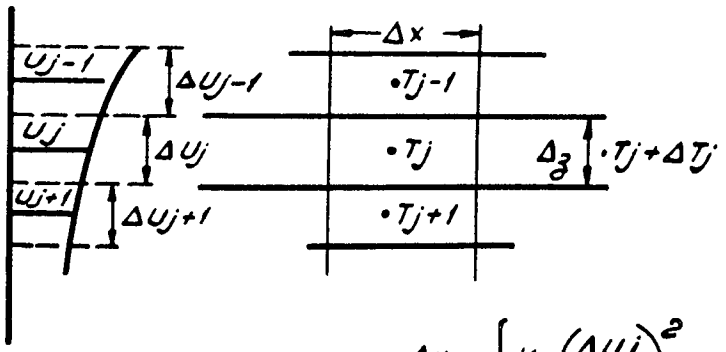

$$\Delta T_j = \frac{\Delta x}{\rho c u_j} \left\{ \eta_j \left(\frac{\Delta u_j}{\Delta z} \right)^2 + \frac{2k}{\Delta z^2} \left(\frac{T_{j+1} + T_{j-1}}{2} - T_j \right) \right\}$$

FIG. 6.12. THE GRID FOR NUMERICAL CALCULATION.

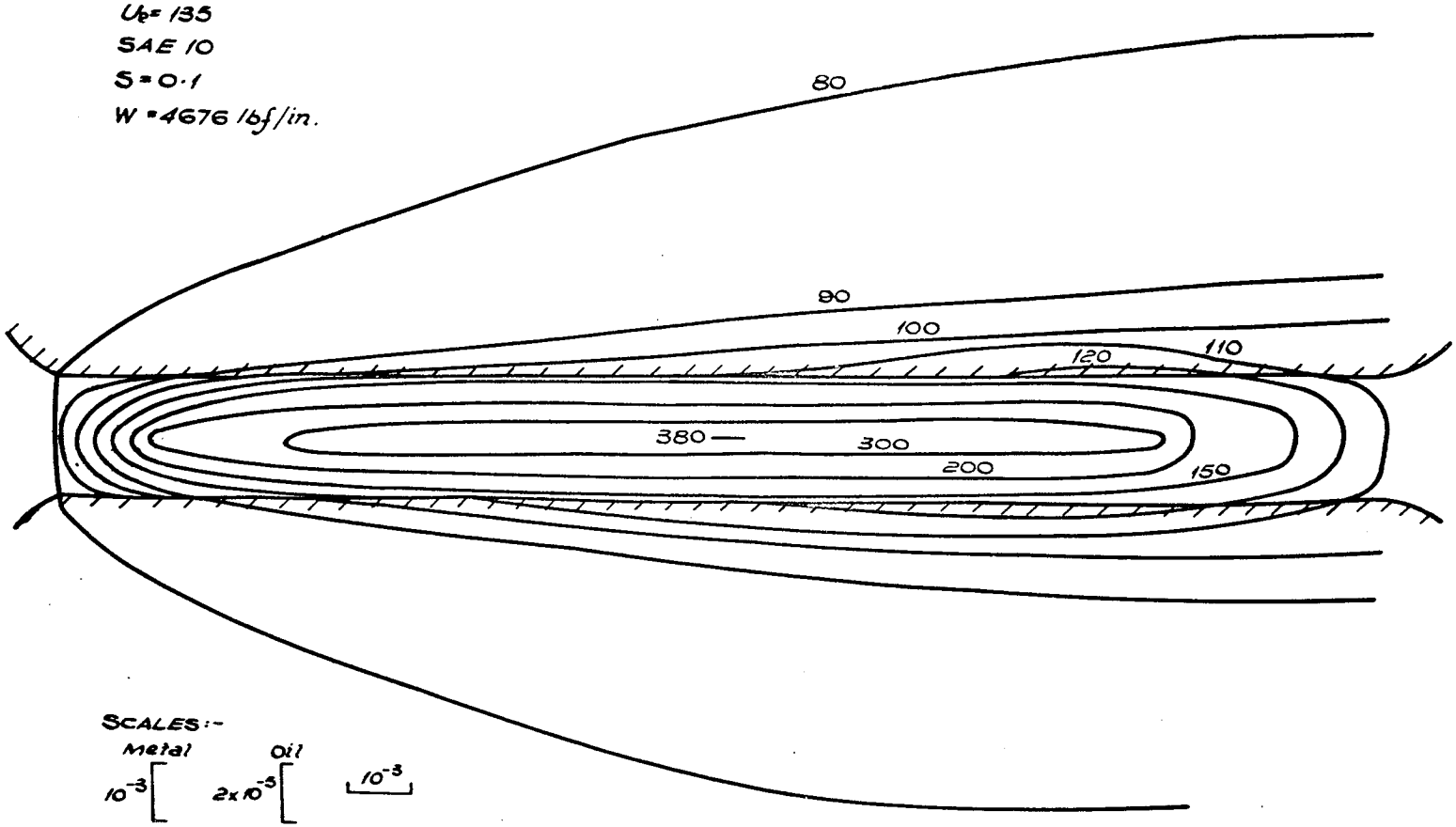

FIG. 6.13. TYPICAL TEMPERATURE DISTRIBUTION THROUGH CONTACT.

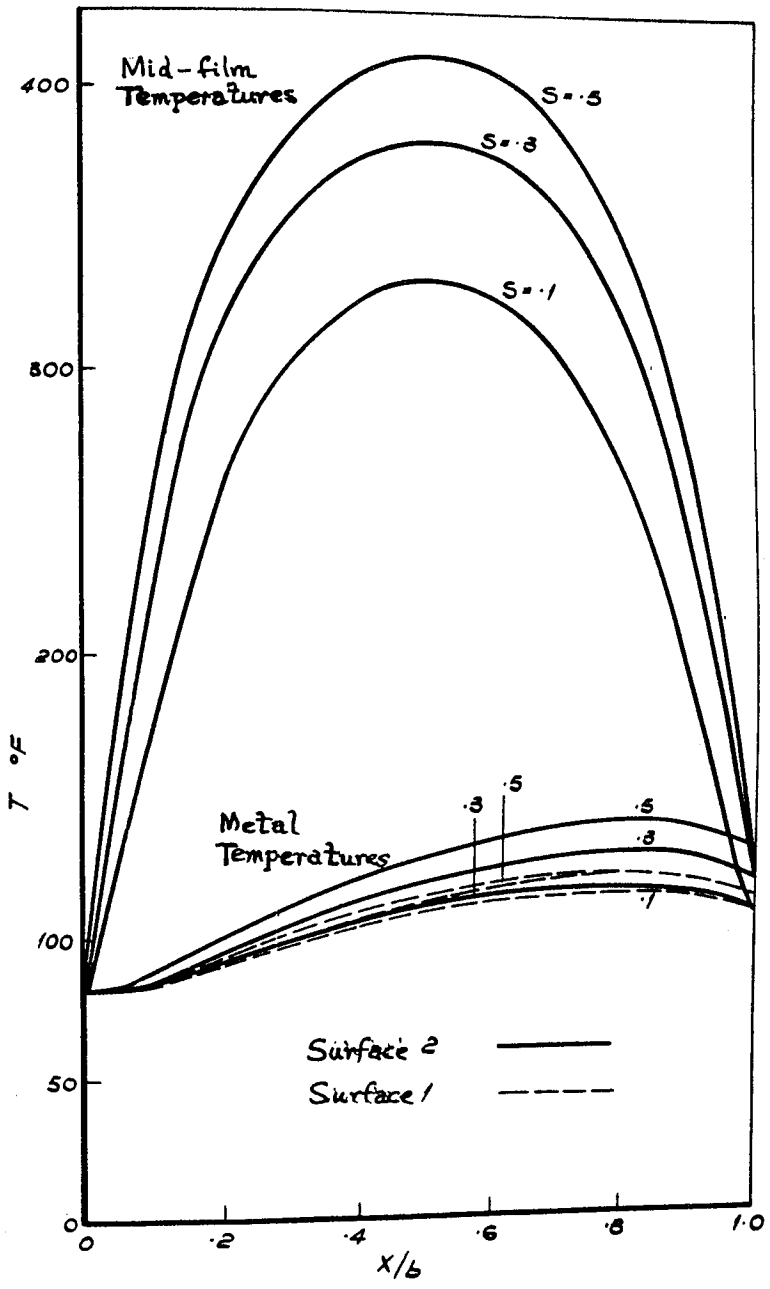

FIG.6.14 EFFECT OF SLIP ON TEMPERATURE DISTRIBUTION

U_e = 135 in/s W = 4·676 lbf/in SAE.10.

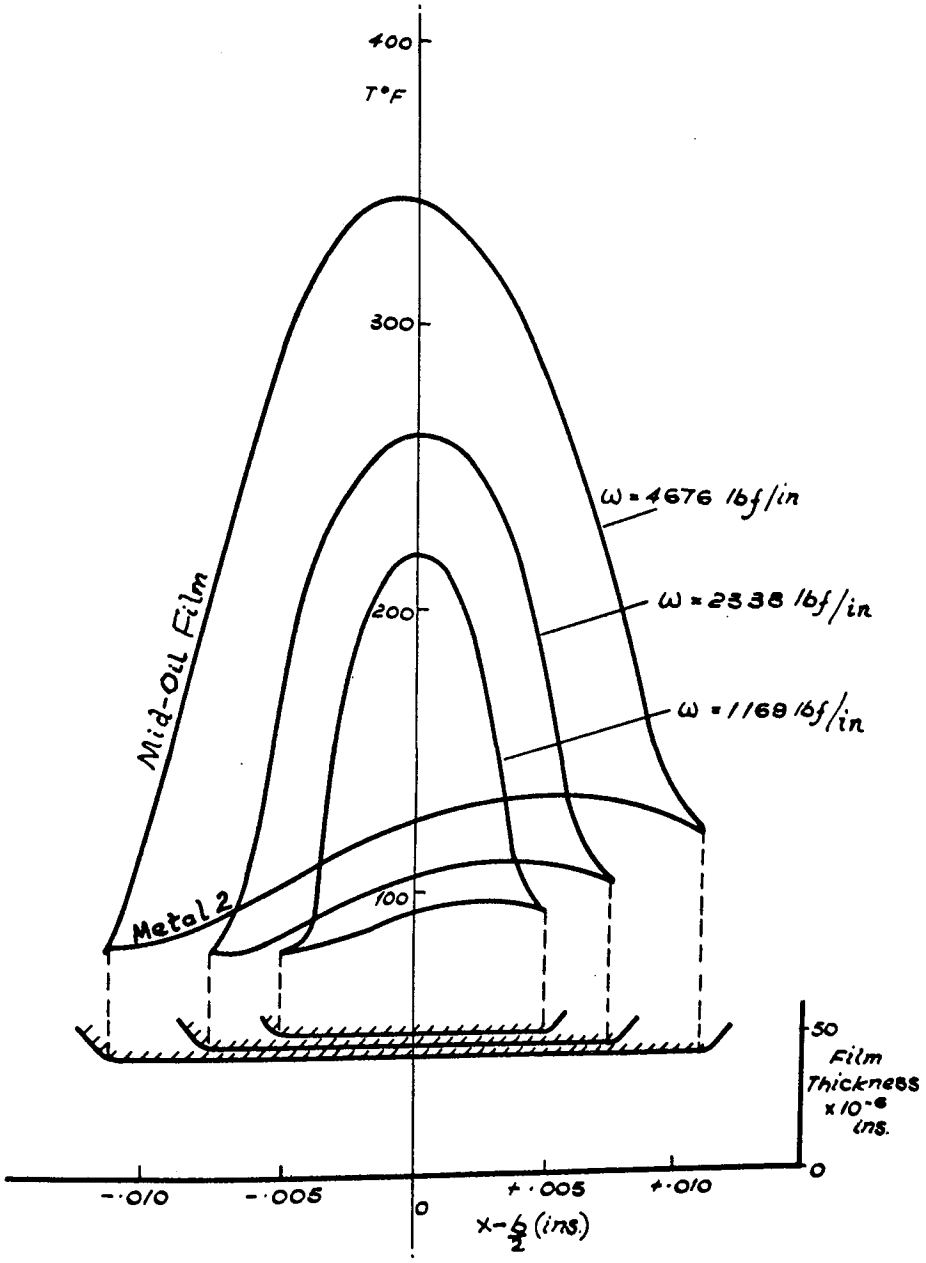

FIG.6.15 EFFECT OF LOAD ON TEMPERATURE DISTRIBUTION

U_a = 135 in/s S = 0·1 S.A.E. 10.

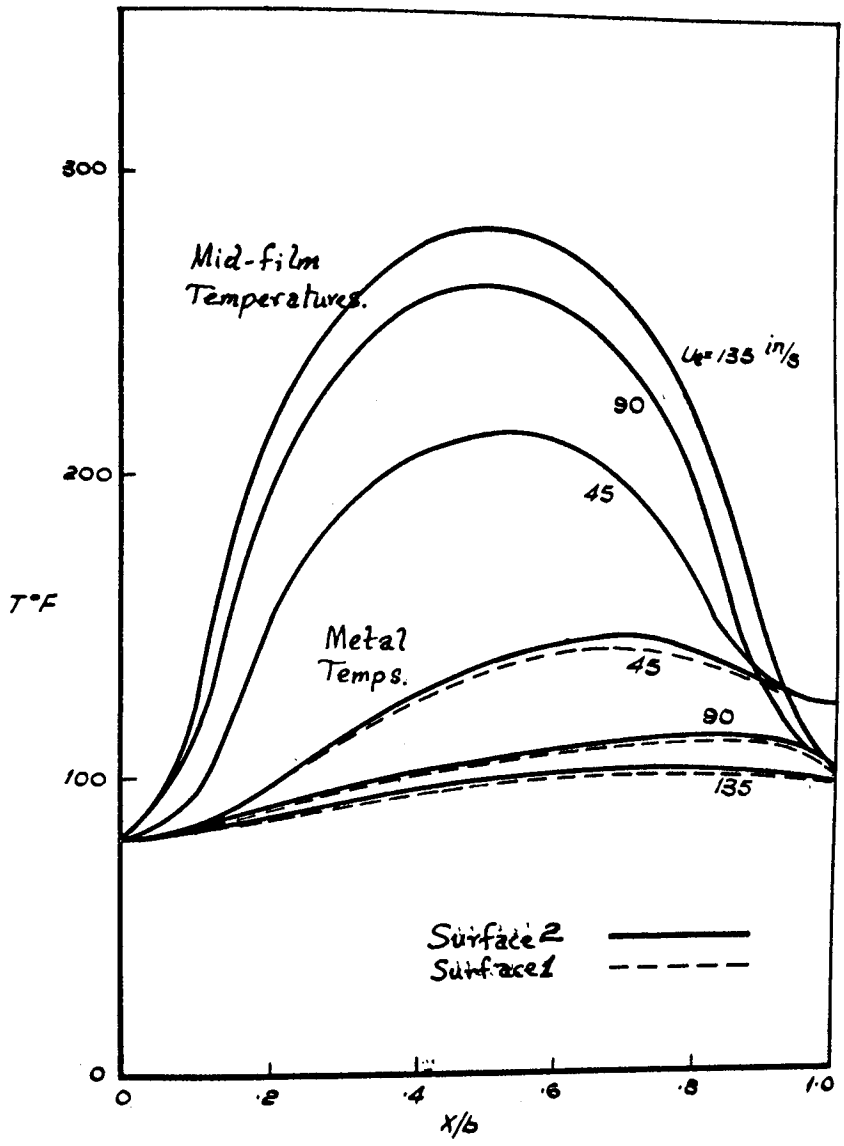

FIG. 6.16. EFFECT OF ENTRAINING VELOCITIES ON TEMPERATURE DISTRIBUTIONS. SAE 10. W 4676 lbf/in. S = 0.1.

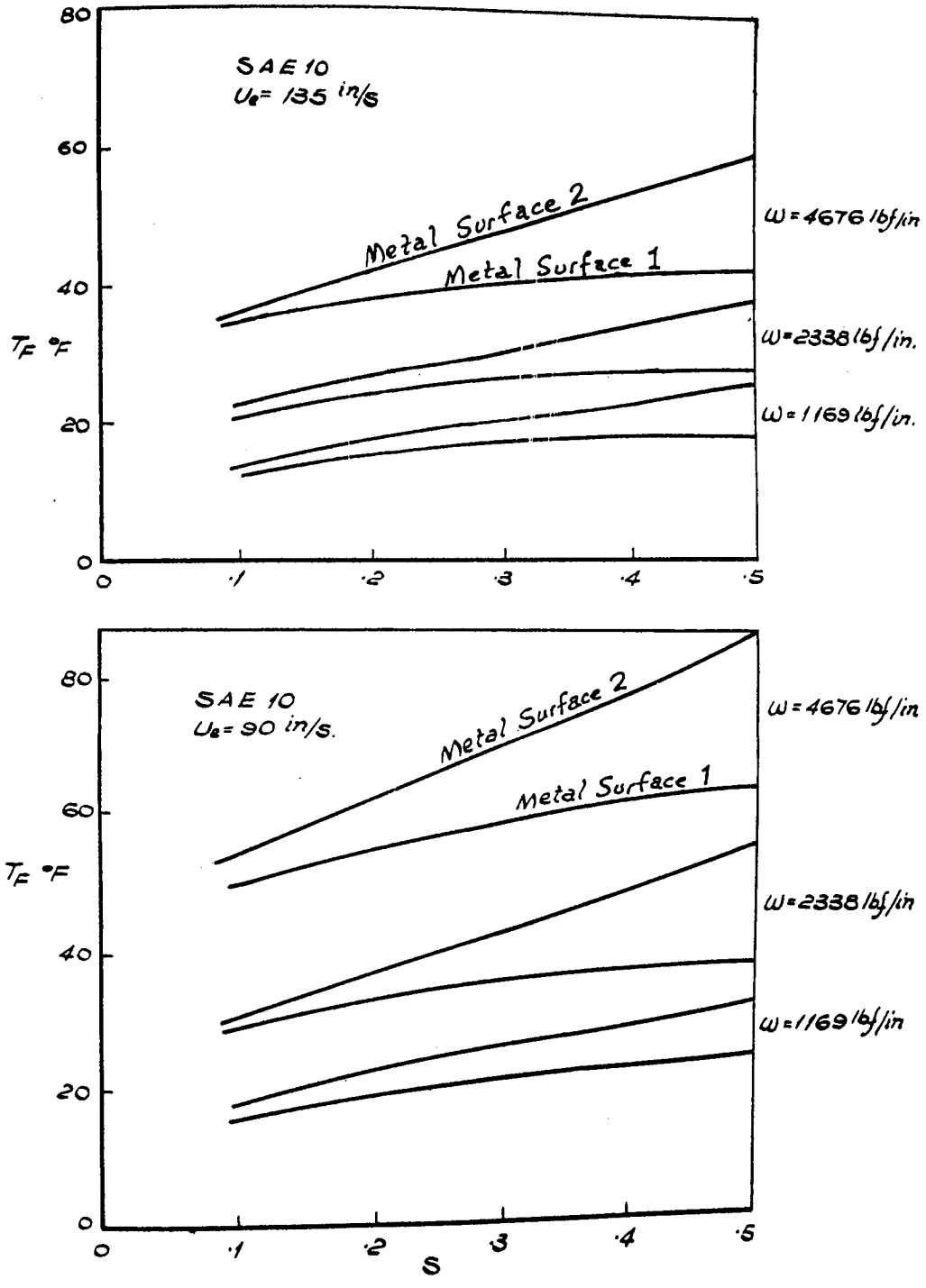

FIG. 6.17.
TEMPERATURE RISE AT METAL SURFACES.
FOR VARYING ENTRAINING SPEED, SLIDE RATIO, AND LOAD.

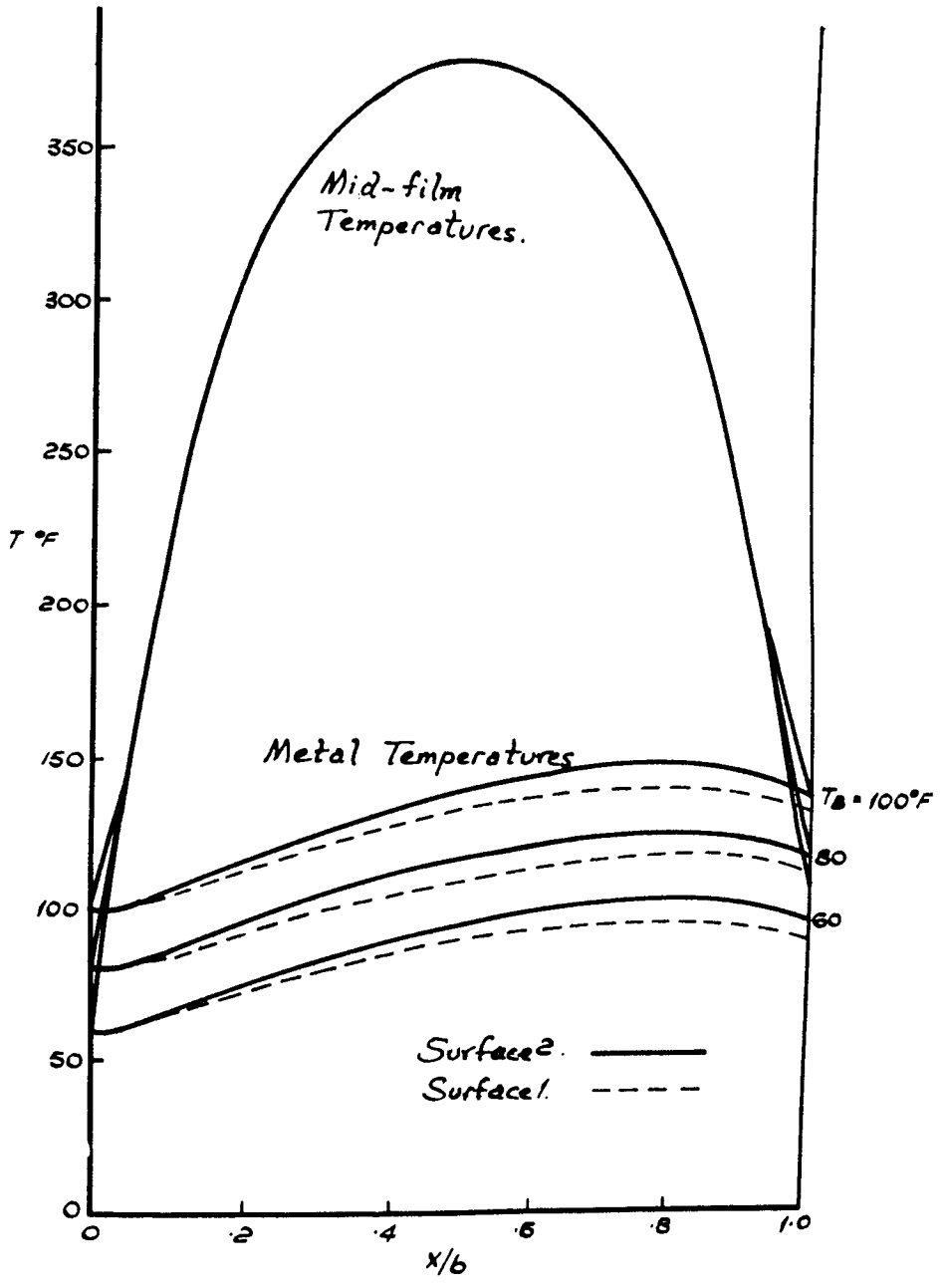

FIG. 6.18 EFFECT OF INLET TEMPERATURE ON PEAK TEMPERATURE RISE OF SURFACES.
U = 135 in/s W = 4676 lbf/in. SAE 10. S = 0.1.

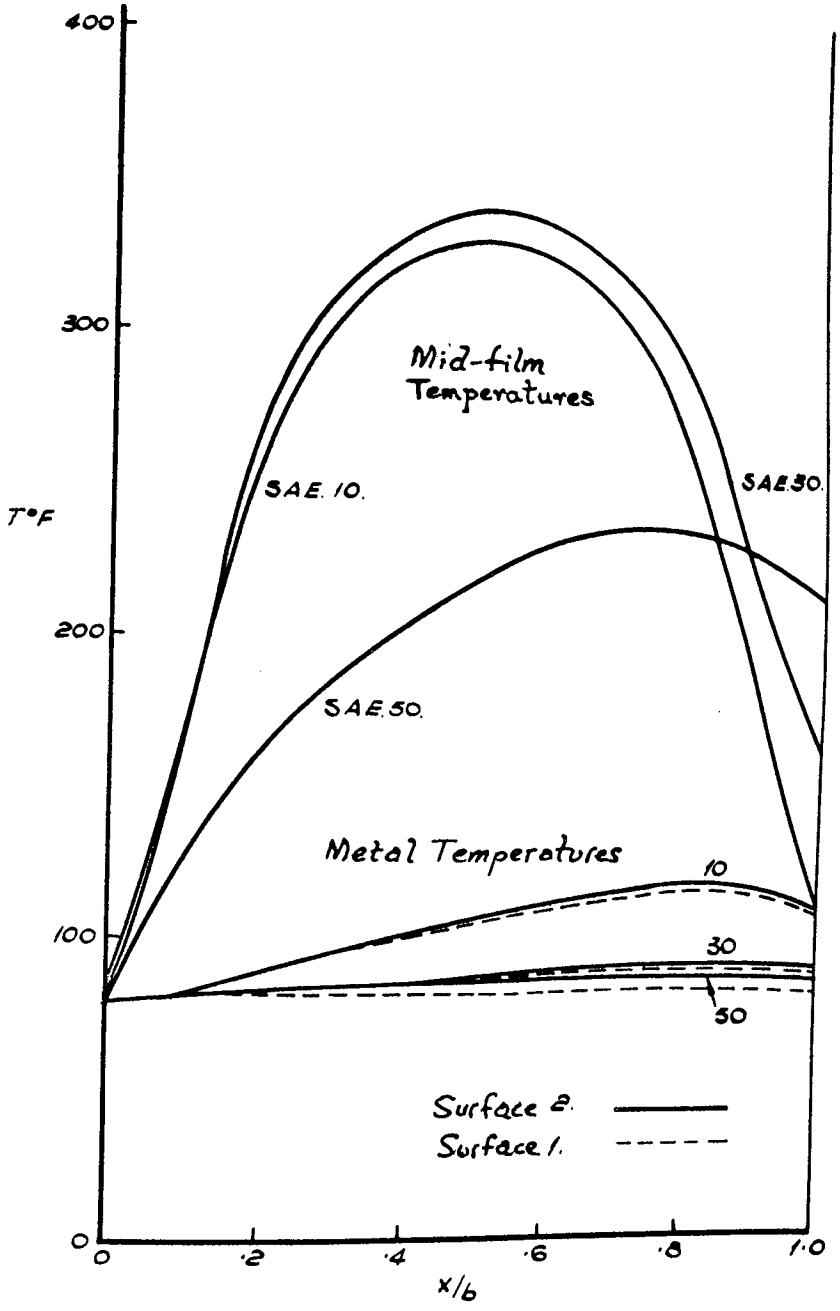

FIG. 6.19 EFFECT OF VISCOSITY ON TEMPERATURE DISTRIBUTION $U = 135$ in/s $W = 4676$ lbf/in. $S = 0.1$.

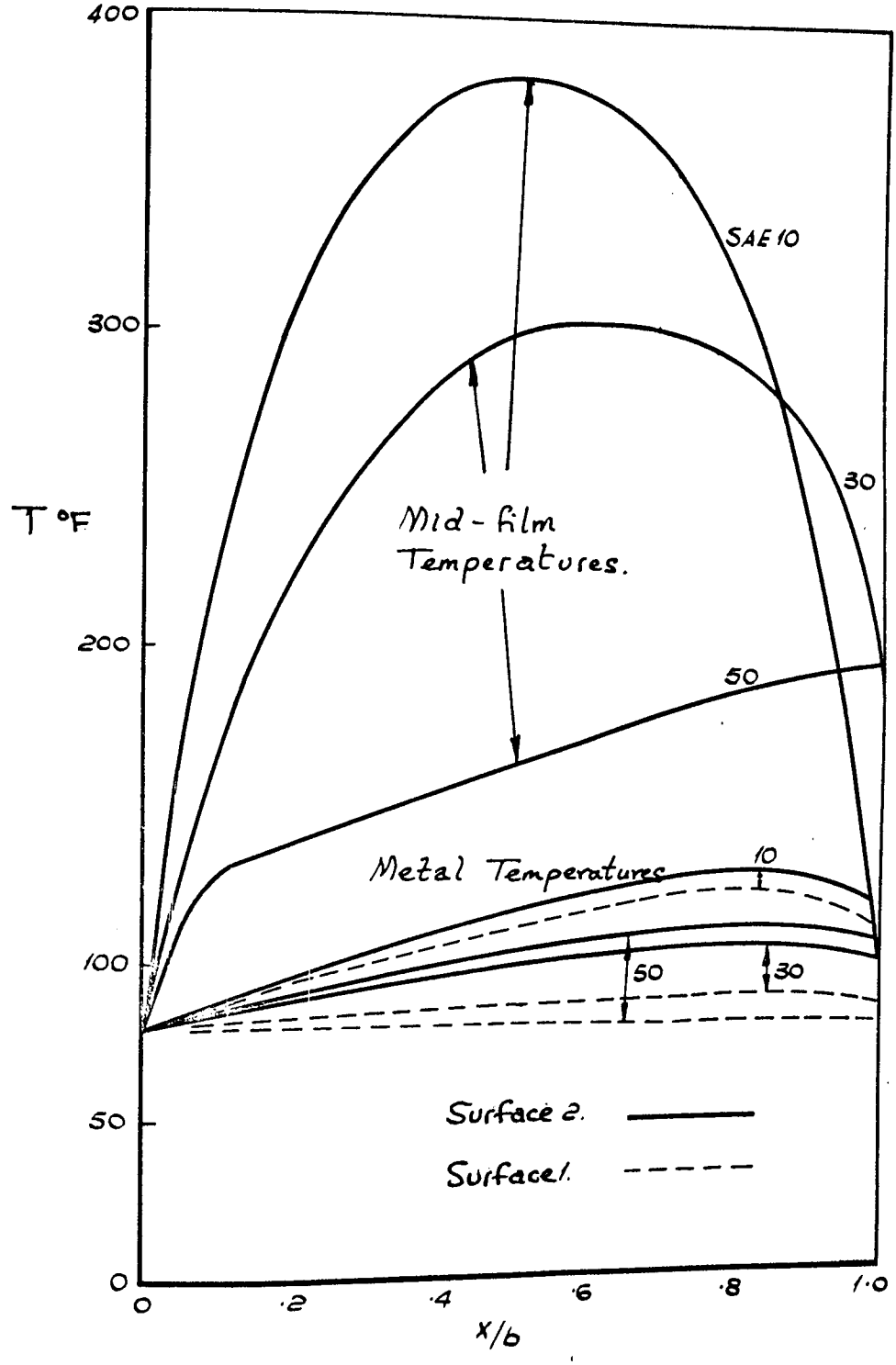

FIG. 6.20. EFFECT OF VISCOSITY ON TEMPERATURE DISTRIBUTION. $U_0 = 135$ in/s. $W = 4767$ lbf/in. $S = 0.3$

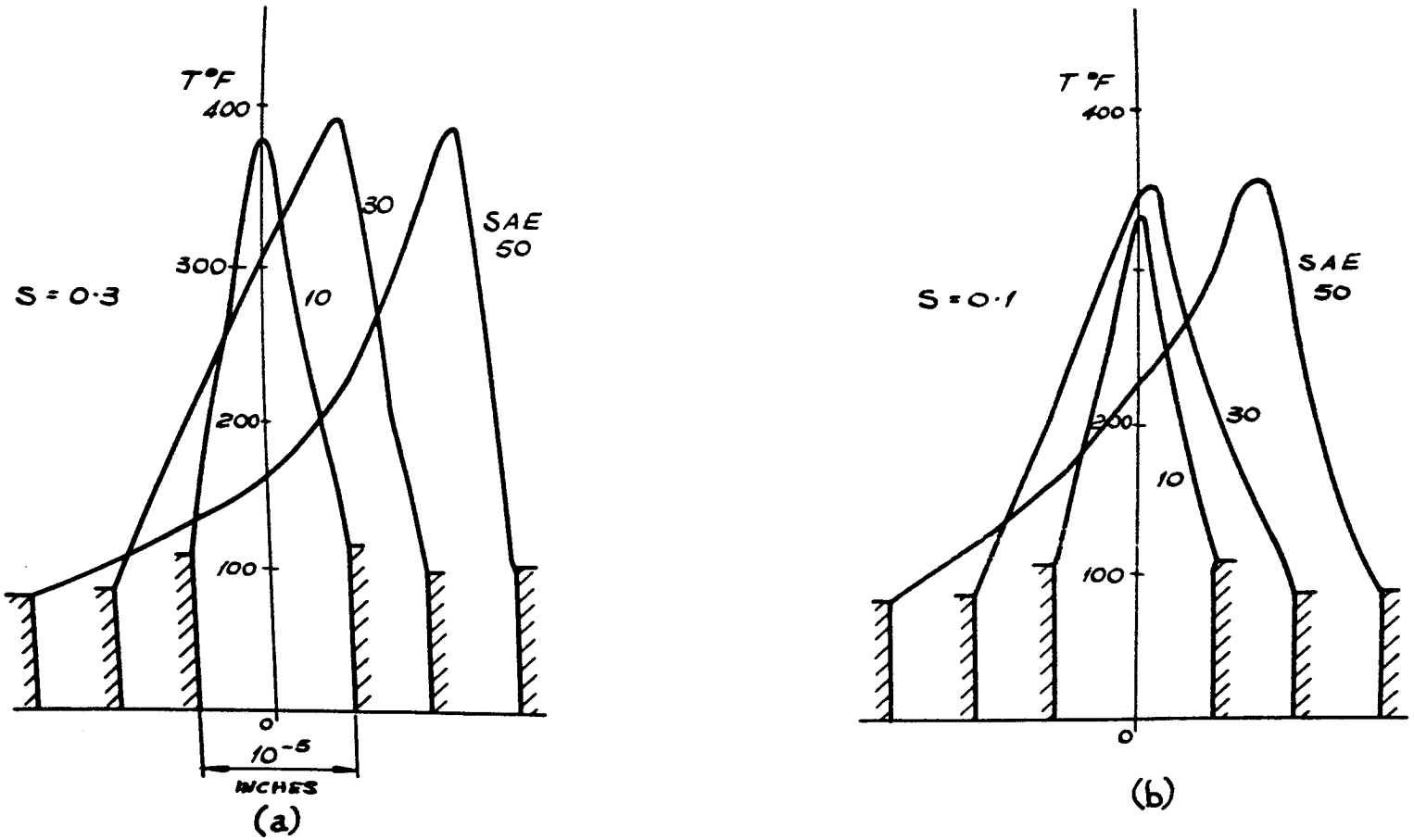

FIG.6.21 EFFECT OF VISCOSITY ON TEMPERATURE DISTRIBUTION ACROSS FILM.

U_e = 135 in/s. W = 4676 lbf/in.

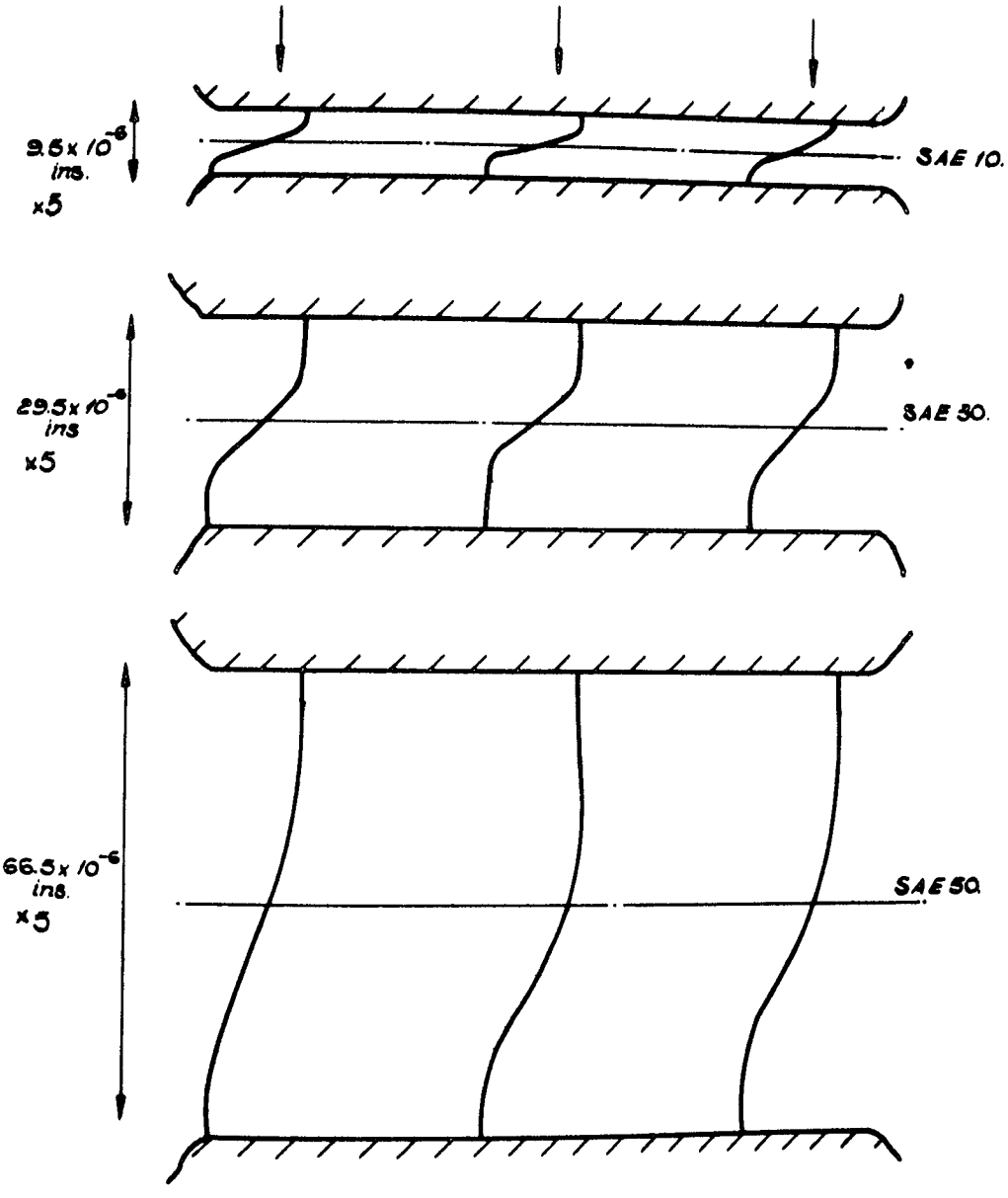

FIG. 6.22. VELOCITY PROFILES FOR DIFFERENT VISCOSITIES

U = 135 in/s W = 4767 lbf/in. S = 0.1.

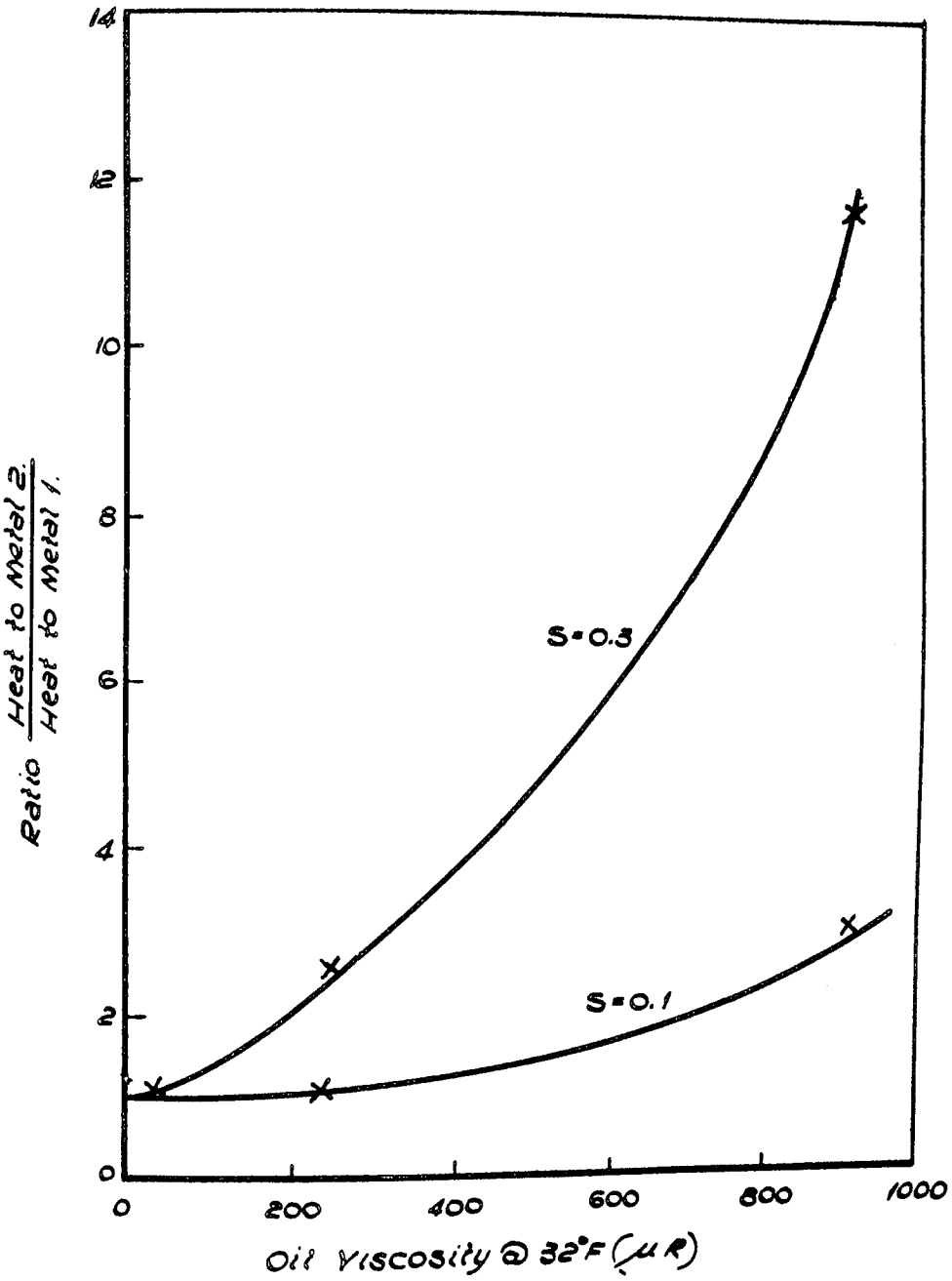

FIG. 6.23 HEAT PARTITION BETWEEN METAL SURFACES FOR DIFFERENT VISCOSITIES.
U_R = 135 in/s W = 4676 lbf/in.

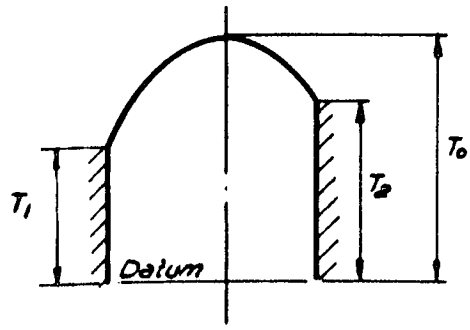

Temperature Distribution Across the Oil Film.

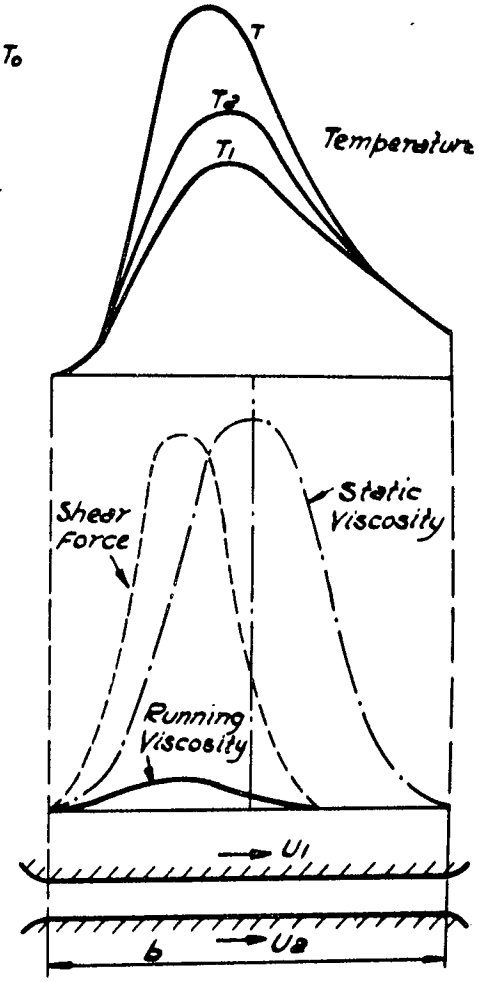

Temperature And Viscosity Variation Across the Band of contact.

FIG. 6.24
TEMPERATURE DISTRIBUTIONS PREDICTED BY MERRITT (Reproduced from ref. 89)

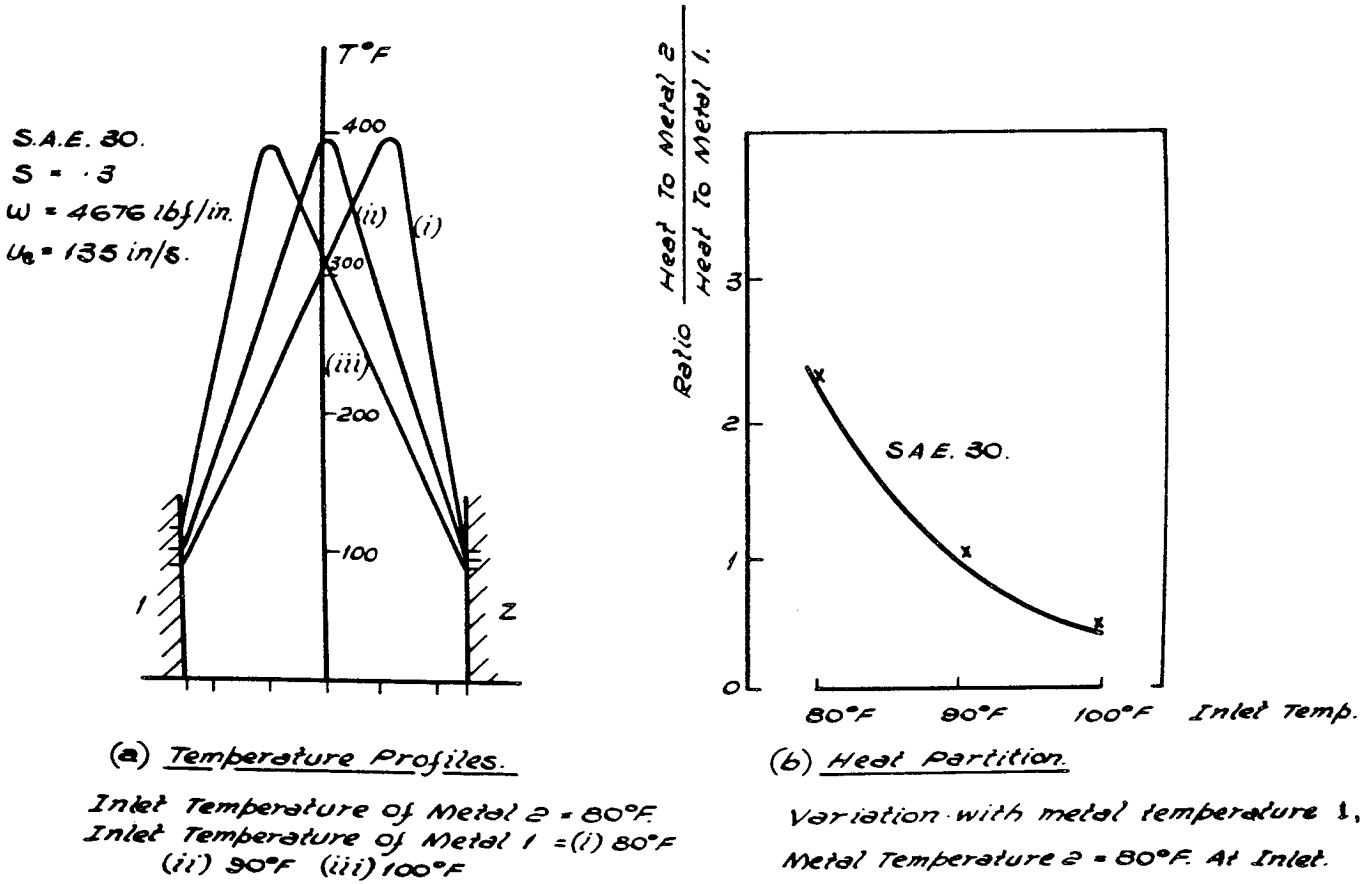

(a) Temperature Profiles.

Inlet Temperature of Metal 2 = 80°F.
Inlet Temperature of Metal 1 = (i) 80°F
(ii) 90°F (iii) 100°F

(b) Heat partition.

Variation with metal temperature 1,
Metal Temperature 2 = 80°F. At Inlet.

FIG.6.25 VARIATION OF HEAT PARTITION WITH INLET TEMPERATURE.

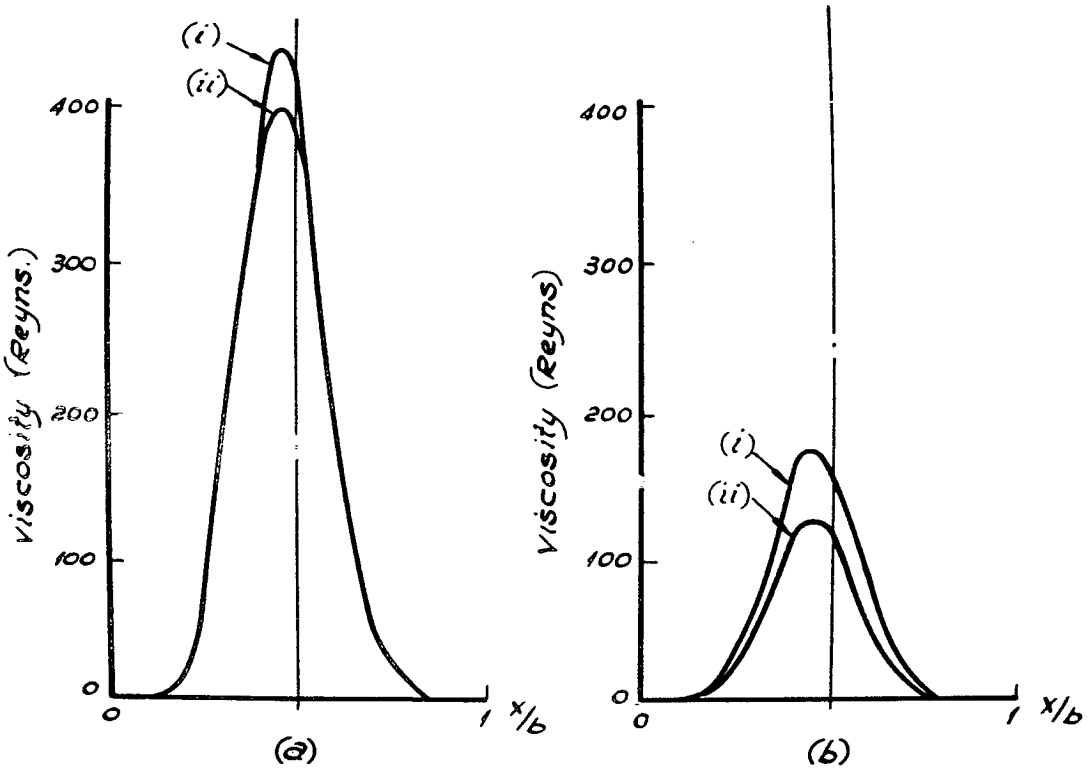

FIG. 6.26 VISCOSITY VARIATIONS AT METAL SURFACES.

(i) Metal surface at U1.

(ii) Metal surface at U2.

U_e = 135 in/S, W = 4676 lbf/in. (a) S = 0·1, (b) S = 0·3.

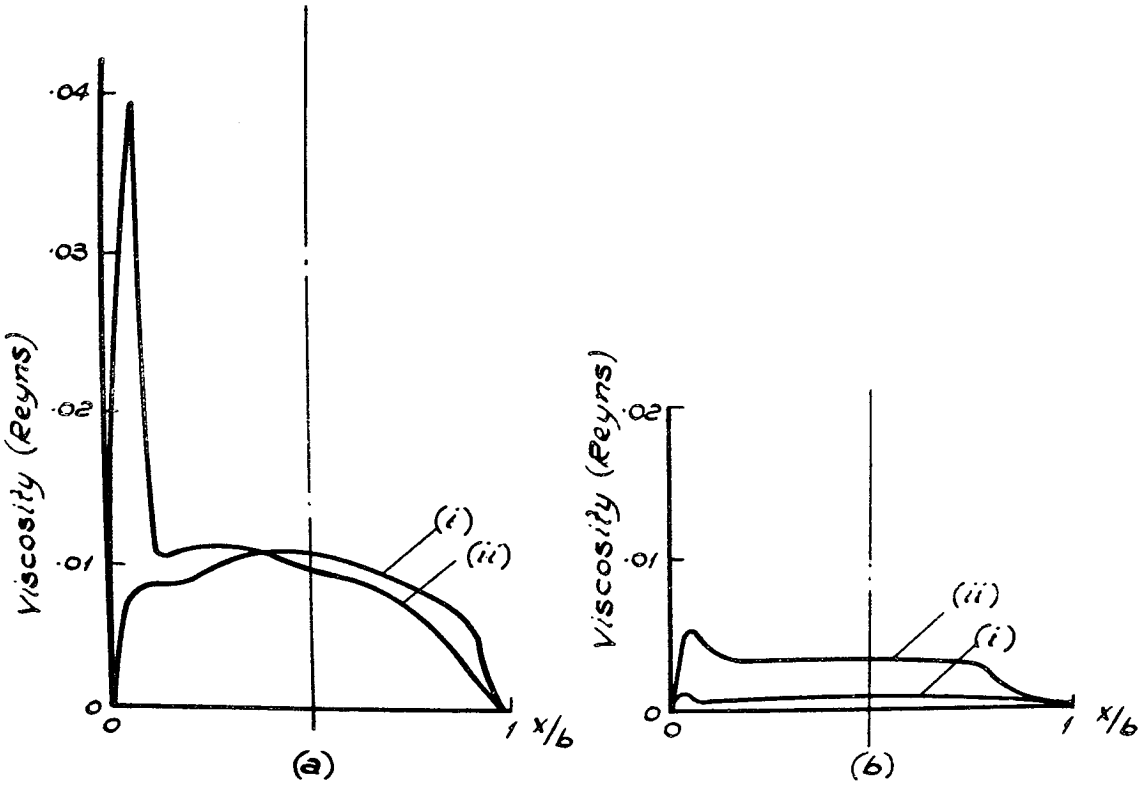

FIG. 6.27.

VISCOSITY VARIATION AT PLANE OF MAXIMUM OIL TEMPERATURE.

U_e = 135 in/S.; W = 4676 lbf/in., (a) S = 0·1, (b) S = 0·3; (i) S.A.E. 10. (ii) S.A.E. 30.

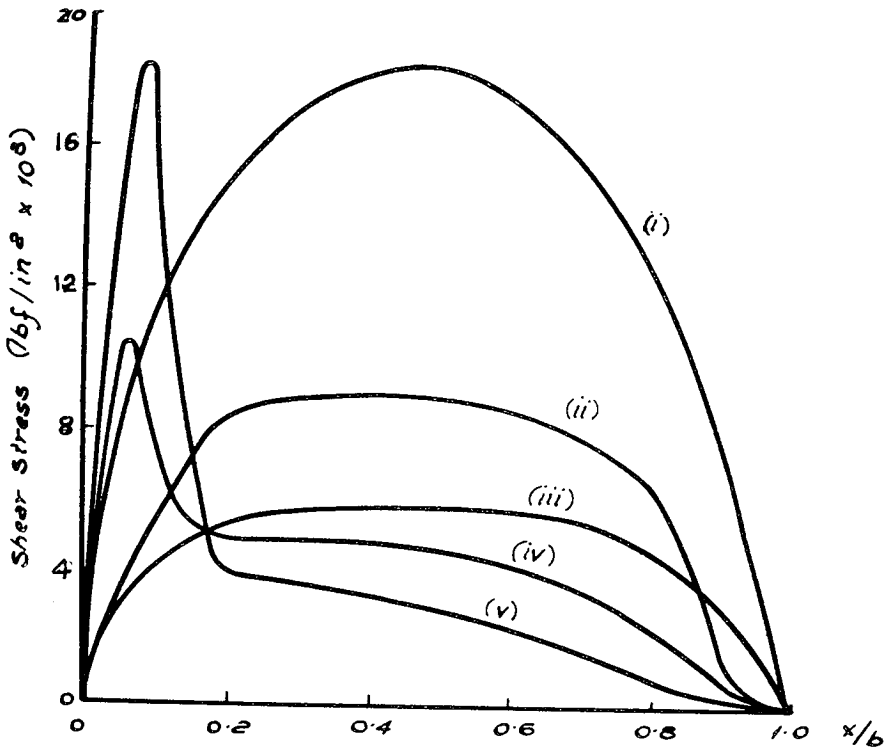

FIG. 6.28. THE SHEAR STRESS DISTRIBUTION FOR VARIATIONS IN LOAD, SLIP RATIO, AND VISCOSITY.

U_e = 135 (i) W = 4676 lbf/in, S = 0·1, S.A.E. 10.
(ii) W = 1169 lbf/in, S = 0·1, S.A.E. 10.
(iii) W = 4676 lbf/in, S = 0·3, S.A.E. 10.
(iv) W = 4676 lbf/in S = 0·1. S.A.E. 30.
(v) W = 4676 lbf/in S = 0·1 S.A.E. 50.

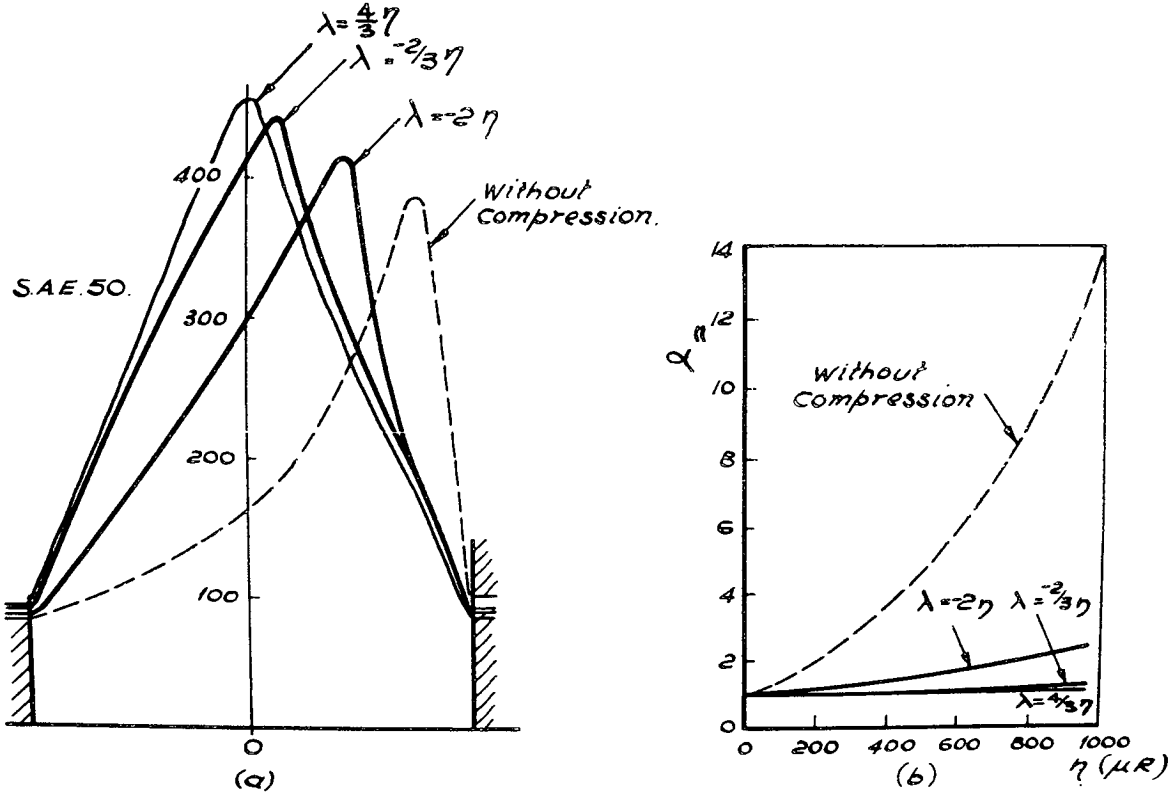

FIG. 6.29. TEMPERATURE DISTRIBUTIONS AND HEAT PARTITION FOR COMPRESSIBLE LUBRICANT.

$W = 4676$ lbf / in. $S = 0.3$. $U_e = 135$ in/s.

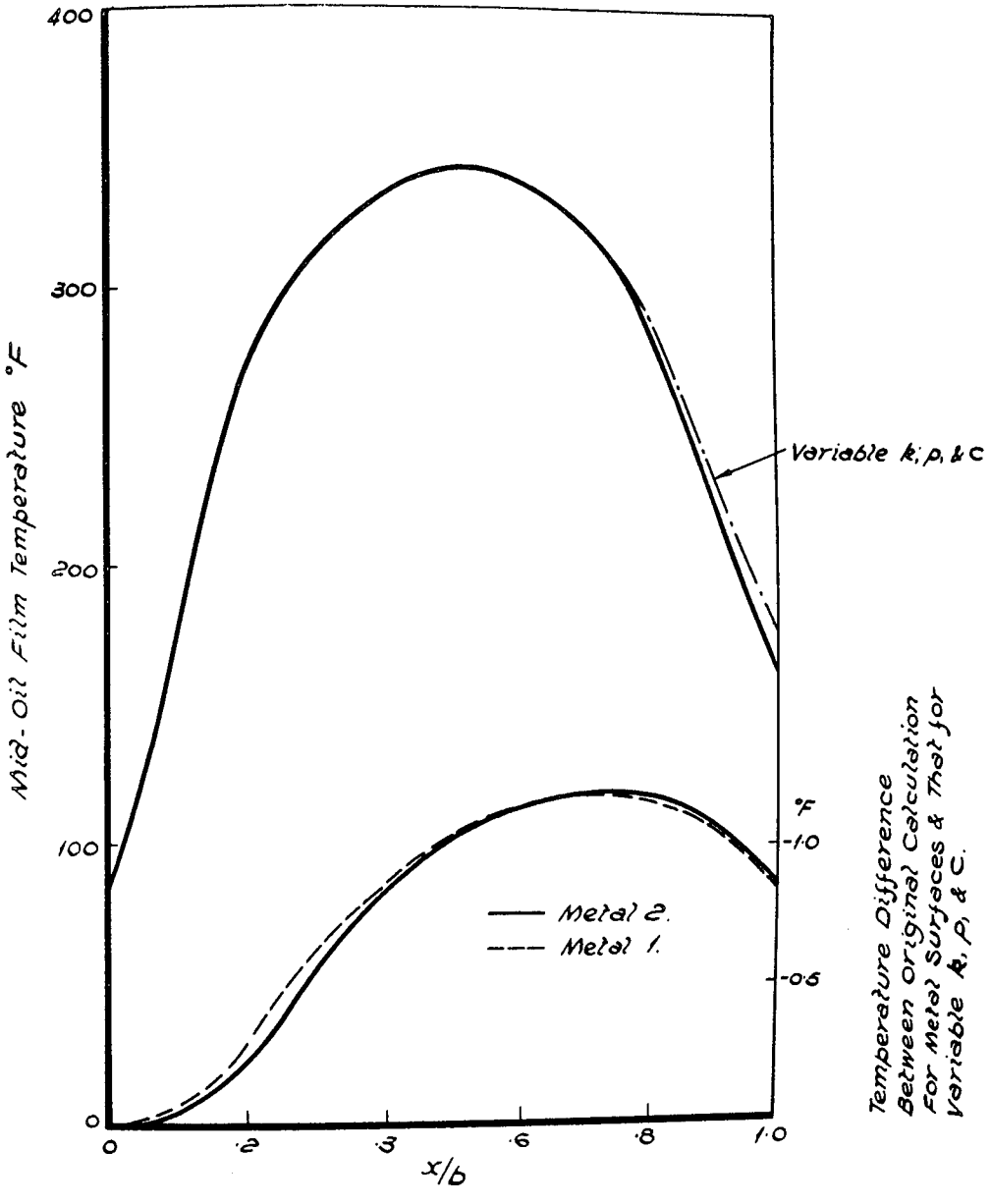

FIG. 6.30. EFFECT OF VARIABLE k, ρ, & c. ON OIL & METAL TEMPERATURES FOR SAE 30 OIL [U = 135 in/s, S = 0·1, W = 4676 lbf/in.]

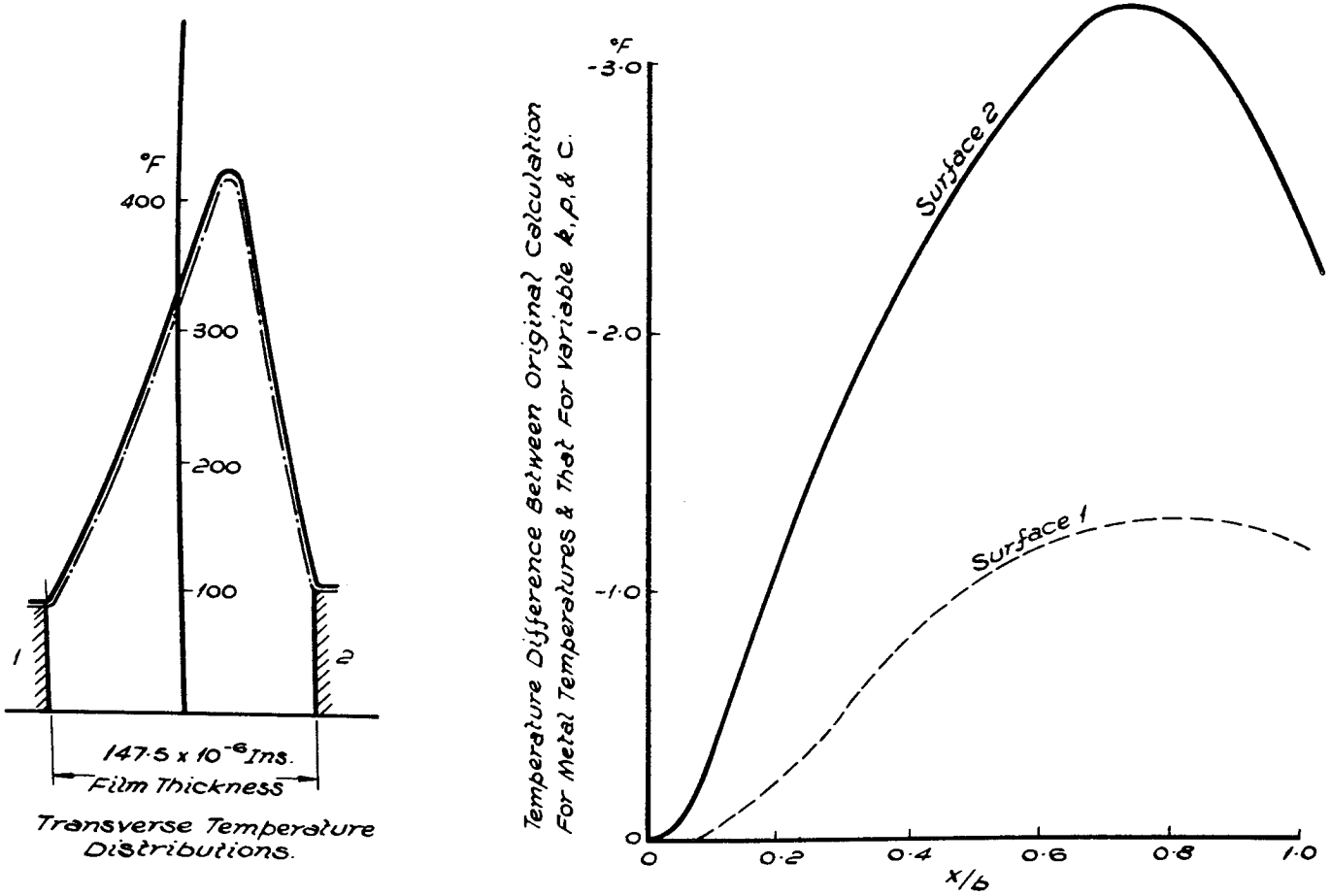

FIG. 6.31. EFFECT OF VARIABLE k, ρ, & C. ON OIL & METAL TEMPERATURES FOR SAE 30 OIL [U = 135 in/s, S = 0·5, W = 4676 lbf/in]

7.0 FRICTION AT LUBRICATED ROLLING/SLIDING CONTACTS

The preceding sections have been concerned with the determination of the temperatures generated at lubricated rolling/sliding contacts and relating these to the scuffing failure of gears and discs. From the calculations of temperature distribution however, additional information concerning the behaviour of the lubricant between the contacting surfaces has been obtained. Of particular interest are the viscosity and velocity distributions, from which may be calculated the shear stresses and overall "coefficients of friction".

Since the pitting of cams and gears is a failure associated with metal fatigue, the surface loading conditions at the contact are important in determining the life to pitting and will include shear stresses as well as the normal Hertzian pressures.

The total tangential force due to the shear stresses in the contact may be represented by a coefficient of friction. In gears, this friction appears as a resistance to sliding, with the work done against the friction dissipated as heat into the oil.

In friction-drives however, the friction is used to transmit torque from one disc to another and the slip between the discs is adjusted to provide the required shear rate in the lubricant in order to transmit the shear stress. In general, for a given contact, there is a limit to the amount of torque that can be transmitted and the optimum is found to depend upon the contact conditions and the lubricant properties.

The thermal analysis of the oil film presented in this thesis is extended to predict shear stresses and coefficients of friction. The results are then used in an examination of the characteristics of traction at elastohydrodynamic contacts.

7.1 Previous work on the traction at elastohydrodynamic contacts

Crook (91) in his classical work on the lubrication of rollers used a two disc machine to measure frictional traction as a function of sliding speed for a range of loads and entraining speeds. The machine consisted of a 3" diameter disc driven by a variable speed motor and a second 3" diameter disc supported in self-aligning bearings and loaded onto the first disc by two cables. A disc brake on the shaft of the second disc determined the torque transmitted and the friction was measured by a calibrated spring mechanism so designed that bearing friction was not included in the reading.

The results are summarised in fig. 7.1 where the frictional traction is seen to increase as the load is increased and at constant load rises, reaches a maximum and then falls. The sliding speed at which the maximum traction occurs increases as the load is reduced. At constant load, sliding speed and inlet viscosity, the frictional traction falls as the entraining speed is increased. If the inlet viscosity is increased, the friction rises more rapidly with sliding speed, reaches a maximum at a lower sliding speed and then falls more rapidly with sliding speed than did the lower viscosity case.

Crook was able to interpret the characteristics of the curves by considering the effective viscosity at the contact, defined as that constant viscosity throughout the zone which would give the same frictional traction as the system actually exhibits.

i.e. Torque $= \bar{\eta}_m \frac{(U_1 - U_2)}{h} b$ ..... (7.1)

and also Torque $= \frac{U_1 - U_2}{h} \int_0^b \eta_m \, dx$

Hence, $\bar{\eta}_m = \frac{1}{b} \int_0^b \eta_m \, dx$ ..... (7.2)

where $\bar{\eta}_m$ is the effective viscosity.

By expressing η_m in terms of ψ from the theoretical thermal analysis outlined in Section 6.3 of this thesis, Crook was able to calculate $\bar{\eta}_m$ by assuming a Hertzian pressure distribution. The results are reproduced in fig. 7.2. By approximating the expression for η_m in terms of ψ, a simple expression for $\bar{\eta}_m$ was evolved that avoided the need for numerical integration of Eq. 7.2.

i.e. $$\bar{\eta}_m = \frac{4k}{b/2\,\Upsilon\,(U_1-U_2)^2}\left[\frac{1}{2}\,\delta F + b \ln.\,(U_1 - U_2) + \frac{b}{2}\ln\left(\frac{\eta_s}{2k}\right)\right] \quad \text{..... (7.3)}$$

Substitution of this expression into the traction Eq. (7.1) produced a relationship between tractive force and sliding speed (U_1-U_2). The curves shown in fig. 7.3 also involved the assumption that entraining speed and hence film thickness was constant for a constant inlet viscosity.

Crook (66) explained the shape of the calculated curves in fig. 7.3 by considering that at small slip there was little frictional heating to affect viscosity and consequently the traction increased proportionately with slip, while at high slip the reduction in viscosity due to frictional heating could become the dominant influence and eventually the traction would fall as slip increased.

Comparing fig. 7.3 with fig. 7.1 shows the agreement between theory and experiment to be only qualitative with the

calculated tractions well in excess of the experimental values. Crook (91) observed however that the lubricant properties used in the calculation were drawn from available results of experiments and might not therefore agree with the properties of the lubricants at the condition of the disc tests, particularly with the variations in temperature occurring within the film.

Calculations of effective viscosity from the experiments were made from Eq. 7.1, employing the values of film thickness deduced from the measurements of disc capacitance. By resubstitution of these values of effective viscosity into Eq. 7.3, suitable values of k/γ and δ were determined and the corresponding theoretical curves of $\bar{\eta}_m$ replotted.

The agreement between theory and experiment was of course much closer than in the traction experiments but the same departure of the theoretical from the experimental curves at low values of sliding speed was observed as noted earlier when the calculated peaks in friction were much higher and sharper than the actual ones. By taking values of k/γ both implausibly large and small, Crook established that the sharp fall in $\bar{\eta}_m$ with sliding speed exhibited by the experimental curves at low speeds could not be explained in terms of temperature. It was concluded that in addition to temperature effects there had to be an effect of shear rate upon the viscosity of the oil. The theory of the heat balance within the oil film accounted for the larger phenomena.

Recently, further studies of the shear behaviour of rolling/sliding contacts have been carried out at the University of Cambridge Engineering Laboratory. Jefferis and Johnson (92) reported the design and development of a power circulating rolling contact disc machine in which each disc was mechanically

coupled to a separately excited d.c. electrical machine whose armatures were connected electrically. With the discs transmitting torque, power circulated from one machine acting as a motor to the other acting as a generator. In this way it was possible to control traction with a stepless variation of sliding speed between the discs.

In a companion paper, Johnson and Cameron (93) presented the results of a series of experiments conducted on the same disc machine in which contact pressures of up to 260,000 lbf/in^2 were investigated. The highest pressure used by Crook was 100,000 lbf/in^2 and Johnson and Cameron found that above this pressure, the oil film showed a marked change in its shear behaviour from that at the lower pressures.

Up to contact pressures of 175,000 lbf/in^2 the traction results showed the same general features as Crook's results; the coefficient of friction increased with contact pressure and reduced with entraining speed. At higher contact pressures however, there appeared to be a ceiling to the friction coefficient which could not be exceeded and to which all the curves approached. This same phenomenon had been observed by Plint (94) in experiments conducted with a very different oil.

Provided therefore, that contact pressures were sufficiently high and rolling speeds and temperatures sufficiently low, the traction ceiling would be reached and a relationship between friction and sliding speed not dependent upon load, speed or temperature was applicable. This conclusion is in accordance with the commonly used values for coefficients of friction of .05 - .08 which are often quoted in practical engineering texts, as for example in reference 95. There is still the provision however, that if maximum friction at

minimum slip is the requirement, as in friction drives, then a high contact pressure and low rolling speed and disc temperature are necessary. Crook was unable to explain the magnitude of the traction peak in terms of thermal effects alone and the same thermal analysis when applied to Johnson and Cameron's results also produced theoretical tractions far in excess of the experimentally determined ceiling.

Closer agreement between theory and experiment was obtained by introducing into the calculations a higher value of thermal conductivity given by the extrapolation of experimental data to the pressures occurring in the contact. Also required in the calculation were values of the viscosity η_m through the contact.

From the initial slopes of their curves Johnson and Cameron calculated the effective viscosities and by manipulation of the equations given in the earlier part of this section, produced curves of apparent viscosity $\bar{\eta}_m$ as a function of contact pressure and disc temperature, fig. 7.4, which referred to zero entraining speed. The effective viscosity was found to reduce with increase in entraining speed, an observation that Crook had also made, fig. 7.5. The contact pressures used by Crook however did not take the effective viscosity into the zone detected by Johnson and Cameron where a marked change in the variation of viscosity with pressure occurred. The change appeared to take effect when the viscosity reached a value between 10^4 and 10^5 Poise.

Even with these directly measured viscosities taken into account, theory produced values of friction far in excess of those recorded, with the conclusion that the assumption of a Newtonian fluid was probably invalid. Several proposals for alternative mechanisms of oil film shear have been made and these are the subject of the following sections.

7.2 Non-Newtonian Effects in Lubricants

7.2.1 The plastic shear plane hypothesis

It was Smith (96) in 1965 who introduced the concept of a lubricant behaving in a similar manner to a plastic solid, when subjected to the extreme pressures of elastohydrodynamic contacts. At these pressures oils had viscosities in the order of 10^5 Poise, something between butter and plasticine in consistence. The hypothesis was that shear traction is limited by the oil reaching a limiting critical shear strength and plastically shearing at the central plane of the oil film.

From the traction experiments on a point contact machine, Smith found that the maximum coefficient of traction and hence the critical shear stress increased with pressure and reduced with temperature. The decrease with temperature was in accordance with the assumption that plastic shear occurred on the central plane of the oil film, where the temperatures would be highest.

The hypothesis therefore suggests that in traction the shear stress at the contact can be increased up to the critical value given by the contact pressure and the oil temperature. Plastic shear then occurs in the film at the plane with the highest temperature. Smith and others have assumed this to be the central plane but the temperature distributions determined in this thesis show that this need not be the case. With increased sliding, the lubricant can no longer be assumed a Newtonian fluid, as the total slip is made up of viscous shear and plastic shear at the central plane. Calculations based on the total slip, and assuming a Newtonian fluid will produce shear stresses well in excess of the critical value and hence those measured.

The principle has been supported in further work by Plint (94) but probably a more significant contribution to the

hypothesis is made by Johnson and Cameron (93) on their line contact machine. From the traction-sliding speed curves, outlined in the previous section, and from which emerged an apparent traction ceiling, they were able to produce an expression for the critical shear stress dependent upon pressure and temperature only, fig. 7.6. The reduction in critical shear stress with temperature was in agreement with the observed reduction in coefficient of friction with increased shear rate for sliding speeds in excess of that giving the maximum friction. In this region, the oil film temperatures increase with sliding speed and the critical shear stress reduces.

Up to the peak friction, the lubricant behaves as a Newtonian fluid with the traction increasing proportionally with sliding speed until the critical shear stress in the oil is reached when plastic shear takes place. Although this hypothesis has proved useful in the instances given, it is not generally accepted as the reason for non-Newtonian effects in lubricants under extreme pressure.

Viscoelasticity has for a long time been the preferred explanation and several rheological models have been introduced. In the discussion to references (93) and (94), Dyson commented on the unacceptable nature of the sharp transition point identifiable with the proposed discontinuity in the behaviour of the lubricant film. Dyson argued that the change in behaviour occurred over a narrow transition zone and that the change in the sign of the dependence of traction on sliding speed could be attributed to the thermal mechanism already proposed by Crook. Dyson considered that the viscoelastic analogy, which he had long preferred, offered an explanation in principle of the experimental facts. What was required for a more quantitive analysis was information regarding the physical properties of lubricants but these were

not yet available.

7.2.2 Viscoelastic behaviour of lubricants

In the study of viscoelasticity, mechanical models have proved extremely valuable (97). Fig. 7.7 shows how these various models can be used to represent any physical phenomenon. In this figure the elastic components are represented by a Hookean spring and the viscous components by a Newtonian dashpot. When these two are placed in series, the Maxwell model is obtained. When these are placed in parallel the Kelvin model is obtained. However several combinations of these basic elements are often employed in an attempt to represent more complex phenomena.

The Kelvin model is particularly valuable for representing creep-relaxation phenomena, as shown in fig. 7.7 where for a given applied stress, the strain increases with time. The Maxwell model is useful in representing stress relaxation phenomena, where for a given strain the stress will gradually reduce with time. It is this model that has been employed extensively in representing viscoelasticity in lubricants. A small element of fluid is considered to be subjected to a shear stress τ that varies with time. This will be the condition occurring in elastohydrodynamic lubrication where the element of fluid as it passes through the contact experiences a change in shear stress, being zero at entry and exit and reaching a maximum somewhere inside the contact.

Under the action of this varying shear stress there will be viscous and elastic shear according to the Maxwell model. If the shear stress did not vary with time then the elastic shear would remain a constant value and the rate of shear contributed by elasticity would be zero.

Hence if the viscous shear rate $= \frac{\partial}{\partial t}\left(\frac{\partial e_1}{\partial z}\right) = \frac{\tau}{\eta}$

and the elastic shear rate $= \frac{\partial}{\partial t}\left(\frac{\partial e_2}{\partial z}\right) = \frac{\partial \tau}{G \partial t}$

then the total shear rate $\frac{\partial U}{\partial z} = \frac{\tau}{\eta} + \frac{\partial \tau}{G \partial t}$

Putting $\frac{\partial \tau}{\partial t} = \frac{\partial \tau}{\partial x}\frac{\partial x}{\partial t} = \frac{\partial \tau}{\partial x} U$

the equation for a Maxwell fluid becomes

$$\frac{\partial U}{\partial z} = \frac{\tau}{\eta} + \frac{U}{G}\frac{\partial \tau}{\partial x}$$

The effect of these considerations on the shear stresses and hence the total traction at a rolling/sliding contact is most clearly demonstrated by considering a certain shear rate between the contacting surfaces. If elasticity effects are negligible then the expression is purely Newtonian.

i.e. $\tau = \eta \frac{\partial U}{\partial z}$

If the elasticity term in the Maxwell equation is significant then the shear stress willbe given by

$$\tau = \eta \left(\frac{\partial U}{\partial z} - \frac{U}{G}\frac{\partial \tau}{\partial x}\right)$$

which results in lower values of shear stress and coefficient of friction at the contact.

Crouch and Cameron (98) applied the Maxwell fluid to a Hertzian pressure profile and by non-dimensional analysis of the

Maxwell fluid equation and graphical integration found that viscoelasticity is only significant when the quantity η_{MAX}/G, $b/2U$ defined as the relaxation number is greater than unity. The relaxation number is simply the ratio of peak relaxation time of the lubricant to half the transit time of the fluid through the contact zone.

The calculations relied upon assumed values for the lubricant properties, in particular the shear modulus G. Unfortunately, direct experimental measurement of these properties at the conditions of pressure and temperature corresponding to those in rolling/sliding contacts is very difficult. Practically the only source of information independent of actual elasto-hydrodynamic tests, is that obtained from studies of lubricants under oscillatory shear. Here the stress cycle times are so small that viscoelasticity is very predominant. Recent research by Lamb (99) and his co-workers have shown that viscoelasticity can be detected in certain lubricants with this type of test.

For alternating shear stresses of the form $\exp(j\omega t)$ the time differential is replaced by $(j\omega)$ and the Maxwell fluid equation becomes

$$\tau(1 + j\omega Y) = j\omega \eta \frac{\partial e}{\partial z} \qquad \ldots\ldots (7.4)$$

where $Y = \eta/G$, defined as the relaxation time.

At low frequencies $\omega Y << 1$ and $\tau = j\omega \eta \frac{\partial e}{\partial z}$ and the response is entirely viscous.

At high frequencies $\omega \cdot Y >> 1$, $\tau = \frac{\eta}{Y} \frac{\partial e}{\partial z}$ and the response is entirely elastic.

$\underline{\eta}$ is therefore a shear modulus, termed the limiting high
Y

frequency shear rigidity modulus, G_∞

At any other frequency of stress alternation, the ratio of shear stress to shear strain is represented by the complex shear modulus

$$G^* = G^1 + j\,G^{11}$$

Hence, $\underline{G^1} = \dfrac{\omega^2 Y^2}{1 + \omega^2 Y^2}$ $\qquad \underline{G^{11}} = \dfrac{\omega Y}{1 + \omega^2 Y^2}$

from Eq. G_∞ $\qquad$ G_∞

7.4

and the dynamic viscosity $\eta^1 = \dfrac{\eta}{1 + \omega^2 Y^2} = \dfrac{G^{11}}{\omega}$

In practice the quantities G^1, G^{11}, and η^1 are not measured but calculated from the components R_L and X_L of the shear impedence Z_L which are determined experimentally.

$$Z_L = R_L + jX_L = -\frac{\tau}{\frac{\partial e}{\partial t}}$$

Applying Newton's law of motion to an elementary volume of the fluid gives:-

$$Z_L^2 = \rho\, G^*$$

from which, equating real and imaginary parts of each side,

$$\rho\, G^1 = R_L^2 - X_L^2; \qquad \rho\, G^{11} = 2R_L X_L$$

The predicted behaviour for a Maxwell model having a single relaxation time $Y = \eta/G_\infty$ is reproduced from (99) in fig. 7.8(a) where the impedences have been plotted in a normalised fashion. The viscosity ratio η^1/η falls from 0.9 to 0.1 as the frequency increases. G^1/G_∞ increases proportionally to ω^2.

Lamb showed that certain fluids such as molten zinc chloride exhibited relaxation behaviour conforming to the Maxwell model

and the measurements agreed with the theoretical curves.

Hence the set of curves given in fig. 7.8(a) represent the viscoelastic behaviour of fluids but implicit in the method is the ability to vary both frequency and/or temperature in order to vary the quantity ($\omega\eta/G_\infty$), thereby giving a wider range than would otherwise be possible on the given apparatus.

Measurements on a wider range of fluids therefore, involved change in viscosity by adjustment of temperature and a new fluid model was introduced by Barlow et al (100) to correlate the results. The model, consisting of a combination of an elasticity element and a viscous element in parallel, produced the characteristics given in fig. 7.8(b) and agreed well with a wide range of measurements on different fluids

The viscoelasticity of three mineral oils of different viscosity was examined by Barlow and Lamb (101) and within experimental accuracy, G_∞ was found to be independent of temperature and for most purposes could be taken to have the value 10^{10} dyn/cm^2. Results for mineral oil, white oil and castor oil are given in fig. 7.(b) where the white oil characteristic agrees well with the model but the mineral oil and castor oil are displaced to higher values of ($\omega\eta/G_\infty$). There are considerable differences of opinion regarding the validity of relating the results of the oscillatory shear tests to the continuous shear conditions occurring in elastohydrodynamic lubrication.

Crook (91) assumed simply that the oil behaved according to the Maxwell fluid equation and by developing the equation in a similar way to Crouch and Cameron (98), determined the reduction in effective viscosity as a function of relaxation number. From this it was possible to tie-up the experimental results that suggested a reduction in effective viscosity for increased

rolling speed, fig. 7.9(a). In the process of making these calculations, Crook obtained estimates of G_∞ in fig. 7.9(b), which by comparison with published data from oscillatory tests (91) lay in the configurational regime of elasticity as opposed to the crystalline elasticity of $G_\infty = 10^{10}$ dyn/cm^2 given by Barlow and Lamb (101).

Dyson (102) however objected to the use of the Maxwell model for the fluid behaviour in continuous shear on the grounds that it did not explain why actual shear stresses were less than calculated for a Newtonian fluid. From the criterion given by Crouch and Cameron, Dyson calculated that for the transit time to be of the same order as the relaxation time, η_{MAX} had to be about 10^3 Poise for $U_e = 10^2$ cm/s, $b = 2 \times 10^{-2}$ cm, and $G_\infty = 10^{10}$ dyn/cm^2. This Dyson considered to be far removed from practice as it implied a shear stress of 1,500,000 lbf/in^2 at a sliding speed of 10 cm/s and a film thickness of 10^{-4} cm.

An alternative model, based on the Oldroyd theory (103) was put forward by Dyson and used to correlate the continuous shear results of Crook and Smith (96) with the oscillatory results of Barlow and Lamb. The method involved the introduction of a shift factor K where the shear stress in continuous shear became $1/K$ times the value of G^{11} at an angular frequency of $\omega = KD$; D equalled the rate of simple shear. K was varied between 0.4 and 12 in order to bring the continuous shear results into line with the oscillatory shear results, although the oils used were entirely different.

Other viscoelastic materials were recognised as having constant shift factors K of about unity and Dyson commented later (104) that there was recent evidence to suggest that lubricants might also have a constant K of about unity and that

his previous treatment needed amendment. Barlow, Lamb, Matheson, Rahmani, and Richter (100) produced results that suggested β_∞ decreased with temperature and increased with pressure. This would have the same effect in terms of correlating the two sets of data, as the variation in K made by Dyson. It is interesting to note that the calculations of Crook based on the assumption of a Maxwell fluid already indicated an increase in β_∞ with pressure as shown in fig. 7.3(b), where the increase in η_m, the effective viscosity was due to pressure. The calculations were at constant pressure but at different temperatures further suggested that β_∞ reduced with temperature. Hence, the calculation of β_∞ from the continuous shear results of Crook are in qualitative agreement with the present oscillatory shear results.

The application of the Maxwell fluid equation therefore appears to be justified as a first approximation to describing the viscoelasticity of lubricants. Such an approximation would enable the calculation of shear tractions, until now confined to the assumption of a Newtonian fluid, to be modified in an attempt to obtain better correlation between experiment and theory.

The original objection to the use of the Maxwell fluid equation made by Dyson, that impossibly high shear stresses would result needs to be modified. Firstly, Crook assumed that when the viscosity reached the value at which viscoelastic effects became significant, then the shear rate was given by the sliding speed divided by the film thickness. However, this represents the mean shear rate of the oil film and as seen in the thermal analysis developed in this thesis, the maximum viscosities occur at the outer edges of the film. Here the shear rates are only 10% of the mean rate and since the critical viscosity will be first attained in the cooler outer edges of the film, the shear

rate at these planes must be used in the calculation of shear stress. The value given by Dyson is therefore reduced from 1,500,000 lbf/in^2 to about 150,000 lbf/in^2. A further modification is the variation of G_∞ with temperature and pressure. Taking a value one decade lower than 10^{10} dyn/cm^2 which falls in the configurational regime determined by Crook, the shear stress reduces to 15,000 lbf/in^2 a value within the range determined experimentally.

It is the aim of the work presented in this section of the thesis, to calculate shear tractions for a Maxwellian fluid and compare these with experimentally measured tractions on a disc machine.

7.3 Extension of the thermal solution to calculate friction

The thermal solution of the elastohydrodynamic contact developed in section 6.7 may be extended to predict coefficients of friction. Other thermal solutions, for example those of Crook (91) and Cheng and Sternlicht (79) have been limited by the assumption of a Newtonian fluid and correlation with empirical coefficients of friction is poor. With the increased support for non-Newtonian behaviour in the form of a Maxwellian fluid, the Maxwell fluid equation is introduced into the thermal solution for friction. Both Newtonian and Maxwellian coefficients of friction will be calculated by suitable modification of the thermal solution.

From section 6.7, variations of viscosity both across and through the contact were obtained in the process of calculating the oil temperature rises. These were due to the viscous dissipation of energy resulting from the shearing of the oil film between the contacting surfaces. The shear rates across the film were also obtained; these were given by:-

$$\left(\frac{\partial U}{\partial z}\right)_i = \frac{\tau}{\eta} = \frac{S.U_1}{h}\left/\int_0^h \frac{1}{\eta}\right.$$

This relationship, relies on the assumption that the shear stress at a point in the contact is transmitted across the film from one metal surface to the other. Consequently, knowing the shear rate and viscosity at one of the elements across the film, the value of τ is given by...

$$\tau = \eta_j \left(\frac{\partial U}{\partial z}\right)_j$$

The tangential force on the element of the surface is given by:-

$$\Delta F = \tau (\Delta x) \quad \text{per unit width.}$$

Hence, by summing all the tangential forces at points Δx apart through the contact from inlet to outlet, a value for the total shear force at the contact is obtained. Dividing this figure by the contact load per unit width produces the calculated coefficient of friction for a Newtonian fluid.

The Numerical treatment for a Maxwellian fluid is not so straightforward.

The shear rate is given by the Maxwell fluid equation,

$$\frac{\partial U}{\partial z} = \frac{\tau}{\eta} + \frac{\dot{U}}{G_\infty}\frac{\partial \tau}{\partial x}$$

As for a Newtonian fluid in section 6.7,

$$S.U_1 = \Sigma \Delta \dot{U}$$

$$\therefore \quad S.U_1 = \Delta z \sum_{0}^{h} \frac{\tau}{\eta_j} + \frac{U_j}{G_\infty}\frac{\Delta \tau_j}{\Delta x}$$

$$= \tau \Delta z \sum_{0}^{h} \frac{1}{\eta_j} + \frac{\Delta z}{\Delta x}\frac{(\Delta \tau)}{G_\infty} \sum_{0}^{k} U_j$$

An approximation for $\Delta\tau$ is the difference in shear stress between the previous element position through the contact and the present one i.e. $(\tau - \tau^1)$

$$\text{Hence} \quad \tau = \tau^1 + \frac{\Delta z}{\Delta x} G_\infty \Sigma U_j$$

$$\Delta z \quad \Sigma \frac{1}{\eta_j} + \frac{\Delta z}{\Delta x} G_\infty \Sigma U_j$$

The numerical method used in the computer program for the thermal solution is a step-by-step process as described earlier and with the unknowns τ and U_j the above equation cannot be solved directly.

A simplification that only introduces small errors if the grid size is small may be made by taking ΣU_j as represented by the ΣU_j^1, the velocities at the previous position. This is not too inaccurate when it is remembered that velocity has been introduced as part of the relaxation number and will not differ greatly between adjacent elements. The error is certainly no greater than that incurred by the viscosity relationship employed. The same reasoning applies to the calculation of $\Delta\tau$.

The equation may therefore be solved for τ and then the shear rate, given by

$$\frac{\Delta U_j}{\Delta z} = \frac{\tau}{\eta_j} + \frac{U_j^1 (\tau - \tau^1)}{G_\infty \Delta x}$$

produces the true values of U_j which may then be carried over to the next position through the contact zone, at which the corresponding values of τ may be calculated.

It is interesting to see whether viscoelasticity will be significant in the particular solutions given for the cases in section 7.0, according to the Crouch and Cameron (93) criterion:-

$$\eta \frac{\Delta U}{\Delta z} >> 1$$

$$b^2 G$$

As an example,

$$G = .0001$$

$$b = .002 \text{ ins}$$

$$\text{Hence} \quad \tau = \tau_1 + \tau^1 \frac{\Delta z}{\Delta x . G_\infty} \Sigma U_j$$

$$\Delta z \quad \Sigma \frac{1}{\eta_j} + \frac{\Delta z}{\Delta x . G_\infty} \Sigma U_j$$

The numerical method used in the computer program for the thermal solution is a step-by-step process as described earlier and with two unknowns τ and U_j the above equation cannot be solved directly.

An approximation that only introduces small errors if the grid size is small may be made by taking ΣU_j as represented by the ΣU_j^1, the velocities at the previous position. This is not too inaccurate when it is remembered that velocity has been introduced as part of the relaxation number and will not differ greatly between adjacent elements. The error is certainly no greater than that incurred by the viscosity relationships employed. The same reasoning applies to the calculation of $\Delta\tau$.

The equation may therefore be solved for τ and then the shear rate, given by

$$\frac{\Delta U_j}{\Delta z} = \frac{\tau}{\eta_j} + \frac{U_j^1 (\tau - \tau^1)}{G_\infty \Delta x}$$

produces the true values of U_j which may then be carried over to the next position through the contact zone, at which the corresponding values of τ may be calculated.

It is interesting to see whether viscoelasticity will be significant in the particular solutions given for the cases in section 6.8, according to the Crouch and Cameron (98) criterion:-

$$\frac{\eta . \Delta U_j / \Delta z}{b/2U} >> 1$$

As an example,

$S = .0001$

$b = .022$ ins

$U = 135$ in/s

$G_\infty = 145 \times 10^3$ lbf/in^2 from Barlow and Lamb (101)

η_{max} SAE 30 at 270,000 lbf/in^2

$= 0.6 \times 10^{4}$ Reyns $\left(\frac{lb}{in.s}\right)$ from thermal solution

$$\therefore \frac{\eta_{max}/\beta}{b/2U} \simeq 420$$

On this basis, the effects of including the Maxwellian fluid equation into the calculation for friction would reduce the values to below that calculated for a Newtonian fluid.

7.4 Discussion of Preliminary Results

7.4.1 The calculated coefficients of friction for a Newtonian fluid

Adopting the same contact model used in section 6.0, the preceding extension of the thermal theory for a Newtonian fluid was applied to the contact conditions for which temperature distributions have already been obtained.

The results are given in figs. 7.10 and 7.11 where the coefficients of friction are in the same order as both measured and predicted by previous research workers (91 - 94). Fig. 7.10 in particular indicates that at increased entraining speed, the curves lie very close together and resemble the traction ceiling measured by Johnson and Cameron (93). The overall trend of the friction curves and the effect of entraining speed, contact load, and viscosity have already been explained by previous authors (91, 93) in terms of thermal action. With increased slip the oil film temperatures are raised, as confirmed by reference to fig. 6.14, and the viscosities in the contact reduce. The reduction in viscosity far outweighs the increase in shear rate and the net result is a reduction in shear stress.

At increased entraining speed the film temperatures increase considerably, as illustrated by fig. 6.16, and in the same way as before a reduction in shear stress is experienced. For an increase in contact load, the film viscosities are greater for a given slip and an increase in friction is observed. By raising the viscosity at inlet to the contact, and in the cases considered this is achieved by selecting a higher viscosity grade lubricant, there is a more severe reduction in friction with increase in slip. These results are in agreement with the overall characteristics predicted by Crook (66).

For conditions of slip below 0.1 the friction rises to greater than 0.1 and for the conditions given in fig. 7.12 and 7.13 reaches the improbable value of 1.8 at a slip of .0002. The thermal effects are insufficient at low slip to reduce the film viscosities and for a Newtonian fluid the friction rises to values not obtainable in practice. Crook produced the same order of discrepancy between his theory and experiments and deduced that the thermal properties and rheology of the lubricant were jointly the important factors determining the peak friction.

By including a further term of the energy equation in the calculation, the heat of compression, a slight reduction in the friction is observed but this does not modify the overall characteristics of the curve, fig. 7.13. Inclusion of the second coefficient of viscosity λ, as detailed in section 6.8.3, produced very little further change in the friction characteristic

7.4.2 Shear stress distributions for a Newtonian fluid

At a given slip, the coefficient of friction for a given set of contact conditions, represents the summation of the shear stresses through the contact zone. The numerical solution may

be programmed to provide the distributions of shear stress and these are given in fig. 6.28. Further results are plotted in fig. 7.14 for SAE 30 oil.

It is interesting to note that for the SAE 10 lubricant, the shear stress increases from zero at the inlet to a maximum near the centre of the contact. For the higher viscosity lubricants, the shear stress distribution is remarkably different, a sharp rise in shear stress due to the pressure dependence of viscosity exists at inlet.

At a short distance inside the contact, the temperature rise in the oil film is sufficient to overcome the rise in viscosity due to pressure. At the same time, the heat dissipation within the oil film is reduced and the rate of temperature rise decreases. The pressure influence on viscosity is subsequently regained but in combination with the higher film temperatures does not raise the viscosity or shear stress to as high as that at inlet where the oil is much cooler. With the SAE 10 oil, the changes in pressure and temperature do not affect the viscosity to the same extent, and the rate of rise of shear stress is reduced considerably.

The inlet "peak" in the shear stress distribution is reflected in the viscosity distributions previously given in fig. 6.28, where agreement with the general predictions of Merritt (89) was observed.

Closer examination of the curves shown in fig. 7.14 indicates that at inlet to the contact the slopes of the shear stress curves are in accordance with the pressure-viscosity relationship and that the rate of increase of shear stress is greater for high slip, where shear rate is correspondingly higher for the same viscosity. The high shear rates however

produce higher film temperatures and the temperature effect on viscosity takes over much earlier in the contact and reduces the overall magnitude of the shear stresses. The areas under the curves represent the tractive force or coefficient of friction and the influence of entraining speed, contact load, and inlet viscosity are once more clearly illustrated.

7.4.3 Results for a Maxwellian Fluid

The shear stress equations derived for a Maxwellian fluid are applied to the example given in figs. 7.12 and 7.13. By a comparison between the Maxwellian and Newtonian coefficients of friction, the predictions of the Crouch and Cameron criterion (38). are confirmed. At the given contact conditions there is a significant reduction in the calculated friction. With the high viscosities generated at the contact and the short transit times of the oil, the stress relaxation effects become very important. The elastic shear of the highly viscous lubricant has insufficient time to relax and the total slip is made up of viscous and elastic shear. A lower shear stress therefore produces the same slip between the surfaces, inducing both elastic and viscous shear. The results show a reduction in the peak friction from a coefficient of 1.0 to .08 with the slip at which the peak occurs increasing from .0002 to .005.

A more detailed analysis of the effect of viscoelasticity according to the Maxwell fluid model is given by examination of the shear stress distribution as the slip is increased. Figs. 7.15 to 7.18 show the mechanism to be complex.

At a slip of .001, the Newtonian fluid exhibits very high shear stresses with the characteristic "peak" stress in the first half of the contact. The viscoelastic effect is predominant

under these conditions and the Maxwellian fluid exhibits a very low shear stress, the slip consisting largely of elastic shear. The Maxwellian shear stress rises towards the end of the contact where the viscosities and the elastic shear components have been reduced by the local reduction in pressure and increased oil temperatures.

Increasing the slip to .005 in fig. 7.16 effects a reduction in the overall magnitude of the Newtonian shear stresses. This is a direct result of the reduction in film viscosities due to increased heat dissipation. In the Maxwellian fluid, the lower viscosities give rise to increased viscous shear and the elastic shear component of the total slip is reduced. The shear stress is consequently higher than at low slip and increases towards the centre of the contact zone. This is accompanied by an increase in the heat dissipation within the film and the peak film temperatures are reached in the second half of the contact figs. 7.19 and 7.20(a). What is then observed is the same abrupt reduction in shear stress as detected in the Newtonian fluid but with a Maxwellian fluid it is delayed till later in the contact. By inspection of the temperature and viscosity curves in figs. 7.19 and 7.20(a) it is apparent that the abrupt reduction in shear stress is associated with a reduction in film viscosity as before, but this time in the outer edges of the film rather than at the mid-plane. The reason for this is explained by the balance between thermal and viscoelastic effects on shear rate.

In the first half of the contact, the outer edges of the film have the lowest oil temperatures and as the viscosity rises due to pressure, the viscoelastic effect becomes more predominant at the edges. The elastic shear component increases and the net shear rate at the mid-plane of the film is reduced. The initial

mid-plane temperature rise is consequently lower than for a Newtonian fluid, and the associated reduction in viscosity is more gradual, fig. 7.19.

With the increased shear rate at the outer edges of the film the viscous shear rate is apparently increased, producing higher oil temperatures and lower viscosities than with a Newtonian fluid, fig. 7.20.

Towards the centre of the contact, the viscosity at the film edges rises gradually whilst the mid-plane viscosity decreases. An increasingly larger part of the total shear rate is transferred to the mid-plane of the film and the viscous dissipation reduces at the outer edges. The elastic shear rate component is also reducing due to the decrease in the rate of shear stress rise, fig. 7.16, the net effect being a further increase in the viscosity of the outer elements of the film.

However, just past the centre of the contact the shear stress begins to reduce, with the effect of relieving the elastic shear induced in the elements as they passed through the region of increasing shear stress in the first half of contact. Reference to fig. 7.20(b) assists in explaining the series of events that follow.

The velocity profiles in this figure, substantiate the remarks already made about the transference of most of the shear rate to the mid-plane. At a distance of $^{x}/_{b} = .6$, the velocity profile is almost identical to that of a Newtonian fluid. The difference lies in the fact that the Maxwellian fluid elements at this point possess an elastic shear distortion although possessing the same velocities as corresponding Newtonian elements. The strain energy associated with the Maxwellian fluid elements is about to be released by the field of reducing shear stress,

through which the elements must now pass. This energy is shown to be recovered in the form of viscous dissipation, increasing the velocities of the elements at the edges of the film and increasing the heat generation throughout. This is clearly illustrated by reference to the velocity profiles and oil temperature rises in the region of $x/b = .7$. An abrupt reduction of viscosity in the outer edges of the film is experienced, resembling that observed on the mid-plane of a Newtonian fluid. The accompanying reduction in shear stress is also in evidence and for the remainder of the contact, the shear stresses are low, rising only slightly as a result of the local pressures and lower oil temperatures.

The double rise in shear stress is more prominent when the slip is increased, fig. 7.17. Here, the higher rate of viscous dissipation produces higher film temperatures with a maximum occurring nearer the centre of the contact. The same characteristics of the shear stress distribution are again observed but with a larger second rise in shear stress due to higher local pressures. The Newtonian and Maxwellian shear stress distributions are seen to be much closer than previous curves.

Eventually the Maxwellian shear stress profile merges with the Newtonian profile as in fig. 7.18 and the double rise in shear stress of the Maxwellian fluid adopts the Newtonian shear stress distribution, including the inlet "peak". At values of slip greater than .05, the thermal action is to reduce the contact viscosities to the extent of eliminating significant viscoelasticity effects so that the behaviour of the Maxwell fluid is no different from that of the Newtonian fluid.

7.4.3 Application to Crook's results

Section 7.1 gave details of Crook's (91) experimental disc results for the traction-sliding speed characteristics of elasto-hydrodynamic contacts. Crook's theory, based on a Newtonian fluid (66) produced coefficients of friction far in excess of the experimental results and the two separate theoretical and experimental graphs given by Crook have been combined in fig. 7.21 for two different contact loads. Full details of the contact conditions are given by Crook and these have been used in the present analysis to recalculate the friction and include visco-elasticity.

The solutions are seen to give better correlation with experiment provided adjustments are made to the value of the thermal diffusivity of the lubricant. The thermal diffusivity giving the best correlation is 40% greater than the usually quoted value at standard temperature and pressure, which is within the 100% increase proposed by Johnson and Cameron (93) from measurements at high pressures.

Further to this, in fig. 7.21(a) it is observed that in the low slip region, the agreement between theory and experiment is improved marginally by the assumption of a Maxwellian fluid ($G_\infty = 10^{10}$ dyn/cm^2). In the high slip region, the friction force reduces at a greater rate than measured experimentally. Crook's theoretical curve exhibits the same tendency.

This may be explained by the increase in surface temperature of the discs in the experiment, i.e. blank temperature of the discs as the sliding speed is increased. The effect is one of reducing the inlet viscosity and hence the film thickness. By comparison with similar experiments conducted by Jefferis and Johnson (92), this results in an increase in the shear stress at

the contact.

The theoretical calculations have not taken into account any increase in blank temperature with sliding speed and therefore predict friction forces increasingly lower than those measured.

For the lower contact load condition in fig. 7.21(b) the surface temperature rise effects are smaller and the theoretical curve provides a better fit to the experiment than Crook's original theory.

From the foregoing preliminary analysis and comparison with existing experimental data, it is evident that while the viscoelastic properties of a lubricant are significant in the low slip region of sliding friction the thermal diffusivity of a lubricant affects the magnitudes of friction over the whole range of sliding speeds.

7.5 The Traction Experiments

7.5.1 The Low-Slip Machine

The preliminary calculations of friction completed so far have not taken into account the variation in blank temperature with sliding speed. In comparing the proposed theory with experiment it is necessary therefore to measure the disc surface temperatures as well as friction as the sliding speed is increased. Published results to data have not included this. Also with the apparent dependence of friction upon the thermal diffusivity of the lubricant it is essential that the thermal conductivity of the lubricant under test and its variation with temperature and pressure are known. Only then can reasonable comparisons between theory and experiment be made.

Measurements of thermal conductivity of lubricants upto pressures of 30,000 lbf/in^2 and for a range of temperatures are available (105). With regard to the viscoelastic properties of

lubricants, approximate values for the shear modulus G_∞ are recorded in the literature, but the dependence upon temperature and pressure is not yet defined.

By conducting further experiments into the frictional behaviour of rolling/sliding contacts it should be possible to make a more accurate appraisal of the present theory by lubricating with an oil of known viscosity and thermal conductivity characteristics. Viscoelasticity may then be introduced into the calculations in the form of the Maxwell model as a first approximation and the published values of G_∞ assessed by the degree of correlation between the predicted and actual friction-slip characteristics.

Such an experiment was conducted on the machine shown in fig. 7.22, which in principle is the same as that used in references 92 and 93.

The machine is constructed on the "back-to-back" system using two shunt-wound 12 HP DC motors, wired so that one of them operates as a motor and the other as a generator. The motor drives the generator through a friction drive provided by two discs loaded together. The circuit diagram in fig. 7.23, assists in the description of the operation of the machine.

Considering the motor, its speed and output torque depend upon the characteristics of the DC machine. At a given field current, the speed of the shaft, U_1 reduces as the torque requirement is increased. The original speed can be maintained by a reduction in the field current. This is achieved by increasing the series field resistance.

The speed of the second shaft, U_2 however is determined by the intersection of the characteristics of the DC machine and the lubricated contact, fig. 7.24.

If the generator is considered to be a motor to begin with, then with a low field resistance, the field is strong and the speed is low for the no-load condition. If instead of requiring a torque and reducing the speed and back emf (as for a motor) the speed is increased by applying a torque, the back emf becomes larger than the applied voltage. The machine then becomes a generator with the torque supplied by the first motor via the discs. The output of the generator is wired as the input to the first motor with a make-up generator coupled into the circuit to replace the frictional and windage losses in the loop.

If the generator field is increased by reducing the series resistance, the "motor" effect would be to slow up the machine and maintain the balancing emf. Hence upon rotation of the machine at the same speed as before, the back emf is greater. Consequently the generator output is increased. However with the requirement of higher torque for the same speed, the discs slip and reduce U_2 from its previous value, lowering the torque required at that field current, fig. 7.24.

The above arrangement provided an infinitely variable range of entraining and sliding speeds and by manipulation of the field series resistances to the make-up generator and the two DC machines, the full range of sliding and entraining speeds upto 1500 rev/min was available.

The torque was measured by strain gauging the flexible coupling on shaft number 1. Both flexible couplings were mounted outside the bearing assemblies supporting the discs and the loading lever, fig. 7.25. The amplified signal from the torque tube therefore included bearing friction as well as the contact friction.

The loading system consisted of weights attached to the

lever protruding from the back of the machine and pivoting about a point vertically below the point of contact between the discs The moment was transmitted via the loading-pin arrangement shown in fig. 7.25, to the self-aligning blocks supporting the second disc. The drive from the second disc was transmitted to the generator via the second flexible coupling.

Blank temperatures were measured with trailing thermocouples of the type described in section 3.9.2 lightly loaded onto each of the discs. (Further evidence of the accuracy of these thermocouples has been presented recently in reference 93)

The discs were 3 inches in diameter and $^{3}/_{16}$ inch wide, and lubricated by an oil supply fed from a reservoir below the disc compartment, fig. 7.26. The surface speeds of the discs could be calculated from the rotational speeds of the shafts. These were measured by the magnetic transducer method, whereby pulses were received from a toothed-wheel mounted on each shaft and displayed by a digital counter. The counter had the facility for displaying the individual speeds of the shafts or expressing the speeds as a ratio of one another. The toothed-wheel consisted of 60 teeth, so that by counting the pulses on one wheel for a period of 10 seconds, the speed could be expressed as rev/min to the first decimal place. For a speed ratio display the counter was triggered by taking the pulses from shaft 2 for instance, and counting the number of pulses received from shaft 1 for 10,000 pulses from shaft 2. The ratio was then displayed to one part in 10,000. The ratio could be inverted by taking 10,000 pulses from shaft 1 and counting the number of pulses from shaft 2. For example, if 9,975 pulses were received from shaft 2 for 10,000 pulses from shaft 1, then the slip was given by $(10,000 - 9,975)/10,000 = .0025$.

The separate speed measurements in rev/min of the two shafts were useful in monitoring the disc speeds to give the desired entraining speed ($U_e = (U_1 + U_2)/2$) whilst the ratiometer facility provided an accurate and direct measurement of slip.

Jefferis and Johnson (92) have experienced severe torsional oscillations with this type of machine at the high slip conditions. In the design of the present version of this machine, therefore, the lengths of shafts were kept short and the torsional stiffness as high as possible. An oscilloscope trace of the torquemeter output gave no indication of torsional vibration except for low load conditions at 420 - 440 rev/min. Either side of the resonant condition, the torquemeter output was smooth and the application of viscous dampers therefore considered unnecessary, provided the resonant condition was avoided.

The oscillations are inherent in the system due to the negative damping offered by the reduction in torque as slip increases and it has been found that significant modification to the measured friction characteristics result when oscillations are present (92).

7.5.2 The Experimental Procedure

The procedure consisted of selecting a suitable contact load and entraining speed and running the machine upto speed after the reservoir had been filled with the test lubricant. The correct balance between the field series resistances was obtained that gave the required slip between the discs whilst maintaining the desired entraining speed. Time was then allowed for the blank temperature readings to settle out at the equilibrium values. As the temperatures rose in a similar manner to that described in section 4.3, the resulting speed changes were corrected

The microstrain output of the torquemeter was then recorded and the controls adjusted once more to set a new slip, but maintain the same entraining speed.

Initial results for test oil I (Appendix I) are given in fig. 7.27 and 7.28 where the friction torque is plotted against sliding speed for various entraining speeds and contact loads. The simultaneously recorded blank temperatures are also recorded. No significance should be attached to the relative magnitudes of the temperatures as these are a consequence of running tests consecutively and there being insufficient time for the heat stored in the oil reservoir to be dissipated between tests. What is important is that the temperatures of the disc surfaces are known so that these can be used in the theoretical predictions.

The traction results are replotted in fig. 7.29 where the curves are observed to lie very close to one another. In the low slip region of the characteristics, the curves do not pass through the origin because the measured traction includes both the sliding and rolling friction of the contact and also the bearing friction of the supports. At zero slip, therefore, the measured traction represents the rolling and bearing frictions.

A further test was carried out to investigate this effect. The machine is so arranged that the DC machines can be operated as either motor or generator and there is no reason why the system employed above cannot be reversed and shaft 2 drive shaft 1. In this way a negative slip is introduced with $U_2 > U_1$ and the curve extends past the zero friction point on the curve, as in fig. 7.30.

This method was employed for all subsequent tests so that rolling and bearing friction could be separated from the sliding friction. A direct comparison between actual and predicted

sliding frictions at the contact would then be possible.

7.5.3 The test lubricant

The lubricant was supplied by H. Naylor of the Thornton Research Centre.

It was an MVI oil of properties given in Appendix I. A viscosity equation of the Vogel type was fitted to the measured values and this was found to be.

$$\eta = .00645\, e^{1790/\mu_R + 170}$$

The measurements of thermal conductivity for the lubricant have been plotted in fig. 7.31. Measurements upto pressures of 29,200 lbf/in^2 were available and extrapolation of the results into one line for all temperatures at higher pressures is possible. The approximate expression for thermal conductivity is given as:-

$$k = \frac{1}{180}\,(3 + .03\,P) \times 10^{-4}\ \text{BtU/in.s}^{\circ}\text{F}$$

where P is pressure in 10^3 lbf/in^2

At pressures below 30,000 lbf/in^2, the relationship does not hold for high temperatures, but the numerical treatment is somewhat simpler if the straight-line relationship is assumed throughout the range of pressures. In the inlet region of the contact where temperatures are low, the error in the value of thermal conductivity is no more than 3%. At outlet where temperatures will be in the region of 60 - 90°C the error will be a little more, 5%. This is insignificant compared to the assumed extrapolation of the curve where at pressures of 300,000 lbf/in^2 the thermal conductivity will be given as 12 x 10^{-4} cal/cms$^{\circ}$C or 6. x 10^{-6} BtU/ins$^{\circ}$F, compared to 3.0 x 10^{-4} cal/cms$^{\circ}$C at atmospheric pressure.

7.6 Discussion of experimental results and comparison with theory

The friction results for the test lubricant specified in section 7.5.3 are given in fig. 7.32 and accompanied by blank temperature readings in figs. 7.33(a) and (b). The conditions of load and speed were those stated in the figures, all other conditions being identical to those given in section 7.5.1.

The points are observed to fall very closely upon one curve and agree with the traction ceiling reported by Johnson and Cameron (93). The preliminary friction results from the traction machine also exhibited the same phenomenon, fig. 7.29 but the peak friction was .055 compared to .072 for the test lubricant. Reference (93) quoted maximum coefficients of friction between .06 and .07, reducing to .04 at high sliding speeds.

It was unfortunate that in the present investigation, slip was limited to .05. This was quite adequate for the purposes of identifying the maximum friction but did not include the high slip regions of the characteristics.

This limitation arose from the inadequate cooling afforded by the closed-loop oil flow system. Rapid increases in the oil inlet and blank temperatures were experienced, as indicated by fig 7.33 and in some instances resulted in scuffing of the disc specimens.

However, the main purpose of the investigation was to examine the low slip region and the rheological behaviour of the lubricant so that the above restrictions were considered not to be a serious disadvantage.

Subsequent modifications to the traction machine involving the installation of a water-cooler on the oil supply demonstrated that the oil inlet temperature could be controlled.

The theoretical predictions of friction and their comparison

with experiment are presented in figs. 7.34 - 7.39.

The values of G_∞ in the Maxwell model were varied to give the best fit to the experimental curves whilst retaining the expressions for the physical properties of the lubricant as detailed in section 7.5.3.

The thermal solution was made to produce quite reasonable estimates of the friction-slip characteristics for the range of conditions considered in the present investigation. A compromise however had to be reached at which the difference between the theoretical and experimental curves was negative in the very low slip region and positive at high slip. Adjustments to the value of G_∞ , as in fig. 7.35 to obtain better agreement in the very low slip region resulted in overestimates of the friction at higher slip.

The effect is attributable to the assumption of the simple Maxwell fluid element representing the non-Newtonian behaviour of the lubricant. From the results, it is clear that the behaviour of the lubricant is more complex and a more accurate model of the fluid element is required for closer agreement between theory and experiment.

Nevertheless the solutions produce better predictions of the friction characteristics than the Newtonian fluid theory and the values of G_∞ necessary to achieve this are within the range of values quoted elsewhere (99,100).

In agreement with the findings of Crook (91) fig. 7.9(b), the values of G_∞ are below the often quoted value of 10^{10} dyn/cm^2 but the dependence upon pressure is the inverse of that predicted by Crook. The solutions presented here involve a reduction in G_∞ with increase in contact pressure which upon extrapolation to low pressure indicates a high value of G_∞ .

with experiment are presented in figs. 7.34 - 7.39.

The values of G_∞ in the Maxwell model were varied to give the best fit to the experimental curves whilst retaining the expressions for the physical properties of the lubricant as detailed in section 7.5.3.

The thermal solution was made to produce quite reasonable estimates of the friction-slip characteristics for the range of conditions considered in the present investigation. A compromise however had to be reached at which the difference between the theoretical and experimental curves was negative in the very low slip region and positive at high slip. Adjustments to the value of G_∞ , as in fig. 7.35 to obtain better agreement in the very low slip region resulted in overestimates of the friction at higher slip.

The effect is attributable to the assumption of the simple Maxwell fluid element representing the non-Newtonian behaviour of the lubricant. From the results, it is clear that the behaviour of the lubricant is more complex and a more accurate model of the fluid element is required for closer agreement between theory and experiment.

Nevertheless the solutions produce better predictions of the friction characteristics than the Newtonian fluid theory and the values of G_∞ necessary to achieve this are within the range of values quoted elsewhere (99,100).

In agreement with the findings of Crook (91) fig. 7.9(b), the values of G_∞ are below the often quoted value of 10^{10} dyn/cm^2 but the dependence upon pressure is the inverse of that predicted by Crook. The solutions presented here involve a reduction in G_∞ with increase in contact pressure which upon extrapolation to low pressure indicates a high value of G_∞ .

This suggests a condition of pure viscous shear at low

pressures which is in agreement with the generally accepted principles of lubrication..

The variation of G_∞ with the lubricant temperature is indicated by the comparison of results for the different speed conditions in figs. 7.34 - 7.39. At increased entraining speed, the oil film temperatures are higher and reductions in the value of G_∞ are experienced.

Further work will be necessary to establish an accurate relationship between G_∞ and pressure and temperature. The theoretical predictions presented in this thesis for instance, may be further modified by varying G_∞ as the slip is increased for any given load and speed. This could possibly overcome the discrepancies occurring in the shape of the curves by enabling higher values of G_∞ to be assumed for the initial part of the characteristic and reduced values in the high slip region where oil film temperatures are increased.

Only by seeking correlation over a complete range of operating conditions may relationships for the dependence of G_∞ upon pressure and temperature be established.

7.7 A note on pitting

The shear stress results obtained in the present investigation may be of some importance to the study of pitting.

Pitting is a phenomenon associated with the fatigue failure of the contacting bodies in areas of high stress alternation. Failure is promoted by local stress concentrations in the form of inclusions or micro-cracks in the material and the initiation of pits may be attributed to either surface or sub-surface origins.

Inspection of the stress field at the contact shows that the maximum shear stress occurs some distance below the surface

of the material (106) but its location and magnitude varies with the surface loading conditions. Early solutions considered only the Hertzian contact pressures (107, 108) but tangential forces were later introduced (109, 110) by adopting a uniform coefficient of friction through the contact zone. The tangential stresses were therefore represented by a parabolic or semi-elliptic distribution, the ratio between tangential and normal stress at any point being the coefficient of friction.

The full elastohydrodynamic pressure distribution has recently been introduced (111, 112) but no further information relating to the tangential stress distribution has been made available and the parabolic distribution is retained (112).

The effect of the tangential stresses is to increase the maximum sub-surface shear stresses but above a friction coefficient of about $\frac{1}{3}$, the shear stresses at the surface rise to a greater magnitude than the sub-surface values (113). Consequently for increased friction at the contact, the life to pitting is reduced and initiation of the failure is transferred from below the surface to the surface of the metal.

In fluid film lubrication however, coefficients of friction rarely exceed 0.1 to 0.15 and it becomes increasingly difficult to explain the occurrence of the surface initiation of pitting. The alternative frictional force distributions provided in this thesis may assist in developing the analysis still further as the shape and magnitudes of the tangential forces will affect the stress field pattern.

Once crack initiation at the surface has been explained then it is quite possible that the hydraulic theory of Way (114) for the propagation of cracks may be applied. The sharp peak in tangential stress predicted in the present work would assist in

opening the surface cracks before entry into the contact zone, whereupon they would become pressurised with oil and undergo propagation.

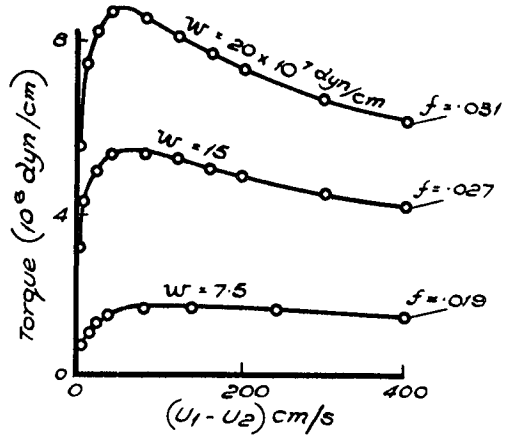

Constant Ue = 400 cm/s

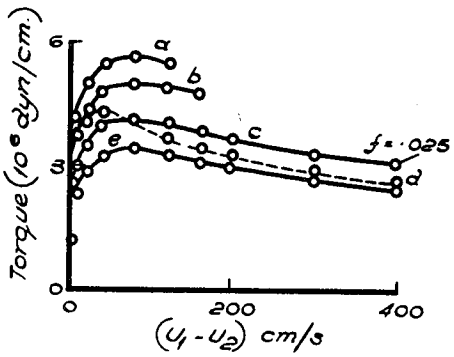

Constant $W = 12{\cdot}5 \times 10^7$ dyn/cm.

a)	$\eta_s = {\cdot}4$ P	Ue = 120 cm/s
b)	·4	200
c)	·4	400
e)	·7	400
f)	·4	600

FIG. 7.1. FRICTIONAL TRACTION AS A FUNCTION OF SLIDING SPEED FROM DISC MACHINE RESULTS OF CROOK (91)

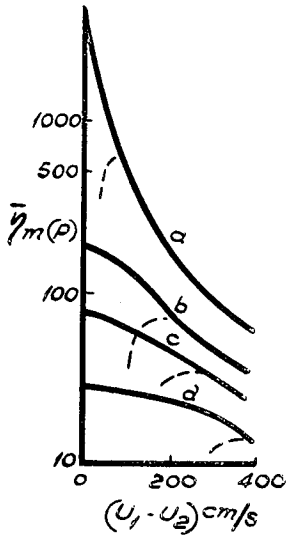

FIG 7.2. EFFECTIVE VISCOSITY ($\bar{\eta}_m$) AS A FUNCTION OF SLIDING SPEED, CALCULATED BY CROOK (66)

a) 20×10^7 dyn/cm
b) 10×10^7
c) $7{\cdot}5 \times 10^7$
d) 5×10^7

} $\eta_s = {\cdot}4$ P

– – – – – from approximate expression.

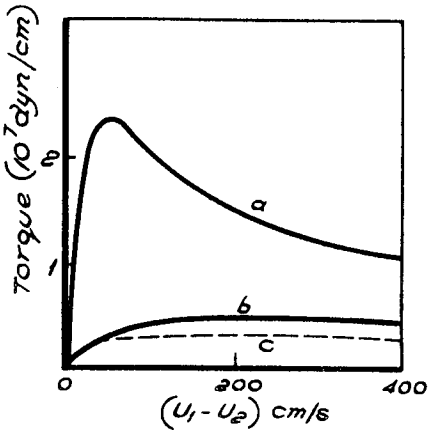

U_e = 500 cm/s, η_s = ·4P
a) $W = 20 \times 10^7$ dyn/cm
b) $W = 10 \times 10^7$
c) U_e = 500 cm/s
η_s = 1P
$W = 10 \times 10^7$ dyn/cm.

FIG. 7.3. FRICTIONAL TRACTION WITH SLIDING SPEED AS CALCULATED BY CROOK (66)

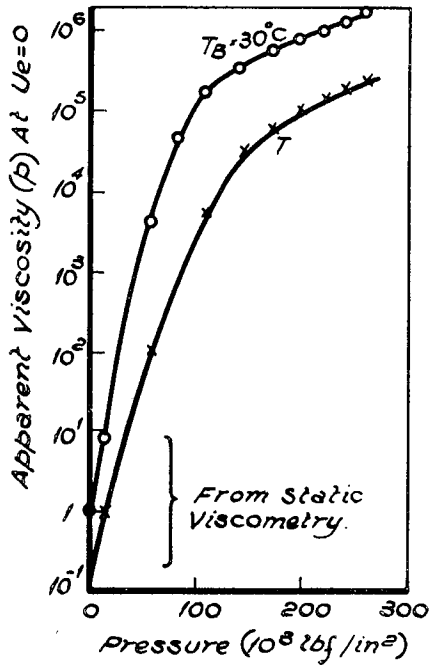

FIG. 7.4. APPARENT VISCOSITIES FROM REF (93)

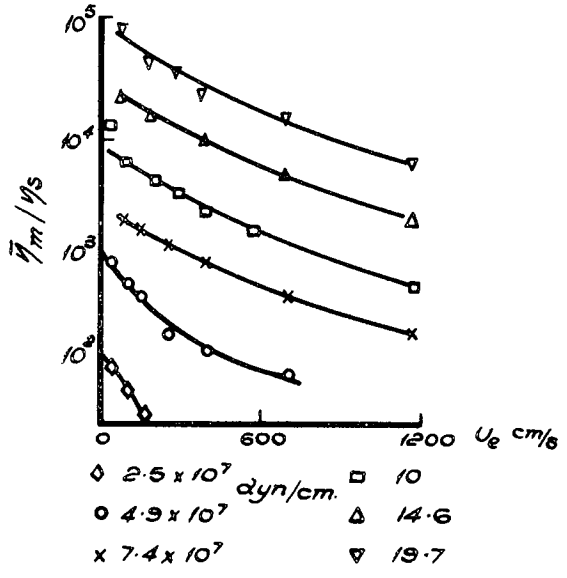

FIG 7.5 EFFECTIVE VISCOSITIES IN PURE ROLLING FROM REF (91)

T.5390.

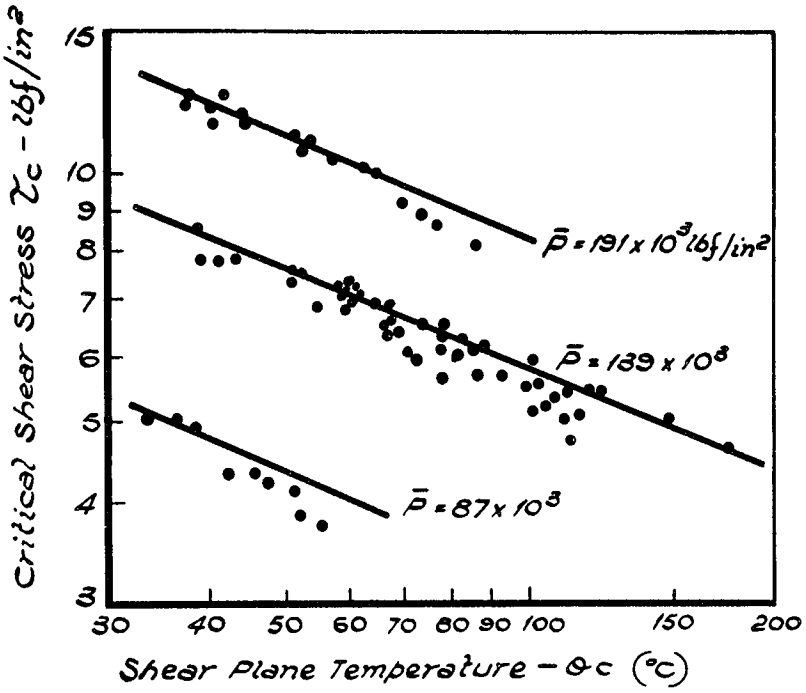

$$\frac{\tau_c}{\bar{P}} = 0.083 \left(\frac{\bar{P}}{139{,}000}\right)^{.2} \left(\frac{\theta_c}{30}\right)^{-.4}$$

Where $\bar{P}$ - Mean Contact Pressure.

FIG. 7.6. CRITICAL SHEAR STRESS RELATIONSHIP DERIVED IN REF. (93)

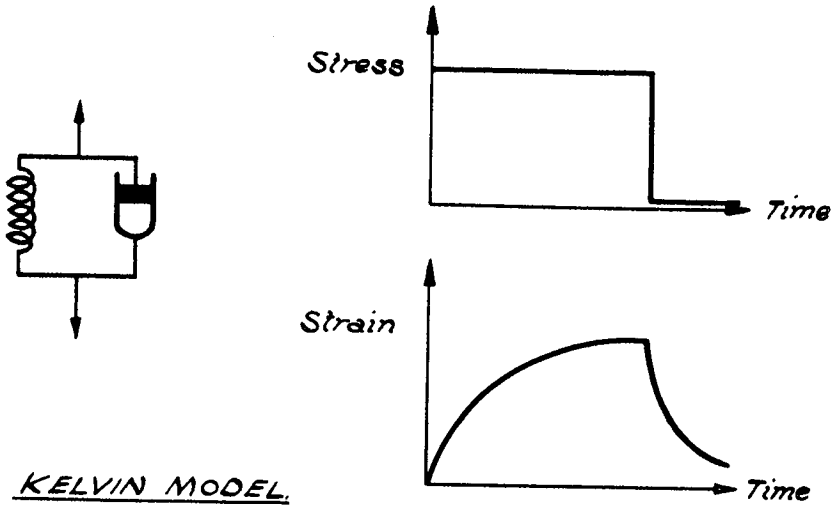

KELVIN MODEL.

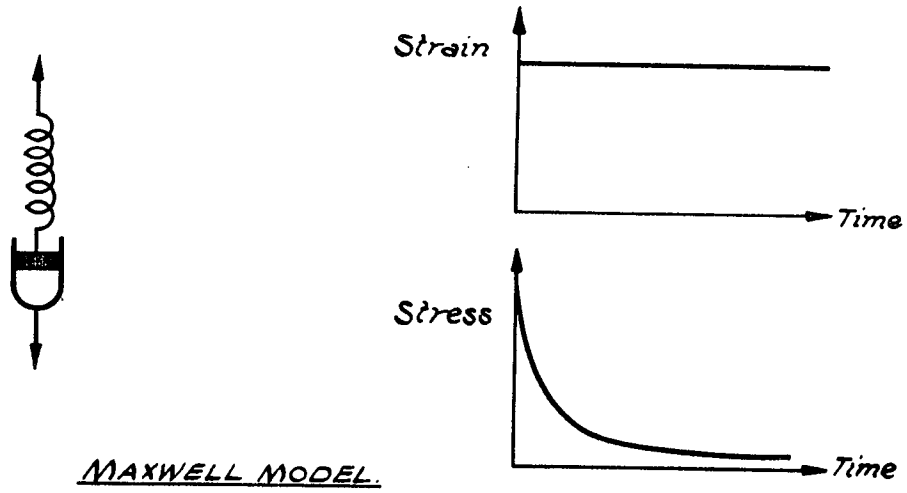

MAXWELL MODEL.

FIG. 7.7. VISCOELASTIC MODELS.

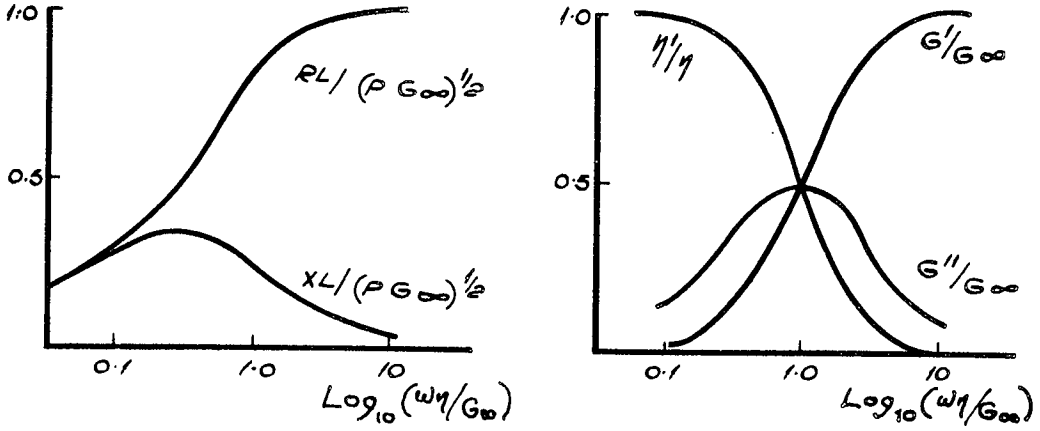

FIG 7.8(a) CALCULATED BEHAVIOUR OF THE VISCOELASTIC PARAMETERS IN CYCLIC SHEAR FOR A MAXWELL FLUID FROM REF (99)

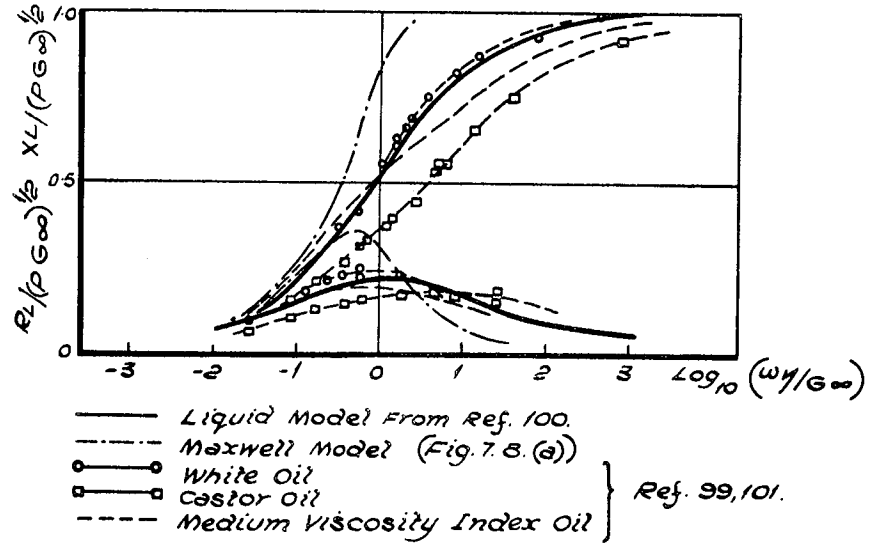

FIG. 7.8(b) NORMALISED PLOTS OF VISCOELASTIC PROPERTIES OF VARIOUS OILS FROM REF. 99, 101. AND COMPARED WITH NEW VISCOELASTIC MODEL FROM REFERENCE (100)

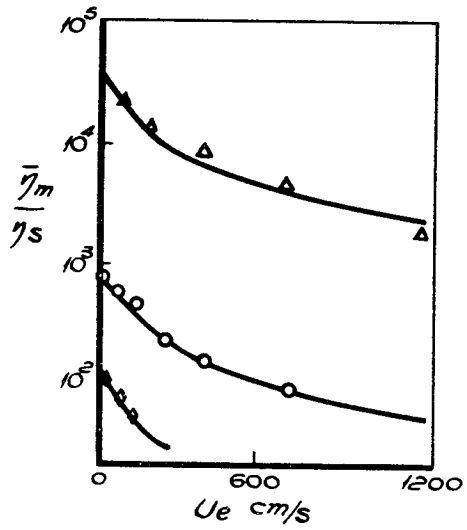

(a) Calculated Reduction In Effective Viscosity (Points from Experiment Reproduced In FIG. 7.5)

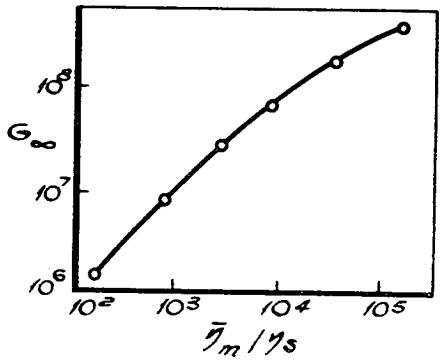

(b) Shear Modulus As A Function of $\bar{\eta}_m/\eta_s$

FIG. 7.9. CALCULATIONS BASED ON VISCOELASTICITY HYPOTHESIS FROM REF.(91.)

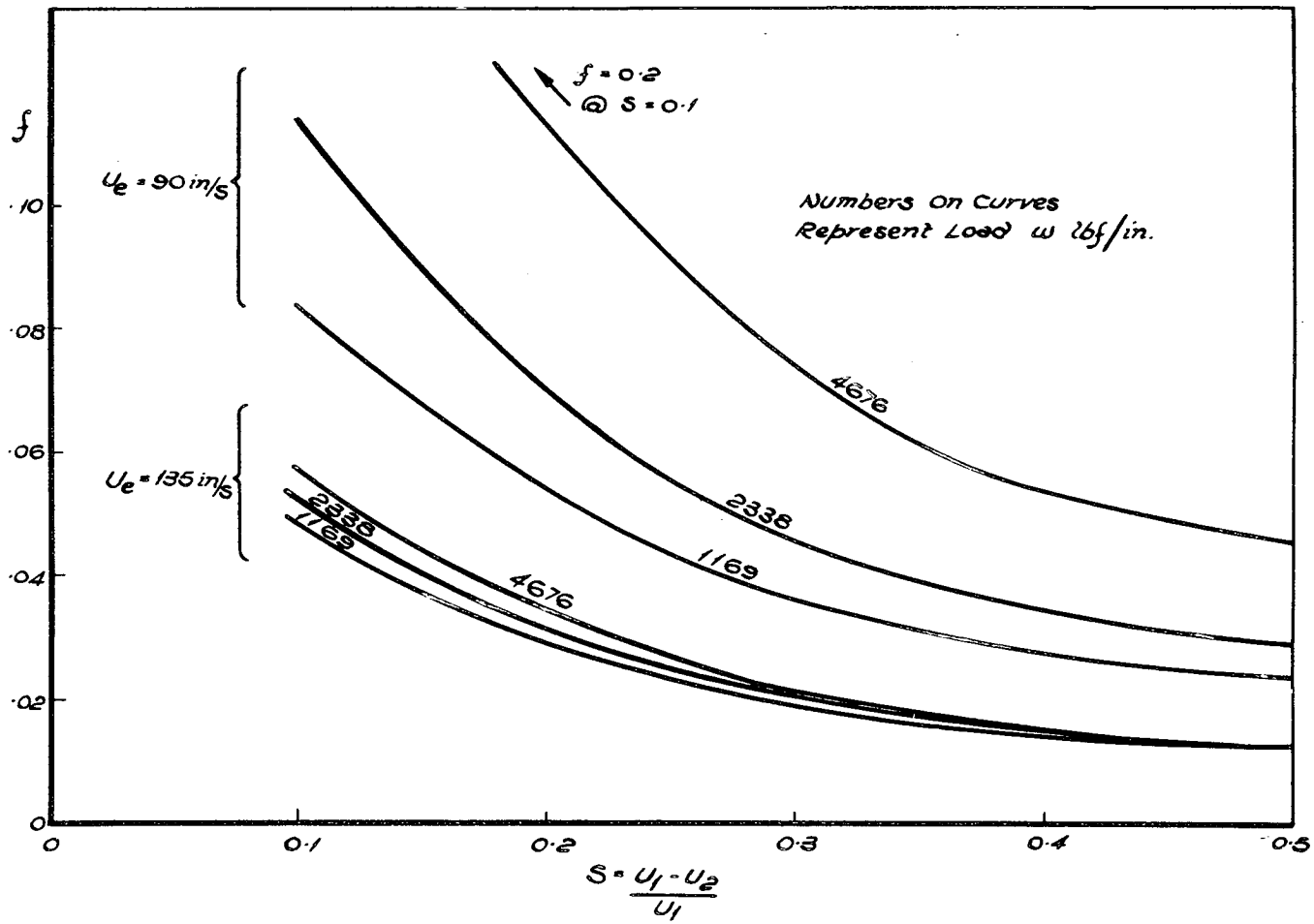

FIG. 7.10. CALCULATED COEFFICIENTS OF FRICTION WITH SLIP FOR SAE. 10. OIL.

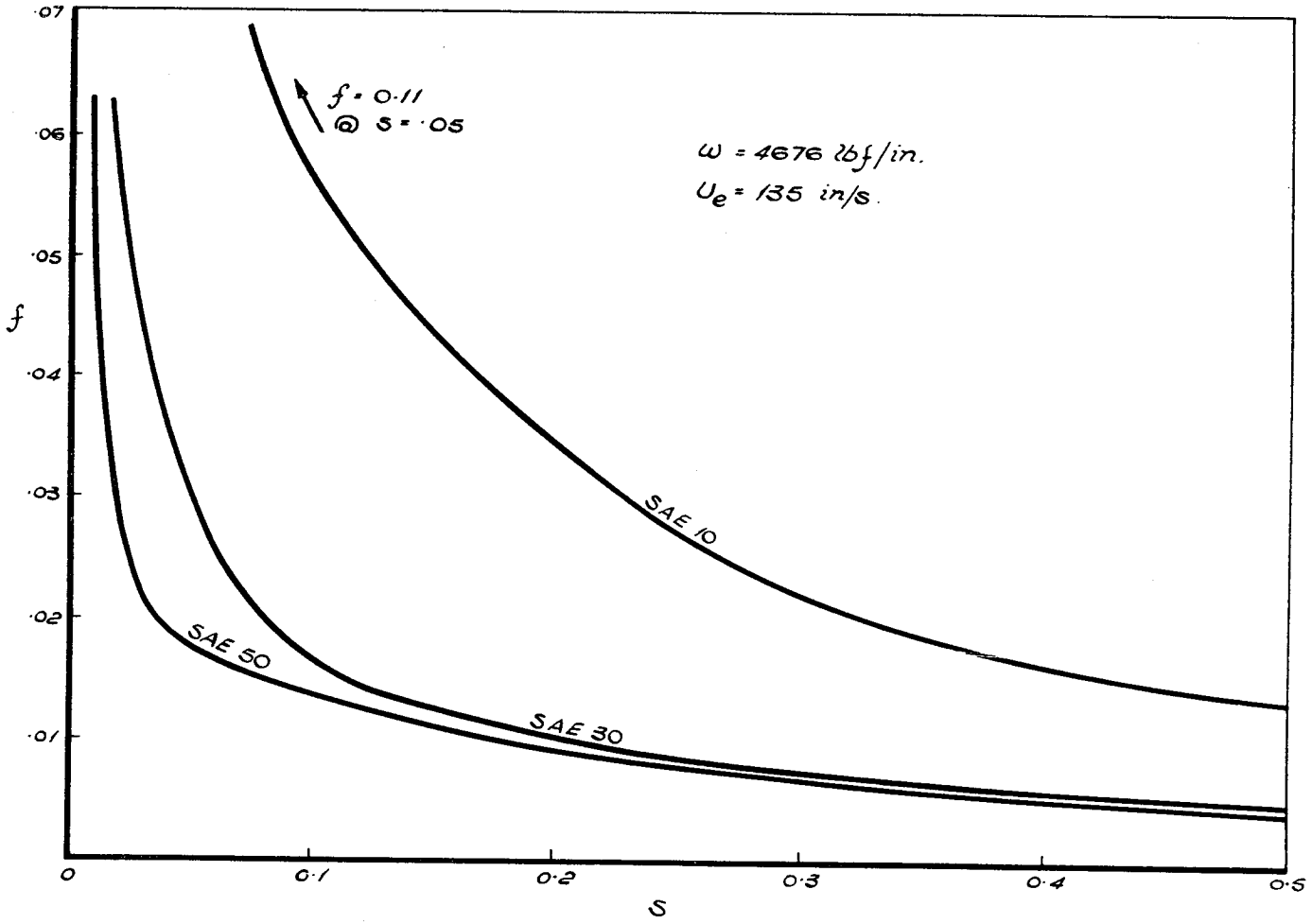

FIG. 7.11. EFFECT OF VISCOSITY ON COEFFICIENT OF FRICTION WITH SLIP

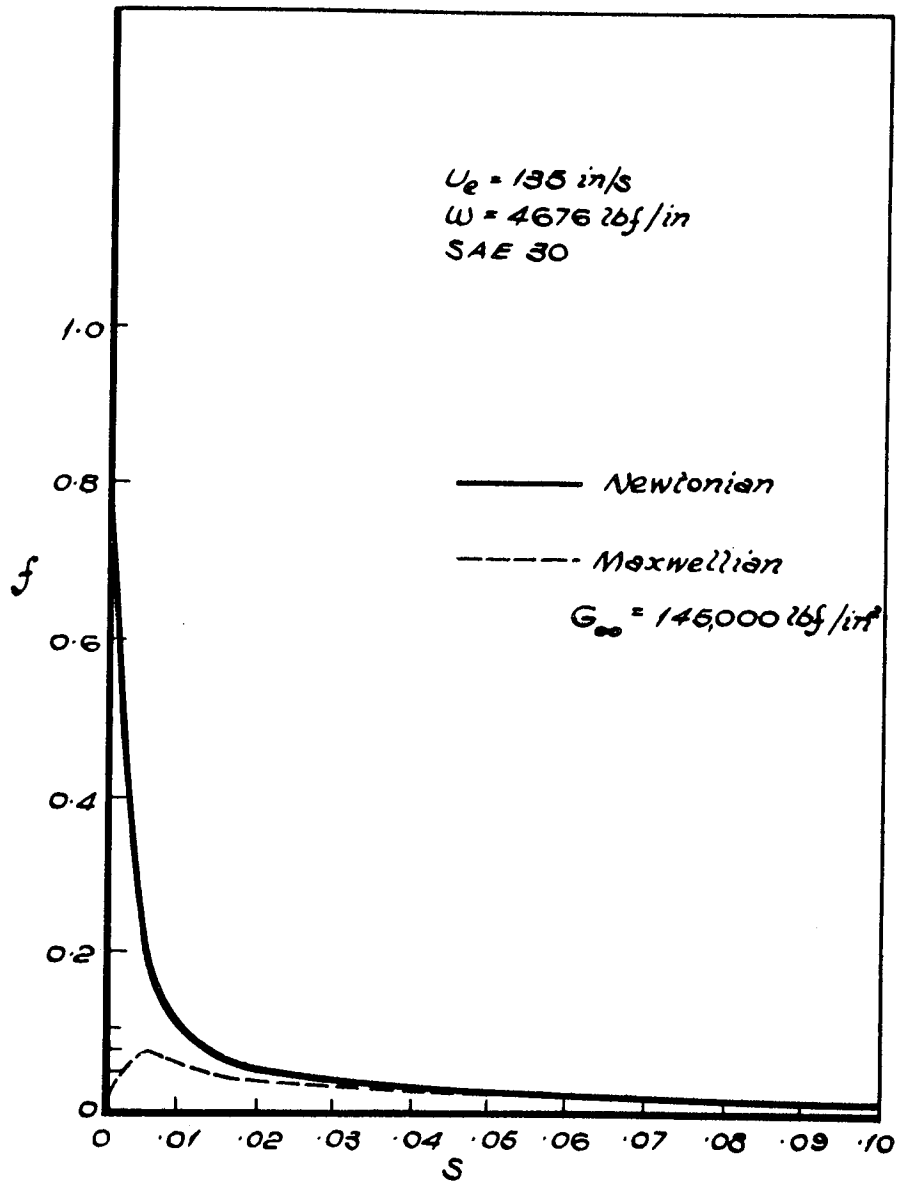

FIG. 7.12. FRICTION BEHAVIOUR OF NEWTONIAN AND MAXWELLIAN FLUIDS UP TO 0·1 SLIP

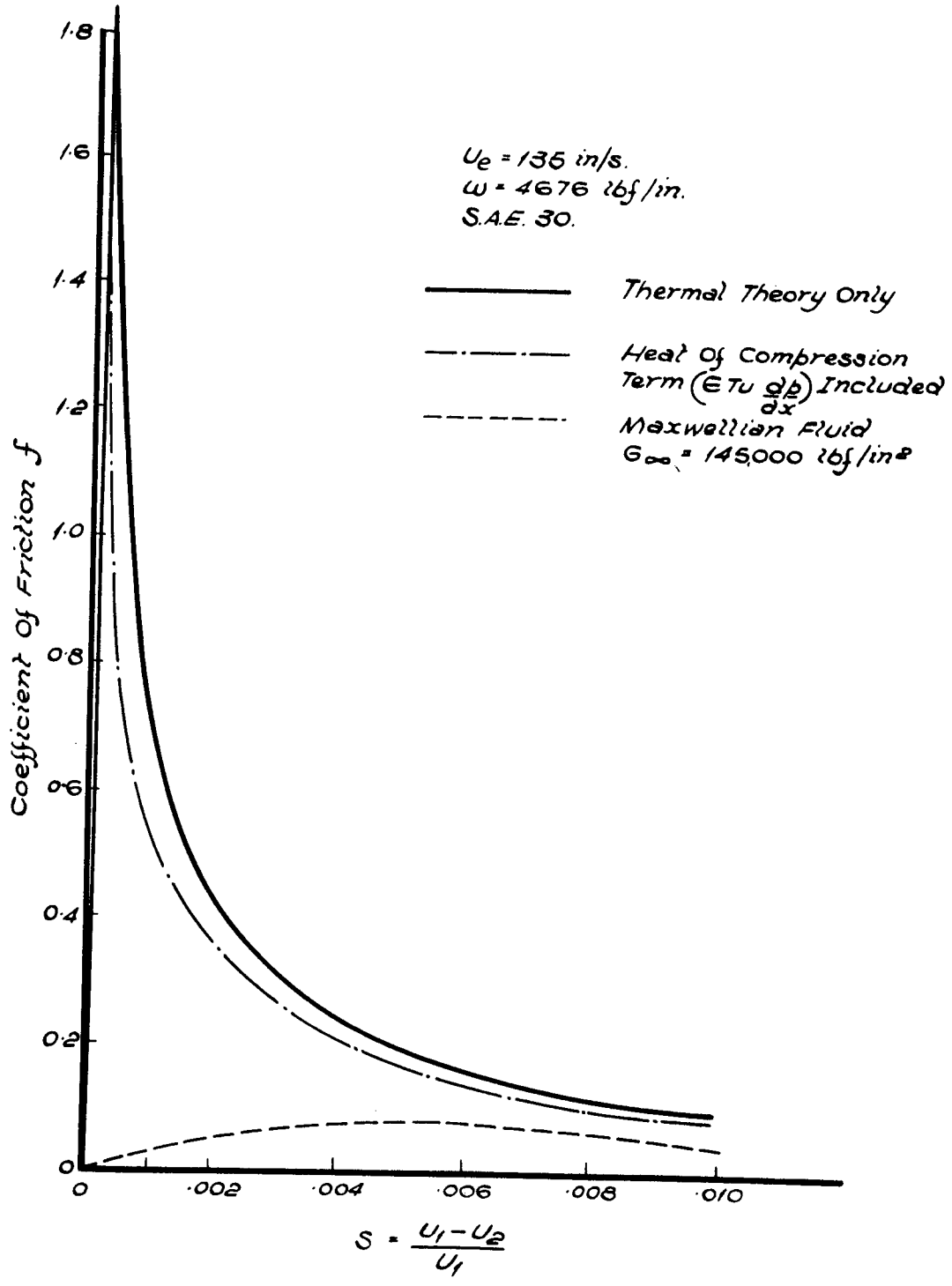

FIG. 7.13. FRICTION UP TO ·01 SLIP INCLUDING (a) Compression and (b) Non-Newtonian Effects.

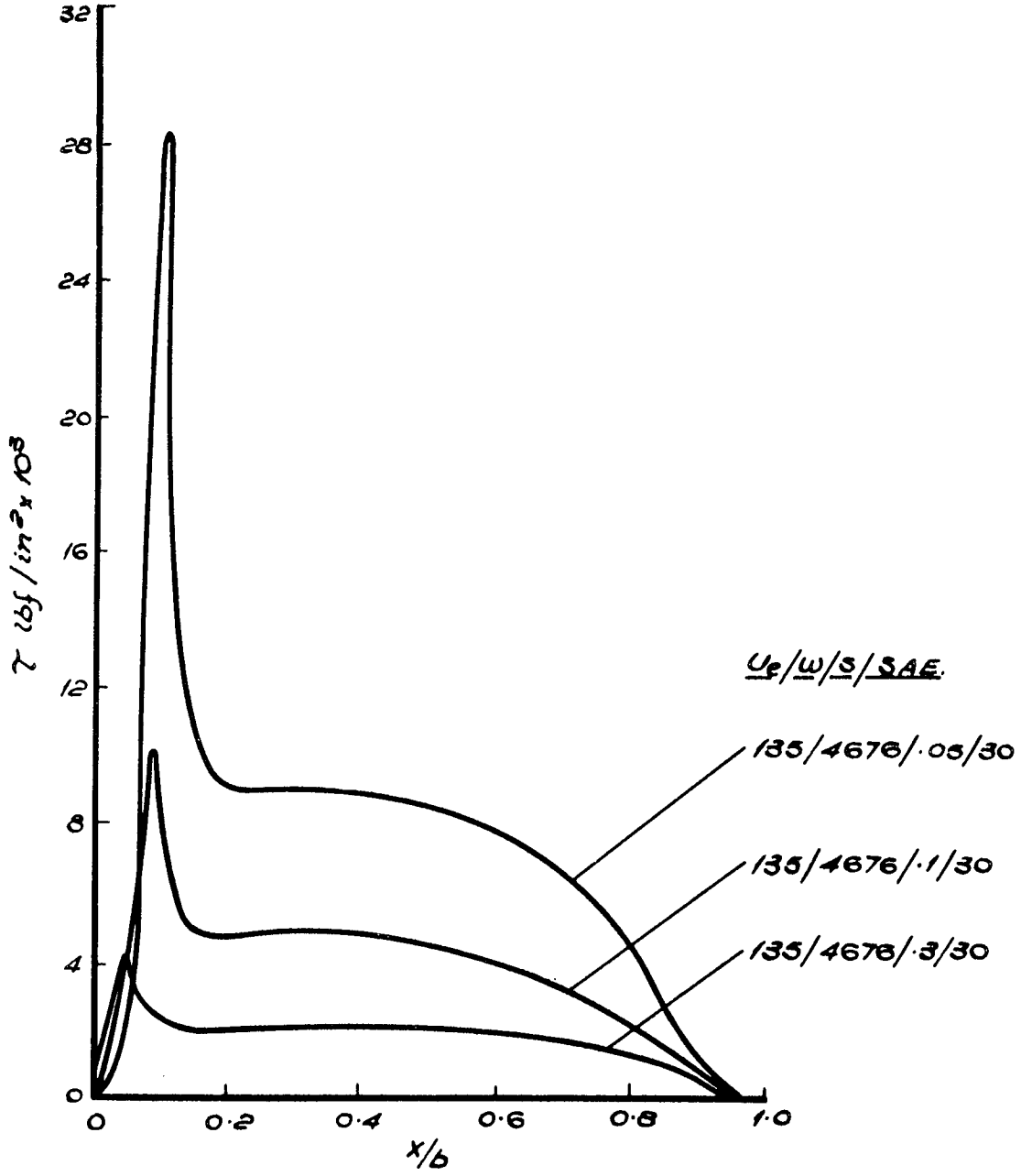

FIG. 7. 14. SHEAR STRESS DISTRIBUTIONS FOR SAE 30. LUBRICANT

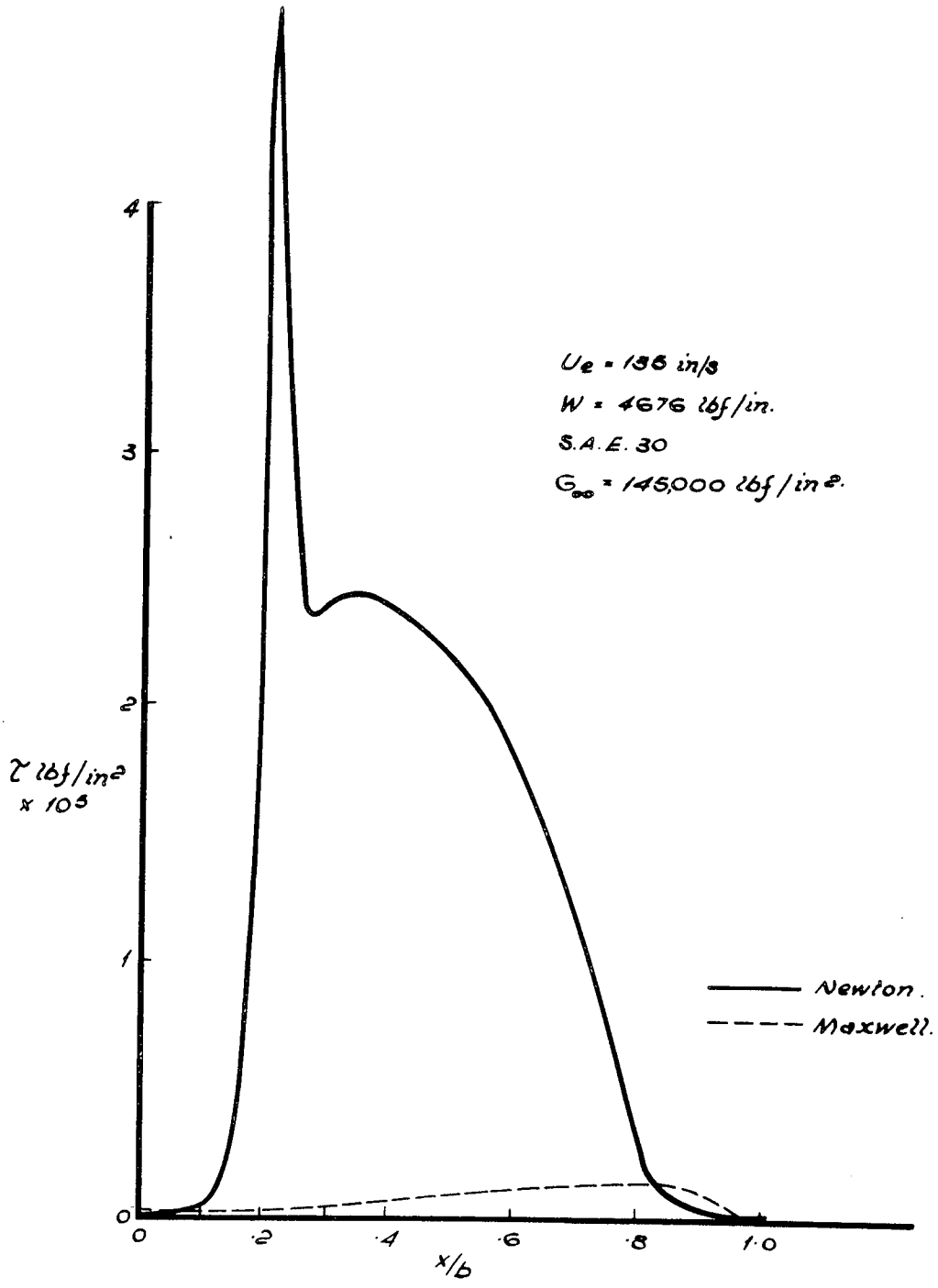

FIG. 7.15. SHEAR STRESS DISTRIBUTIONS FOR NEWTONIAN AND MAXWELLIAN FLUIDS AT S=·001.

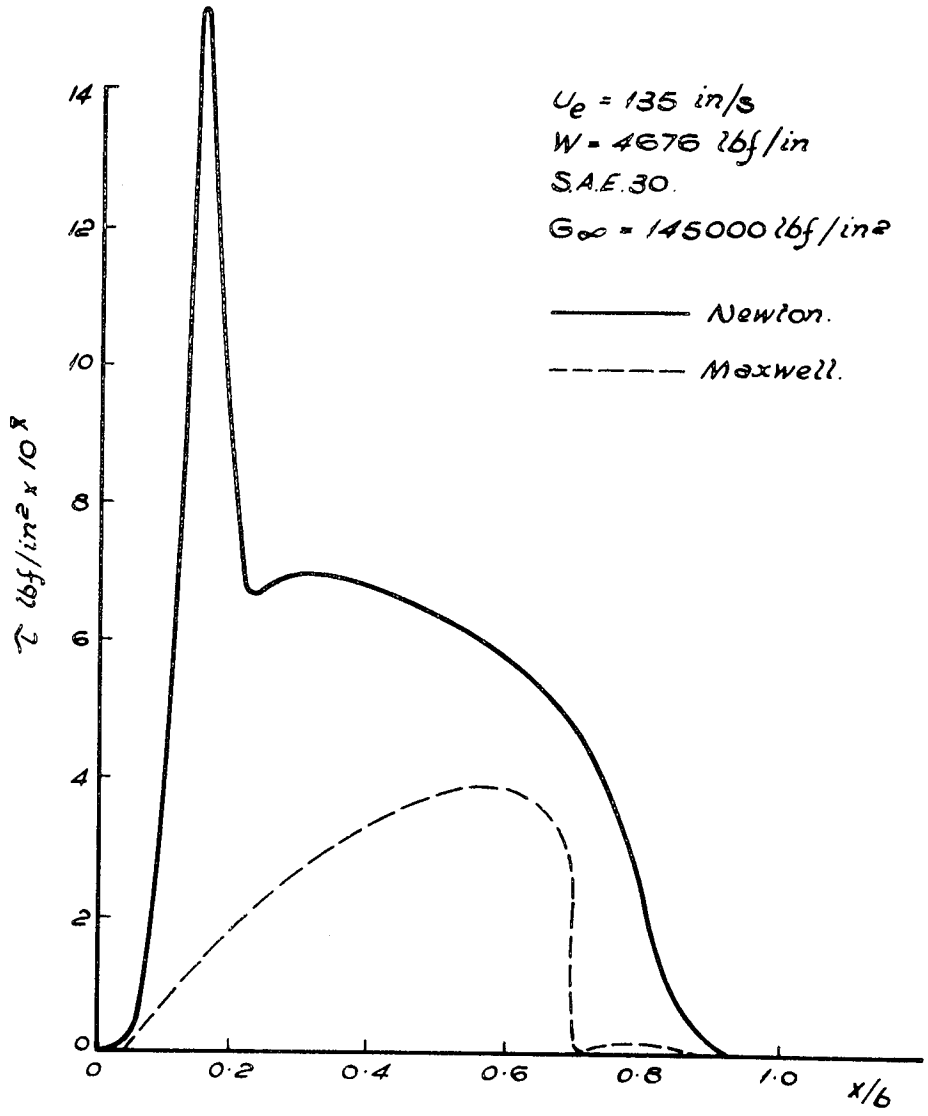

FIG. 7.16. SHEAR STRESS DISTRIBUTIONS FOR NEWTONIAN AND MAXWELLIAN FLUIDS AT S = ·005.

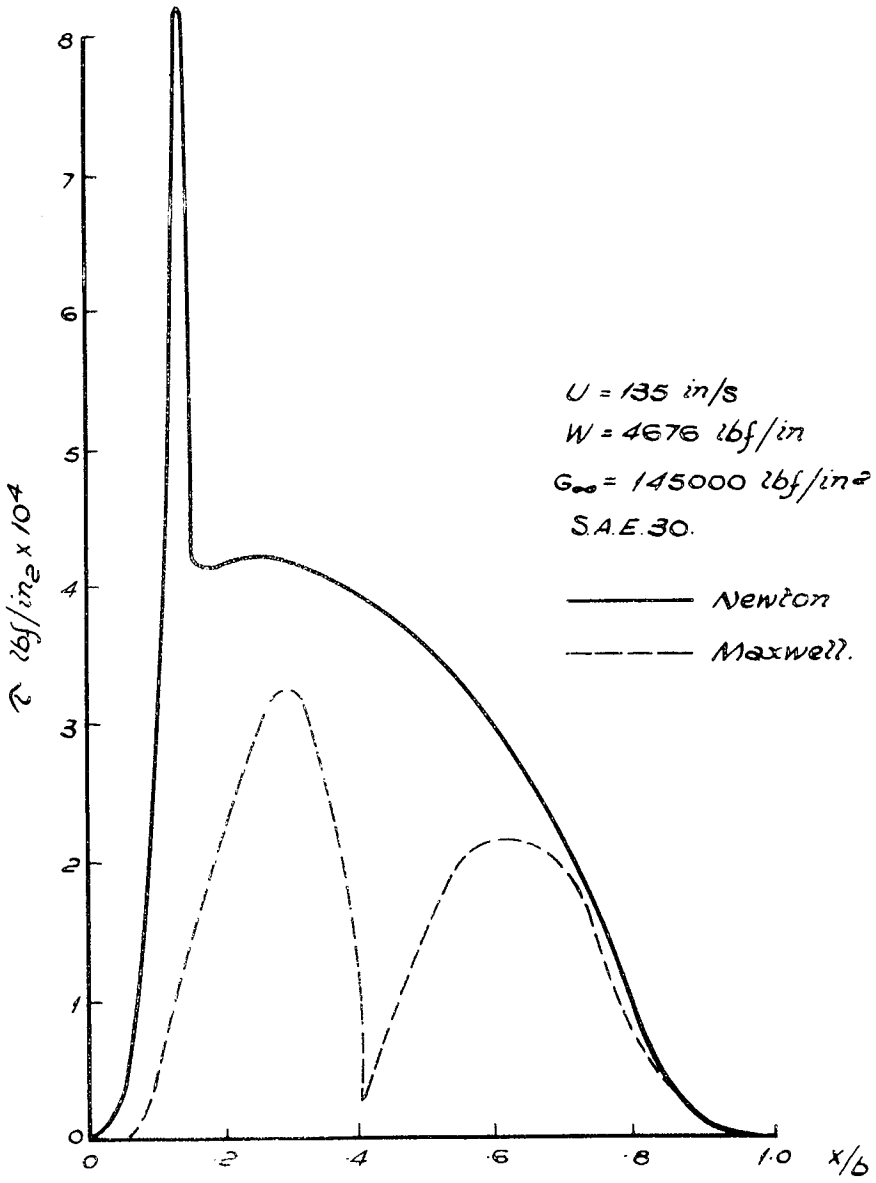

FIG. 7.17. SHEAR STRESS DISTRIBUTIONS FOR NEWTONIAN AND MAXWELLIAN FLUIDS AT S = ·01.

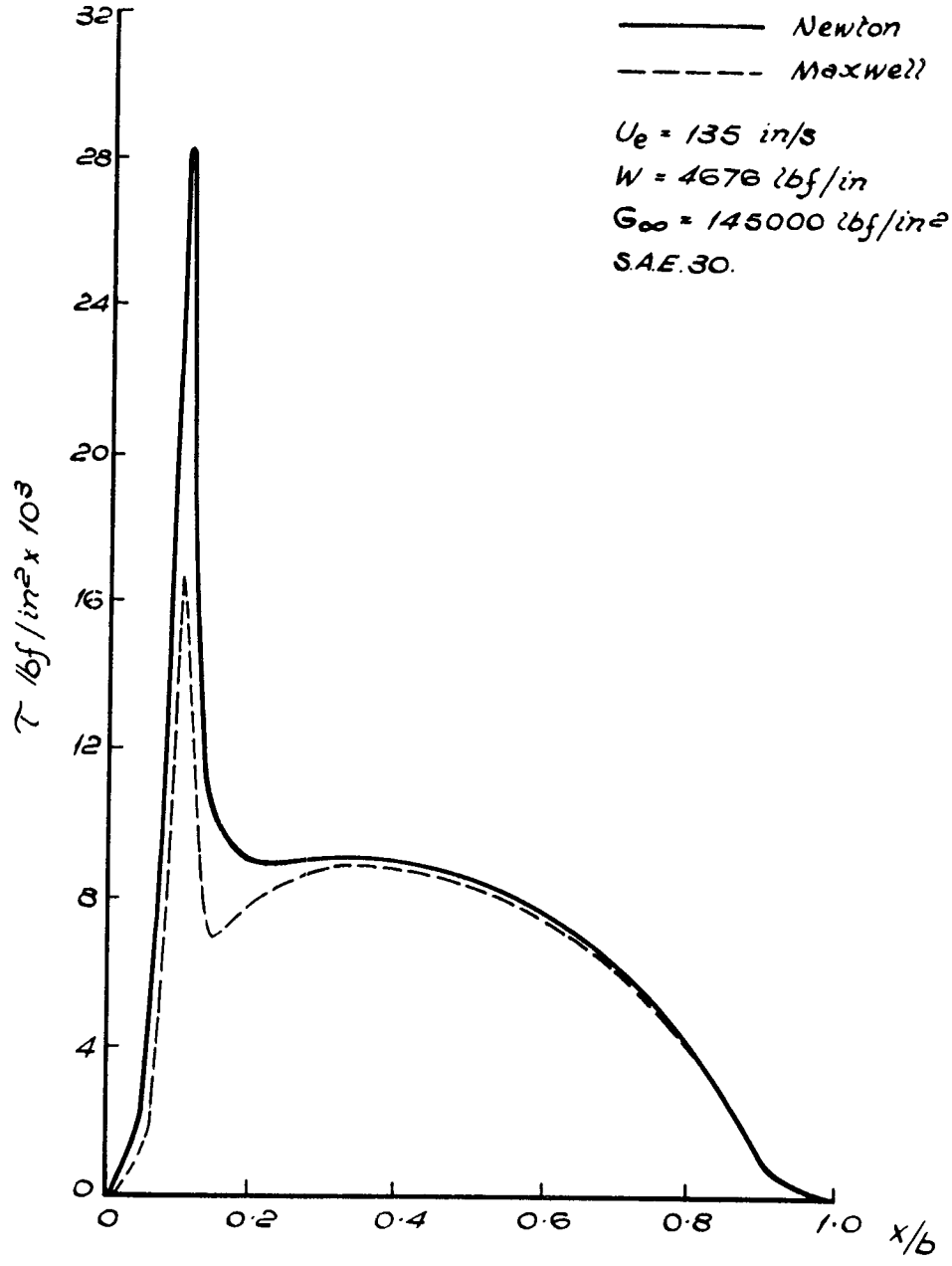

FIG. 7.18. SHEAR STRESS DISTRIBUTION FOR NEWTON AND MAXWELL FLUIDS AT S = ·05.

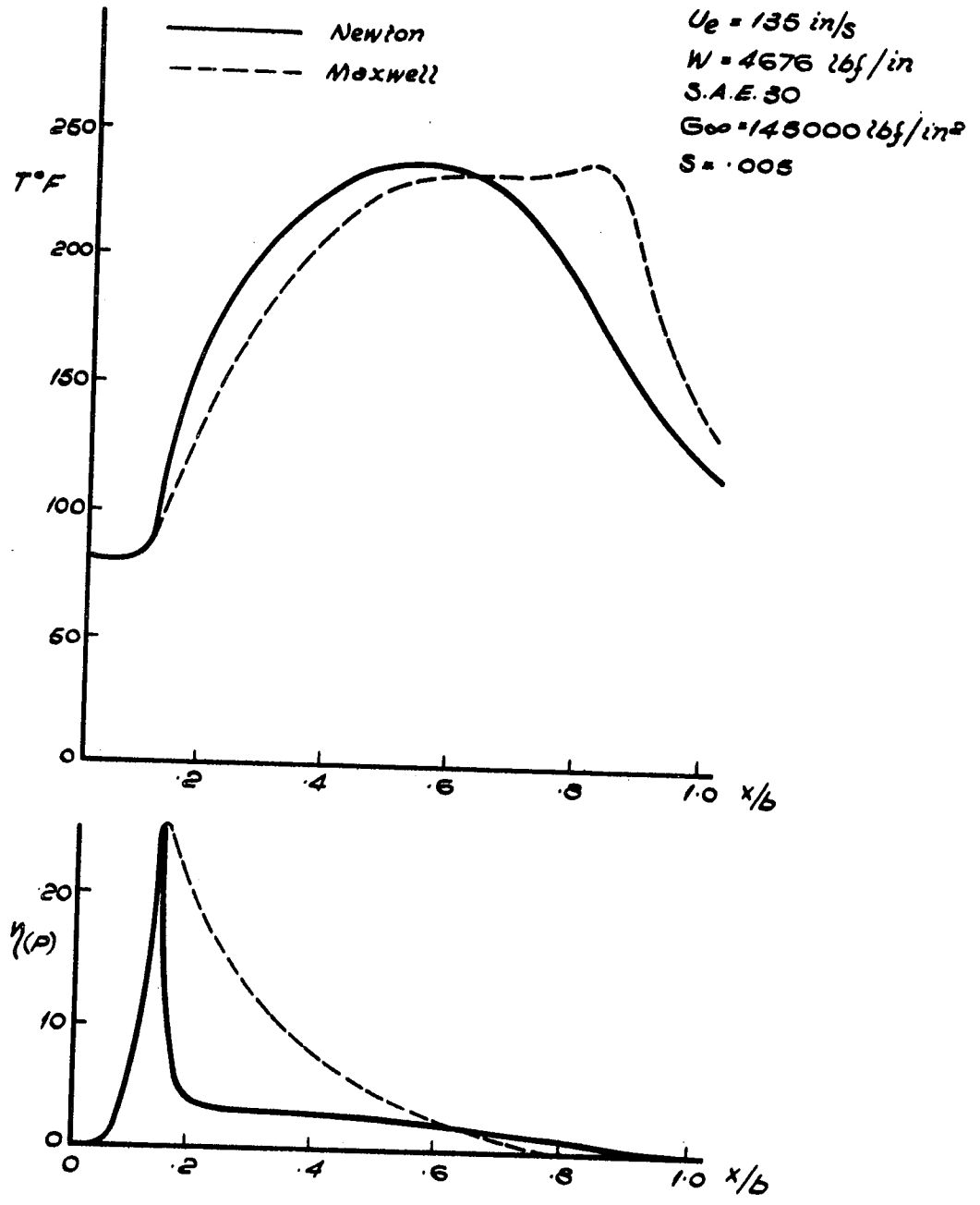

FIG. 7.19. TEMPERATURE AND VISCOSITY DISTRIBUTIONS AT MID-PLANE FOR NEWTONIAN AND MAXWELLIAN FLUIDS.

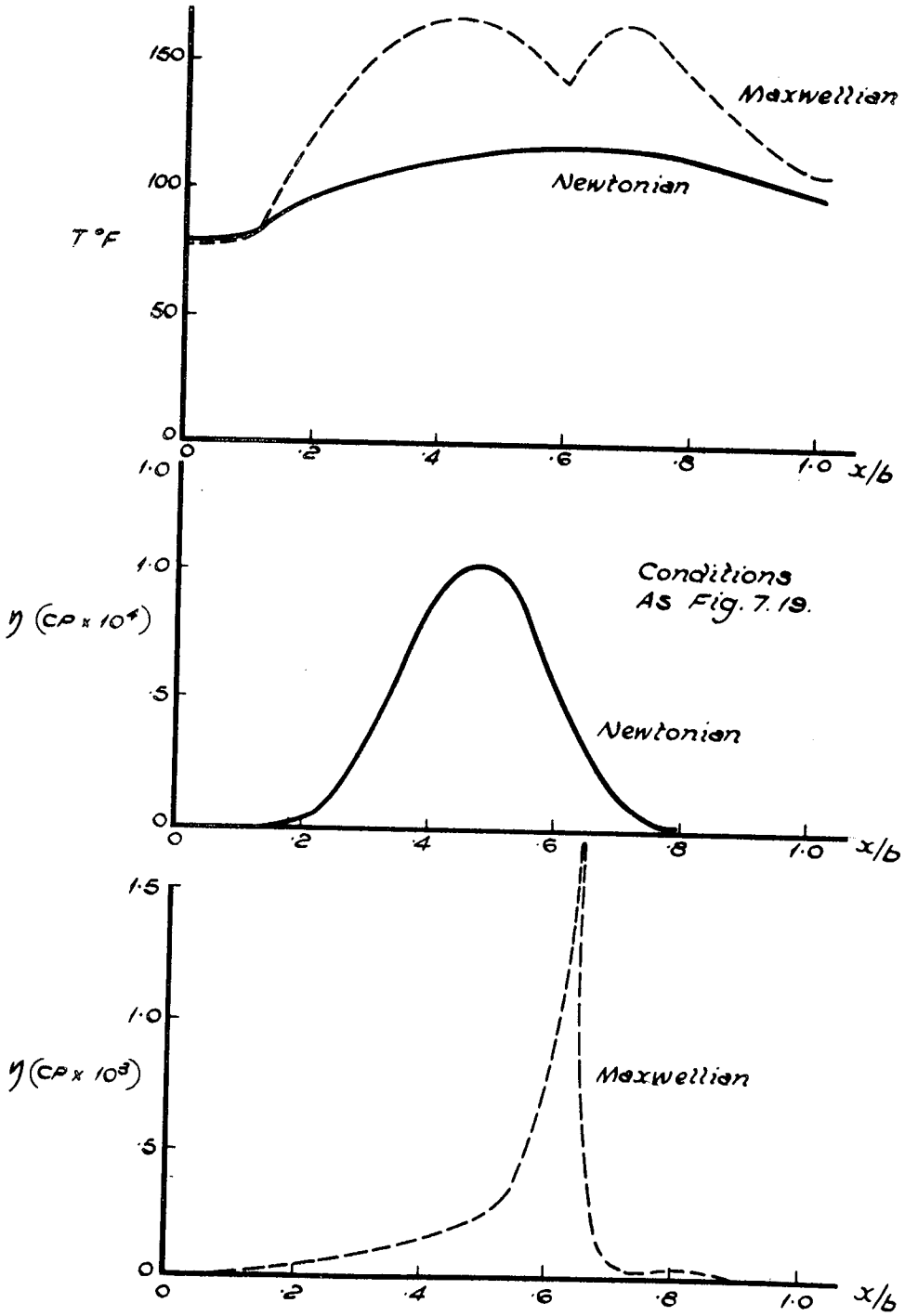

FIG. 7.20.(a) TEMPERATURE AND VISCOSITY DISTRIBUTIONS AT FILM EDGE FOR NEWTONIAN AND MAXWELLIAN FLUIDS.

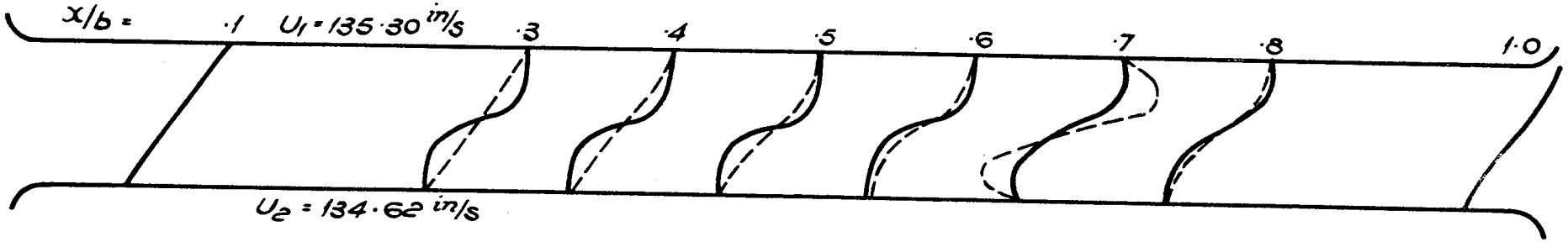

Conditions as Fig. 7.19.

——— Newtonian
– – – – Maxwellian

FIG 7.20(b) VELOCITY PROFILES THROUGH CONTACT FOR NEWTONIAN AND MAXWELLIAN FLUIDS.

$\frac{U_1 + U_2}{2}$ = 400 cm/Sec. ; η Inlet = ·4 P OM 100 Oil 3 ins. Dia. Discs. (·75" Wide)

$T_B \simeq 60°C$.

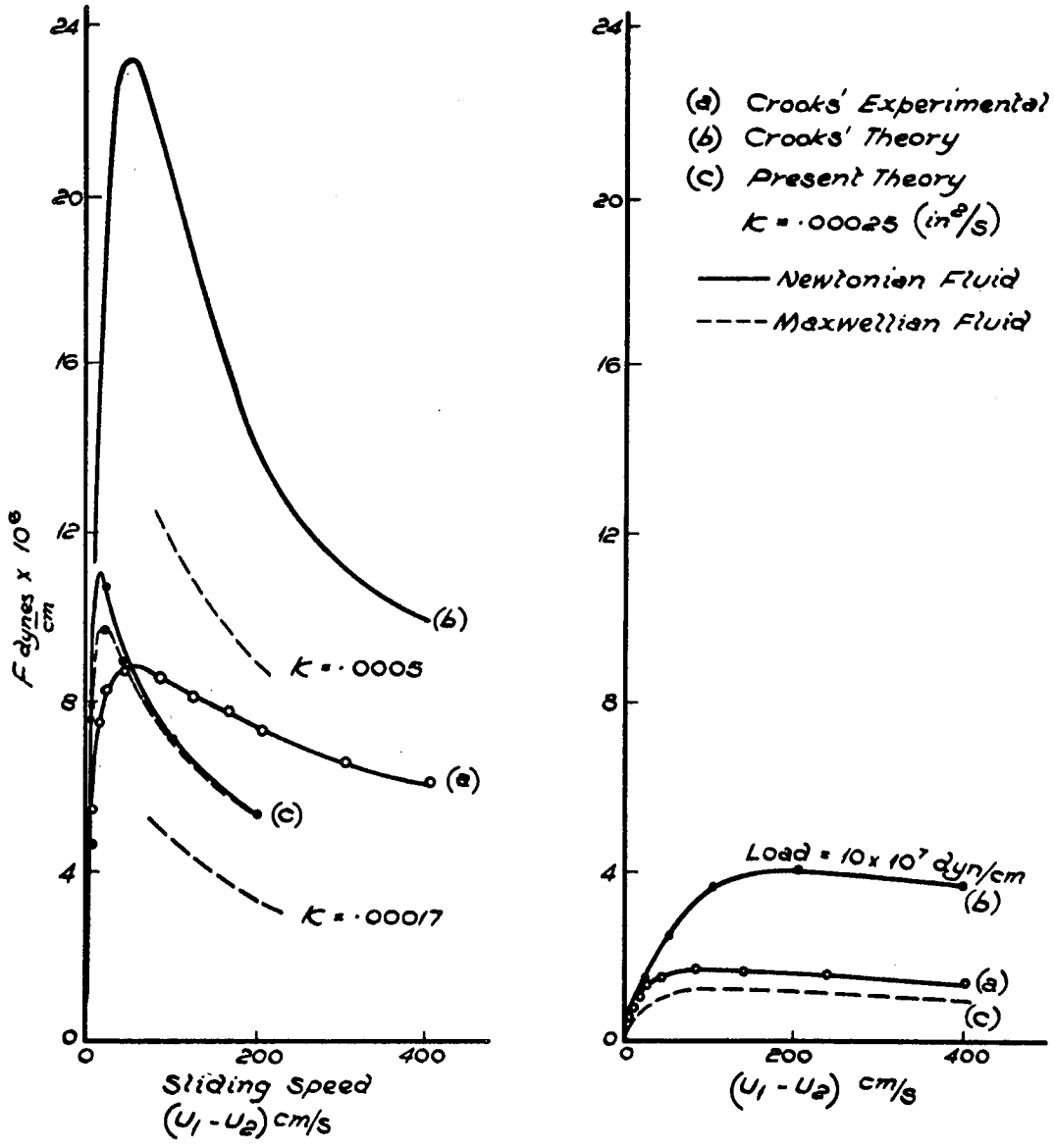

(a) Load = 20 x 10^7 dyn/cm. (b) Load = 7·5 x 10^7 dyn/cm.

FIG. 7.21. COMPARISON WITH CROOKS' THEORY AND EXPERIMENT.

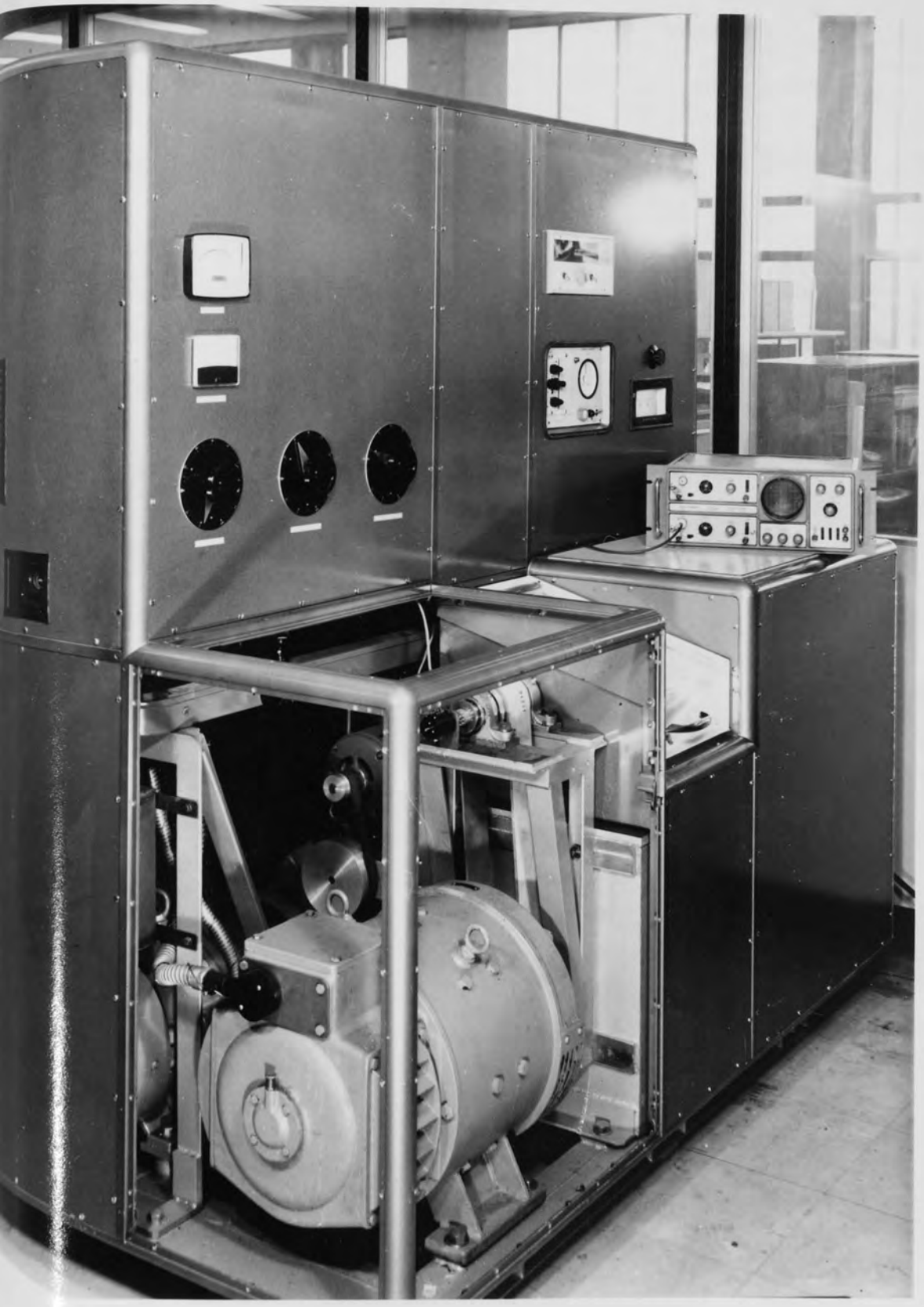

Fig. 7.22 The traction machine

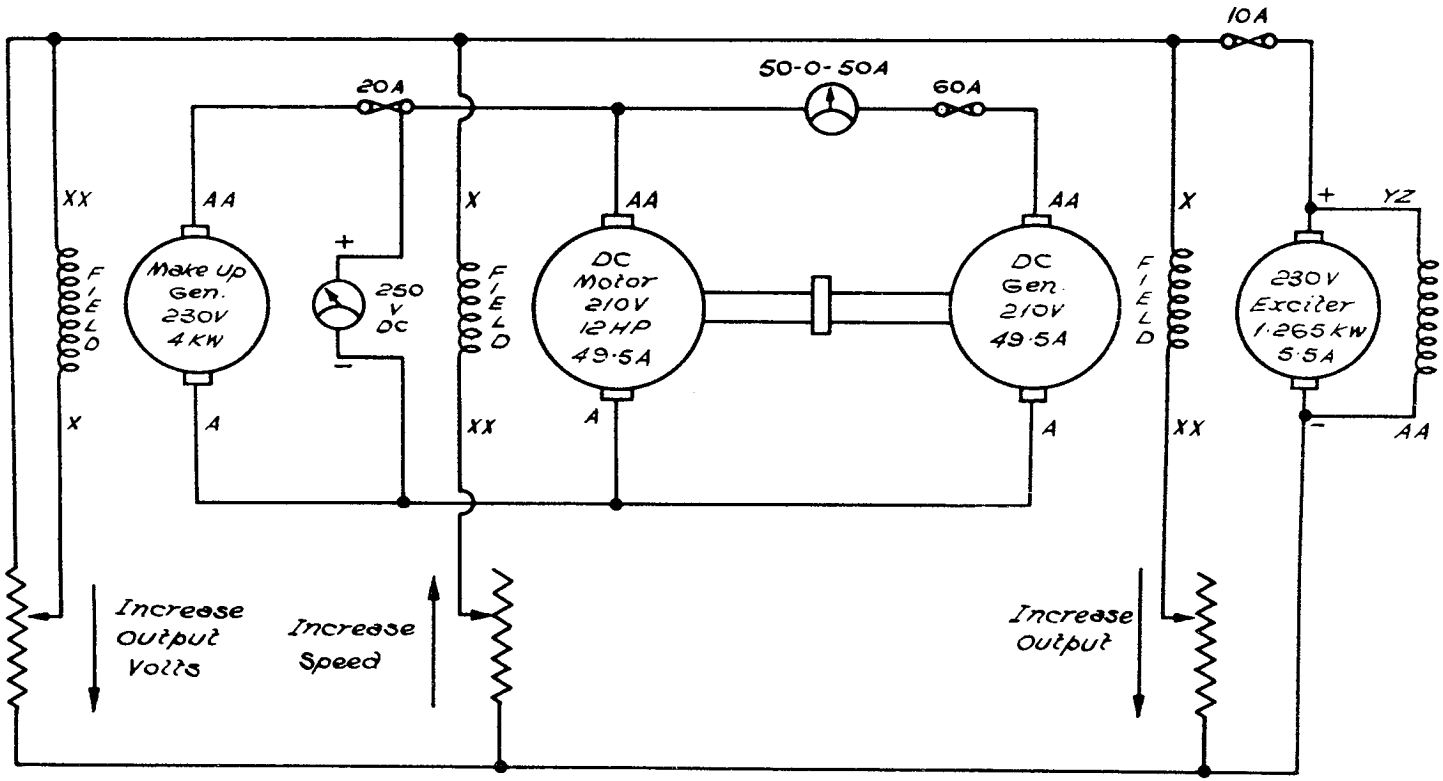

FIG 7.23. CIRCUIT DIAGRAM FOR WIRING OF TRACTION MACHINE.

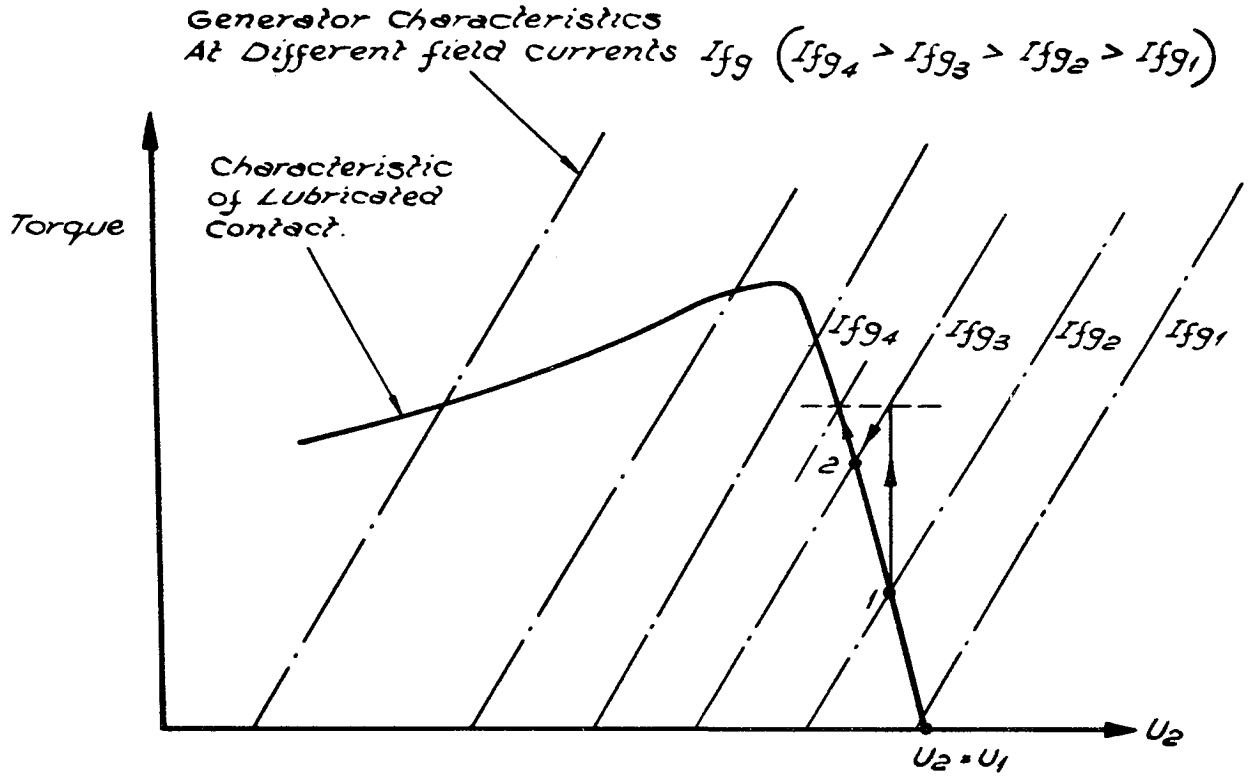

FIG. 7.24. OPERATING CONDITION OF GENERATOR.

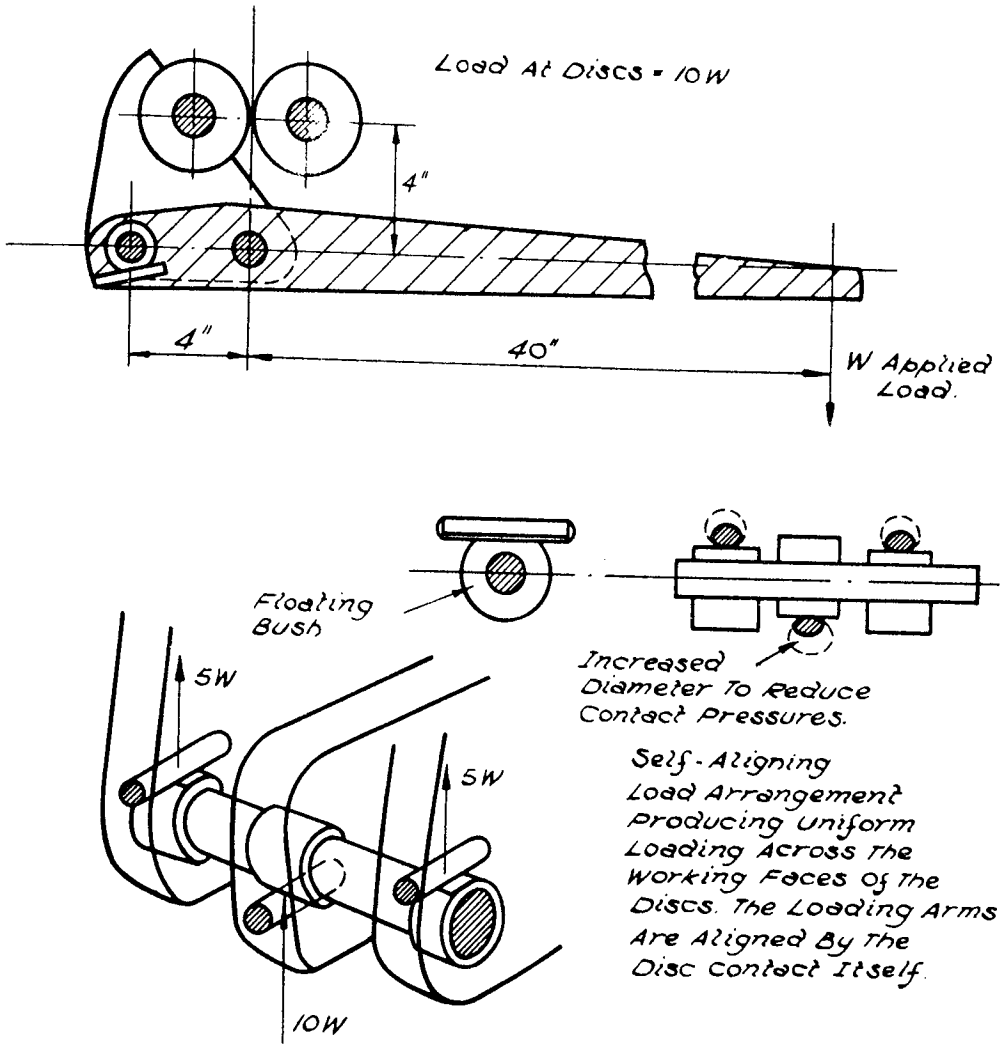

FIG. 7.25. LOADING ARRANGEMENT OF TRACTION MACHINE.

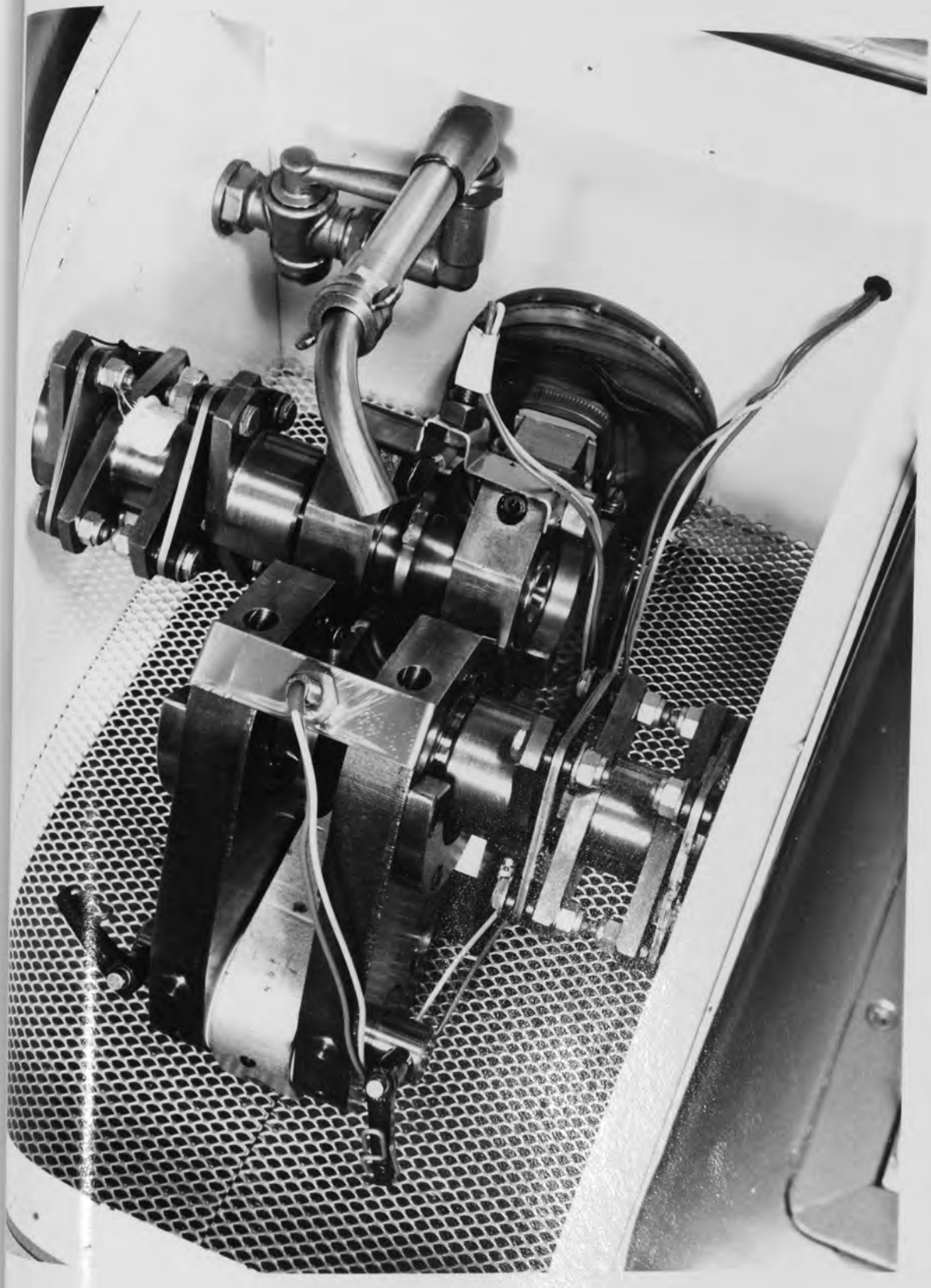

Fig. 7.26 The disc compartment of the traction machine

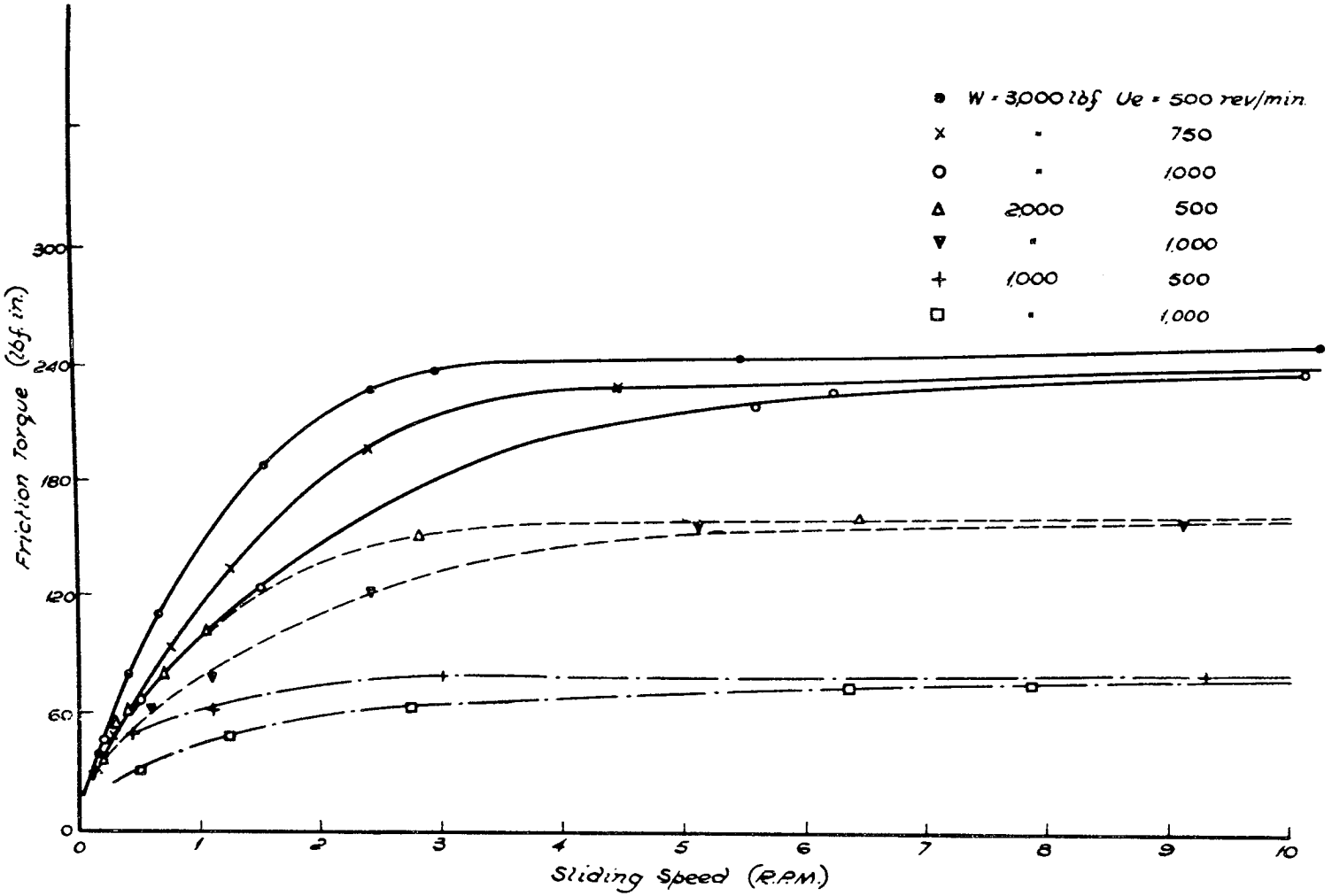

FIG. 7.27. INITIAL FRICTION TORQUE AGAINST SLIDING SPEED RESULTS FOR OIL I.

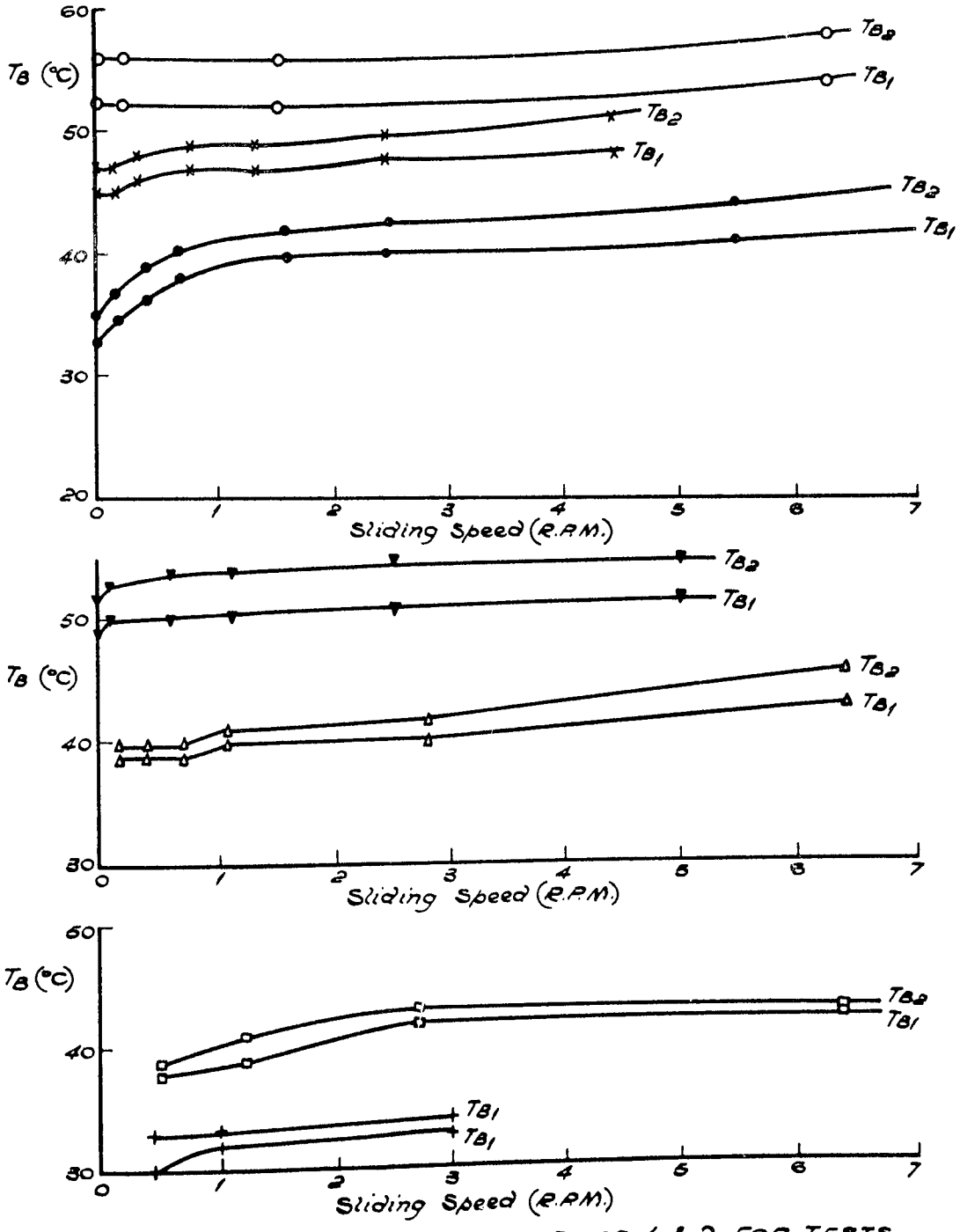

FIG. 7.28. BLANK TEMPERATURES OF DISCS 1 & 2 FOR TESTS ON OIL I. (Symbols same as in FIG 7.27)

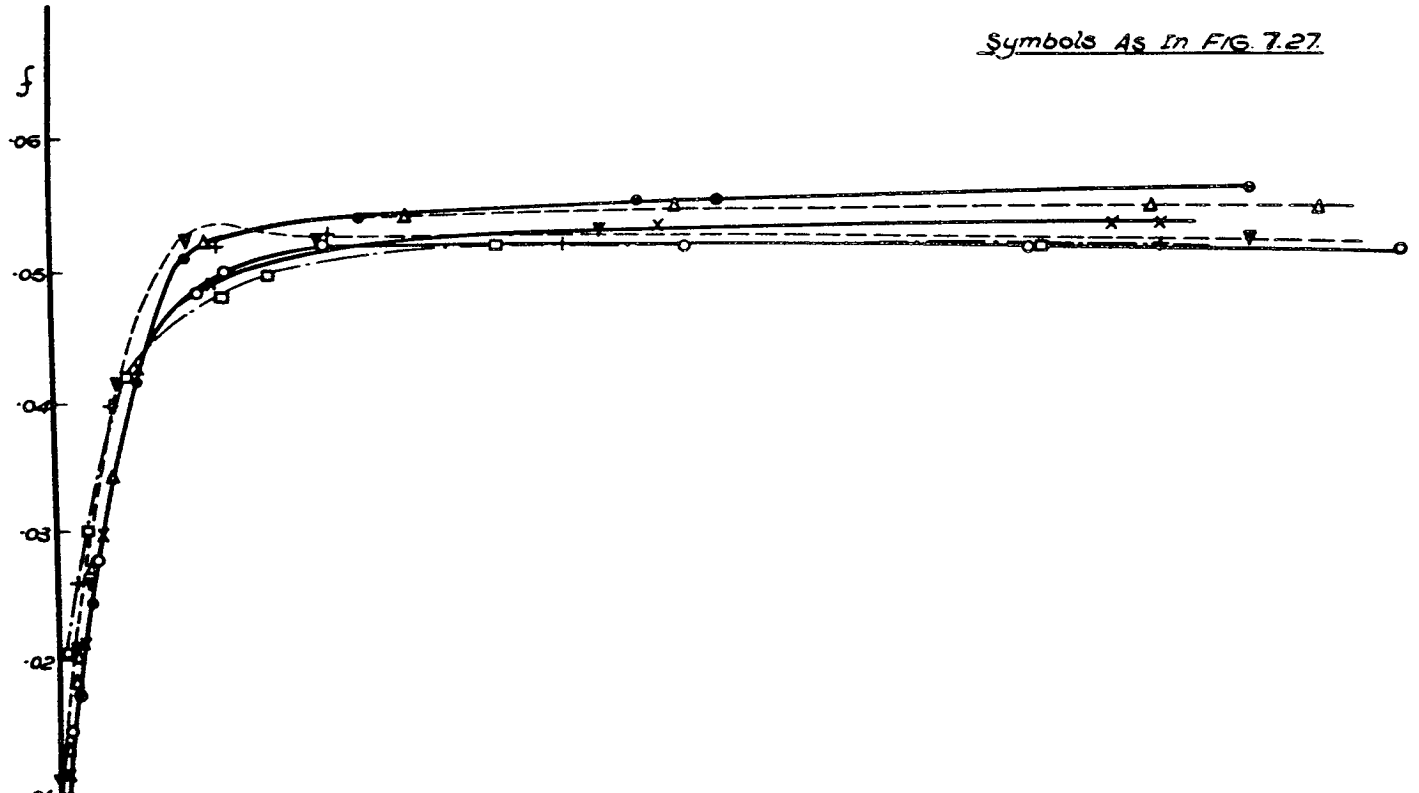

FIG. 7.29. COEFFICIENT OF FRICTION AGAINST SLIP FOR OIL I.

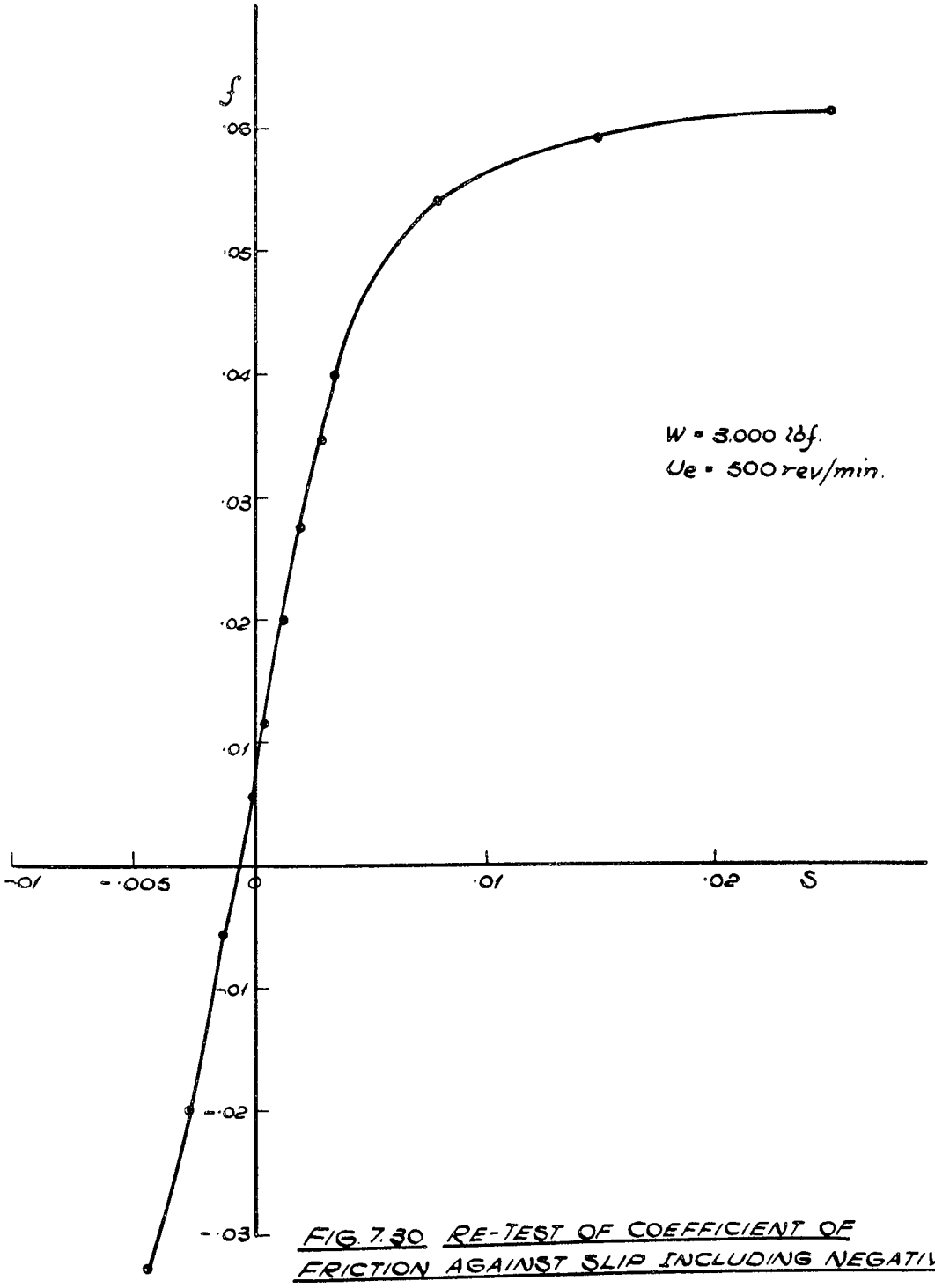

FIG. 7.30 RE-TEST OF COEFFICIENT OF FRICTION AGAINST SLIP INCLUDING NEGATIVE SLIP FOR OIL I.

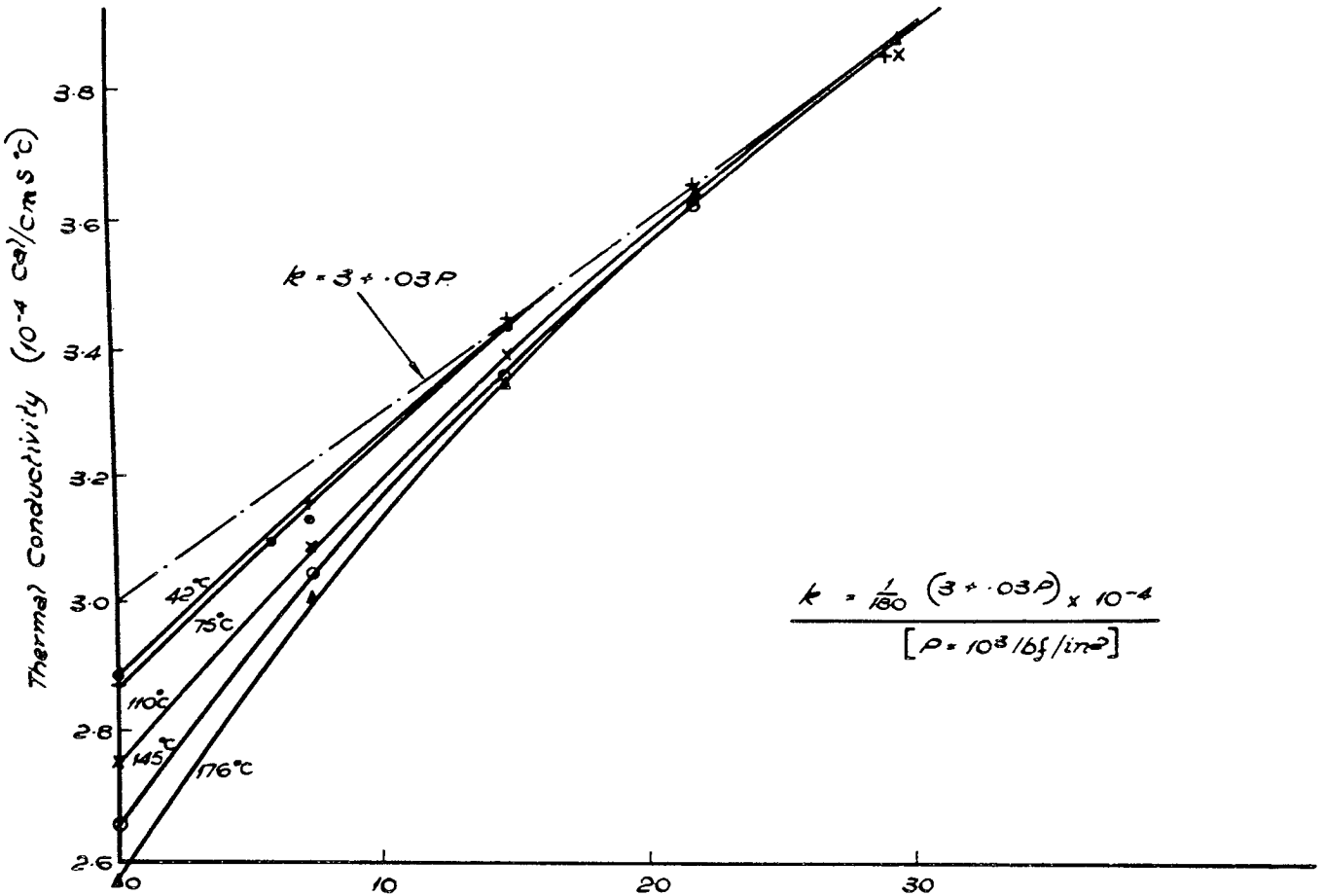

FIG. 7.31. THERMAL CONDUCTIVITY OF OIL II - THE TEST LUBRICANT.

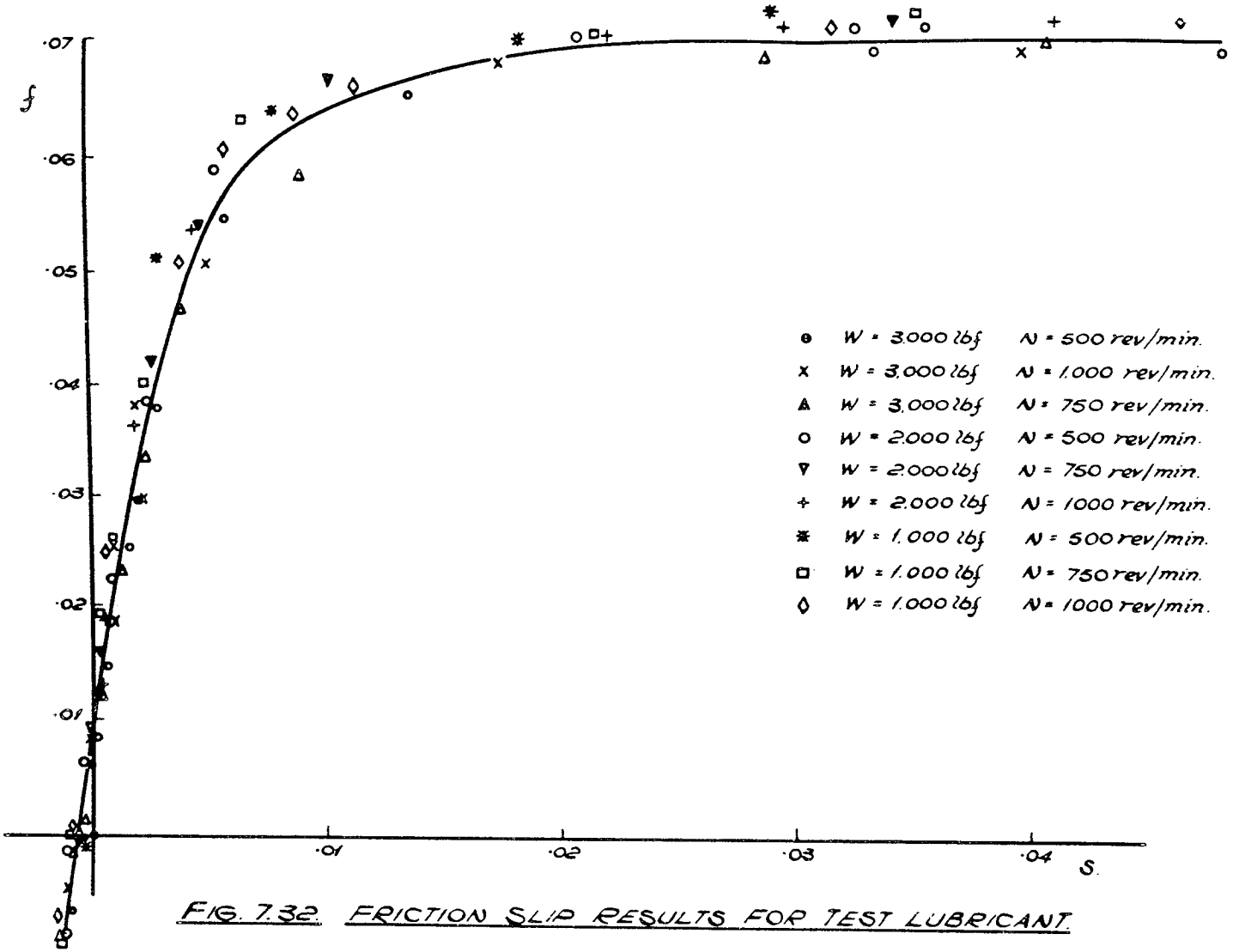

FIG. 7.32. FRICTION SLIP RESULTS FOR TEST LUBRICANT.

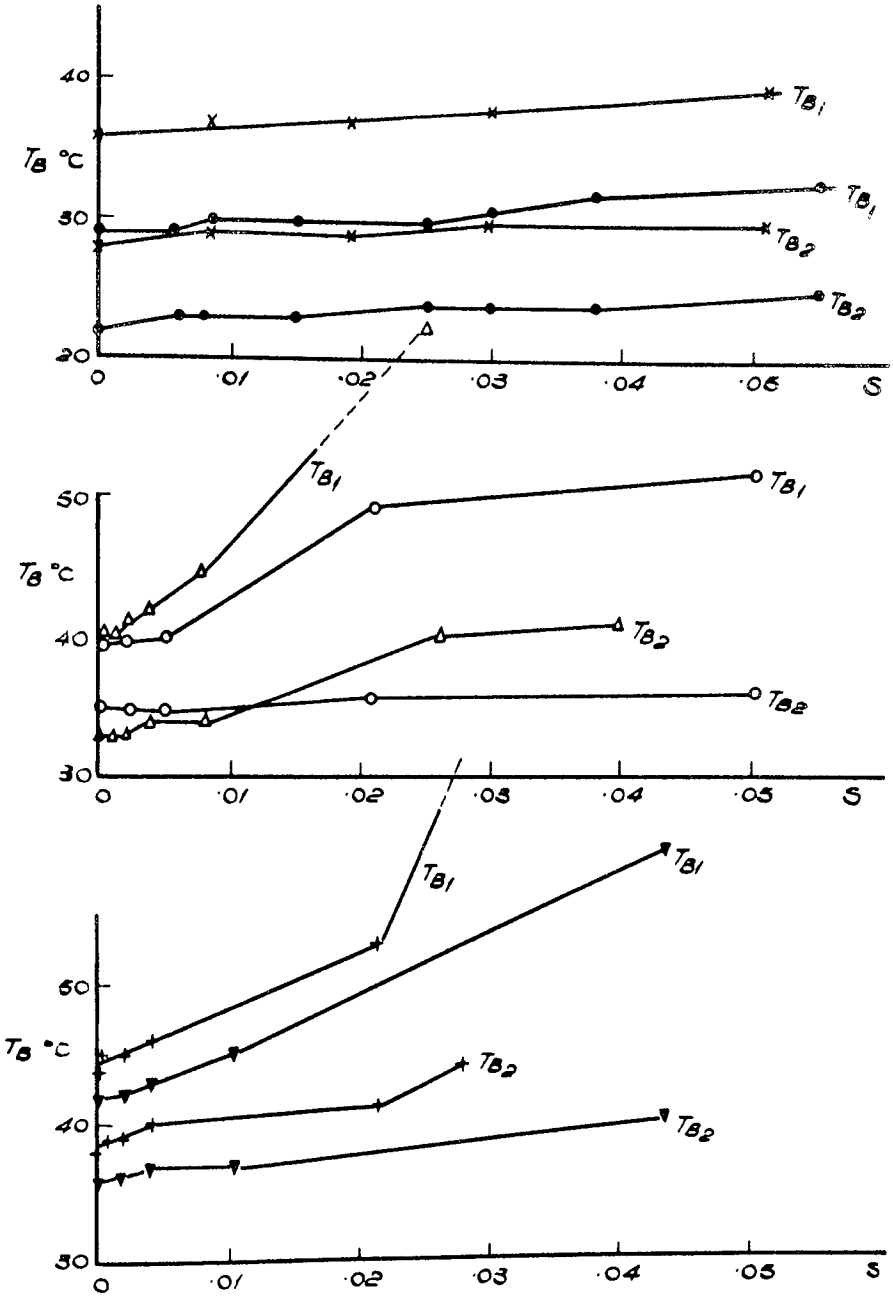

FIG. 7.33.(a) BLANK TEMPERATURE READINGS FOR TESTS IN FIG. 7.32.

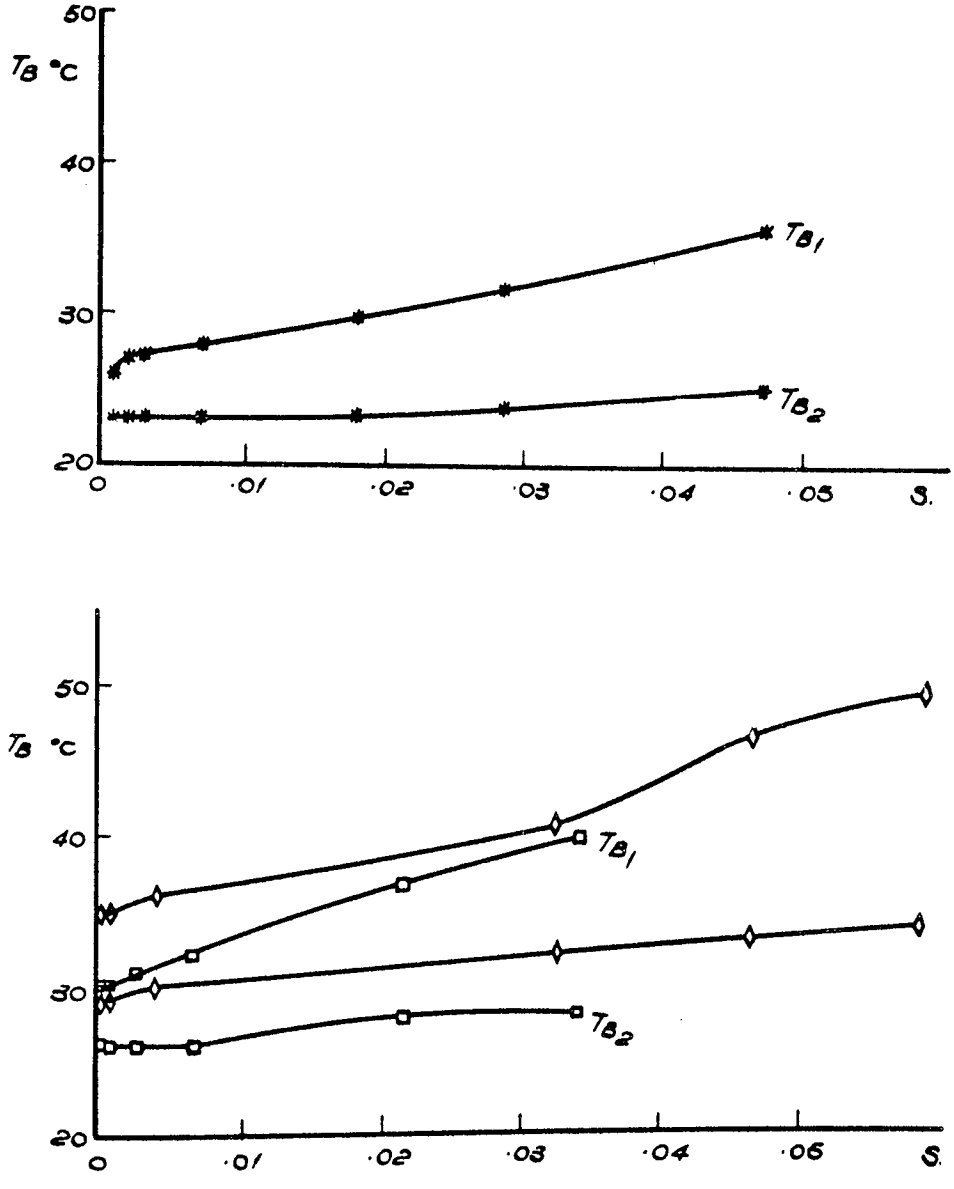

FIG. 7.33 (b) BLANK TEMPERATURE READINGS FOR TESTS IN FIG. 7.32

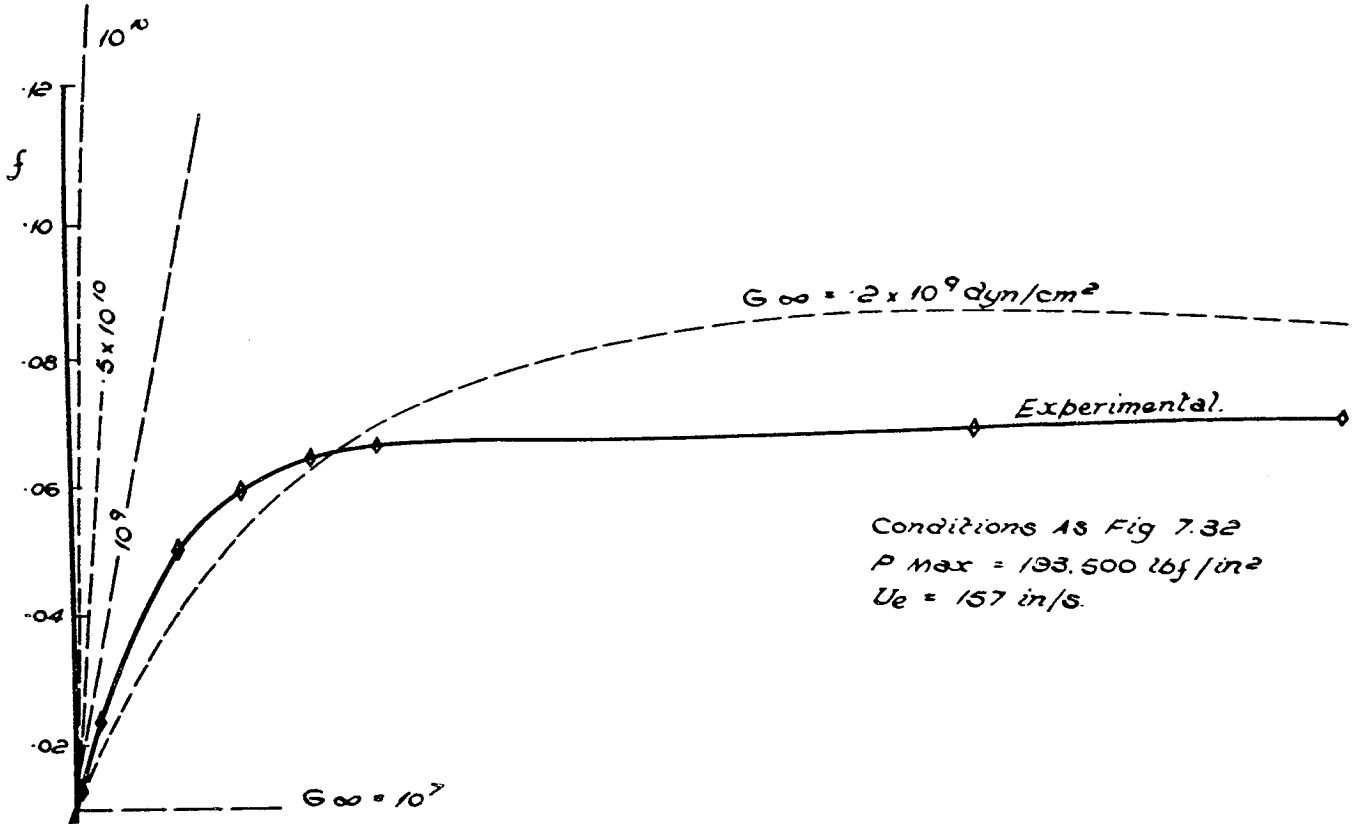

FIG. 7.34 PREDICTIONS OF FRICTION — SLIP CHARACTERISTICS.

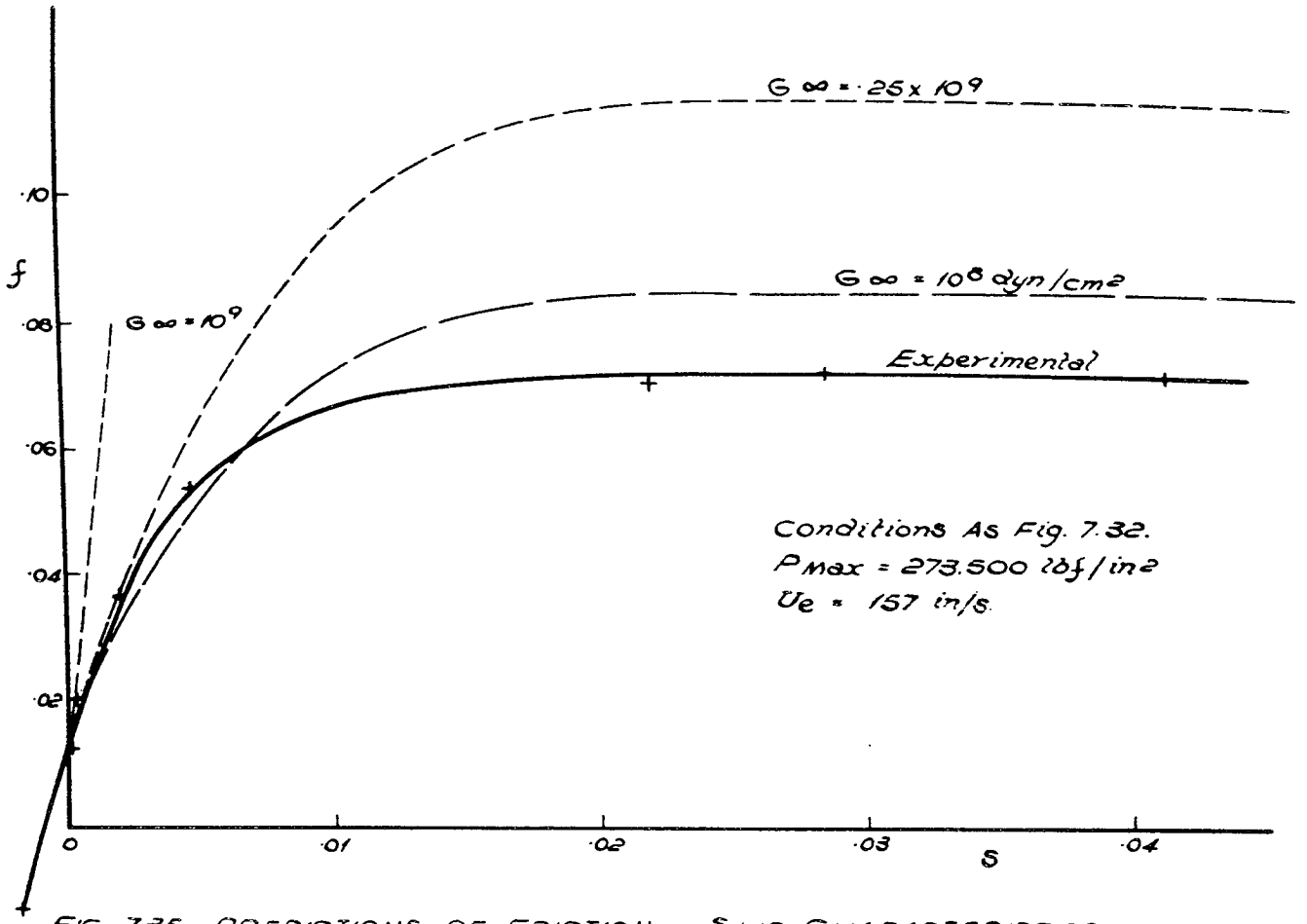

FIG. 7.35 PREDICTIONS OF FRICTION - SLIP CHARACTERISTICS.

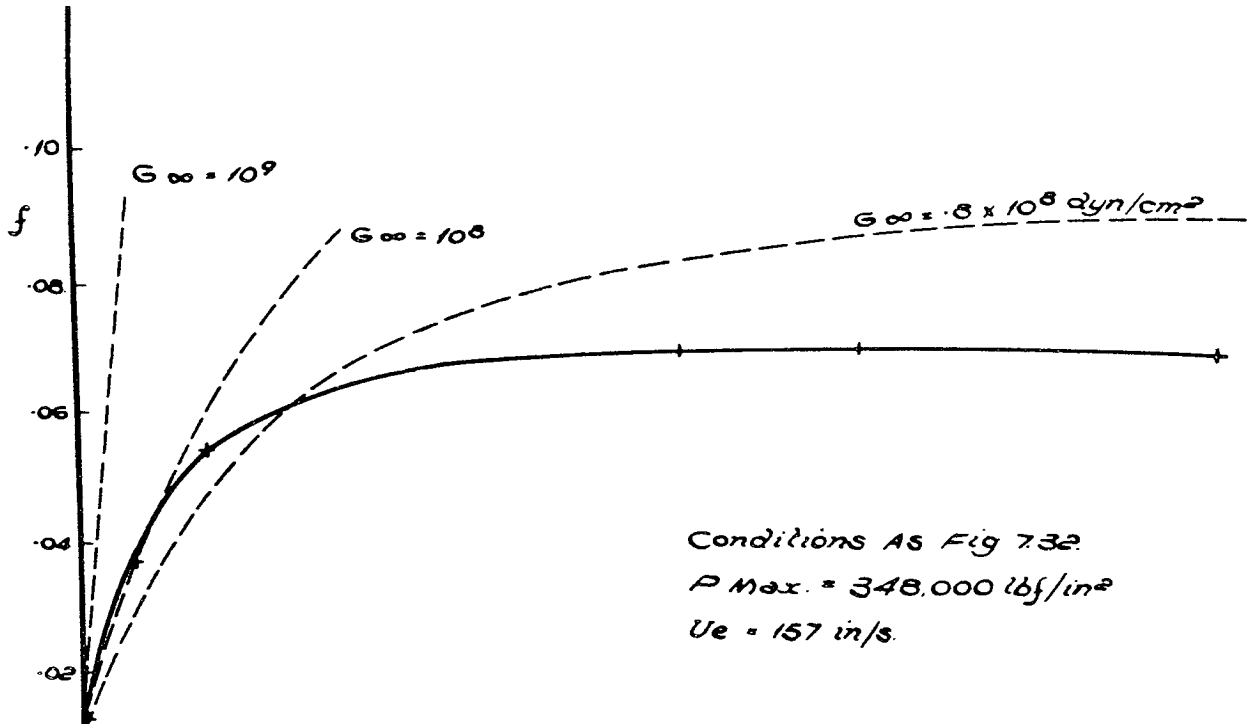

FIG. 7.36. PREDICTIONS OF FRICTION-SLIP CHARACTERISTICS

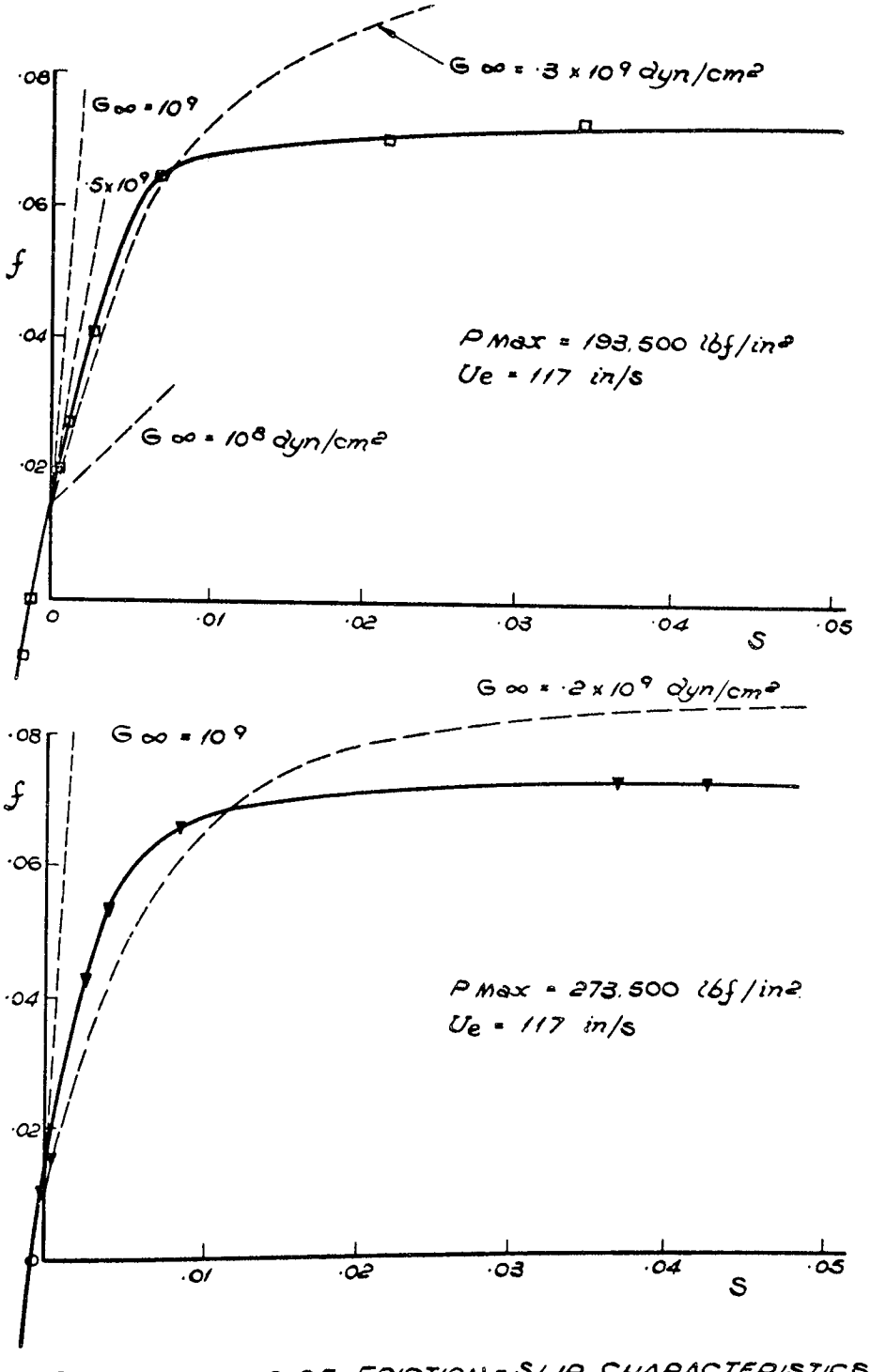

FIG. 7.37 PREDICTIONS OF FRICTION - SLIP CHARACTERISTICS

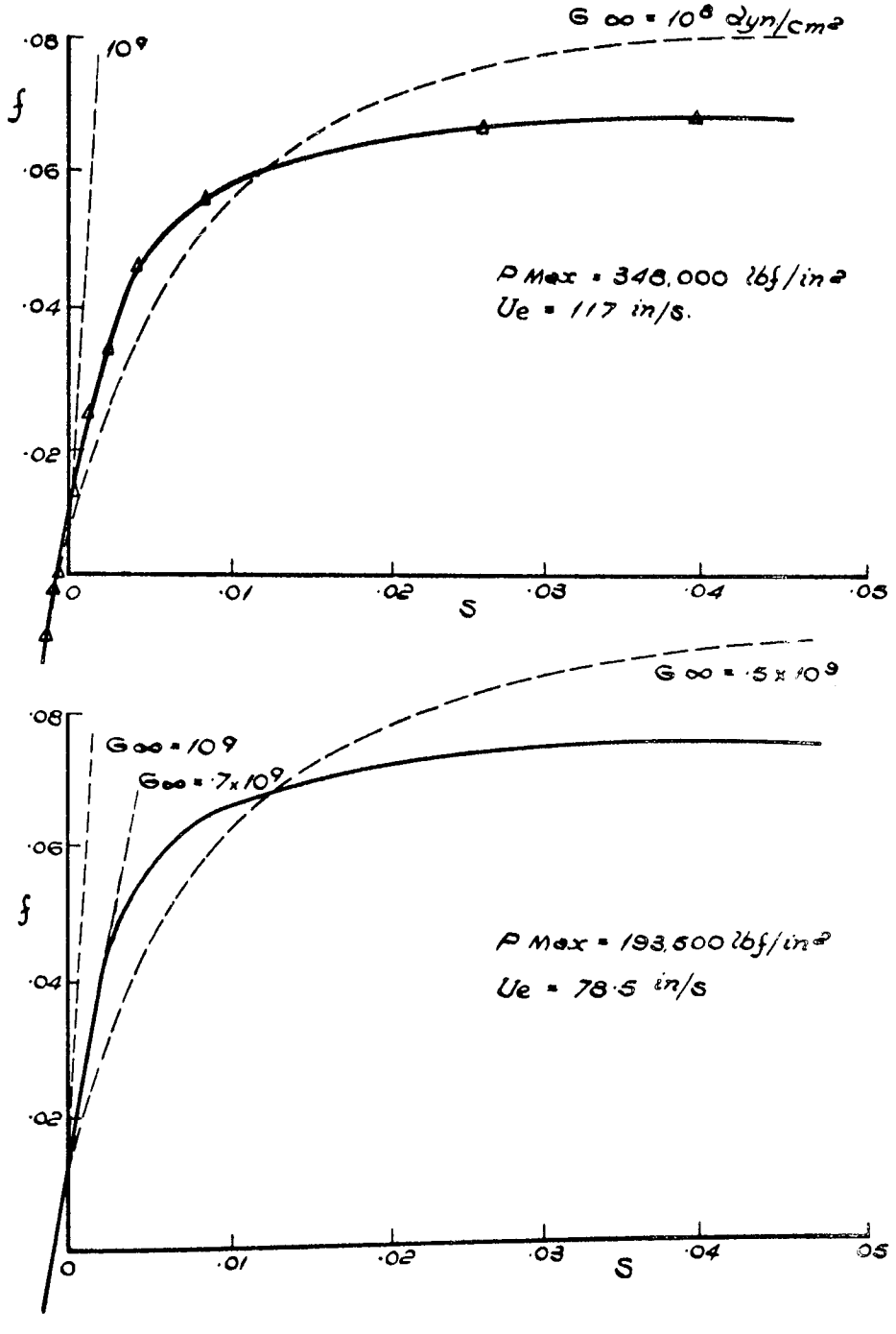

FIG. 7.38 PREDICTIONS OF FRICTION-SLIP CHARACTERISTICS.

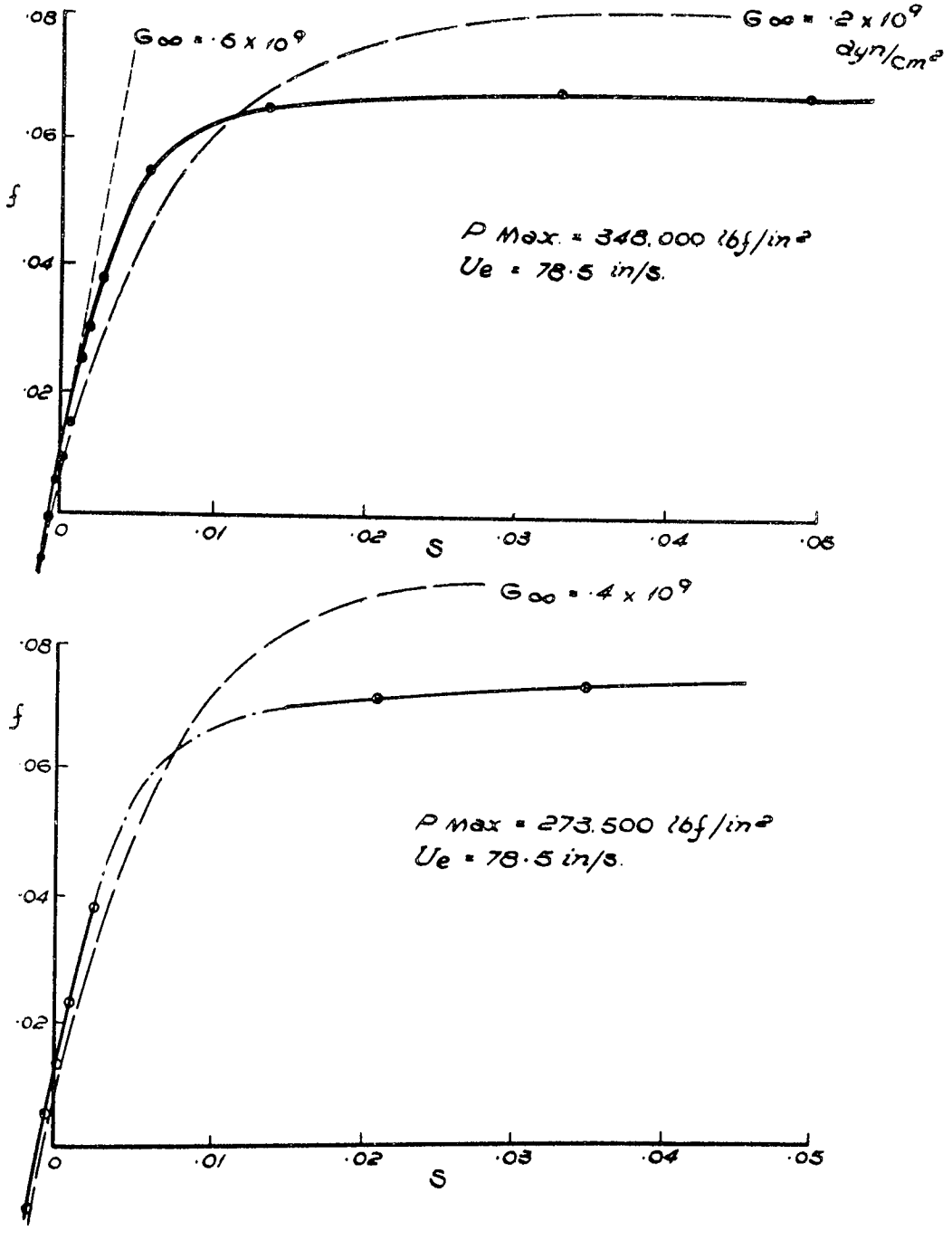

FIG. 7.39 PREDICTIONS OF FRICTION - SLIP CHARACTERISTICS.

8.0 GENERAL DISCUSSION

The various parameters affecting the thermal and frictional characteristics of lubricated rolling/sliding contacts have been investigated. From an analysis of the behaviour of the lubricant entrained between the contacting bodies, a complete description of the temperature, viscosity and shear stress field has been made available against which the experimental data relating to the failure of these contacts may be compared.

Once the contact conditions have been established, it has been shown that the physical properties of the lubricant play an important role in the magnitude of the temperatures reached within the contact. The numerical treatment is quite suitable for the introduction of any known relationships between the properties of the lubricant and these should be included wherever possible. It is also advisable to employ the full pressure profiles and film shapes of the contact if these are known. Generally they are not and the expressions quoted in this thesis are quite adequate, particularly for heavily-loaded conditions where the full elasto-hydrodynamic profiles have been shown to approach very closely those of dry contacts.

Thus by selecting the parameters describing the conditions and geometry of the contact and collecting as much information about the lubricant as possible, the gear designer is provided with a method of calculating the temperature in a particular application. There is a limitation to the use of the technique, and this is the need for prior knowledge of the inlet temperature of the surfaces to the contact. This temperature is given by the operating temperature of the machine components, and has been defined in this thesis as the blank temperature.

The blank temperature depends upon the geometry of the

installation and such factors as whether or not the gears are mounted in an enclosure or lubricated by splash-jet. Chapter five gathered together a range of empirical expressions for the heat transfer coefficients from cylinders and discs that may be relevant to the problem and extended these to consider the effect of enclosures. The results were correlated in terms of a self-induced crossflow but further work will be necessary to relate the crossflow velocity to the enclosure size, so that the established expressions for heat transfer with crossflow may be used in these instances.

Actual measurements of blank temperature showed that for gears lubricated by splash-jet, most of the heat was carried away by the oil flowing over the surfaces. Subsequent analysis of the results indicated a method by which the effective heat transfer coefficients under these conditions might be assessed and provided as design data.

The limitation in the use of the thermal theory may consequently be overcome, if the effective heat transfer coefficient is known. It is necessary to carry out a re-iterative process of calculation whereby blank temperatures are initially assumed for each of the contacting bodies. The theory then not only calculates the resulting total temperatures in the contact but also the heat conduction to each of the bodies. No results for actual heat flow into the surfaces are given in this thesis but are simply obtained by the product of the thermal capacities of the elements in the metal and their respective temperature rises from the computer print-out sheet. At this point, it is important to recall the asymmetry of the temperature profiles across the film and their dependence upon the physical properties of the lubricant. The heat sharing between the metal bodies will be significantly

influenced by this asymmetry and the need for accurate expressions of the lubricant properties must be emphasised.

The next stage of the numerical process involves the calculation of new blank temperatures. These are derived directly from the heat injected into the metal component and the effective heat transfer coefficient losing the heat to the surroundings. The new values of inlet temperature are then re-introduced into the calculation of total contact temperature and the process repeated until eventually a consistent value for blank temperature is obtained.

The result will apply to the conditions of steady operation, where the heat lost to the surroundings equals the heat injected at the contact. The transient condition in which the heat input is greater than that lost, and the blank temperature is rising should also be possible but is of little practical significance except where short periods of operation are envisaged.

With the full temperature distribution at the contact so obtained, the possibility of failure by scuffing of a pair of gears for example, may be assessed. It has for some time been indicated that gears scuff when a particular temperature is attained within the contact. Most of the evidence has been obtained by large scale gear and disc tests but the work on boundary lubrication has lead to a theory based upon the transition temperatures at which metal soaps attached to the metal surfaces are softened and removed to expose the clean metal beneath.

As the loads and speeds of operation of gears and discs are increased, the maximum temperature reached by the surfaces in the contact, defined as the total contact temperature also increases. When this temperature reaches the transition temperature of the metal soaps formed by the adsorption of the

naturally occurring surfactant compounds found to exist in mineral oils, then desorption or "softening" of the protective surface layer occurs. Contact between the metallic surfaces is then possible, either by chance contact with debris carried by the oil and bridging the film thickness or by high asperities piercing the oil film. The progressive welding and tearing of the surfaces then results in failure by scuffing, where the original surface profiles are destroyed and a severe increase in friction is observed.

The temperature at which scuffing is initiated has been defined as a property of the lubricant and called the critical temperature. The experiments in Chapter three of this thesis have shown that critical temperatures cannot be related to viscosity as this is no direct indication of the nature of the surface active compounds present in the oil. A short and simple technique has been developed in the present work for the direct measurement of critical temperatures. The equipment necessitated the use of stainless steel specimens to avoid the chemical reaction effects observed with other steels at the sustained high temperatures of the machine. The results gave good agreement with a series of gear and disc tests. A worthwhile excercise however would be to reduce the "soak" time of the apparatus, by reducing the volume of lubricant to be heated or to arrange for removal of the deposited layer by mechanical means. Further experiments could then be attempted using a range of gear steels.

The proposed technique is ideal for the industrial rating of oils, and provides the designer with a figure of merit by which to assess the lubricant.

Against this additional data for the lubricant, may be compared the total temperature reached by a pair of gear teeth

in mesh. To avoid failure by scuffing, the total contact temperature would have to be lower than the quoted critical temperature of the lubricant to be used or conversely a lubricant would have to be selected that possessed a critical temperature greater than the predicted total temperature of the contact.

It is conceivable, that when lubricant properties are established and heat transfer coefficients more thoroughly documented than the above trial and error process could be programmed onto a computer to provide a rapid selection procedure for gear lubricants.

The discussion has so far concentrated on the lubricated rolling/sliding contacts occurring in gear teeth. A further example of these contacts is found between the discs and rollers of friction drives. Various designs are commercially available, but all rely on the transmission of torque from one cylindrical or spherical member to another in the presence of a lubricant.

It has been possible by extending the thermal theory developed in this thesis, to study the frictional characteristics of lubricated contacts. The predicted relationships between traction (or friction coefficient) and sliding speed (or slip) agree in general with previous analytical solutions and exhibit the same overestimation of the coefficients of friction at low slip. All theories to date are based upon the assumption that the lubricant behaves as a Newtonian fluid. With the recent evidence to suggest that lubricants possess non-Newtonian characteristics that in some instances resemble the Maxwellian fluid, it is important that an attempt be made to include this effect in the solutions of the traction problem.

Measured values of the shear modulus of elasticity are available from oscillatory tests but their applicability to the

continuous shear situation is not clear. The exact viscoelastic model of a lubricant is anticipated to be more complex than the simple Maxwell element but as a first approximation the latter has been introduced into the numerical analysis of traction presented in Chapter seven.

The solution was applied to the contact conditions obtained by an experimental rig specially constructed to measure the transmission provided by a lubricant of known physical properties. These included the thermal conductivity of the oil over a range of pressures and temperatures, which in a preliminary analysis had been found a significant parameter in determining the magnitude of the traction. By comparing the predicted and actual friction-slip relationships, the value of the shear modulus was adjusted to provide the best correlation. The values of G_∞ so obtained were within the range quoted by other authors from different experiments.

When further details of the viscoelastic properties of lubricants become available and more exact models of the fluid element are developed then the present solution may be adapted to include these. More accurate analysis of friction drive performance will then be possible, pointing the way to improved transmission fluids with higher torque transmission and reduced heat dissipation. For the present however, solutions of the type given in this thesis assist the engineer in assessing suitable design changes to improve the performance of the friction drive unit.

A by-product of the friction analysis is the shear stress distribution through the contact zone. The results for Newtonian and Maxwellian fluids differed considerably but both provided surface shear loading distributions not previously determined. The nature of the surface loading at the contact is the key factor

in determining the stress field in the subsurface material of the contacting bodies and has an important effect upon the life to pitting of rolling elements. The shear stress results obtained here could therefore be introduced into an examination of the stress distribution of rolling elements and so contribute to the understanding of failure by pitting.

9.0 CONCLUSIONS

From a series of scuffing tests on gears and discs, agreement has been obtained between the calculated scuffing temperatures and the critical temperature of the lubricant measured directly on the proposed two-disc machine. The simplicity of the apparatus and short period of each test makes the technique suitable for the industrial rating of lubricants, it having been shown that other properties of the lubricant, such as the viscosity, do not necessarily give an indication of the critical temperature.

The relationship between blank temperature and heat transfer coefficient has been investigated by temperature measurements on actual gears and discs. This has resulted in the proposal of a method for assessing the heat transfer coefficients of particular machine installations whatever the method of lubricant application employed. Further to this, the well established expressions for convective heat transfer to surrounding homogeneous fluids have been extended to examine the effect of enclosures and the presence of a self-induced crossflow has been detected.

The thermal analysis of the lubricant film at rolling/sliding contacts presented in this thesis has demonstrated the important roles played by the physical properties of the lubricant in determining the heat sharing between the metal surfaces and maximum contact temperatures attained at the metal-oil interfaces. An asymmetry in the heat generation across the oil-film has been discovered and attributed to the relative blank temperatures of the two surfaces and is observed to be affected by the second coefficient of viscosity, λ .

Predictions of total contact temperature, which are

more accurate than those obtained by the Blok equation, therefore require a precise knowledge of the lubricants physical properties.

The same analysis has been used to calculate the effective coefficients of friction at rolling/sliding contacts Previous analytical and numerical solutions have all assumed Newtonian behaviour of the fluid as it passes through the contact but by the introduction of the Maxwell fluid model into the analysis, the present work has shown that the agreement between theoretical and measured friction is far better than previously obtained.

Shear stress distributions within the contact have been obtained for both Newtonian and Maxwellian fluids and differ considerably from the usual assumptions of a semi-elliptic or parabolic distribution. A double-rise profile is found, the first rise producing a sharp "peak" in shear stress at inlet to the contact with a Newtonian fluid. The latter results are of particular relevance to the study of contact stresses and their relation to pitting.

Appendix I

Viscosities of lubricants

	Viscosity, cS	
	21°C	60°C
*SAE 10 plain mineral oil	.90	17
*SAE 30	400	45
*SAE 90	1100	80
*650 Brightstock	2500	160
Ali & Thomas 'B'	335.8	34.9
Ali & Thomas 'C'	158	28.5
OIL I plain mineral oil	1743	147
	100°F	210°F
OIL II MVI mineral oil:*	33.52	4.77

Specific Gravity

@ 30°C .875

@ 100°C .833

* Supplied by Shell Petroleum Ltd

Thornton Research Centre

Appendix II

The calculation of critical temperature from the friction-temperature trace of the two-disc critical temperature machine

For the SAE 30 plain mineral oil Fig. 13, the following applies:-

On trace, time scale = 2 minutes per division
and 1 mV represented by 1 large division
(equal to 10 small divisions).

∴ Mean torque before rise = .90 mV

Calibration of torque tube is 8.75 lbf.in per mV.

∴ torque = 7.86 lbf.in.

friction force at 1.25 in radius = 6.28 lbf.

shared equally between discs.

Load on machine arm = 5 lbf.

Load at discs = 3.5 x 5 = 17.5 lbf.

∴ Coeff. of friction = .18

Blok flash temperature equation is:-

$$Tf = \frac{1.11\ f.\ w\ (U_1^{\frac{1}{2}} - U_2^{\frac{1}{2}})}{K\ b^{\frac{1}{2}}}\ {}^{o}F$$

when K = 42.2 lbf.in.s. units

b = Hertzian width contact

$$= 3.04 \sqrt{\frac{w\ R_N}{E}}$$

w = load/unit width

$$= \frac{3.5 \times 5}{3/16}\ \text{lbf./in}$$

= 94 lbf /in

$$R_N = \frac{1.25 \times 1.25}{1.25 + 1.25} = \frac{5}{8} \text{ in.} \quad \therefore \quad b = 4.25 \times 10^{-3} \text{ in}$$

With $N = 26$ rev/min, $U_1 = -U_2 = \frac{\pi DN}{60}$ in/s $= 3.4$ in/S

Rewriting the Blok flash temperature equation in the form:

$$Tf = \frac{1.11 \, f. \, w \, (U_1 - U_2)}{K \, b^{\frac{1}{2}} \, (U_1^{\frac{1}{2}} + U_2^{\frac{1}{2}})}$$

The surfaces of the two discs move at the same velocities past the contact zone, but in opposite directions. This implies that the heat input to the discs due to the friction at the contact will be equally shared as well as the flash temperature being equal.

The $(U_1 - U_2)$ term enters the above equation as the frictional energy dissipated. Hence the difference will be algebraic and $U_1 - U_2 = 2U_1$.

The $(U_1^{\frac{1}{2}} + U_2^{\frac{1}{2}})$ term however is derived as a result of summing the heat input and will be the numerical sum of the square root velocities.

i.e. $(U_1^{\frac{1}{2}} + U_2^{\frac{1}{2}}) = 2U_1^{\frac{1}{2}}$

These conclusions are drawn from ref. 43.

Hence $Tf = 8.5^{\circ}C$

From trace and thermocouple calibration,

$Tb = 180^{\circ}C$

$\therefore Tc = 180 + 8.5 = 188.5^{\circ}C$

Other results are given in fig. 16.

Appendix III

Test gears - specifications and dimensions

5" P.C.D. 20% pressure angle 30 teeth

Radius of Addendum Circle	2.6665 inches
Radius for tip relief to commence	2.5298 inches
Tip relief	0.6×10^{-3} inches
Radius of pitch circle	2.5000 inches
Radius of lowest active point	2.3912 inches
Radius of base circle	2.3492 inches
Base pitch	0.4920 inches

At tip-root contact point:-

R_1, Instantaneous radius of curvature at tip = 1.2614 inches

R_2, " " " " " root = .4487 inches

$$R_N = \frac{R_1 R_2}{R_1 + R_2} = 0.330$$

U_1, Instantaneous surface speed at tip = 132 in/sec

U_2, " " " " root = 47 in/s

At 1,000 rev/min, Sliding speed = $U_1 - U_2$ = 85 in/s

At 1,000 rev/min, Rolling speed = $\frac{U_1 + U_2}{2}$ = 89.5 in/s

$$\text{Slip} = \frac{U_1 - U_2}{U_1} = .64$$

At pitch point:-

R_1 = .8551 inches R_N = .428

R_2 = .8551 inches $U_1 = U_2$ = 89.5 in/s per 1,000 rev/min

Appendix IV

Steel specifications

Steel	Composition per cent	Hardness V.p.n.
KE 961 High duty die steel	1.5 C ; 12 Cr	700
KE 839 Direct Hardening (En 31) steel	1 C ; 1.5 Cr	700 - 800
S.106 60 ton steel (suitable for nitrogen hardening)	0.25 C : 3 Cr ; 0.5 Mn	750 (case) 300 (core)
S.110 Austenite stainless steel	18 Cr : 8 Ni	

Appendix V

Sample results and calculations of heat transfer quantities

Measured					Calculated				
Q watts	N rev/min	Ts mV	T_{BOX} mV mean	$T_{AMBIENT}$ °C	ΔT °C	Re	Nu	Gr $\times 10^5$	Pr
18.8	0	1.81	.08	24.5	45	0	22.8	3.06	.702
18.8	50	1.81	.1	24.5	45	222	22.8	3.06	.702
18.8	75	1.81	.12	23.8	45.7	334	22.4	3.11	.700
18.8	100	1.81	.14	23.8	46.2	445	22.2	3.14	.700
18.8	160	1.88	.19	23.8	47	710	21.8	3.19	.699
18.8	215	1.86	.20	23.8	46.7	955	21.9	3.17	.700
18.8	280	1.82	.21	24	45	1240	22.8	3.06	.702
18.8	310	1.73	.25	25	42.8	1370	23.9	2.91	.703
18.8	400	1.71	.25	25	42	1780	24.4	2.86	.704
18.8	452	1.67	.25	25	41.3	2020	24.8	2.80	.704
18.8	535	1.62	.25	25	40	2380	25.7	2.72	.704
18.8	570	1.59	.25	25	39.5	2540	26.0	2.68	.705
18.8	595	1.57	.25	25	38.8	2640	26.4	2.64	.705
18.8	694	1.54	.25	25	38	3080	27.0	2.58	.706
18.8	870	1.51	.25	25	37.2	3880	27.5	2.53	.706

$$Gr = \epsilon g \Delta T \frac{D^3 \rho^2}{\mu^2}$$

$$Nu = \frac{Q}{\Delta T \pi D.L} \cdot \frac{D}{k}$$

$$Pr = \frac{Cp\,\mu}{k}$$

$$Re = \frac{\rho \pi D^2 N}{\mu}$$

All properties are those of air calculated at the mean temperature of the surface temperature and air temperature inside the enclosure.

Appendix VI

Calculation of heat transfer coefficients for gears

From the blank temperature results in section 4.0 the heat transfer coefficient for 5" PCD gears at 500 rev/min with 4676 lbf/in load has been determined as 308 (230 by approximate calculation).

Also $q/_{2L}$ = 4,800 BtU/hr.ft^2

$$q/_2 = 4{,}800 \times \frac{.4375 \times \pi \times 5}{144}$$

$$= 227.5 \text{ BtU/hr}$$

where .4375 = width of one row of gear teeth to which hc has been referred.

From the heat transfer in air results of O'Donoghue,

$$Nu = 12\ Re^{\frac{1}{4}} \quad \text{for } 2.5 \times 10^3 < Re < 4.5 \times 10^4$$

In this case $Re = \frac{UD}{\gamma} = \frac{\pi D^2 \times N/60}{.00022 \times 144 \text{ in}^2/\text{s}}$

$$= 2 \times 10^4$$

$$\therefore \quad Nu = 142$$

$$hc = \frac{Nu.k}{D} = \frac{142 \times .000058 \times 12 \times 241.9}{5}$$

$$= 5 \text{ BtU/ft}^2\text{.hr.}^\circ\text{F}$$

Now, $T_B - T_{ambient} = 19.8\ ^\circ\text{F}$

$$\therefore \quad q = \frac{5 \times 1 \times 5\pi}{144} \times 19.8 \text{ BtU/hr}$$

$$q = 10.7 \text{ BtU/hr}$$

when q is the heat lost by convection from the cylindrical surface.

From the heat transfer in air results of Cobb and Saunders

$$Nu = .015\ Re^{0.8}$$

$$= 42$$

$$\therefore \quad hc = 1.48 \text{ BtU/ft}^2\text{.hr.}^\circ\text{F}$$

$\therefore$ At $T_B - T_{ambient} = 19.8^\circ\text{F}$, assuming same surface temperature at side of discs as at working surface,

$$q = 1.48 \times \frac{\pi 5^2}{4} \times \frac{2}{144} \times 19.8 \text{ BtU/hr}$$

$$= 4 \text{ BtU/hr}$$

hc referred to cylindrical surface

$$= 5 \times \frac{(10.7 + 4)}{10.7}$$

$$= 6.5 \text{ BtU/ft}^2\text{.hr.}^\circ\text{F}$$

Appendix VII

Derivation of interface heat conduction equation

Consider an element bonded by the interface of dissimilar materials and subjected to a temperature gradient across it:-

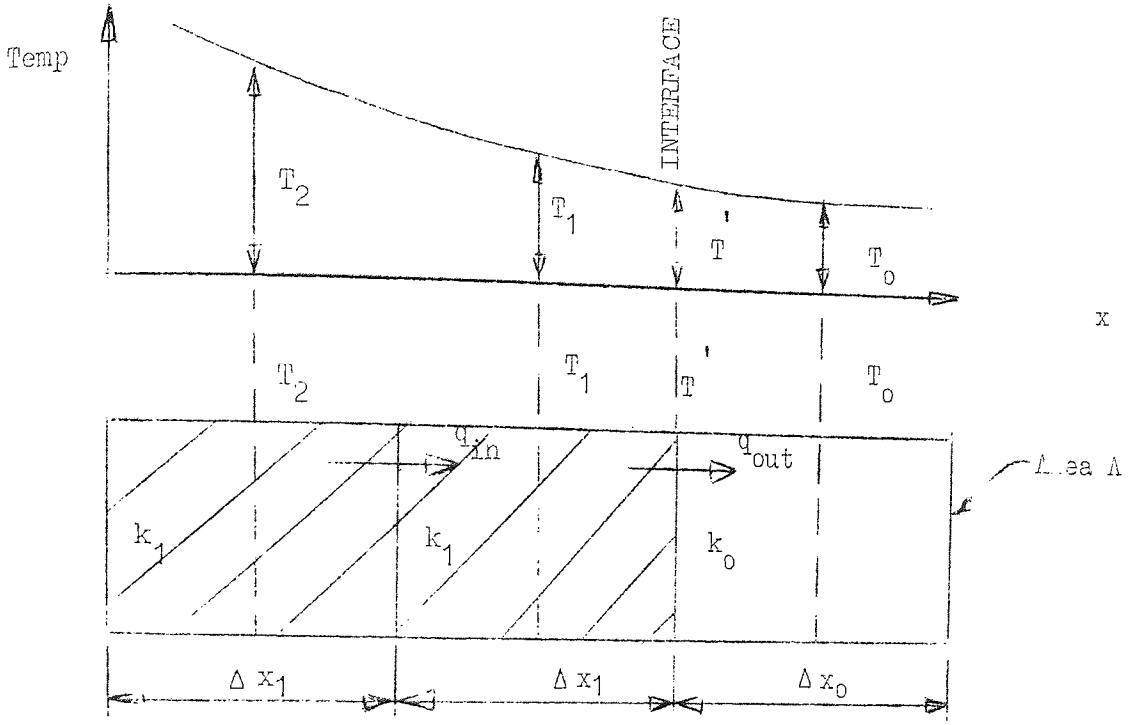

$$q_{in} = k_1 A \left(\frac{dT}{dx}\right)_1 = k_1 A \left(\frac{T_2 - T_1}{\Delta x_1}\right)$$

$$q_{out} = \frac{k_o A}{\frac{\Delta x_o}{2}} (T' - T_o) = \frac{k_1 A}{\frac{\Delta x_1}{2}} (T_1 - T')$$

$$\text{i.e. } (T_1 - T_o) = \frac{q_{out}}{A}\left[\frac{\left(\frac{\Delta x_o}{2}\right)}{k_o} + \frac{\left(\frac{\Delta x_1}{2}\right)}{k_1}\right]$$

$$\therefore q_{out} = A \frac{(T_1 - T_o)}{\left[\frac{\Delta x_o}{2k_o} + \frac{\Delta x_1}{2k_1}\right]}$$

From time t = 0 to Δt, the net heat flow into element 1 produces a temperature rise ΔT_1.

The heat associated with this temperature rise is $\rho_1 C_1 \frac{\Delta T}{\Delta t} \Delta x_1 A$.

$$\therefore \rho_1 C_1 \frac{\Delta T}{\Delta t} \Delta x_1 A = k_1 A \frac{(T_2 - T_1)}{\Delta x_1} - \frac{A (T_1 - T_o)}{\left[\frac{\Delta x_o}{2k_o} + \frac{\Delta x_1}{2k_1}\right]}$$

$$\therefore \frac{\Delta T}{\Delta t} = \frac{1}{\rho_1 C_1 \Delta x_1} \left[\frac{(T_2 - T_1)}{\frac{\Delta x_1}{k_1}} + \frac{(T_o - T_1)}{\left[\frac{\Delta x_o}{2k_o} + \frac{\Delta x_1}{2k_1}\right]} \right]$$

Appendix VIII

Block diagram for computer programme of thermal solution to lubricated rolling/sliding contacts

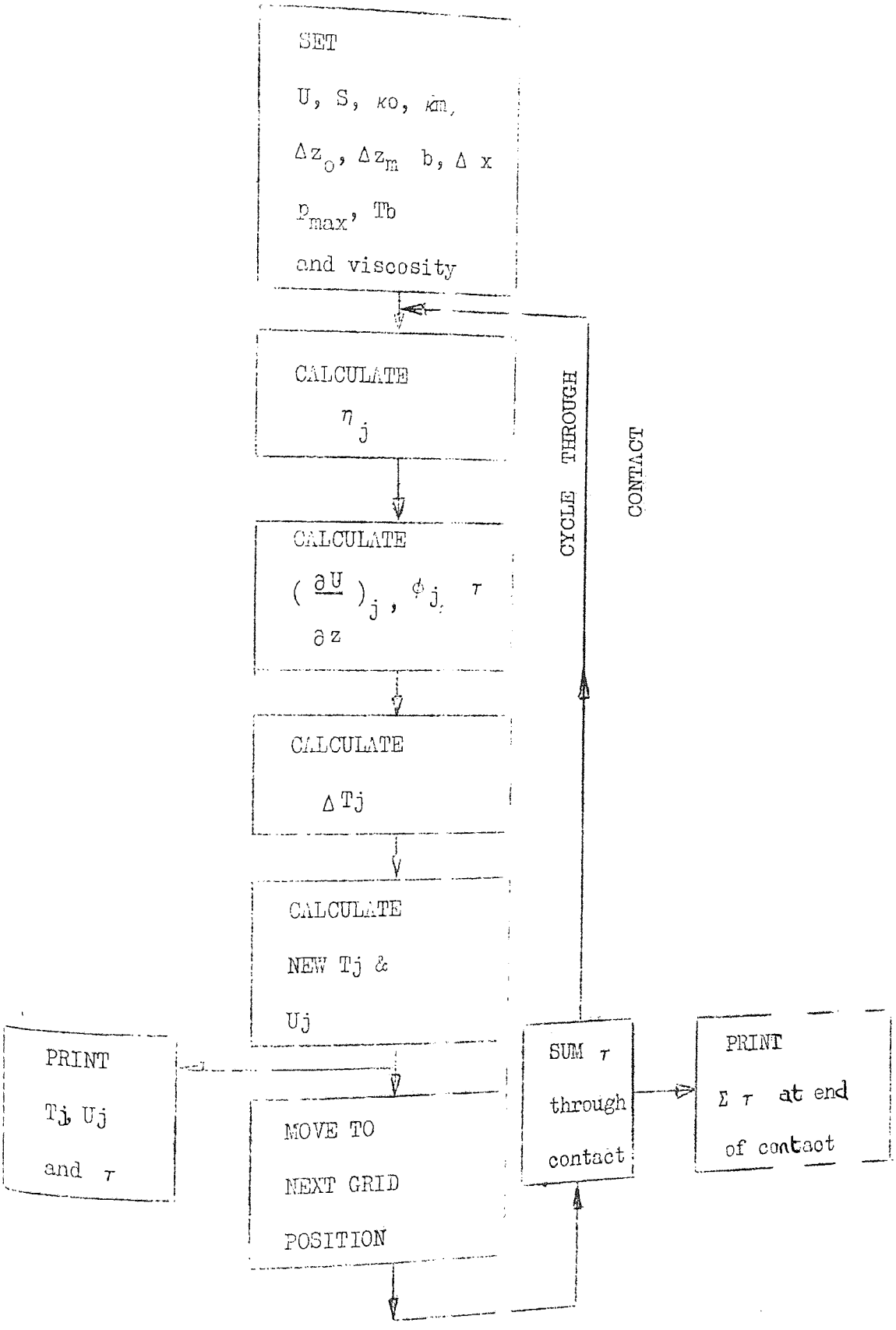

APPENDIX IX A SAMPLE ELLIOT AUTOCODE 803 COMPUTER PROGRAMME

```
::FLASH  TEMPS  VARY K C RO

SETS LJ(I)GO
SETV S(60)ABCEH(2)K(60)P(60)N(60)R(2)T(120)U(120)XYMV(60)Z(5)D(60)N(5)
SETF EXP
SETR 20

1)Z=T(I+1)+T(I-1)
Z=Z-TI
Z=Z-TI
Z=Z/R2
Z=Z/R2
Z=Z*K2
Z=Z*X
Z=Z/UI
Z=Z/2
TI=TI+Z
EXIT

2)Z=T(I+1)+T(I-1)
Z=Z-TI
Z=Z-TI
Z=Z/R1
Z=Z/R1
Z=Z*KJ
Z=Z/R1
Z=Z/PJ
Z=Z*X
Z=Z/UI
Z=Z/2
TI=TI+Z
EXIT

3)READ U50
READ S
READ T
READ K2
READ F
READ O
READ G3
READ M
READ A1
READ H2
READ R1
READ R2
READ C
READ X
READ Y
```

```
S3=1
N=0
O=1
X=X/Y
K4=H2/K2
K4=K4/R2

VARY I=1:1:120
TI=T
REPEAT I

VARY J1=0:1:1501
P=STAND J1
P=P/750
P=1-P
P=P*P
P=1-P
P=P*M
P=P/1000

P1=P/2.24
P2=P1*.02
P2=P2+1
P2=P1/P2
P2=P2*.007
P2=P2+1


 VARY J=51:1:5
 A=TJ/400
 A=A+0.4
 S1=LOG 10
 A=A*S1
 A=EXP A
 Q2=TJ+170
 Q2=Q3/Q2
 Q2=EXP Q2
 Q1=Q*Q2
 B=Q1*6895000
 B=LOG B
 B=.062*B
 B=EXP B
 A=A*B
 A=0.062/A
 S2=A*P
 S2=1+S2
 S2=LOG S2
 S2=16*S2
 S2=EXP S2
 SJ=Q1*S2
 REPEAT J

JUMP UNLESS S3=7504
7)VARY J=51:1:5
LINE
PRINT SJ,6/
REPEAT J
S3=0
4)S3=S3+1
S20=0
VARY J=51:1:5
DJ=1/SJ
S20=S20+DJ
REPEAT J


VARY J=51:1:5
V50=0
VJ=U53*S
VJ=VJ/SJ
VJ=VJ/S20
VJ=VJ/2
UJ=U(J-1)-V(J-1)
UJ=UJ-VJ
N1=V53*S53
N=N+N1


5)QJ=X/UJ
QJ=QJ*SJ
QJ=QJ*VJ
QJ=QJ*VJ
QJ=QJ*4
QJ=QJ/H1
QJ=QJ/H1
QJ=QJ/R1
P3=TJ-60
P3=C*P3
P3=1-P3
P4=TJ*.00045
P4=P4+.388
P4=P4/.934
PJ=P3*P4
PJ=PJ*P2
KJ=TJ-32
KJ=KJ*.0003
KJ=1-KJ
KJ=KJ*.935
KJ=KJ/144
KJ=KJ/3600
QJ=QJ/PJ
QJ=QJ/9336
REPEAT J

U56=1-S
U56=U56*U50
VARY I=51:1:5
TI=TI+QI
REPEAT I
VARY I=56:2:25
JUMP IF I=56@9
UI=U56
SUBR 1
JUMP @10
9)Z1=T55-T56
K3=H1/K55
K5=K3+K4
K5=K5/2
Z1=Z1/K5
Z2=T57-T56
Z2=Z2/K4
Z=Z1+Z2
Z=Z/H2
Z=Z/R2
Z=Z/U56
Z=Z*X
Z=Z/2
T56=T56+Z
10)REPEAT I


VARY I=2:2:25
JUMP IF I=50@11
UI=U50
SUBR 1
JUMP @12
11)Z1=T51-T50
K3=H1/K51
K5=K3+K4
K5=K5/2
Z1=Z1/K5
Z2=T49-T50
Z2=Z2/K4
Z=Z1+Z2
Z=Z/H2
Z=Z/R2
Z=Z/U50
Z=Z*X
Z=Z/2
T50=T50+Z
12)REPEAT I


VARY I=51:2:3
JUMP IF I=51@13
JUMP IF I=55@14
SUBR 2
JUMP @15
13)Z1=T50-T51
K3=H1/K51
K5=K3+K4
K5=K5/2
Z1=Z1/K5
Z2=T52-T51
Z2=Z2/K3
Z=Z1+Z2
Z=Z/H1
Z=Z/R1
Z=Z/P51
Z=Z/U51
Z=Z*X
Z=Z/2
T51=T51+Z
JUMP @15
14)Z1=T56-T55
K3=H1/K55
K5=K3+K4
K5=K5/2
Z1=Z1/K5
Z2=T54-T55
Z2=Z2/K3
Z=Z1+Z2
Z=Z/H1
Z=Z/R1
Z=Z/P55
Z=Z/U55
Z=Z*X
Z=Z/2
T55=T55+Z
15)REPEAT I


VARY I=57:2:24
UI=U56
SUBR 1
REPEAT I


VARY I=1:2:25
UI=U50
SUBR 1
REPEAT I


VARY I=52:2:2
SUBR 2
REPEAT I


JUMP UNLESS O=15006
O=0
8)VARY G=1:5:21
LINE
VARY I=G:1:5
PRINT TI,3:2
REPEAT I
REPEAT G
LINES 2
VARY J=50:1:7
LINE
PRINT UJ
REPEAT J


6)O=O+1
REPEAT J1
LINE
PRINT N,6/
JUMP @3
STOP
START 3
```

Appendix X - List of papers

The following papers were published by the author during the course of the work presented in this thesis.

"The heat transfer coefficie it and lubricated contact temperature"

O'Donoghue J.P., Manton S.M. and Cameron A.

ASLE Trans. Vol. 10 No. 2 Ap il 1967 p. 175.

"An experimental determinati n of the temperature at scuffing"

O'Donoghue J.P., Manton S.M. and Askwith T.C.

I.Mech.E. Tribology Conventi n, Pitlochry 1968, Paper No. 3 p. 20.

"Gear lubricant testing mach nes - are they useful?"

Manton S.M. and O'Donoghue J P.

Tribology, Vol. No. 3 Aug. 1 68 p.146.

"Temperatures at lubricated olling/sliding contacts"

Manton, S.M., O'Donoghue J.P and Cameron A.

Proc. I.Mech.E. 1968-68, Vol 182 part 1 No. 41.

Bibliography

1. Almen, J.O. "Surface deterioration of teeth" Mech. Wear ASM 1950, p. 229.

2. American Gear Manufacturers Association — Progress report by Automotive Bearing Committee Sec. II "PVT Values of gear teeth" AGMA Pub. 101.02 Oct. 1951.

3. Shipley, E.E. "Design and testing consideration of lubricants for gear applications" Lubrication Engineering, 1950 Vol. 14, 4, p. 140.

4. Borsoff, V.N. Accinelli, and Buttnoo — ASME Trans. V. 73, pp. 687 - 95.

5. Hanhoja, J. and Tension, H.D. "The effect of temperature, speed, and type of oil on gear scuffing" M.I.T.A. June 1947.

6. Kelley, E.F. "A new look at the scoring phenomena of gears" Trans. SAE, Vol. 61, p. 175, 1953.

7. Blok, H. "Theoretical study of temperature rise at surfaces of actual contact under oiliness lubricating conditions" General discussion on lubrication, I.Mech.E. Vol. 2, 1937, p. 22.

8. Blok, H. SAE Transactions 1939, 44, 5 May

9. O'Donoghue, J.P. and Cameron, A. "Friction and temperature in rolling/sliding contacts" ASLE Trans. Vol. 9, p. 186, 1965.

10. Benedict, G.H. and Kelley, B.W. "Instantaneous coefficients of friction for gears" Trans. ASLE Vol. 4, 1961, p. 59.

11. Lane, T.B. and Hughes, J.R. "A practical application of the flash temperature hypothesis to gear lubrication" Proc. 3rd World Petrol Congress, p. 320, 1951.

12. Blok, H. "Lubrication as a gear design factor" I.Mech.E. Conf. on Gearing 1958, p. 144.

13. De Gruchy, V.J. and Harrison, P.J. "Development of an edge type disc machine" Proc. Convention on Lubrication & Wear I.Mech.E. Bournemouth 1963.

14. O'Donoghue, J.P. "Gear tooth contact phenomena" Ph.D. thesis University College, Dublin 1964.

15. Heng, V.V. "Investigation of steel seizure in a roller testing machine" 1960 Friction and Wear in Machinery, 14.

16. Genkin, M.D. Kuznin, N.F. and Mishurin, Yu.A. "A study of seizure of steel rollers" National Research Council of Canada Technical Translation 1056.

17. Leach, E.F. and Kelley, B.W. "Temperature - the key to lubricant capacity" ASLE Lub. Conf. 1964, paper 13.

18. Ali, M.S. and Thomas, M.P. "The effect of changes in the physical properties of plain mineral oils on their load carrying capacity" Inst. Pet. Gear Lub. Conf. Oct. 1964.

19. IP/IAE Gear Rig Tests sub-panel "Lubrication evaluation with gear machines" Proc. Symp. "Gear lubrication" Inst. Pet. 1964, I.1.

20. IP/IAE Gear Rig Tests sub-panel "The IAE 3¼ inch centres gear rig estimation of precision" Proc. Symp. "Gear lubrication" Inst. Pet. 1964 I.6.

21. IP/IAE Gear Rig Tests sub-panel "Note on correlation of results from the IAE and Ryder gear rigs" Proc. Symp. "Gear lubrication" Inst. Pet. 1964 I.16.

22. Foyle, T.I. "Correlating the IAE and FZG gear rigs by the critical scuffing temperature theory" Proc. Symp. "Gear lubrication" Inst. Pet. 1964, I.79.

23. Niemann, G. and Ohlendorf, H. "Verlustleistung und erwärmung von stirnradgetrieben" VDI-Z, 102, No. 6, 21 Feb. 1960.

24. Hughes, J.R. and Waight, F.H. "The lubrication of spur gears" I.Mech.E. 1950, Conference on Gearing.

25. Matveevsky, R.M. "The effect of load on the critical temperature of oils in the lubrication of different materials" Year 1961, p. 292.

26. Matveevsky, R.M. "The critical temperature of oil with point and line contact machines" Trans. ASME Se.D. J. Basic Eng. 87, 754-760, 1965.

27. Bowden, F.P. and Tabor, D. "The friction and lubrication of solids" Pt. 1, Clarendon Press. Oxford 1950.

28. Fein, R.S. Discussion to reference 26.

29. Fein, R.S. "Effects of lubricants in transition temperature" ASLE paper no. 64LC-7.

30. Fein, R.S. "Operating procedure effects on critical temperatures" ASLE Trans. 10, 373-385 (1967).

31. Bowden, F.P. and Leben, L. Proc. Roy. Soc. A169, 371 (1939).

32. Dingle, E.D. Nature, 160, 710 (1947).

33. Ibrahim, M. and Cameron, A. "Oil film thickness and the mechanism of scuffing in gear teeth" Proc. Lub. & Gear Conv. I.Mech.E. 1963, paper 20.

34. Askwith, T.C., Cameron, A. and Crouch, R.F. "Chain length of additives in relation to lubricants in thin film and boundary lubrication" Proc. Roy. Soc. A. vol. 291, 500-5 9, (1966).

35. Grew, W. and Cameron, A. "Friction transition effect of matching surfactant and carrier" Nature, vol. 214, p.429 (1967).

36. Cameron, A. Rogers, P.R. and Siripongse, C. "Thin film lubrication" 1958 Engineering 186, p.146.

37. Gross, W.A. "Gas film lubrication" 1962 New York, Wiley, Sect. 6.1, 6.2.

38. Fuks, G.J. "The properties of solutions of organic acids in liquid hydrocarbons at solid surfaces" Research in surface forces (ed. B.V. Derjaguin) pp. 79-88 Moscow (Trans. Consultants Bureau N.Y. 1962).

39. Frewing, J.J. "The heat of adsorption of long chain compounds and their effect on boundary lubrication" 182, 270 (1944).

40. O'Donoghue, J.P. and Cameron, A. "Temperature at scuffing" Proc. Symp. Elastohydrodynamic Lubrication Sept. 1965, I.Mech.E. paper 6.

41. Groszek, A.J. and Palmer, D.J. "Surface active compounds in lubricating oils" J.Inst. Pet. (1961), 47, 295-306.

42. Glasstone, S. "Textbook of physical chemistry" 2nd Ed. 1956, Macmillan, New York and London.

43. Blok, H. "Les temperatures de surface dans les conditions de graissage sans extreme pression" 1937 Second World Petrol Congress, Paris, Section 4.

44. Davies, A.R. and Forrester, J.S. Private Communication J. Lucas Ltd. 1966.

45. Carslaw, H.S. and Jaeger, J.C. "Conduction of heat in solids" Clarendon Press (1947).

46. Cameron, A., Gordon, A.N. and Symm, G.T. "Contact temperatures in rolling/sliding surfaces" Proc. Roy. Soc. Vol. 286, p.45-61 (1965).

47. Gordon and Cameron, A. Private Communication.

48. McAdams, W.H. "Heat transmission" McGraw Hill Book Co. 1954, p.177.

49. Etemad, G.A. "Free convection heat transfer from a rotating cylinder to ambient air, with interferometric study of flow" ASME No. 54-A-74.

50. Anderson, J.T. and Saunders, O.A. "Convection from an isolated cylinder rotating about its axis" Proc. Roy. Soc. A 1953, Vol. 217 p.555.

51. Kays, W.M. and Bjorklund, I.S. "Heat transfer from a rotating cylinder with and without crossflow" Trans. ASME Vol. 70/1958 p.70.

52. McAdams, W.H. "Heat transmission" McGraw Hill Book Co., 1954, p. 258

53. Richardson, P.D. and Saunders, O.A. "Studies of flow and heat transfer associated with a rotating disc" J.Mech.Eng. Sc. I.Mech.E. Dec. 1965.

54. Cobb, E.C. and Saunders, O.A. "Heat transfer from a rotating disc" Proc. Roy. Soc. A. 1956, Vol. 236, p. 343.

55. Eckert, E.R.G. "Introduction to the transfer of heat and mass" McGraw Hill Book Company. Inc. N.Y 1950, p. 120-125.

56. Martin, H.M. "Lubrication of gear teeth" Engineering, London 103, p. 199.

57. Cameron, A. "Principles of lubrication" Longmans Green and Co. Ltd. 1966.

58. Peppler, W. (1936, 1938) referenced in "Elastohydrodynamic Lubrication" by Dowson, D. and Higginson, G.R. Pergamon Press (1966) p. 229.

59. Mendahl, A. "Contribution to the theory of the lubrication of gears and of the stressing of the lubricated flanks of gear teeth" Brown Boveri Review 28, No. 11, 37[illegible] (1941).

60. Catcombe, E.K. "Lubrication characteristics of involute spur-gears - a theoretical investigation" Trans AMSE 67, 177, (1945).

61. Cameron, A. "Hydrodynamic theory in gear lubrication" J. Inst. Petrol 38, 614 (1952).

62. McEwen, E. "The effect of variation of viscosity with pressure on the load carrying capacity of oil films between gear teeth" J. Inst. Petrol 38, 646, (1952).

63. Grubin, A.N. and Vinogradova, I.E. Central Scientific Research Institute for Technology and Mechanical Engineering Book No. 30, Moscow (DSIR Translation No. 337) (1949).

64. Crook, A.W. "The lubrication of rollers, I" Phil. Trans. A250, 387, (1958).

65. Crook, A.W. "The lubrication of rollers, II film thickness with relation to viscosity and speed" Phil. Trans. A254, 223 (1961 a).

66. Crook, A.W. "The lubrication of rollers, III, a theoretical discussion of friction and the temperatures in the oil film" Phil. Trans. A254, 237 (1961b).

67. Dowson, D. and Longfield, M.D. "Distribution of pressure and temperature in a lightly loaded lubricated contact" I.Mech.E. Lubrication and Wear Convention, May 1963.

68. Dowson, D. and Higginson, G.R. "A numerical solution to the elasto-hydrodynamic problem" J.Mech.Eng. Sci. 1, No. 1, 6 (1959).

69. Dowson, D. and Higginson, G.R. "The effect of material properties on the lubrication of elastic rollers" J.Mech.Eng. Sci. 2, No. 3, (1960).

70. Dowson, D., Higginson, G.R. and Whitaker, A.V. "Elasto-hydrodynamic lubrication a survey of isothermal solutions" J.Mech.Eng. Sci. 4, 2, 121 (1962).

71. Dowson, D. and Higginson, G.R. "New roller bearing lubrication formula" Engineering, London, 192, 158 (1961).

72. Sibley, L.B. and Orcutt, F.K. "Elastohydrodynamic lubrication of rolling contact surfaces" Trans. ASLE 4, 2, p.234.

73. Archard, G.P., Gair, F.C. and Hirst, W. "The elastohydrodynamic lubrication of rollers" Proc. Roy. Soc. of London Vol. 262 p. 51 (1961).

74. Dowson, D. and Higginson, G.R. "The theory of roller bearing lubrication and deformation" I.Mech.E. 1963, Lub. and Wear Convention.

75. Dowson, D. and Higginson, G.R. "A theory of involute gear lubrication" Inst. Petrol 1964 Gear lubrication Symposium.

76. Sternlicht, B., Lewis, P. and Flynn, P. "Theory of lubrication and failure of rolling contacts" Trans. ASME J. of Basic Eng. 83, Se.D. 2, 213 (1961).

77. Cheng, H.S. and Sternlicht, B. "A numerical solution for the pressure, temperature and film thickness between two infinitely long, lubricated rolling and sliding cylinders, under heavy loads" ASME paper 64, Lub. 11.

78. Cheng, H.S. "A refined solution to the thermal elastohydrodynamic lubrication of rolling and sliding cylinders" ASLE Trans. 8, 397 (1965).

79. Cheng, H.S. and Orcutt, F.K. "A correlation between the theoretical and experimental results on the EHL of rolling and sliding contacts" Paper No. 13 I.Mech.E. Symp. on Elastohydrodynamic lubrication, Leeds 1965.

80. Archard, J.F. "Experimental studies of elasto-hydrodynamic lubrication" Paper R2, I.Mech.E. Symp, EHL, Leeds 1965.

81. Dowson, D. and Whitaker, A.V. "A numerical procedure for the solution of the EHL problem of rolling and sliding contacts lubricated by a Newtonian fluid" Paper 4, I.Mech.E. Symp. EHL, 1965.

82. Ibrahim, M. "The study of oil films between the teeth of running spur gears" Ph.D. Thesis London (1961), 80-4.

83. SHI-I-PAI "Viscous flow theory - 1 Laminar flow" Van Nostrand (1956).

84. Rosenhead, L. "A discussion on the first and second viscosities of fluids" Proc. Roy. Soc (A) 1954, 226, 1-65.

85. Rogers, G.F. and Mayhew, Y.R. "Engineering Thermodynamics" Longmans, Green & Co. Ltd. p.101, 1957.

86. Barakat, H.Z. and Clark, J.A. "On the solution of the diffusion equations by numerical methods" Trans. ASME J.Heat Transfer, Vol. 88, Se.C, No.4.

87. Jakob, M. and Hawkins, C.A. "Elements of heat transfer" 3rd Ed. J. Wiley & Sons, 1957.

88. Cameron, A. and Chu, P.S.Y. "Pressure viscosity characteristics" J.Inst. Petrol. Vol. 48, No. 461 (1962).

89. Merritt, H.E. "Gear tooth contact phenomena" I.Mech.E. Proceedings, Vol. 176, No.7 1962.

90. Taskoprulu, N.S., Barlow, A.J. and Lamb, J. "Ultrasonic and visco-elastic relaxation in a lubricating oil" J.Acou. Soc. America, Vol. 33, No.3 (1961).

91. Crook, A.W. "The lubrication of rollers - IV. Measurements of friction and effective viscosity" Phil. Trans. Vol. 255, A1056 (1963).

92. Jefferis, J.A. and Johnson, K.L. "Traction in EHL contacts" Paper 1, Proc. I.Mech.E. Vol. 182, (1), No. 14.

93. Johnson, K.L. and Cameron, R. "Shear behaviour of EHL oil films at high rolling contact pressures" Paper 4, Proc. I.Mech.E. Vol. 182 (1) No. 14.

94. Plint, M.A. "Traction in EHL contacts" Paper 3, Proc. I.Mech.E. Vol. 182 (1) No. 14.

95. Merritt, H.E. "Gears" 3rd edition. Pitman 1954.

96. Smith, F.W. "Rolling contact lubrication in the application of elastohydrodynamic theory" Trans. ASME 1965, 87 (Se.D), 170.

97. Van Wazer et al. "Viscosity and its measurement" 1963 Interscience Publishers.

98. Crouch, R.F. and Cameron, A. "Graphical integration of the Maxwell fluid equation and its application" J.Inst. Pet. Vol. 48, No. 436 (1960).

99. Lamb, J. "Physical properties of fluid lubricants rheological and viscoelastic behaviour" Paper 18, p.13 Conf. Lub & Wear I.Mech.E. London (1967).

100. Barlow, A.J., Lamb, J., Matheson, A.J., Padmini, P.R.Kl. and Richter, J. "Viscoelastic relaxation of supercooled liquids Pt. I" Proc. Roy. Soc. 1967, 298, (No. A, 1455) 467.

101. Barlow, A.J. and Lamb, J. "The viscoelastic behaviour of lubricating oils under cyclic shearing stress" Proc. Roy. Soc. 1959, 253, 52.

102. Dyson, A. "Flow properties of mineral oils in elastohydrodynamic lubrication" Phil. Trans. Vol. 258, A1093, p. 259, (1965).

103. Oldroyd, J.G. "Non-Newtonian effects in steady motion of some idealised elasto-viscous liquid" Proc. Roy. Soc. London A Vol. 245 p.278.

104. Dyson, A. Discussion to reference 93.

105. Naylor, H. Private Communication.

106. Durelli, A.J., Phillips, E.A. and Tsao, C.H. "Analysis of stress and strain" p. 212, McGraw-Hill Book Co. 1958.

107 Hertz, H. Quoted by Timoshenko, S. and Goodier, J.N. "Theory of elasticity" p. 372 McGraw Hill Book Co. 2nd Edition.

108. Belajef, N.M. As above. p. 380.

109. Smith, J.O and Cheng Keng Liu "Stresses due to tangential and normal loads on an elastic solid with application to some contact stress problems" J.App.Mech. Trans ASME 1953, 75, 157.

110. Poritsky, H. "Stresses and deflections of cylindrical bodies in contact with application to contact of gears and of locomotive wheels" J. App. Mech. Trans ASME 1950, 72, 191, 465.

111. Dowson, D., Higginson, G.R. and Whitaker, A.V. "Stress distribution in lubricated rolling contacts" Symp. "Fatigue in Rolling Contacts" I.Mech.E. 196, paper 6.

112. Schoeppel, R.A. and Evan-Iwanouski, R.M. "Rolling and sliding contact stress parameters in elastohydrodynamic lubrication" J. App. Mech. Trans ASME 1967, 471.

113. Johnson, K.L. and Jefferis, J.A. "Plastic flow and residual stresses in rolling and sliding contact" Symp. "Fatigue in rolling contacts" I.Mech.E., 1964, paper 5.

114. Way, S. "Pitting due to rolling contact" Trans ASME Vol. 2 1935, p. 49.